Development of an organotypic 3D *in vitro* model of normal human breast tissue: a tool for cancer initiation studies

Claire Elizabeth Nash BSc (Hons)

Submitted in accordance with the requirements for the degree of

Doctor of Philosophy

The University of Leeds

School of Medicine

March 2014

The candidate confirms that the work submitted is her own, except where work which has formed part of jointly authored publications has been included. The contribution of the candidate and the other authors to this work has been explicitly indicated below. The candidate confirms that appropriate credit has been given within the thesis where reference has been made to the work of others.

The work in Chapter 1 and introduction of Chapter 3 of the thesis has appeared in publication as follows:

Nash, C. and V. Speirs, *Pre-Clinical Modelling of Breast Cancer: Which Model to Choose?*, in *Breast Cancer Metastasis and Drug Resistance. Progress and Prospects*, A. Ahmad, Editor 2013, Springer.

I was first author of the chapter. The other author, Prof Valerie Speirs, contributed through reviewing and editing the work prior to final submission to the book editor.

Candidate Achievements

Publications

Nash, C. and V. Speirs, Pre-Clinical Modelling of Breast Cancer: Which Model to Choose?, in *Breast Cancer Metastasis and Drug Resistance. Progress and Prospects*, A. Ahmad, Editor 2013, Springer.

D. Holliday, M. Moss, S. Pollock, S. Lane, A. Shabaan, R. Millican-Slater, **C. Nash**, A. Hanby & V. Speirs. The practicalities of using tissue slices as pre-clinical organotypic breast cancer models. *J Clin Pathol,* 2013, **66**(3), p. 253-5.

Verghese, E., Drury, R., Green, C.A., Holliday, D.L., Lu, X., **Nash, C**., Speirs, V., Thorne, J.L., Thygesen, H.H., Zougman, A., Hull, M.A., Hanby, A.M. and Hughes, T.A. Role of miR-26b in carcinoma-associated fibroblasts and effect on migration and invasion of breast cancer epithelial cells. *The Lancet*, 2014. **383**: p. S103.

Millican-Slater, R., Good, R., **Nash, C.**, Heads, J.A., Pollock, S., Gomm, J., Jones, J.L., Sundara-Rajan, S., Horgan, K., Hanby, A.M., Speirs, V. (2014) Pathobiology of breast tissue and primary cell cultures obtained from a female-to-male transgender patient. *Cell and Tissue Banking.* (submitted)

Poster and Oral Presentations

Nash, C. *A 3D in vitro model of normal breast tissue: A tool for breast cancer initiation studies*. [Poster] National Cancer Research Institute, Liverpool, UK, November 2012.

Nash, C. *A 3D tri-culture model of normal mammary gland: A tool for breast cancer initiation studies.* [Poster] CTRC-AACR San Antonio Breast Cancer Symposium, San Antonio, USA, December 2012.

Nash, C. *Developing and Characterising a Novel 3D in vitro Model of Normal Breast for Cancer Initiation Studies.* The Pathological Society and British Division of the IAP national meeting, Edinburgh, UK, June 2013.

Nash, C. *Developing and Characterising a Novel 3D in vitro Model of Normal Breast for Cancer Initiation Studies.* Leeds Institute of Molecular Medicine Postgraduate Research Symposium, Leeds, UK, April 2013.

Nash, C. *Developing and Characterising a Novel 3D in vitro Model of Normal Breast for Cancer Initiation Studies.* The University of Leeds Faculty of Medicine and Health Postgraduate Conference, Leeds, UK, July 2013.

Awards

Awarded 1st prize for best plenary oral presentation at The Pathological Society and British Division of the IAP national meeting, Edinburgh, UK, June 2013.

Awarded 2nd prize oral presentation at Leeds Institute of Molecular Medicine Postgraduate Research Symposium, Leeds, UK, April 2013.

Awarded 2nd prize oral presentation at The University of Leeds Faculty of Medicine and Health Postgraduate Conference, Leeds, UK, July 2013.

Awarded joint 3rd Postgraduate Researcher of the Year at the Showcase University of Leeds Postgraduate Researcher conference, Leeds, UK, December 2014

Awarded BACR/ CRUK Travel Bursary to attend CTRC-AACR San Antonio Breast Cancer Symposium in USA, December 2012

Acknowledgements

I would like to thank my primary supervisor, Prof Valerie Speirs, for her guidance, dedication, encouragement, passion, and most of all patience throughout the last few years. Without her this PhD would not have been possible. I would also like to thank my co-supervisors: Prof Andrew Hanby for all his help with pathology and for making me laugh throughout these years, Dr Georgia Mavria and Dr Darren Tomlinson for their extensive knowledge and guidance throughout and Dr Debbie Holliday for training me and for her friendship giving me a solid foundation to build my thesis upon. I'd also like to thank our collaborators Dr Fedor Berditchevski and Prof Louise Jones (and her group) for their help throughout.

I'd like to thank the Leeds Institute of Molecular Medicine for funding me and all the patients who donated to the Leeds Breast Tissue Bank for making this work possible.

I big thank you goes out to all of the people I have shared the laboratory and department with who have not just been a massive help but like a family to me over the last few years. Dr Stanley Ko's generosity, knowledge and support was greatly appreciated and Dr Euan Baxter and Dr Laura Smith have been especially helpful with their help and guidance throughout. A special thank you goes out to Emily Smart for being a fantastic friend and keeping me sane throughout my PhD.

I'd like to thank my family for believing in me, getting me through my education and encouraging me to pursue my dreams. Their support has been crucial in allowing me to build a career in science and will never go unappreciated.

Finally I'd like to give a huge thank you to my fiancé Michael Baron. He has supported me both financially and emotionally throughout this project and without him I would have certainly crumbled under the pressure. His continued enthusiasm for life and positive attitude has kept me balanced throughout the entirety of this PhD.

Abstract

The mechanisms involved in breast cancer initiation are not well understood. This may in part be due to a lack of an *in vitro* model that faithfully recapitulates the morphology, phenotype and *in vivo* architecture of the normal human mammary gland. Most *in vitro* models of normal breast have relied on the use of reconstituted basement membrane gels to induce luminal epithelial cell polarity and have neglected the role of myoepithelial cells and fibroblasts in this process. The aim of this thesis was to develop a three dimensional *in vitro* culture system of normal breast which included three of the major functional cell types of breast embedded in a more physiologically relevant collagen I matrix. It was then sought to use the system to investigate the mechanisms behind breast cancer initiation via genetic manipulation of well-known oncogenes and tumour suppressors involved in breast cancer progression.

To achieve this, myoepithelial cells (Myo1089, originally isolated from breast reduction mammoplasty sample, gift of Dr Mike O'Hare) and fibroblasts (isolated and immortalised from breast reduction mammoplasty samples collected with ethical approval in house) were characterised by immunofluorescence to assess their suitability. Following characterisation, these were virally transfected with Turbo Green Fluorescent Protein (tGFP) and dsRed protein respectively to enable tracking. Three-dimensional tri-cultures were established in collagen I and included the non-tumorigenic luminal epithelial cell line HB2 with GFP Myo1089 cells and dsRed fibroblasts. Cells were cultured for three weeks in Transwell™ cell culture inserts. Following fixation these were analysed by haematoxylin and eosin staining, confocal microscopy and immunohistochemistry. Morphology and immunostaining profiles were compared to sections of a normal human *in vivo* breast tissue specimen.

Immunohistochemical characterisation using the following antibodies: E-cadherin, epithelial membrane antigen, vimentin, laminin 5, collagen IV plus luminal and basal cytokeratins, demonstrated polarised epithelial structures with lumen formation and basement membrane

production with a similar immunostaining profile to normal breast tissue. The importance of including myoepithelial cells and fibroblasts in maintaining these structures was demonstrated. We established this model was amenable to genetic engineering by overexpressing HER2 and HER3 in HB2 cells, and knocking out ERβ1 in Myo1089 cells and DOCK4 in fibroblast cell lines using siRNA/shRNA techniques respectively. These were included in separate models with morphological and phenotypic effects determined by haematoxylin and eosin staining, immunohistochemistry and quantification of HB2 structures formed. We further investigated the intracellular signalling cascades stimulated by heregulin in order to validate our findings upon overexpression of HER2 and HER3 and to investigate the cancer initiation potential of heregulin in the breast.

In summary, an *in vitro* model of normal breast tissue that includes three of the major functional breast cell types cultured in a physiologically relevant three dimensional matrix has been developed. The morphology and protein expression profile of the model was validated against a human breast tissue specimen and confirmed that it is a suitable model of normal breast. The model proved to be reproducible, suitable for experimentation using genetic engineering and cell behaviour could be easily visualised using standard laboratory techniques. To conclude, this is a robust *in vitro* model of normal breast tissue offering an alternative cost-effective method of studying genes and processes involved in breast cancer initiation.

Table of Contents

List of Figures

List of Tables

Abbreviations

Abbreviation	Definition
2D	Two-dimensional
3D	Three-dimensional
ADH	Atypical Ductal Hyperplasia
ALH	Atypical Lobular Hyperplasia
ATCC	American Type Culture Collection
BSA	Bovine Serum Albumin
CAFs	Cancer Associated Fibroblasts
cDNA	complementary deoxyribonucleic acid
Coll IV	Collagen IV
DAPI	4', 6-diamidino-2-phenylindole
DBD	DNA Binding Domain
DCIS	Ductal Carcinoma *in situ*
DHR	DOCK Homology Region
DMEM	Dulbecco's Modified Eagle Medium
DNA	Deoxyribonucleic Acid
DOCK4	Dedicator of Cytokinesis 4
DPBS	Dulbecco's Phospho Buffered Saline
ECACC	European Collection of Cell Cultures
E-cad	E-cadherin
ECM	Extracellular Matrix
EDTA	Ethylenediaminetetraacetic acid
EGF	Epidermal Growth Factor
EGFR	Epidermal Growth Factor Receptor
EMA	Epithelial Membrane Antigen
EMT	Epithelial-to-Mesenchymal Transition
ER	Estrogen Receptor
ERα	Estrogen Receptor-alpha
ERβ	Estrogen Receptor-beta
EV	Empty Vector
FACS	Fluorescence Activated Cell Sorting
FCCs	Fibrocystic Changes
FCM	Fibroblast Conditioned Media
FEA	Flat Epithelial Atypia
G418	Geneticin
GEFs	Guanine nucleotide Exchange Factors
H & E	Haematoxylin and Eosin
HB2 HER2/3OE	HER2 and HER3 overexpressing HB2 cells
HB2 HER2OE	HER2 overexpressing HB2 cells
HB2 HER3OE	HER3 overexpressing HB2 cells
HB2 WT	Wildtype HB2 cells
HBSS	Hanks Buffered Salt Solution
HER	Human Epidermal Growth Factor Receptor

Abbreviation	Definition
HGF	Hepatocyte Growth Factor
HI-FCS	Heat-inactivated Foetal Calf Serum
HRG	Heregulin
IDC	Infiltrating Ductal Carcinoma
IDC-NST	Infiltrating Ductal Carcinoma-No Special Type
IHC	Immunohistochemistry
LBD	Ligand Binding Domain
LCIS	Lobular Carcinoma *in situ*
MaSCs	Mammary Stem Cells
MGA	Microglandular Adenosis
MMPs	Matrix Metalloproteinases
MUC-1	Mucin-1
M_w	Molecular weight
NRG	Neuregulin
PBS	Phospho Buffered Saline
PIP_3	Phosphatidylinositol-3,4,5-triphosphate
PR	Progesterone Receptor
PrlR	Prolactin Receptor
qPCR	quantitative real-time Polymerase Chain Reaction
RNA	Ribonucleic Acid
RNAi	RNA interference
RNase	Ribonuclease
RTKs	Receptor Tyrosine Kinases
Sca-1	Stem Cell Antigen-1
SDF-1	Stromal cell Derived Factor-1
shRNA	Short Hairpin RNA
siRNA	Small Interfering RNA
STR	Short Tandem Repeat
TDLU	Terminal Duct Lobular Unit
tGFP	Turbo GFP
TGFβ	Transforming Growth Factor-beta
TIMP-1	Tissue Inhibitor of Metalloproteinase-1
TN-C	Tenascin-C
UDH	Usual Ductal Hyperplasia
Vim	Vimentin
WHO	World Health Organisation
αSMA	α-smooth muscle actin

1 Chapter 1: Introduction

1.1 Normal Breast

1.1.1 Anatomy

The female human breast is a complex structure with networks of ducts and glands designed for lactation (Fig 1.1 & Fig 1.2). These ducts branch out from the nipple and terminate at functional units known as terminal ductal lobular units (TDLU). Lobules are comprised of blind ended tubules called acini which are capable of milk secretion. Ducts and lobules are surrounded by a fibrous tissue known as the stroma. Ducts, lobules and stroma are all embedded within an adipose matrix. Normal breast acini are rich in epithelial cells. These comprise two distinct cell lineages; luminal and myoepithelial cells which share a common stem/basal parentage. Each acinus contains a layer of luminal epithelial cells arranged around a central lumen surrounded by a single layer of myoepithelial cells. These are encased by a protein rich basement membrane and are embedded in the stroma (Fig 1.2).

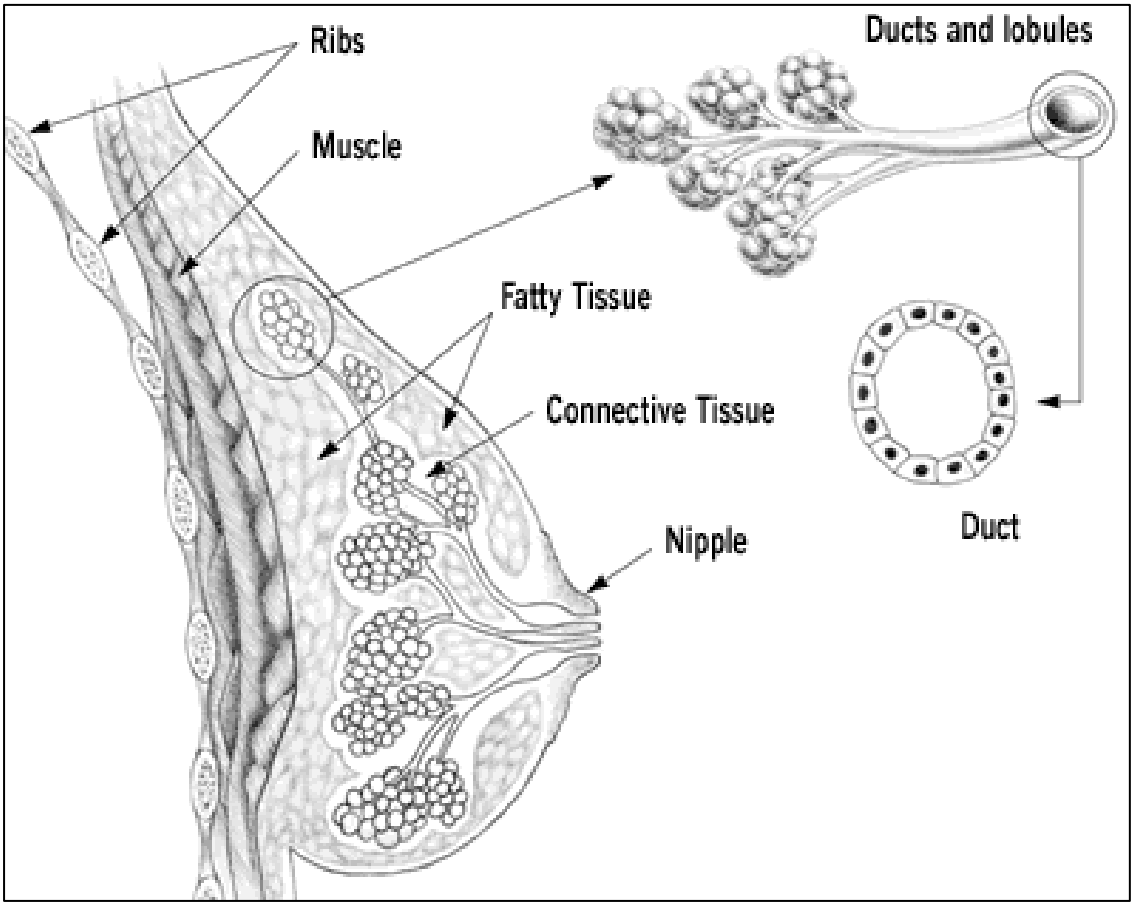

Fig 1.1 Diagrammatic representation of the gross anatomy of the adult female breast

Diagram shows branching network of ducts designed for milk delivery to the nipple. Ducts terminate with lobule structures containing multiple acini. These are surrounded by fibrous stromal tissue (connective tissue) and adipose tissue (fatty tissue).

Adapted from http://www.my-breast-cancer-guide.com/what-is-breast-cancer.html

a)

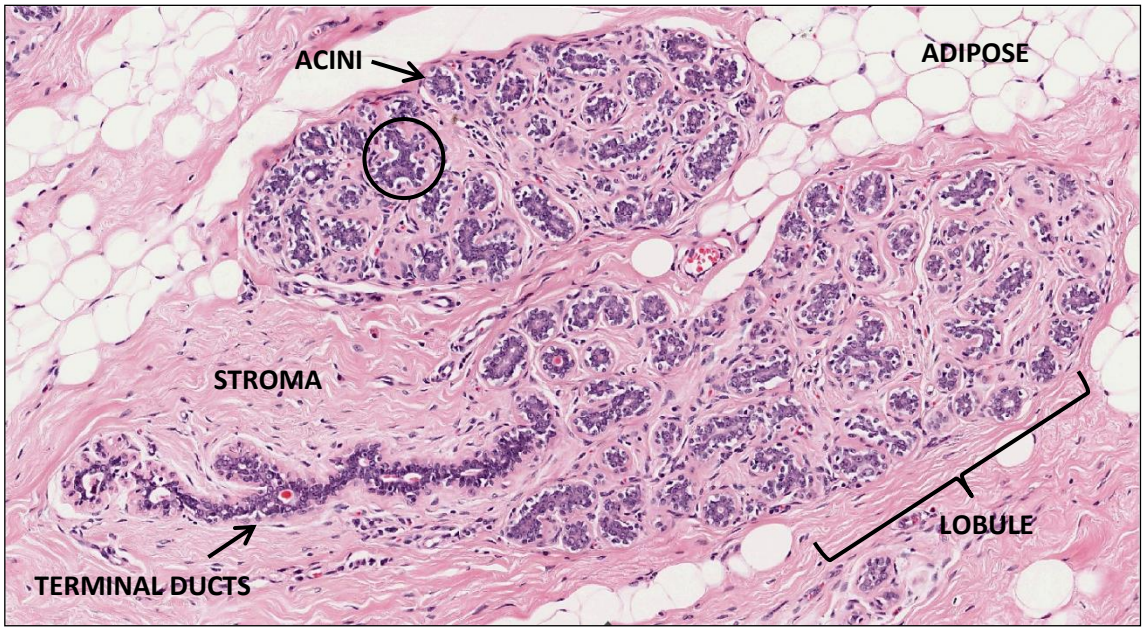

b)

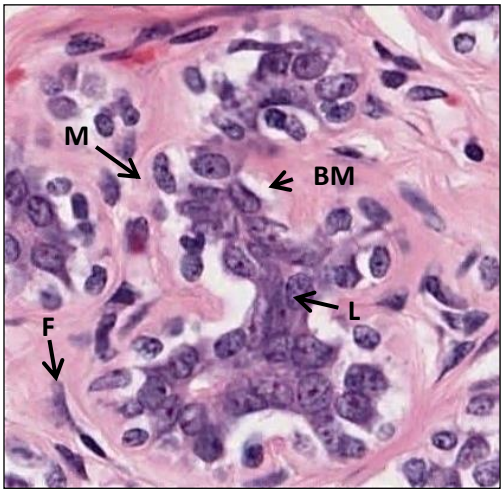

Fig 1.2 Representative haematoxylin & eosin stained cross section of normal adult human breast tissue.

a) Cross section of normal human adult breast shows two breast lobules containing multiple acini situated adjacent to the terminal ducts. These are surrounded by a fibrous stroma and adipose fat tissue. Circle highlights the acinus featured in (b).

b) Cross section of an acinus showing an internal layer of luminal epithelial cells (L). These are surrounded by a layer of myoepithelial cells with clear cytoplasm (M) which sit beneath a protein-rich basement membrane shown in dark pink (BM). The acinus is embedded in a fibrous stroma containing fibroblasts (F).

Images courtesy of Prof Andrew Hanby (Leeds Institute of Cancer and Pathology).

1.1.2 Epithelial cells of the mammary gland

Luminal epithelial and myoepithelial cells of the mammary gland have distinct functions and protein expression profiles. The main function of luminal epithelial cells is to secrete milk during lactation. In order to do this, luminal epithelial cells respond to a variety of hormones such as estrogen, progesterone and prolactin [1]. Accordingly, estrogen receptor alpha (ERα) [2, 3], progesterone receptor (PR) [4] and prolactin receptor (PrlR) [5] are all specific to luminal epithelial cells. However, the expression of hormone receptors is highly dependent on the cell environment with a loss of expression common upon *in vitro* culture. For this reason, luminal epithelial cells are more commonly distinguished from myoepithelial cells by their expression of cytokeratins 8, 18 and 19 [6, 7] and epithelial membrane antigen (also known as MUC-1) [8].

The function of myoepithelial cells during lactation is to contract around the acinus and eject milk into the ducts [9]. These can be distinguished by their expression of cytokeratins 5 and 14 as well as vimentin and α-smooth muscle actin (α-SMA) [10-12]. Myoepithelial cells also play a role in the formation of the basement membrane that surrounds breast acini. This has been proven by their expression of basement membrane proteins such as collagen IV and laminin [10, 13]. Myoepithelial cells form distinct desmosomes with both themselves and with luminal epithelia and unlike luminal epithelia, form hemidesmosomes and attach to the basement membrane [14, 15]. The adhesion properties of myoepithelial cells result in the expression of proteins which can be used to further distinguish them from luminal epithelial cells. These include desmosomal-specific cadherins such as desmocollin 3 and desmoglein 3 [16, 17] and integrins such as β4-integrin [18, 19].

1.1.3 Mammary stem cells

Mammary stem cells (MaSCs) give rise to the luminal and myoepithelial cell lineages described above via a series of progenitor cell intermediates [20]. MaSCs reside in the basal region of the mammary gland alongside myoepithelial cells [21]. The majority of data available on MaSCs has been sourced from studies in mice. The most widely used markers to distinguish MaSCs in mice are positivity for CD24 and CD61 (β3-integrin), high expression of CD29 and CD49f (β1- and α6 integrin respectively) and no expression of stem cell antigen-1 (Sca-1), estrogen receptor (ER), PR, human epidermal growth factor receptor 2 (HER2) and haematopoietic cell markers known collectively as Lin [22-25]. Transplantation studies in mice have revealed that MaSCs are capable of reforming an entire functional mammary gland from a single cell [22]. These give rise to both luminal and myoepithelial cell lineages. MaSCs can be distinguished from luminal epithelial cell progenitors and differentiated epithelium using CD24. CD24 expression is lower (but not lacking) in MaSCs compared with luminal cell lineages [26]. However, perhaps due to their shared basal location, MaSCs are much more difficult to distinguish from myoepithelial cell lineages as these both share high expression of cell surface β1- and α6-integrins and gene expression profiles [23].

In human breast tissue, both bipotent and unipotent progenitor cell populations have been identified. Bipotent progenitors typically have a CD49f high and EpCAM low expression profile and are EMA, CD24, and CD133 negative. Unipotent luminal epithelial progenitors are positive for CD49f, EpCAM, EMA, CD24, and CD133 [27, 28]. Through serial passaging of bipotent progenitors, Stingl et al identified a myoepithelial-restricted progenitor population [27]. More recently, a profile for these cells has been identified which is negative for keratins 5 and 19 with low expression of claudins [29].

The signalling mechanisms that drive this stem cell hierarchy are largely unclear. Few signalling pathways have been identified to induce differentiation down the myoepithelial cell lineage.

However, expression of genes such as Gata-3, Elf5, Notch and PML have all been implicated in driving a luminal epithelial cell fate [25, 28, 30, 31].

1.1.4 Stromal cells of the mammary gland

The stroma is defined as the supportive tissue of an epithelial organ consisting of connective tissue and blood vessels [32]. In the breast, the stroma surrounds the ductal-lobular unit and contains a variety of cell types. These include vascular endothelial cells lining blood vessels, lymphocytes, macrophages and adipocytes [33]. The most abundant cell type within breast stroma is fibroblasts. The main function of fibroblasts is to provide structural support to epithelial structures. Fibroblasts produce a scaffold of extracellular matrix (ECM) proteins which include collagen I [34], fibronectin, and like myoepithelial cells, collagen IV and laminin [35]. Due to these apparent overlapping functions of myoepithelial cells and fibroblasts, there are few immunohistochemical markers that can distinguish between these cells. Like myoepithelial cells, fibroblasts express vimentin. Although fibroblast-specific protein-1 has been identified to be specific to fibroblasts [36], it appears that this is a marker of “active” fibroblasts [37] and may not be applicable to normal breast.

1.2 Breast cancer

1.2.1 Statistics

Breast cancer is one of the most commonly diagnosed cancers in the world with an estimated 1.38 million cases diagnosed worldwide in 2008 [38]. In 2010, over 49,500 women were diagnosed with breast cancer in the UK alone with approximately 80% of those aged 50 or over. Over the last decade, the incidence of breast cancer in the UK has increased by approximately 6% and it is now estimated that a woman has a 1 in 8 risk of developing breast cancer in her lifetime. This disease is not limited to women however with approximately 400 men diagnosed with breast cancer in the UK in 2010 [39].

1.2.2 Heterogeneity

Breast cancer is a highly heterogeneous disease and is categorised into subtypes based on morphological features. The World Health Organisation have reported 18 different histological subtypes of invasive breast cancer [40]. These can fall into two main categories. Those which exhibit unique and easily identifiable morphological features are known as “special type” and include invasive lobular, mucinous, tubular and medullary carcinomas. Those which do not show any classical morphological features and which vary considerably from case-to-case are known as “no special type” and comprise infiltrating ductal carcinomas of no special type (IDC-NST). It is the IDC-NST group of breast tumours that are the most common form of breast cancer and have received the most research interest to date.

Although these morphologic features correlate with patient prognosis [41], classification of breast cancers in this way have been shown to be poorly reproducible with limited clinical value by the National Health Service breast cancer screening programme (UK). Breast cancers are therefore further classified based on their differentiation and mitotic activity. The current classification system used in the UK is derived from work by Page, Elston and Ellis [42] and is based on three parameters. These assess tubular/acinar/glandular formation, nuclear

pleomorphism and number of mitotic bodies. Each of these is scored from one to three, a summary of how these scores are assigned are summarised below in Table 1.1.

Score	Tubule/Acinar Formation	Nuclear Pleomorphism	Mitotic Index (example field diameter of 0.6mm)
1	>75% of tumour exhibit tubular or acinar structures	Small nuclei, little variation in size, uniform chromatin	≤10 mitotic bodies per field of view
2	10-75% of tumour exhibit tubular or acinar structures	Open vesicular nuclei, visible nucleoli, variable size and shape	11-20 mitotic bodies per field of view
3	<10% of tumour exhibit tubular or acinar structures	Vesicular nuclei, marked variation in size and shape, large bizarre forms	≥22 mitotic bodies per field of view

Table 1.1 Summary of how scores are assigned to the grading parameters outlined by the National Health Service breast cancer screening programme for breast tumours

The scores for tubule formation, nuclear pleomorphism and mitotic index are then added together to obtain a total score and overall grade of the tumour as outlined below:

- Total score of 3-5 = Grade 1 tumour (low grade)
- Total score of 6-7 = Grade 2 tumour (intermediate grade)
- Total score of 8-9 = Grade 3 tumour (high grade)

In addition to the morphologic features discussed, heterogeneity has also been demonstrated at a molecular level. The earliest of these studies by Perou et al in 2000 [43] and Sorlie et al in 2001 [44] identified five main subtypes of IDC-NST based on their gene expression profiles (Table 1.2). These subtypes are defined by the expression of the receptors HER2, ER and PR. Sorlie et al [44] found that patient outcome significantly correlated with the expression patterns of these receptors with Basal and HER2 cancers associated with shortest patient survival and Luminal A and B the longest survival time. This classification has enabled more efficient pathological diagnosis of breast cancers and is still used to date.

Tumour Subtype	Receptor Expression	Tumour Characteristics	Targeted Therapies
Luminal A	HER2-, ER+ & PR+/-	Low grade, non-aggressive	Hormone therapy
Luminal B	HER2+, ER+ & PR+/-	Low grade, non-aggressive (worse than Luminal A)	Hormone therapy and Trastuzumab
Basal	HER2 –, ER- & PR-	High grade, aggressive	None
HER2	HER2+, ER- & PR-	High grade, aggressive	Trastuzumab
Normal	Variable- High expression of basal and adipose markers, low expression of luminal markers	Variable	None

Table 1.2 Summary of the Perou classification of IDC-NST based on their receptor expression profiles and their correlation with grade and treatment

Abbreviations: Positive (+), negative (-)

Recently this heterogeneity has been recognised further with breast cancer now classified into at least 10 molecular subtypes [45]. Though this heterogeneity is observed in the epithelial component of breast cancers with the majority of breast cancers arising in the luminal epithelium, it is becoming increasingly apparent that the surrounding stroma may contribute to this [46].

1.3 Role of the stroma in breast cancer

As early as 1975, DeCosse et al demonstrated that an embryonic tissue microenvironment had the capacity to cause differentiation of murine mammary carcinomas [47]. The role of the tumour stroma has since become a major focus for breast cancer research. This saw the advent of several *in vitro* studies highlighting the role of stromal cells in the enhancement of tumour growth and invasion [48, 49]. Conversely, the ability of the normal breast stroma to induce malignant cells to take on a non-neoplastic phenotype [50] as well as direct cells from foreign organs into a mammary epithelial fate [51, 52], has also been reported.

Studies using human tissue have reinforced this concept. In 2008, Finak et al identified that the surrounding stroma from different breast cancer specimens had different gene expression signatures and proved to be a powerful predictor of patient outcome [53]. In addition, the expression of ECM related genes has also been linked to patient survival [46].

Multiple changes in the stroma have been identified and proven to facilitate tumour progression. These include: changes in collagen density and mechanical tension [54, 55], altered levels of ECM proteins associated with wound healing such as collagens, proteoglycans and glycosaminoglycans [33], changes in proteolytic enzymes such as matrix metalloproteinases (MMPs) [56, 57] and genetic changes such as loss of heterozygosity [58] and somatic mutations [59] exclusive to the stromal component. Although these indicate a clear role for the stroma in the progression of breast cancer, these have largely studied the stroma as a whole with the roles of each cell type remaining unclear. However, of central importance is the role of the fibroblasts which is the main component of the tumour stroma. The epithelial cell to fibroblast ratio in normal breast has been estimated at between 2:1 and 3:1 [60] whereas this is altered in breast tumour stroma with an epithelial cell to fibroblast ratio of up to 1:5 reported [61, 62].

1.3.1 Fibroblasts and breast cancer

Many of the changes mentioned above are due to the actions of activated fibroblasts within the tumour stroma known as carcinoma associated fibroblasts (CAFs). There are multiple theories as to the origin of CAFs. These are that resident fibroblasts are activated by paracrine signalling from tumour cells, that mesenchymal stem cells are recruited to the tumour stroma and differentiate into fibroblasts [63], or that adipocytes revert to a fibroblast-like phenotype in response to paracrine signalling from tumour cells [64]. It is possible that CAFs originate from a combination of these sources and may be dependent on the subtype of breast tumour.

CAFs are a heterogeneous population of cells. A subset of CAFs expressing α-SMA akin to fibroblasts associated with wound healing [65] are known as myofibroblasts. Other sub-populations of CAFs include those that express fibroblast activation protein, Thy-1 and Desmin [66]. Significant expression differences have also been reported in CAFs derived from different breast tumour subtypes [67].

It is now well documented that CAFs promote tumour progression. It is widely accepted that CAFs mainly exert this influence through secretion of a variety of tumour promoting factors which either promote epithelial-mesenchymal transition (EMT) of tumour epithelial cells or induce increased vascularisation of tumours. These include hepatocyte growth factor (HGF) [68], transforming growth factor receptor-β (TGFβ) and stromal cell derived factor-1 (SDF-1) [69]. In addition to CAF influence via paracrine signalling, CAFs also have the capacity to induce the changes to the ECM of tumours mentioned in section 1.3 above through production of ECM proteins, remodelling collagen fibrils and release of MMPs.

1.3.2 The importance of myoepithelial cells in breast cancer

One key feature of progression from the non-obligatory benign precursor lesion ductal carcinoma in situ (DCIS, discussed in section 1.4.2) to invasive cancer is the loss of the myoepithelial cell layer. This has indicated that myoepithelial cells may play a tumour

suppressor role. Both *in vitro* and *in vivo* studies have demonstrated that myoepithelial cells have the capacity to inhibit tumour growth. Hu et al showed that co-injection of myoepithelial cells with MCFDCIS.com cells in a xenograft mouse model suppressed the transition of DCIS lesions to invasive carcinoma [70]. One of the hallmarks of breast cancer progression is the loss of normal tissue architecture and polarity. Myoepithelial cells are proven to maintain normal luminal epithelial polarisation and architecture and do so via production of laminin [17, 71]. In addition to their effects on cell arrangement, myoepithelial cells express a number of tumour suppressor proteins such as maspin, structural ECM proteins such as fibronectin, proteinase inhibitors such as tissue inhibitor of metalloproteinase-1 (TIMP1) and angiogenic inhibitors such as thrombospondin-1 [72, 73]. The result of this is to counteract the tumour promoting effects of the surrounding stroma, to build ECM rather than degrade it and thus have a "containment" effect on malignant cells within ducts. Myoepithelial cells derived from DCIS containing breast tissue have an impaired ability to polarise luminal epithelial cells [71] and differ in their gene expression pattern [74]. It is clear from these studies that myoepithelial cells are a vitally important component in the prevention of tumour invasion. Surprisingly, these cells are largely understudied and the mechanisms leading to obliteration of the myoepithelial cell layer during invasion is unknown.

1.4 Benign breast disease

The vast majority of lesions that arise in the breast are benign. The term benign breast disease encompasses a heterogeneous group of lesions which exhibit unique morphological features. The most frequent subgroup of benign lesions is termed fibrocystic changes (FCCs). These are detected in nearly all of the female breast reduction mammoplasty samples examined [personal communication, Prof Andrew Hanby, Leeds Institute of Cancer and Pathology] with the majority not incurring increased risk of breast cancer. There are a variety of subtypes of FCCs. Historically, these have been categorised as non-proliferative lesions, proliferative lesions without atypia and proliferative lesions with atypia [75]. For the purpose of this thesis, only proliferative benign lesions will be discussed.

The most common proliferative benign lesions of the breast occur in the epithelium. The use of terminology such as “hyperplasia” clouds the understanding of the biology of these lesions. For example, usual ductal hyperplasia consists of a polyclonal benign proliferation of cells which are not neoplastic while lobular hyperplasia represents a monoclonal neoplastic proliferation. For purpose of discussion here, proliferative benign lesions will therefore be categorised into non-neoplastic and neoplastic for clarification. Example images of these lesions can be found in Fig 1.3.

1.4.1 Non-neoplastic benign lesions

Usual Type Ductal Hyperplasia

As discussed, in the normal breast, ducts are lined by a single layer of secretory luminal epithelium surrounded by a contractile layer of myoepithelium. Historically, epithelial hyperplasia has been defined as an increase in number of cells within the ductal space. Aberrant proliferation of the luminal epithelium (usually in response to environmental cues such as systemic hormones) can occur resulting in lumen filling within the ducts. When these proliferating cells do not induce distortion of architecture of the ductal space, these are

denoted usual ductal hyperplasia (UDH). These can be graded as mild whereby the luminal cell layer is three to four cells thick, moderate if the layer is more than four cells thick or florid if the lumen is considerably distended or obliterated. Historic works have implied a neoplastic character to these lesions; however, there is little evidence to confirm this. Typically, immunohistochemistry for cytokeratin markers will show a mixture of cells with both luminal and myoepithelial phenotype [76]. This is uncharacteristic of "true" neoplasia which consists of a uniform cell population. Cytogenetic analysis of these lesions have demonstrated abnormalities such as loss of heterozygosity and chromosomal alterations such as losses at 1p, 16p, 17q and 22q as well as amplification in 20q [77-79], some of which are also conserved in atypical ductal hyperplasia (ADH) [80]. However, these genomic alterations are usually rare and randomly distributed.

Columnar cell lesions

Columnar cell lesions are characterised by dilation of the acini of TDLUs lined by columnar epithelial cells. These can be divided into two broad subgroups: columnar cell change which is non-neoplastic and columnar cell hyperplasia which are neoplastic (discussed in section 1.4.2). Both these subgroups are further classified by the presence or absence of cytological atypia [81]. Lesions classified as columnar cell change feature one or two layers of columnar epithelial cells with ovoid nuclei orientated perpendicular to the acini basement membrane. These cells may feature "snouts" and lesions sometimes feature calcification [82]. Unlike UDH, cells of columnar cell change are predominantly luminal in phenotype, are ER and PR positive but negative for myoepithelial cytokeratins and HER2 [76]. Albeit with a limited sample size, in 2006, Dabbs et al demonstrated that columnar cell change lesions show no loss of heterozygosity [83]. Patients with columnar cell change lesions are considered to have a low risk of developing breast cancer and it is generally recommended that patients with these lesions require no clinical intervention [84].

1.4.2 Neoplastic benign lesions

Flat Epithelial Atypia

Flat epithelial atypia (FEA) are a type of columnar cell hyperplasia that exhibit cytological atypia. These generally consist of more than two layers of columnar epithelial cells and unlike columnar cell change lesions, lining epithelia have an increased nuclear-cytoplasmic ratio with round nuclei not orientated perpendicular to the basement membrane [85]. These may form small micropapillae and commonly form snouts with luminal secretions and calcification. Like columnar cell change lesions, FEA lesions have luminal characteristics, express ER and PR and do not feature cells with a myoepithelial phenotype or that express HER2 [81]. These commonly feature a loss of heterozygosity at chromosomes 16q, 17p and X and gains on 15q, 16p and 19 [58, 76]. FEA lesions are reported to be associated with only a slight increase in risk of developing breast cancer [86] and thus their clinical management is still under intense debate.

Atypical ductal hyperplasia

Unlike UDH, atypical ductal hyperplasia (ADH) usually features a uniform population of luminal type proliferative cells [87, 88]. Like FEA, these are usually ER positive, negative for myoepithelial markers and tend to only occupy small ducts of <2mm [89]. Women who have ADH are four to five times more likely to develop breast cancer and usually do so 10 to 15 years post diagnosis [90]. This risk is one-two times for UDH [91]. In 2008, Xu et al demonstrated that ADH lesions feature up to five times more chromosomal alterations than UDH [92]. These share many of the chromosomal alterations with FEA with loss of 16q being the most characteristic and most reported alteration [76, 78]. Chromosome 16q contains the E-cadherin gene CDH1 [93] but does not always correlate with a loss of E-cadherin protein expression [94].

Ductal carcinoma in situ

Ductal carcinoma *in situ* (DCIS) is defined as the proliferation of cells with features of malignancy with no evidence of basement membrane penetration [95]. Like ADH, proliferation of cells occurs within lumen of ducts and acini and results in the loss of a hollow lumen and distortion in duct and acini architecture. The morphological differences between ADH and some cases of DCIS are subtle and are often only distinguished by the size of the lesion.

DCIS can be categorized into seven groups based on their morphologic features: cribriform (malignant cells oriented to leave a glandular lumen), papillary (malignant cells form large papillations into luminal space), micropapillary (malignant cells form smaller finger-like protrusions into luminal space) and solid (malignant cells fill the ductal space), apocrine (consist of large cells with abundant eosinophilic cytoplasm and large nuclei), flat and other. In the UK, these are further classified as high, intermediate or low grade based on cytonuclear features and the presence of comedo necrosis. High grade DCIS feature highly mitotic cells with large irregularly spaced pleomorphic nuclei cells and often contain areas of necrosis and calcification. Low grade DCIS are much more similar to ADH featuring uniform small and rounded cells with small nuclei, few mitoses with little necrosis. Intermediate grade DCIS show moderate pleomorphism of nuclei which are larger than in low grade DCIS with a high nuclear to cytoplasmic ratio [96].

Examination of biologic features can distinguish DCIS from other benign breast lesions. These include chromosomal imbalances with loss of heterozygosity reported in more than 70% of high grade DCIS cases as opposed to 42% in ADH [78]. The presence of molecular markers such as HER2 also differentiates DCIS from ADH. Overexpression of the HER2 protein has been identified in up to 50% of DCIS cases [97] with no evidence of overexpression in cases of ADH [98]. Diagnosis of DCIS confers a strong risk of developing breast cancer in the future. Retrospective studies have shown that 30% of DCIS lesions will progress to breast cancer [99,

100]. Current thinking is that cells within DCIS lesions acquire further genetic abnormalities conducive to cell migration and invasion such as loss of E-cadherin [101]. These become capable of penetrating through the basement membrane and invading into the surrounding stroma. This process is aided by proteinases such as MMPs [102] and is associated with a loss of the myoepithelial cell layer [13]. This theory is supported by the fact that greater than 95% of breast cancers are of luminal epithelial origin. In addition, DCIS lesions have been demonstrated to exhibit some of the heterogeneity of IDC and can often be categorised into the Perou subtypes of breast cancer discussed in section 1.2.2.

Lobular Lesions

Unlike ductal lesions, lobular epithelial lesions are less heterogeneous exhibiting a similar morphology and are collectively termed lobular neoplasia. Like ductal hyperplasia, epithelial cells proliferate uncontrollably to fill luminal spaces but do so in the acini of the lobules. In 1941, Foote and Stewart defined lobular neoplasia as a monomorphic population of cells that arise from and expand the TDLU and spread through the ductal system [103]. Lobular neoplasia can be subdivided into atypical lobular hyperplasia (ALH) and lobular carcinoma *in situ* (LCIS) (see Fig 1.3 for examples). These have very subtle differences and are generally only distinguished by the extent of epithelial cell proliferation and distension of the lobular unit. When less than one half of the acini of a given lobule are affected, the term ALH is used. When more than half are affected, this is classed as LCIS. The cells within these lesions as mentioned are uniform, usually small and round and have a high nuclear-cytoplasmic ratio. They may also contain clear vacuoles [104]. The risk of developing breast cancer differs with these lesions as women with ALH are four to five times more likely to develop breast cancer whereas this increases to eight to ten times more likely with LCIS [105].

Non-neoplastic benign breast lesions

Neoplastic benign breast lesions

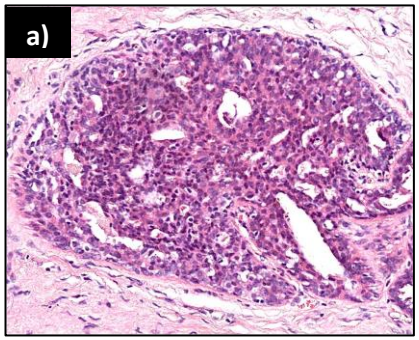

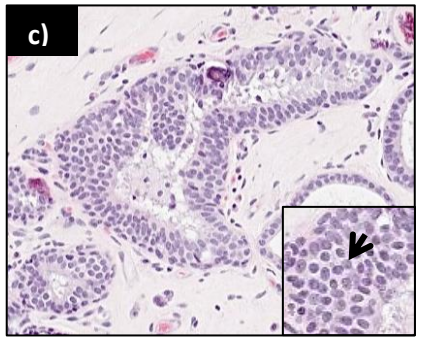

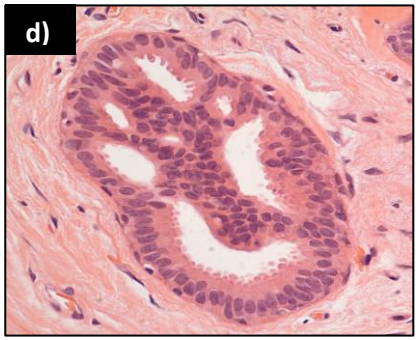

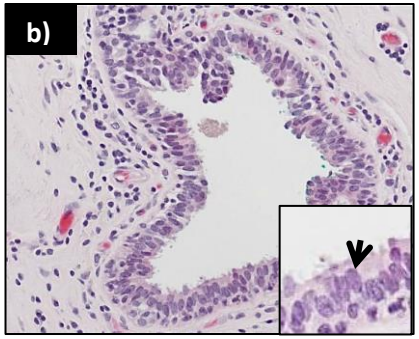

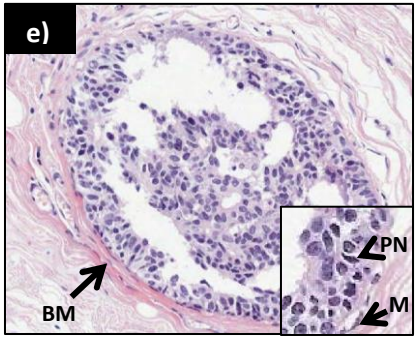

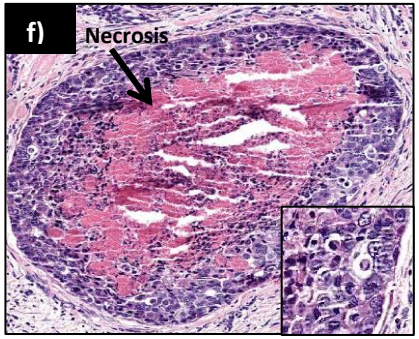

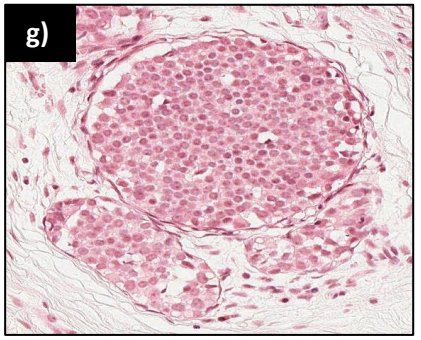

Fig 1.3 Histology of benign lesions of the breast

Example images of H & E stained breast tissue specimens containing benign lesions.

(a-b) Non-neoplastic benign lesions include usual ductal hyperplasia and columnar cell change. Usual ductal hyperplasia lesions (UDH, a) consist of lumens filled with small rounded cells. Non-neoplastic columnar cell change lesions feature two layers of columnar shaped epithelial cells with ovoid nuclei orientated perpendicular to the basement membrane (arrow, b).

(c-g) Neoplastic benign lesions include flat epithelial atypia, atypical ductal hyperplasia and DCIS. Flat epithelial atypia lesions feature multiple layers of epithelial cells with rounded nuclei not perpendicular to the basement membrane (arrow, c). Atypical ductal hyperplasia lesions contain uniform populations of proliferative epithelial cells (d). Example of an intermediate grade cribriform ductal carcinoma in situ (DCIS) lesion without comedo necrosis which feature multiple layers of epithelial cells with pleomorphic nuclei (PN, e) surrounded by spindle-shaped myoepithelial cells (M, e) and an intact basement membrane (BM, e). Example of a high grade solid pattern DCIS lesion with comedo necrosis which feature pink necrotic material (necrosis, f) and multiple layers of epithelial cells which are large, irregularly spaced and highly pleomorphic (inset, f). Lobular carcinoma in situ lesions consist of small rounded epithelial cells with a high nuclear-cytoplasmic ratio (g).

Images courtesy of Prof Andrew Hanby (Leeds Institute of Cancer and Pathology)

1.5 Evolution of breast cancer from preinvasive lesions

Histological and epidemiological evidence over the last century has resulted in the proposal of a linear model of breast cancer progression. This is that an initiating event occurs in the luminal epithelium of normal breast and results in FEA. This therefore proposes that FEA is the earliest stage of preinvasive ductal carcinoma. A growth advantage of the cells of FEA is then thought to result in the development of ADH which then spreads and is classified as DCIS. When these cells gain the ability to breach the basement membrane, this gives rise to IDC [106]. Genomic and transcriptomic analysis of benign breast lesions largely support this hypothesis but have also proposed that this may be specific to the progression of low grade IDC. It is now thought that low grade IDC and high grade IDC have distinct pathways of progression which has led to the categorisation of low grade neoplasia and high grade neoplasia families.

FEA, ADH and DCIS have been reported to occur in the same breast [107]. This has indicated that these lesions are related and may represent an evolutionary continuum. This is supported by the fact that FEA, ADH and low grade DCIS all have overlapping morphological and immunohistochemical features [108, 109]. All these lesions share an ER positive, PR positive and HER2 negative profile [110, 111]. Perhaps the most striking evidence for the existence of a low grade neoplasia "family" has been gained through genomic and transcriptomic analysis. All these lesions have shared genomic alterations, the most frequently reported of which are a gain in 16p and 17q and a loss in 16q and 17p [58, 76, 83]. These alterations have been shown to correlate with low grade IDC and coupled with the ER/PR/HER2 profile suggest that FEA, ADH and low grade DCIS are precursor lesions for low grade luminal IDC [43, 76].

Until recently, it was thought that there was no precursor lesion to high grade DCIS. However, it is now proposed that microglandular adenosis (MGA) may be a precursor to high grade DCIS and IDC. These lesions often occur in association with IDC [112, 113]. The vast majority of

these lesions are ER, PR and HER2 negative [114] and share genetic aberrations with high grade DCIS and IDC such as loss of 17q [115, 116]. High grade DCIS and IDC possess uniquely different gene expression patterns to the low grade neoplasia family. These profiles are associated with mitotic activity and are generally ER and PR negative and may be HER2 positive or negative [76, 109]. Chromosomal alterations of high grade DCIS and IDC also differ from the low grade neoplasia family with gains in 8q and 17q and loss of 13p reported [77].

Regardless of the specific pathway, the concept that DCIS is a non-obligatory precursor for IDC is widely accepted. Nearly all breast cancers are accompanied by DCIS [117] and progression of DCIS to IDC has been demonstrated in mouse models [118].

A summary of the low grade and high grade pathways to IDC is provided in Fig 1.4

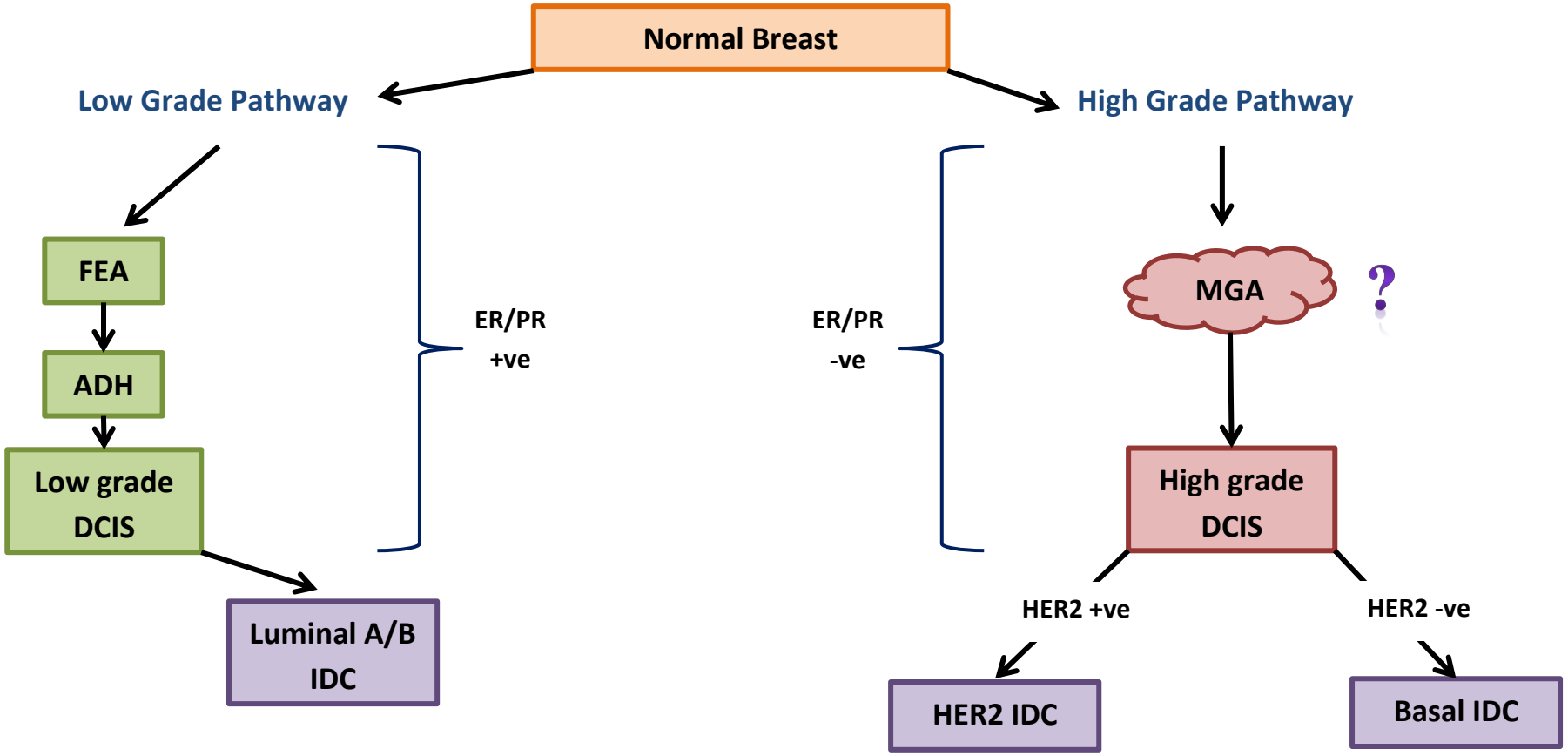

Fig 1.4 Summary schematic of the proposed low grade and high grade pathways to breast cancer

Low grade pathway involves a linear progression through the benign breast lesions flat epithelial atypia (FEA), atypical ductal hyperplasia (ADH), low grade DCIS and results in luminal type invasive ductal carcinoma (IDC). These are estrogen receptor (ER) and progesterone receptor (PR) positive (+ve). The high grade pathway may initiate with microglandular adenosis (MGA) leading to high grade DCIS which if are human epidermal growth factor receptor 2 (HER2) positive leads to HER2 IDC but if are HER2 negative (-ve) leads to basal IDC. These are ER and PR negative.

1.6 Cell of origin of breast cancer

The origin of aberrant epithelium in all these conditions is still under debate. Two theories have been suggested. These are the sporadic clonal evolution model and the cancer stem cell model.

The sporadic clonal evolution model proposes that any epithelial cell can acquire genetic mutations and those which confer a growth advantage are selected over time and contribute to tumour progression [119]. Since epithelia of normal breast are known to harbour genetic changes also, it is plausible that a random combination of these may sporadically induce aberrant proliferation and tumorigenesis [120, 121].

The cancer stem cell model proposes that the self-renewal properties of stem cells and their propensity to remain in the tissue for long periods of time means that they are more likely to accumulate genetic and epigenetic modifications [122, 123]. It is thought that these cells undergo asymmetric division to both self-renew and produce progenitor cells that give rise to different breast cancer subtypes [124, 125]. An alternative hypothesis is that it is the progenitor cells that are the cell of origin for certain subtypes of breast cancer. Luminal progenitors have been shown to have a similar genetic signature to HER2 and BRCA1 basal breast tumours [126-128]. In this scenario, it is thought that the mature differentiated luminal epithelia give rise to the less aggressive luminal subtypes of breast tumours.

1.7 Preclinical *in vitro* models of breast cancer

The highly heterogeneous nature of breast cancer poses a challenge to researchers when attempting to model it in the laboratory, with one single experimental system unlikely to be able to recapitulate this. As a result, a variety of models are used to fully dissect the complex signalling pathways involved in breast cancer initiation and metastasis. One of the biggest challenges researchers face is finding a relevant model that allows manipulation of genes and proteins in a controlled laboratory environment while accurately reflecting the characteristic

features of human breast tissue and tumours. Numerous models have been developed which have aided our understanding of breast disease progression. These range from simple cell lines grown in two dimensions used to aid discovery of cell signalling pathways, to complex *in vivo* systems, typically mouse, used for validation of drug response and metastasis studies. With the amount of different models available for breast cancer research increasing (each with their own advantages and disadvantages), choosing the right model to address specific biological questions becomes increasingly complex. For the purpose of this thesis, only *in vitro* models will be discussed. However, it is recognised that *in vivo* mouse models play an integral role in breast cancer research. A summary of their suitability to different areas of breast cancer research can be found in our published review book chapter of pre-clinical models of breast cancer [129].

1.7.1 Two dimensional (2D) *in vitro* models

The simplest and most commonly used method of investigating breast cancer biology is the use of cell lines grown *in vitro* in 2D on tissue culture plastic. Several different cell lines representing the molecular subtypes of breast cancer defined by Perou et al [43] are available, a selection of which are summarized in Table 1.3. Cell lines representative of DCIS include SUM225 [130] and MCF10DCIS.com [131] have enabled studies of early breast lesions. In addition, advances have been made in the isolation of breast cancer stem cells offering researchers good models to understand stem cell biology [Reviewed in 132]. It is yet to be established whether existing breast cancer cell lines can represent the heterogeneity of breast cancer highlighted by Curtis et al [45]. Cell lines have many advantages in that they are readily available, easy to propagate and are amenable to genetic manipulation. Further details on their biology and provenance can be found in some excellent reviews [Reviewed in 133, 134, 135]. However, it is increasingly acknowledged that a major problem with 2D culture is a loss of polarity and the lack of extracellular cues known to regulate breast tissue architecture *in vivo* [136]. While convenient, 2D culture cannot recapitulate *in vivo* conditions. Cells are highly

sensitive to their environment and even defining the appropriate culture media to retain their *in vivo* phenotype remains a challenge. For this reason, more sophisticated systems are required to assess cell behaviour that take into account the surrounding cell microenvironment.

Cell Line	Biomarker Expression	Representative Breast Cancer Sub-group
MCF-7	ER+,HER2-, $ki67^{Lo}$	Luminal A
ZR-75	ER+,HER2+, $ki67^{Hi}$	Luminal B
MDA-MB-468	ER-,PR-, HER2-, $ki67^{Hi}$	Basal
SKBR3	ER-,PR, HER2+, $ki67^{Hi}$	HER2
MDA-MB-231	ER-,PR-, HER2-, $ki67^{Lo}$, $Claudin^{Lo}$, $E\text{-}Cadherin^{Lo}$	Claudin-low

Table 1.3 Examples of breast cancer cell lines and their molecular classification

Abbreviations: positive (+), negative (-), high expression (Hi) and low expression (Lo)

1.7.2 Three dimensional (3D) *in vitro* models

As discussed, the cell microenvironment plays a pivotal role in maintaining epithelial cell morphology and phenotype. This has led to a move towards developing methods of culturing cells in 3D. For several decades, a simple approach has been taken whereby single cell types have been cultured in 3D but have proven remarkably similar to aspects of differentiated tissues [137, 138]. The simplest form of 3D *in vitro* model developed takes advantage of the fact that many cell types have the propensity to aggregate together. This can be achieved through various methods including rotary cell culture [139] and hanging drop cell culture [140] and typically results in cell spheroids. These can be mono- or multicellular depending on the research question. Typically, these are used for modelling growth and invasion of solid tumours [141, 142]. These are advantageous in that they are easily applied to high-throughput screens [143] and are thus valuable for anti-cancer drug screening and testing [144]. The use of

spheroids has also revolutionised research into mammary stem cell biology which are easily analysable and quantifiable [145-147]. However, spheroid cultures lacks influence from the surrounding ECM and may not accurately reflect tissue *in vivo*.

Alternatively, cells can be cultured in 3D in the presence of an *in vivo*-like ECM. Two methods are commonly used to generate 3D acini-like structures. The "embedding" technique involves completely embedding epithelial cells in an ECM. Epithelial cells are pre-aggregated through centrifugation or rotary culture and then suspended in liquid ECM solution and then gels left to set or, single cells can be suspended in the ECM solution before setting permitting organisation of the cells in 3D matrix. Once embedded, gels are layered with culture media and can either be left fixed to the bottom of the cell culture plastic, or, be freed and allowed to float in culture media [148] or suspended using Transwell® inserts [149]. Another commonly used method is the "overlay" technique whereby cells are seeded onto a bed of ECM gel and may be layered with culture media with diluted ECM [150]. The types of ECM material available and the choice of cells to include in models such as these will be discussed in Chapter 3.

There are several advantages to culturing cells in a 3D ECM. A comprehensive study by Kenny et al [151] demonstrated that the culture of different breast tumour cell lines in ECM to some extent mimicked the heterogeneity of breast cancers *in vivo*. The phenotypes of these cultures even correlated with the different sub-groups of breast cancer highlighted in Table 1.2. Mammary luminal epithelial cells respond to ECM by forming acini-like structures [152] which resemble *in vivo* breast. Changes in polarisation and disruption of these acini-like structures are factors that can be used to distinguish between non-transformed and transformed cells which are not apparent in 2D [153, 154]. The use of 3D *in vitro* cultures enables the researcher to tightly control the condition of the surrounding microenvironment and tailor the cultures to address specific hypotheses. By culturing tumour cells with specific ECM constituents, *in vivo* cell-cell and cell-ECM interactions can be represented in the laboratory [155]. Such studies

have shed light on the various cell surface molecules important for cell-ECM interactions such as Tetraspanin CD151 [156] and α6, β1- and β4-Integrins [50]. Another benefit of culturing cells in 3D ECM is the ability to study cell migration and locomotion in a physiologically relevant context. 3D *in vitro* cultures in ECM have helped elucidate novel mechanisms of cell migration such as collective cell migration [157] with ECM proving to control motile properties of cells [158]. These have also facilitated the discovery of key cell surface signalling proteins important for cell invasion. These include desmosomal cadherins, e-cadherin and carcinoembryonic antigen-related cell adhesion molecule 1 [17]. These interactions can be studied in conjunction with intracellular signalling pathways to better our understanding of the link between extracellular environment and cell transformation. Signalling molecules such as PI3K and PTEN have been studied in this manner [159]. What's more, like 2D cultures, 3D *in vitro* cultures are amenable to genetic manipulation. These have identified novel mechanisms of action for various tumour suppressors and oncogenes. Examples include the tumour suppressors NM23-H1 [160, 161], retinoblastoma [162], AZU-1 [163] and dystroglycan [164] and oncogenes such as HER2 [165]. 3D cultures also have the potential for genetic manipulation via RNAi techniques facilitating further study of complex signalling pathways. New technologies being developed are also providing platforms to study processes such as breast cancer metastasis in a complex 3D *in vitro* tri-culture context through the use of microfluidics [166]. The resemblance of 3D *in vitro* cultures to mammary acini morphology and biology provides new opportunities to study cancer initiation mechanisms which may not have been possible with 2D cultures. The establishment of culture systems that accurately resemble disease-free breast tissue architecture hold the key to investigating the subtle changes that occur during the early stages of tumorigenesis. This is a field that is largely unexplored but has recently been recognised internationally by panel of expert breast cancer scientists and healthcare professionals to be of great importance to our understanding of breast cancer

progression and the development of preventative treatments [167]. The current disease-free 3D *in vitro* models available will be further discussed in Chapter 3.

Potential disadvantages of 3D cultures include difficulty in tracking different cell populations in models consisting of multiple cell types. Labelling individual cell types with tracker dyes prior to incorporation into 3D culture allows cells to be tracked, but many of the cell tracker reagents available for this purpose are only stable for relatively short periods of time [149]. For longer term experiments, this can be overcome by stable transduction with proteins such as Enhanced Green Fluorescent Protein. However, this aside, including just one or two cell types still does not account for influences imposed by adipose cells, immune infiltrates and cues from vascular endothelium which exists *in vivo*.

One of the biggest challenges with the use of 3D *in vitro* cultures is the subsequent analysis and quantification of observations. Biochemical analysis is problematic due to difficulties in separating cells from the surrounding ECM [168]. Imaging of these cultures requires specialised and often not readily available equipment due to the necessity of an excellent signal to noise ratio, optical sectioning ability, good spatial resolution and ample penetration of thick specimens [169]. In addition, collagen ECM causes considerably background fluorescence making visualisation of collagen based cultures even more challenging [170]. This can be overcome by the use of multiphoton microscopy [171] or optical coherence/projection tomography [172, 173] but can be both expensive and time consuming. However, recent technological advances have been made and have proven that 3D co-culture models can not only be cultured for long periods of time (up to 23 days) but can also be imaged in real time to observe cell to cell interactions [174].

The obvious limitation of all 3D *in vitro* models is the lack of a complex *in vivo* system complete with blood supply, immune infiltrates and regulation by hormonal cues. This limits these

models to the study of cell interactions and signalling pathways. In order to study tumour progression and metastasis, animal models are required.

1.7.3 *Ex vivo* culture

An alternative *in vitro* approach developed more recently employs small fragments of breast tumours embedded in collagen I and grown in 3D [175]. This has allowed tamoxifen-sensitivity to be determined [176] suggesting that the model could prove valuable in assessing drug responses of individual patients. Allied to this is the tissue slice model [177], in which we have shown that 250µm tissue slices can be maintained in a viable native state for up to seven days post-surgery [178]. The ability to culture intact human tissue as outlined in these two models could provide an opportunity to validate new drugs on human tissue with fewer ethical implications which are associated with animal models. One could foresee the benefits of pre-testing patient samples with a range of drug therapies via *ex vivo* culture enabling a more accurate and individual treatment regime to be developed. Models such as these could improve current 3D models and start to bridge the gap between laboratory research and clinical practice.

1.7.4 Summary of pre-clinical *in vitro* models of breast cancer

Due to the complexity and heterogeneity of breast cancer there is no single model that can fully recapitulate all aspects of the breast microenvironment. Given this diversity, it is likely that not only different models will be required to simulate breast tumours, but that multiple different cell types with a variety of genetic aberrations will need to be included. While cell lines grown in 2D have contributed much to our understanding of breast cancer biology, it is now clear that 3D systems are more biologically relevant. However there is still a need to refine current 3D *in vitro* models to encompass multiple components of the breast microenvironment. 3D *in vitro* models of normal breast in particular are limited and often omit key functional cell types of normal breast. This will be discussed further in Chapter 3.

Hypothesis & Aims

A three-dimensional *in vitro* model of normal breast can be achieved in the laboratory that includes three of the major functional cell types of breast in a physiologically relevant matrix and accurately reflects the morphology and phenotype of normal human *in vivo* breast tissue. Such a model could be used as a tool to study breast cancer initiation.

Specific aims were to:

- Optimise a three dimensional *in vitro* breast culture system that contained normal luminal epithelial cells, myoepithelial cells and fibroblast cell lines in the physiologically relevant matrix collagen I
- Validate the model by comparing morphology and phenotype to a human breast reduction mammoplasty specimen
- Prove that the model was amenable to cancer initiation studies by genetic engineering in both the luminal epithelium and the stromal components

2 Chapter 2: Materials and Methods

This chapter details methods used throughout this project that are common to all or more than one results chapter. Chapter specific methods can be found in the corresponding chapter.

2.1 Cell Culture

A list of all the cell types used throughout this project, where they were obtained, appropriate references (if applicable) and how they were maintained and passaged are summarised in Table 2.1. All cells were maintained at 37^{o}C in humidified incubators and 95% air and 5% CO_2 and passaged when 70-80% confluent. All cells were cultured using vented cap cell culture flasks (Corning). Multiple cryovials (Nuncbrand) of cells at earliest possible passage were frozen down as stocks in liquid nitrogen. These were frozen in 90% heat inactivated foetal calf serum (HI-FCS) with added 10% dimethyl sulphoxide (Sigma). Cells that were cultured beyond 20 passages from their first use were discarded and replaced with a new stock vial. All cells were regularly tested for mycoplasma infection (Lonza mycoplasma test kit) and no cells used in this project tested positive. With the exception of fibroblasts isolated in house, all cell types used were Short Tandem Repeat (STR) profiled courtesy of the in house Genomics facility (Leeds Institutes of Molecular Medicine) to confirm identity of cell lines used and no cellular cross-contamination was detected. Phase contrast images were taken using an Olympus CKK41 microscope with an Olympus Camedia C-7070 camera attached. Details of the microscope used to take fluorescent images will be provided in appropriate results chapters.

Cell Type	Source and reference	Medium Used	Passage Protocol
HB2	ECACC (Cat No. 10081201) Ref: [179]	DMEM+GlutaMAX™ I (Invitrogen) + 10% HI-FCS + 10µg/mL Insulin + 5µg/mL Hydrocortisone	Cells washed with DPBS (Invitrogen), 0.1% EDTA in DPBS added for 5 mins. 0.5% Trypsin/EDTA (Invitrogen) added for ~2mins and cells resuspended in medium. Cells were centrifuged at 290 x g for 3 mins, pellet resuspended in medium and replated at a 1:25 dilution
HER2 and HER3 overexpressing HB2 cells	Gift of Dr Fedor Berditchevsky (University of Birmingham) Unpublished.	As per HB2	As per HB2
Myo1089	Gift of Prof Mike O'Hare (Ludwig Institute, London) Ref: [149]	Nutrient Mixture HAM F-12 (Sigma) + 10% HI-FCS + 5µg/mL Hydrocortisone + 10µg/mL Insulin + 10ng/mL Epidermal Growth Factor	As per HB2. Cells replated at 1:10 dilution. Regularly purified using β4-Integrin coated Dynabeads (see section 2.2)
GFP Myo1089 & dsRed Myo1089	Generated in house from Myo1089 (see Chapter 3)	As per Myo1089	As per Myo1089
MCF10A	ATCC (Cat No. CRL 10317) Ref: [180]	Advanced DMEM F12 (Invitrogen) + 5% Horse Serum + 5µg/mL Hydrocortisone + 10µg/mL Insulin + 10ng/mL Epidermal Growth Factor + 50µg/mL Cholera Toxin	As per HB2. Cells replated at 1:4 dilution.
HMFU19	Gift of Prof Mike O'Hare (Ludwig Institute, London) Ref: [181]	DMEM+GlutaMAX™ I (Invitrogen) + 10% HI-FCS	Cells washed with DPBS, 0.5% Trypsin/EDTA added for ~2mins and cells resuspended in medium. Cells were centrifuged at 290 x g for 3 mins, pellet resuspended in medium and replated at a 1:10 dilution
SkBr3	ATCC (Cat No. HTB-30) Ref: [182]	As per HMFU19	As per HMFU19. Cells replated at a 1:3 dilution
Primary and hTERT fibroblasts	Isolated in house (see Chapter 3)	As per HMFU19	As per HMFU19. Cells replated at a 1:4 dilution

Table 2.1 Details of source, media conditions and maintenance of cells used throughout this study

Table 2.1 Abbreviations: HI-FCS- Heat-inactivated foetal calf serum, DPBS- Dulbeccos Phospho Buffered Saline, EDTA- Ethylenediaminetetraacetic Acid

2.2 Purification of Myo1089 and MCF10A cells using β4-Integrin coated beads

Pan Mouse IgG Dynabeads (1.5 x 10^5, Invitrogen) were washed in 1mL sterile filtered Dulbeccos Phospho Buffered Saline (DPBS, Invitrogen) + 0.1% bovine serum albumin (BSA) and pulled out of solution via a Magnarack (DRI Ltd). Wash was repeated twice before Dynabeads were resuspended in 0.5mL DPBS + 0.1% BSA. β4-Integrin antibody (5µg/mL, Clone 3E1, Millipore) was added to the resuspended Dynabeads before solution was rotated for 18 hours at 4°C. Cells were trypsinised as per Table 2.1, counted using a haemocytometer and 1.5 x 10^5 cells centrifuged at 290 x g for 3 mins. Cells pellet was resuspended in 1mL DPBS + 0.1% BSA. β4-Integrin coated Dynabeads were washed 3x with 1mL DPBS + 0.1% BSA using a Magnarack. β4-Integrin coated Dynabeads were pulled out solution and resuspended in 1mL of cell solution. Cells were rotated with the β4-Integrin coated Dynabeads for 30 mins at 4°C. β4-Integrin coated Dynabeads were pulled out of solution using a Magnarack and supernatant containing β4-Integrin negative cells was retrieved. β4-Integrin coated Dynabeads were resuspended in 1mL DPBS + 0.1% BSA and process repeated twice to separate β4-Integrin negative and positive cell populations. β4-Integrin coated Dynabeads were resuspended in 3mL DPBS + 0.1% BSA and both β4-Integrin negative (if required) and positive cell populations centrifuged at 290 x g for 3 mins. Cells were resuspended in appropriate medium (see Table 2.1) and plated out into vented cap cell culture flasks (Corning) before incubation at 37°C and 95% air and 5% CO_2.

2.3 3D gel culture

Rat Tail Collagen I (BD Biosciences) was diluted with DPBS to achieve a 2mg/mL collagen concentration (previously optimised [149]) and mixed with the following: eight parts of collagen solution (2mg/mL) was added to one part 10x Hanks Buffered Salt Solution (HBSS,

Sigma). The pH of the gel mixture was neutralised by adding sodium hydroxide drop-wise until a pink-orange colour was achieved. Cells were trypsinised as per Table 2.1, counted using a haemocytometer and appropriate number of each cell type (as indicated in relevant chapters) mixed together and centrifuged at 290 x g for 3 mins. Cell pellet was resuspended in appropriate medium (as indicated in relevant chapters) to a volume that constituted one part of the final gel volume. These were added to achieve a total cell density of $4x10^5$ cells /mL of gel mixture. The gel-cell mixture (200µl) was added to 12-well plate cell culture inserts with a PET membrane with 8.0µm pore size (Falcon) and these placed within wells of a 12-well culture plate (Costar, Corning Inc). Gels were left to solidify for 20 mins before 500µl of appropriate medium (as indicated in relevant chapters) was added on top of each gel within the insert and 1mL added to the bottom of each well in the cell culture plate. Gels were cultured at 37°C and 95% air and 5% CO_2 for 21 days unless otherwise specified with 50% of the medium being replaced every three days during this time. Gels were fixed in 10% Formalin (Sigma) for five hours before being processed in a Leica ASP 200 tissue processor (Leica Microsystems), paraffin embedded and 5µm sections taken using a Leica RM2235 microtome (Leica Microsystems) ready for analysis.

2.4 Preparation of conditioned medium

The non-tumorigenic fibroblast cell line HMFU-19 and tumour epithelial cell line SkBr3 were passaged (Table 2.1) and allowed to recover in normal growth conditions for 24 hours. Cells were rinsed in DPBS and incubated for 48 hours in serum-free medium. Medium was aspirated and cell debris removed by centrifugation at 290 x g for 3 mins before being stored at -80˚C until used.

2.5 Haematoxylin and Eosin (H & E) staining

Gel sections (5µm) were dewaxed with xylene (VWR International, 4 x 3 mins) and rehydrated with 100% ethanol (4 x 3 mins) and graded ethanols of 75%, 50% and 25% diluted in water (3

mins each). Sections were rinsed in water for 2 mins and stained with Mayers Haematoxylin (11.4mM haematoxylin, 2mM sodium iodate, 3mM citric acid, 173mM chloral hydrate, 61mM aluminium potassium sulphate, 2% ethanol, 12% glycerol, prepared from reagents from Sigma in house courtesy of the Histopathology team, Leeds Institute of Cancer and Pathology) for 2.5 mins. Sections were rinsed in water for 2 mins and then counterstained with eosin (14mM eosin-Y in distilled water, prepared from powder from BDH in house courtesy of the Histopathology team, Leeds Institute of Cancer and Pathology) for 2 mins. Sections were rinsed in water for 1 min and then dehydrated in 100% ethanol (10 secs, 30 secs and 2 x 5 mins) and xylene (3 x 3) mins before being mounted onto coverslips with DPX (CellPath).

2.6 Immunohistochemistry (IHC)

Gel sections (5µm) were dewaxed with xylene and rehydrated with ethanol (as for H & E above) before incubating in 10% H_2O_2 (VWR International) in methanol at room temperature for 10 mins to block any endogenous peroxidase. For proteolytic digestion antigen retrieval, sections were incubated at 37^{o}C for 20 mins in 20µg/mL Proteinase K (Fungal, Invitrogen) in Phosphate Buffered Saline (PBS, 137 mM NaCl, 2.7 mM KCl and 10 mM phosphate buffer solution pH 7.4, prepared from ready-made tablets, Sigma). For heat-induced antigen retrieval, sections were placed in boiling distilled water containing 0.9% Antigen Unmasking Solution (Vector Laboratories Inc) in a pressure cooker. Once full pressure was achieved, antigen retrieval was timed for 2 mins before cooling sections. Sections were placed in Sequenza coverplates (Shandon) and rinsed with PBS. Non-specific binding sites for all sections were blocked with 1 x Casein (Vector Laboratories Inc) diluted 1:10 in PBS for 20 mins at room temperature. Where extra blocking steps were required, sections were rinsed twice with 2% BSA (Sigma) in PBS before adding 100µl 20% goat serum (Dako) in PBS and incubating at room temperature for 20 mins. All sections were rinsed with PBS before the addition of 100 µl of primary antibodies (Table 2.2) diluted in Antibody Diluent (Invitrogen). Primary antibody was

omitted to serve as negative controls. Sections were incubated either overnight at 4^{o}C or for 2 hours at room temperature (see Table 2.2), rinsed twice in PBS and stained using Dako Envision Detection System according to manufacturer's instructions. Sections were incubated in Copper Sulphate for 2 mins, rinsed in water and counterstained with Mayer's Haematoxylin (Sigma) for 1 min, before incubation in Scotts Tap Water Substitute (Sigma) for 2 mins. Sections were subsequently dehydrated in 100% Ethanol and Xylene (as per H & E) before being mounted onto coverslips with DPX (CellPath).

2.7 Image acquisition of gel and tissue sections

Throughout this study, digital images of H & E and IHC stained gel and human tissue sections were acquired through slide scanning courtesy of the in house Virtual Pathology facility (Leeds Institute of Cancer and Pathology). Glass slides were scanned using Aperio CS and Aperio AT scanners (Aperio Technologies Inc) using x20 and x40 objectives producing images with a final resolution of 0.23 and 0.43µm per pixel respectively. Images were acquired using Aperio Imagescope software version 11 (Aperio Technologies Inc).

Antibody Against (abbreviation)	Manufacturer	Clone	Type	Dilution	Antigen Retrieval Method	Extra blocking step used	Incubation time
Collagen IV (Coll IV)	Sigma	COL-94	Mouse Monoclonal	1:1000	Proteolytic Digestion	Yes- Goat serum	Overnight at 4°C
Tenascin-C (TN-C)	Sigma	BC-24	Mouse Monoclonal	1:1000	Proteolytic Digestion	Yes- Goat serum	Overnight at 4°C
Vimentin (Vim)	Dako	Vim 3B4	Mouse Monoclonal	1:200	Heat induced	No	Overnight at 4°C
Epithelial Membrane Antigen (EMA)	Dako	E29	Mouse Monoclonal	1:5000	Heat induced	No	Overnight at 4°C
α-Smooth Muscle Actin (αSMA)	Dako	1A4	Mouse Monoclonal	1:200	Heat induced	No	Overnight at 4°C
E-Cadherin (E-Cad)	Dako	NCH-38	Mouse Monoclonal	1:100	Heat induced	No	Overnight at 4°C
Ki67	Dako	MIB-1	Mouse Monoclonal	1:1000	Heat induced	No	Overnight at 4°C
M30	Roche	M30	Mouse Monoclonal	1:50	Heat induced	No	Overnight at 4°C
Turbo GFP (tGFP)	Pierce	N/A	Rabbit Polyclonal	1:500	Heat induced	Yes- Goat serum	2 hours room temperature
dsRed	Clontech	N/A	Rabbit Polyclonal	1:200	Heat induced	Yes- Goat serum	2 hours room temperature

Table 2.2 Details of antibodies, their dilutions and methods used for IHC

2.8 Isolation of primary fibroblasts from clinical specimens

Breast tissue that was surplus to histopathological diagnosis was selected from reduction mammoplasty samples after patients provided informed consent. All samples were collected via the Leeds Breast Tissue Bank following ethical approval (Rec: 09/H1306/108, Leeds Teaching Hospital Trust R+D No. HTA 11_0001). Samples were selected on the condition that patients had received no prior chemotherapy and that samples were received no later than 6 hours after operation was carried out.

Primary fibroblasts were isolated using a method adapted from one used by Gomm et al previously [183]. Tissue was minced with a scalpel before being placed in a vented cap cell culture flask (Corning) with 5mL RPMI-1640 (Gibco) + 5% HI-FCS containing 2.5µg/mL of Fungizone and 100U/mL of Penicillin/Streptomycin antibiotics (both Invitrogen). Tissue was incubated overnight at 37^{o}C and 95% air and 5% CO_2 in a humidified incubator. Tissue was digested the following morning with 10mg/mL of Collagenase IA (Sigma) with gentle shaking and monitoring every 30-60 mins. If required, another 10mg/mL of collagenase IA was added to ensure thorough digestion of sample. Once tissue was digested, sample was diluted with 25mL DPBS (Invitrogen) and passed through a 70µM Nylon BD Falcon cell strainer (BD Biosciences) to harvest fibroblasts. Fibroblast-rich solution was centrifuged for 3 mins at 290 x g and cell pellet resuspended in 15mL DPBS to wash. This was repeated twice to give a total of 3x DPBS washes. Fibroblasts were plated out onto vented cap cell culture flasks coated with 20µg/mL Fibronectin (Sigma) in DMEM-GlutaMAX^{TM}-I + 10% HI-FCS, 2.5µg/mL Fungizone and 100U/mL Penicillin/Streptomycin antibiotics and incubated at 37^{o}C and 95 % air and 5% CO_2 in a humidified incubator. Antibiotics were removed following one week in culture. Stocks of cells were frozen as per section 2.1 between passages 0 and 2.

2.9 Lentiviral Transduction

Lentiviral transduction was carried out using the 2nd generation calcium phosphate method developed by Prof Didier Trono [184]. This was performed in a Genetically Modified Category II cell culture facility that was approved for viral work under permission obtained by Dr Georgia Mavria (Leeds Institute of Cancer and Pathology). Details of lentiviral expression plasmids used will be detailed in relevant chapters.

2.9.1 Production of expression and packaging plasmids

Lentiviral expression plasmids, pMD2.G envelope plasmid (gift from Dr Georgia Mavria, Fig 2.1) and psPAX2 packaging plasmids (gift from Dr Georgia Mavria, Fig 2.2) were transformed into XL1-Blue Supercompetent bacterial cells (Agilent) and cultured on LB-agar plates (prepared using Lennox LB Broth with Agar powder as per manufacturer's instructions, Sigma) containing 100µg/mL of Ampicillin (Sigma). Colonies were picked and plasmid DNA purified using Qiagen Plasmid Maxi-Prep Kit (Qiagen) following manufacturer's instructions.

2.9.2 Production of lentiviral particles

Replication-deficient lentiviral particles containing expression or shRNA constructs were generated using Lenti-X 293T cells for lentiviral packaging (Clontech). Lenti-X 293T cells were maintained in DMEM-GlutaMAX-1™ medium (Invitrogen) + 10% HI-FCS at 37°C and 95 % air and 5% CO_2 in a humidified incubator. For routine passage, cells were washed with DPBS, 0.5% Trypsin/EDTA added for ~2mins and cells resuspended in medium. Cells were centrifuged at 290 x g for 3 mins, pellet resuspended in medium and replated at a 1:10 dilution.

Lenti-X 293T cells were seeded into 15cm round cell culture dishes (Corning) with a seeding density of 2.5 x 10^6 cells and left to recover for 48 hours until ~70% confluent. Medium was

replaced 2 hours prior to transfection. The following transfection solution was prepared in a 50 mL centrifuge tube (Falcon®, Corning) with each of the components added in order:-

- 22.5µg lentiviral expression plasmid
- 7.9µg pMD2.G envelope plasmid
- 14.6µg psPAX2 packaging plasmid
- 660µl 0.1 x Tris EDTA (1mM Tris, 0.1mM EDTA, pH 8.8)
- 350µl molecular biology grade water (Calcium Phosphate Transfection kit, Sigma)
- 113µl 2.5M Calcium phosphate (Calcium Phosphate Transfection kit, Sigma)

The transfection solution was mixed briefly by pipetting. 1.14mL of 2 x Hepes Buffered Saline (Calcium Phosphate Transfection kit, Sigma) was added dropwise under agitation by vortexing and solution left to incubate at room temperature for 20 mins. Transfection solution was then added dropwise to Lenti-X 293T cells and rocked gently to mix. Cells were left to incubate for 16 hours at 37^{o}C and 95 % air and 5% CO_2 in a humidified incubator. Medium was then replaced and cells left to incubate for 8 hours. Medium containing lentiviral particles was then harvested, centrifuged at 290 x g for 3 mins to remove cell debris and passed through a 0.45µm sterile filter (Sartorius). Virus supernatant was then stored at -80^{o}C until ready to use.

2.9.3 Transduction of cells with lentiviral particles

Target cells were cultured in 25cm^3 vented cap cell culture flasks (Corning) until 60% confluent. Medium was replaced with viral supernatant either neat (pFURW expression vector), or, diluted 1:5 in DMEM-GlutaMAX-1™ medium (Invitrogen) + 10% HI-FCS (pGIPZ expression vectors) containing 8µg/mL Polybrene (Sigma). Cells were incubated in viral supernatant for 5 hours before washing 3 x DPBS and medium replaced with appropriate target cell medium. Cells were left to recover for 72 hours and growth monitored daily. The transduction efficiency was determined by

assessing the percentage of fluorescent cells using an EVOS fl microscope (Advanced Microscopy Group). This was performed by counting the number of fluorescent cells from three separate fields of view at 10 x magnification and expressing as a ratio of the total number of cells counted from the corresponding phase contrast fields of view at 10 x magnification. In the event that less than ~90% of the cells were fluorescent, fluorescent cell populations were enriched using Fluorescence-activated cell sorting (FACS) courtesy of the in house flow cytometry facility (Leeds Institutes of Molecular Medicine). Un-transduced cells were used as negative controls to define the flow-cytometry gates.

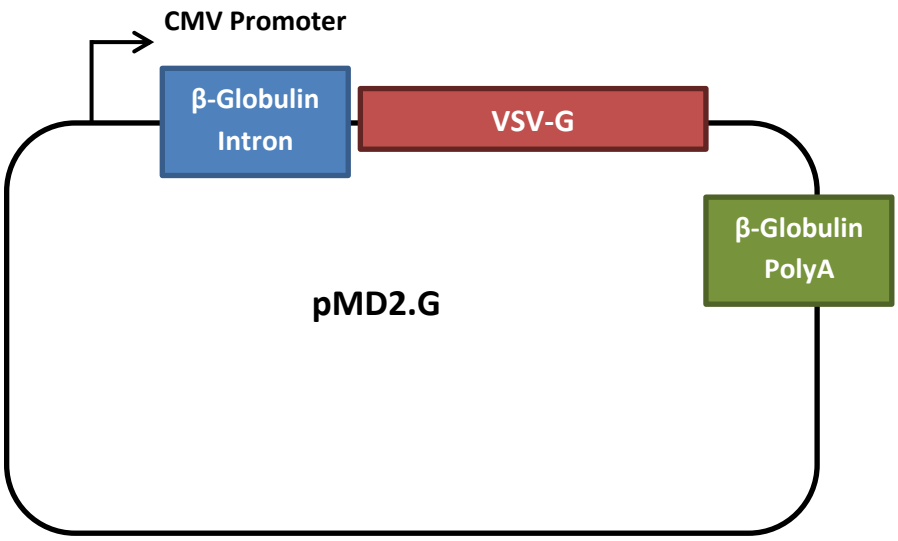

Fig 2.1 Simplified plasmid map of pMD2.G envelope plasmid

Diagram represents key elements contained within the pMD2.G envelope plasmid (gift from Dr Georgia Mavria, Leeds Institute of Cancer and Pathology) used for lentiviral transduction. Key elements are as follows:- Cytomegalovirus promoter (CMV), β-Globulin Intron, G glycoproteins of the vesicular stomatitis virus gene (VSV-G), β-Globulin polyadenylation sequence (PolyA).

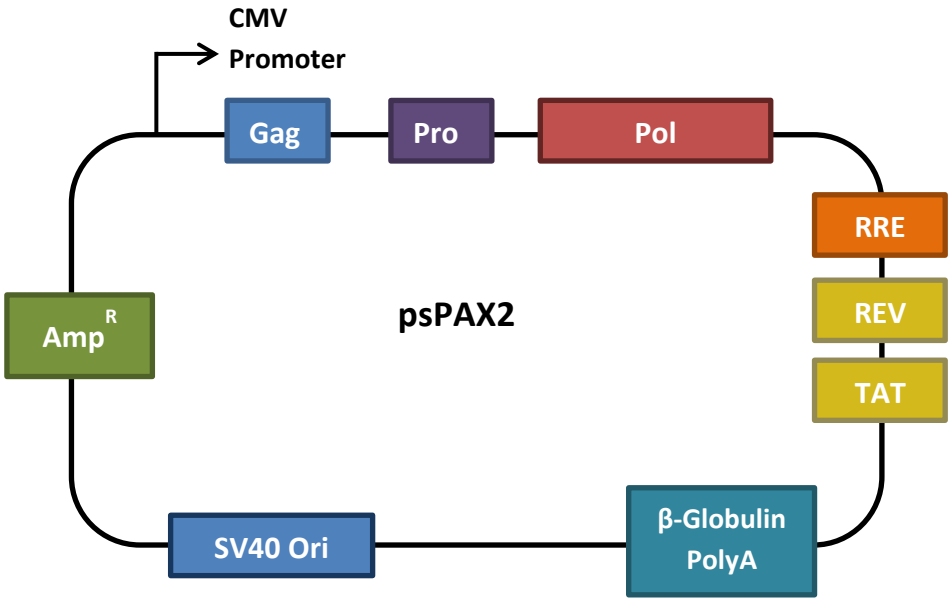

Fig 2.2 Simplified plasmid map of psPAX2 packaging plasmid

Diagram represents key elements contained within the psPAX2 packaging plasmid (gift from Dr Georgia Mavria, Leeds Institute of Cancer and Pathology) used for lentiviral transduction. Key elements are as follows:- Cytomegalovirus promoter (CMV), Group Antigen polyprotein gene (gag), Viral Protease gene (Pro), reverse transcriptase gene (Pol), Regulator of Expression of Virion Protein gene (Rev), Trans-activator of Transcription gene (Tat), β-Globulin polyadenylation sequence (PolyA), Simian Vacuolating Virus 40 origin of replication (SV40 Ori) and Ampicillin resistance gene (Amp^R).

2.10 Retroviral transduction

Retroviral transduction was carried out by Dr Euan Baxter, Leeds Institute Cancer and Pathology. This was performed in a Genetically Modified Category II cell culture facility that was approved for viral work under permission obtained by Prof Margaret Knowles (Leeds Institute Cancer and Pathology). Viral supernatant comprised of retroviral particles containing pBabe-neo-hTERT plasmid expression constructs in DMEM-GlutaMAX-1™ medium (Invitrogen) + 10% HI-FCS (see Fig 2.3 for plasmid map) was provided courtesy of Dr Julie Burns, Leeds Institute Cancer and Pathology.

Target cells were cultured in 25cm^3 vented cap cell culture flasks (Corning) until 60% confluent. Medium was replaced with viral supernatant diluted 1:5 in DMEM-GlutaMAX-1™ medium (Invitrogen) + 10% HI-FCS containing 1µg/mL Polybrene (Sigma). Cells were incubated in viral supernatant overnight before washing 3 x DPBS and medium replaced with DMEM-GlutaMAX-1™ medium (Invitrogen) + 10% HI-FCS containing 500µg/mL Geneticin (G418, Sigma). Cells were maintained and passaged using this medium for 10 days before G418 was removed. Cell growth was monitored daily thereafter.

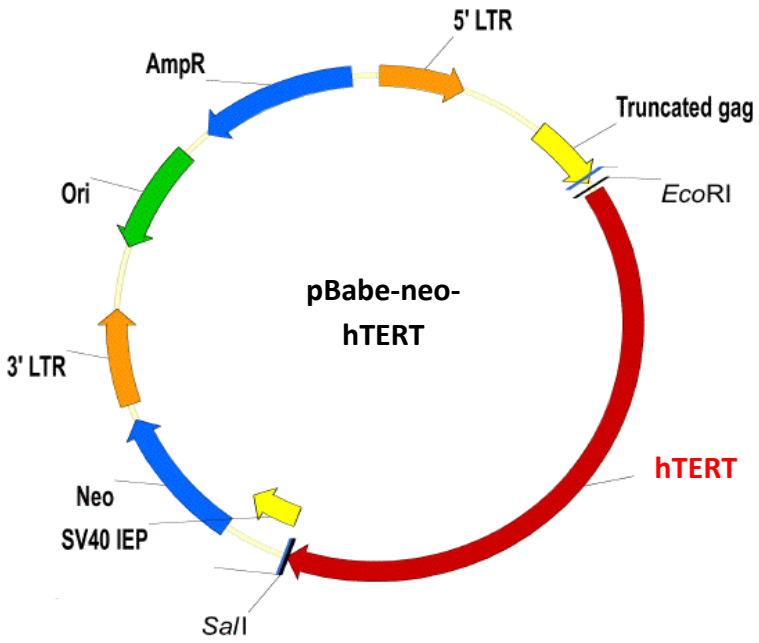

Fig 2.3 Plasmid map of pBabe-neo-hTERT retroviral plasmid used to insert the hTERT gene into primary fibroblasts

Diagram represents key elements contained within the pBabe-neo-hTERT plasmid used for retroviral transduction of primary fibroblasts with the hTERT gene. Key elements are as follows:- 5'-long terminal repeats (5'-LTR), truncated gag gene (truncated gag), human Telomerase Reverse Transcriptase gene (hTERT), Simian Vacuolating Virus 40 promoter (SV40 IEP),Neomycin resistance gene (Neo), 3'-LTR, origin of replication (Ori), Ampicillin resistance gene (Amp^R) and restriction enzyme sites for *Eco*RI and *Sal*I.

Diagram adapted from [185].

2.11 Protein extraction and quantification

Cells for protein extraction were cultured in vented cap cell culture flasks until 60% confluency was reached with any treatments performed in situ before protein extraction was carried out. Lysis buffer used contained 1x modified RIPA buffer (300mM NaCl, 4mM EDTA, 2% NP40 (Sigma) and 0.5% Na deoxycholate (Sigma)), with 1x protease inhibitor (Roche mini protease cocktail tablet made up to 1ml in nuclease-free water, Ambion). Cells were washed with ice cold PBS and flask placed on ice. Pre-chilled lysis buffer (500µl per T25 flask) was applied and incubated on ice for 4 mins with intermittent swirling of flask. Cells were scraped with a cell scraper and lysate transferred to a chilled eppendorf tube and left on ice for 20 minutes. Lysate was centrifuged in a microcentrifuge at 15682 x g for 15 minutes and the supernatant transferred to a new chilled tube. Protein extracts were ideally used fresh or stored at -80°C.

Protein concentration was determined using the colorimetric DC protein assay according to manufacturer's instructions (BioRad). Briefly, 5 µl of BSA protein standards ranging from 2 - 0.1875mg/ml as well as 5 µl of protein samples were added to separate wells of a flat-bottomed 96 well microtitre plate (Corning). A solution of alkaline copper tartrate solution was prepared (Reagent A + Reagent S) and 25µl added to each of the wells containing standards and samples. This was followed by addition of 200µl of Folin's reagent (Reagent B) to each sample. Colour change was allowed to develop for 15 minutes before optical density was measured at 670nm using an Opsys MRTM microplate reader (Dynex Technologies Ltd). The protein concentration was calculated using the standard curve from BSA protein standards.

2.12 Western Blotting

All protein samples were diluted to ensure equal concentrations using deionised water and 20µl of sample transferred to a new pre-chilled eppendorf tube. To each sample, 7.5µl of 4x NuPAGE® LDS sample buffer (Life Technologies) and 2.5µl of beta-mercaptoethanol (Sigma) was added to make a final volume of 30µl. Samples were denatured for 5 mins at 105^{o}C using a Grant QBD2 dry block heater, vortexed and allowed to cool on ice. Precast NuPAGE® Novex® 4-12% Bis-Tris Gels were used with Xcell SureLock™ Mini-Cell system and submerged in 1 x NuPAGE® MOPS SDS Running Buffer (all Invitrogen). 20 µl of the samples and 7 µl of the BioRad Dual Color Protein Plus protein standard (BioRad) were loaded into the gels and electrophoresis was performed for 1 to 1.5 hours at 150V.

Proteins were transferred to a Polyvinylidene difluoride membrane (Amersham). Briefly, membrane was activated with methanol for 30 secs, and soaked in 1 x NuPAGE® Transfer buffer diluted with distilled water and 10% methanol. Proteins were transferred in transfer buffer using the Xcell II Blot Module SureLock™ system (Invitrogen) overnight at 4^{o}C at 13v.

Membrane was blocked with 5% skimmed milk in TBST (10mM Tris-HCl, pH 8.5, 150mM NaCl, 0.1% Tween-20) for 8 hours at 4^{o}C with gentle rocking. Membrane was then incubated with primary antibody diluted in blocking buffer overnight at 4^{o}C with gentle rocking. Membrane was washed 3 x 10 mins with TBST before incubating with secondary antibody diluted in blocking buffer for 1 hour at room temperature. Following 3 x 10 min washes in TBST, membrane was developed using SuperSignal West Pico Chemiluminescent Substrate (Thermo Scientific) and visualised using ChemiDoc® MP imaging system.

Primary antibodies used: anti-HER2 IgG (Rabbit Polyclonal, Cell Signalling Technology, dilution 1:1000), anti-HER3 IgG (Mouse monoclonal, Clone 2F12, Millipore, dilution 1:1000), anti-β-actin

IgG (Clone AC-15, Sigma, dilution 1:10000), anti-DOCK4 IgG (Rabbit polyclonal, Bethyl Laboratories Inc, dilution 1:500), anti-phospho-Akt Ser473 IgG (Rabbit monoclonal, Clone 193H12, Cell Signalling Technology Inc, dilution 1:1000), anti-phospho-PLCγ1 Ser1248 IgG (Mouse monoclonal, Clone D25A9, Cell Signalling Technology Inc, dilution 1:1000).

Secondary antibodies used: HRP-conjugated polyclonal goat anti-rabbit antibody (Santa Cruz Biotechnology, dilution 1:10000), HRP-conjugated polyclonal goat anti-rabbit antibody (Santa Cruz Biotechnology, dilution 1:10000).

2.13 Quantification of H & E stained 3D HB2 structures

The method used for quantification of 3D *in vitro* HB2 co-cultures was developed in house courtesy of Dr Darren Treanor (Virtual Pathology facility, Leeds Institute of Cancer Pathology). Gels were serial sectioned, H & E stained and 20x magnified digital images acquired as per sections 2.5, 2.6 and 2.7. For the purpose of optimisation, 10 serial sections encompassing a total depth of 50µm were taken. Quantification thereafter was based on sections taken from a depth between 15µm and 40µm (see Chapter 3 for validation).

Quantification was performed using Aperio Imagescope software version 11. Annotation tools were used to outline the perimeters of the whole gel section, any holes within the gel section and around HB2 units manually using a computer equipped with a Wacom Cintiq touchscreen monitor. Example annotations are shown in Fig 2.4. A viable HB2 unit was defined as a cohesive cluster of four or more cells with discernible nuclei. To ensure that units quantified were comprised of HB2 cells and not Myo1089 and fibroblast cells, IHC was performed alongside H & E of the gels as per sections 2.5 and 2.6 to confirm that the structures being annotated did not contain tGFP or dsRed positive cells. HB2 units on the periphery of the gel section or holes were excluded as they were not representative of the majority of HB2 structures within the gels. Aperio Imagescope software

calculated the area of each annotation in μm^2 and the number of units was based on the number of annotations drawn. Lumen formation was defined as a space within HB2 units that was enclosed by a continuous chain of cells and was counted manually. Any HB2 units that contained spaces with breaches in the surrounding cells were excluded. Example images of what was defined as a viable lumen and a non-viable lumen are shown in Fig 2.5.

The area of the gel section was calculated by subtracting the area of holes in the gel from the total area of the gel section. Due to the inherent variation between the size of gel sections and therefore the number of units within each gel, the area of HB2 units were normalised by expressing the area of the unit per μm^2 of gel. This was calculated by taking the area of each HB2 unit and dividing by the area of the gel section (μm^2).

For each experiment, one section from three replicate gels for each variable was quantified. Raw data obtained from Aperio Imagescope was inputted into GraphPad Prism 6 software where the mean and standard error of the mean (SEM) was calculated along with any statistical analysis was performed.

a)

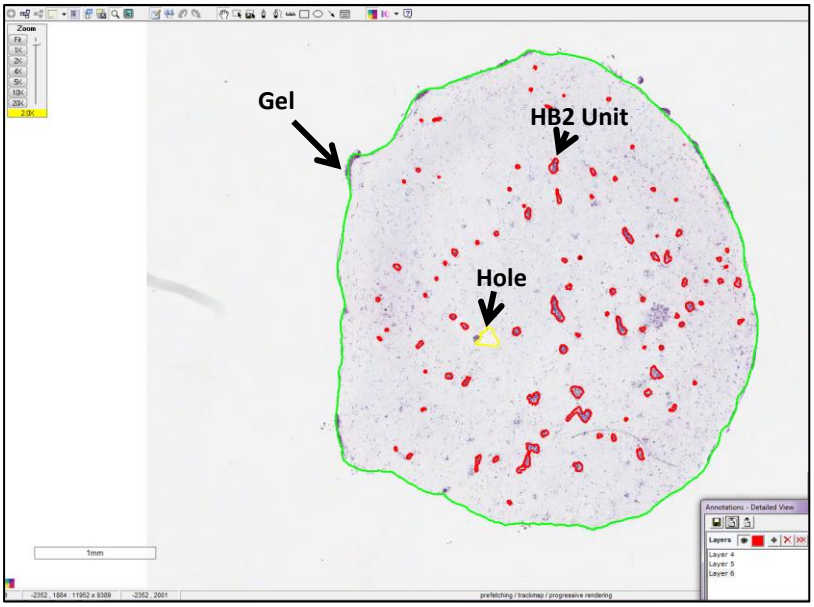

b)

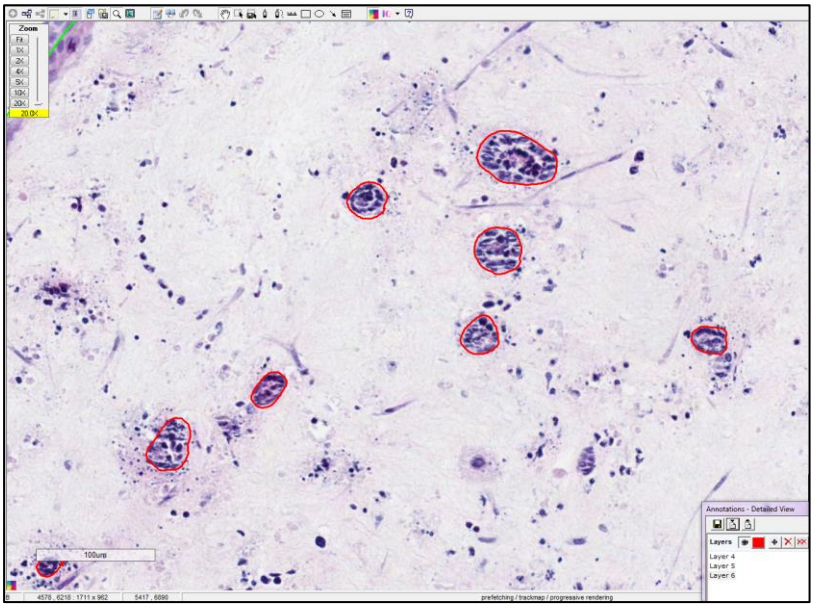

Fig 2.4 Representative images of annotations drawn in Aperio Imagescope software used for quantification of HB2 units in 3D *in vitro* culture

a) Example image showing representative annotations drawn to calculate the total area of each gel section (Gel, green), any holes within gel sections (Hole, yellow) and of HB2 cell units (HB2 Unit, Red).

b) Example image at 20x magnification showing representative annotations drawn around HB2 units.

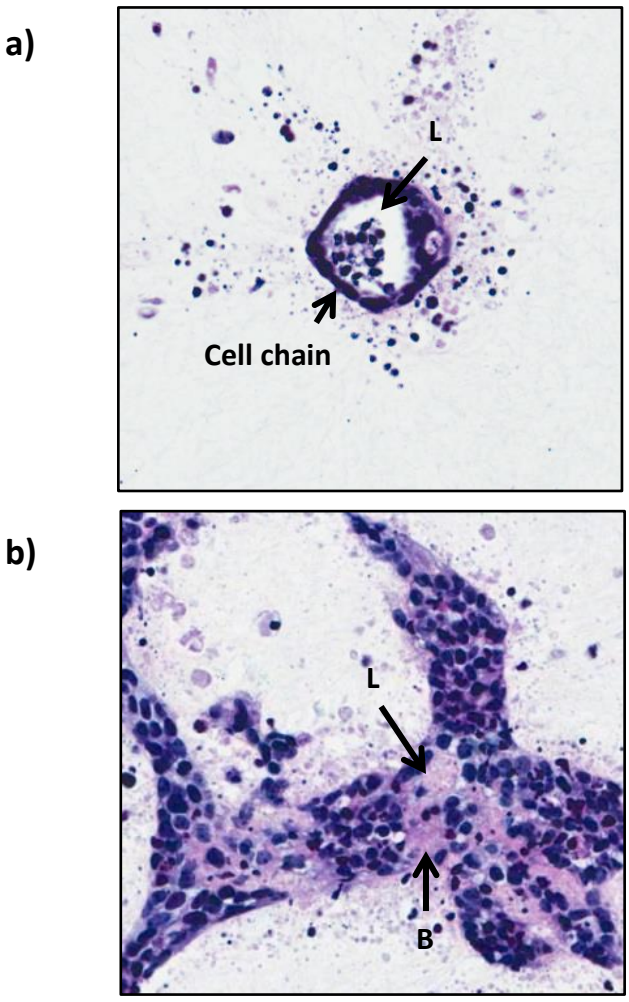

Fig 2.5 Representative images to demonstrate what constituted a viable and a non-viable lumen for quantification

a) Example of a HB2 unit containing a luminal space that was considered viable for quantification. Unit contains a luminal space (L) that is surrounded/enclosed by a continuous chain of rounded HB2 cells (Cell chain) that contains no breaches. b) Example of a HB2 unit containing a luminal space that was considered not viable for quantification. Unit contains a luminal space (L) that is not fully enclosed by a chain of HB2 cells. HB2 cell layer surrounding the space is discontinuous featuring breaches (B).

3 Chapter 3: Optimisation of a 3D *in vitro* tri-culture model of normal breast

3.1 Introduction

The basic principle of 3D *in vitro* culture is to incorporate either single or multiple cell types into a 3D matrix in order to recapitulate an *in vivo* tissue environment. Therefore, there are two main considerations when developing a 3D *in vitro* model of normal breast; choice of an appropriate matrix and selection of cells to include.

3.1.1 Choice of Matrix

Natural ECM materials isolated from murine sources are preferred for 3D models. Various techniques using natural ECM materials have been extensively reviewed [186-188] and under the right conditions, support cell growth in 3D. The most commonly used ECM material is the commercially available compound Matrigel™. Matrigel is derived from the Engelbreth-Holm-Swarm mouse sarcoma and is rich in the basement membrane proteins laminin and collagen IV, as well as several extracellular growth factors [189]. Culture of breast epithelial cells in 3D Matrigel™ has seen the formation of acini-like structures [190] with evidence of milk protein expression [152]. However, materials such as Matrigel™ should be used with caution. Levels of growth factors within Matrigel™ can vary, and components such as collagen IV can differ in subunit composition to *in vivo* components [191] potentially increasing susceptibility to remodelling and proteolysis not commonly found *in vivo.* Matrigel™ may also provide tumour cells with additional survival and proliferative signals facilitating tumorigenesis [192]. Although these caveats can be overcome by the use of growth factor reduced Matrigel™, there are alternative ECM materials to Matrigel™ that may be more appropriate for the culture of breast cells *in vitro*.

As demonstrated by our group in Fig 3.1 and reported by Parmar and Cunha [193], the main constituent of normal breast stroma consists predominantly of collagen I. The remodelling and mechanical tension of collagen I has been proven to influence breast tumour cell invasion [54] and the morphology of breast cells [194, 195]. An increase in collagen density has also been linked to increased risk of breast cancer [196, 197]. It therefore seems prudent that the influence of collagen I matrix be accounted for in 3D *in vitro* models of breast and may provide a more physiologically relevant environment for culture of breast cells. Production of successful acini- and duct-like structures akin to those cultured in Matrigel™ has already been achieved [198, 199] through culture of mammary epithelial cells in collagen I perhaps making collagen I a viable and more appropriate choice of ECM matrix for 3D models of breast.

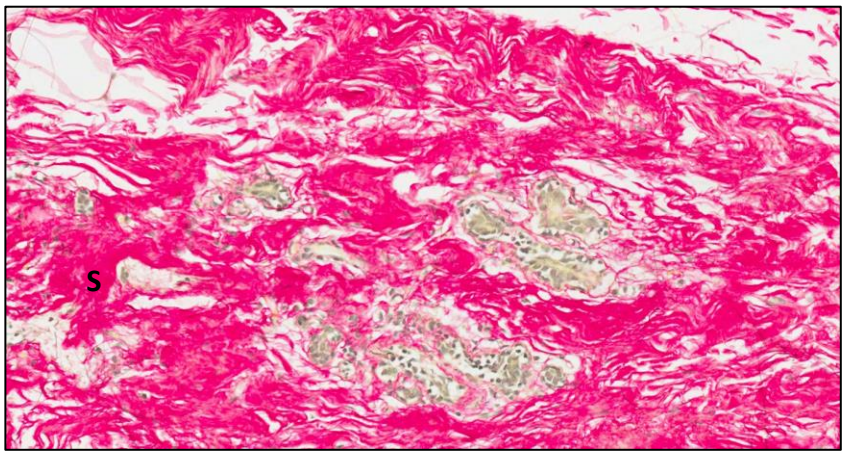

Fig 3.1 Sirius red staining of collagen I in normal breast tissue

Example of a normal breast tissue sample stained with Sirius Red highlighting the abundance of collagen I fibrils in the breast stroma (S). Image courtesy of Prof Valerie Speirs (Leeds Institute of Cancer and Pathology).

3.1.2 Choice of Cells

Despite the vast amount of breast cancer cell lines available, there is a scarcity of normal breast epithelial cell lines. The MCF10A cell line has customarily been chosen as a representative of normal luminal breast epithelium. MCF10A cells are a spontaneously immortalised mammary epithelial cell line derived from a patient with fibrocystic change. They are non-tumorigenic as don't exhibit anchorage-independent growth and they exhibit features of normal luminal cells such as ultrastructural similarities to breast luminal epithelial cells and expression of breast epithelial cytokeratins and sialomucins, [180, 200]. Culture in Matrigel^{TM} has yielded some impressive acini-like structures which are polarised, contain hollow lumens and produce basement membrane proteins [154, 190]. This has also been recapitulated in collagen I matrix [201]. Another less commonly used representative for normal luminal breast epithelium is the HB2 cell line. HB2 cells are a sub-population of the MTSV1-7 cell line [202] which have luminal epithelial characteristics and were originally isolated from breast milk. Branching 3D duct-like structures have been achieved through culture of HB2 cells in collagen I [199].

While culture of these cells in 3D matrix has resulted in structures akin to *in vivo* breast acini and ducts which cannot be achieved through culture in 2D, *in vivo* breast architecture is much more complex including a variety of other cell types that influence epithelial architecture. This has led to a rise in 3D co-culture with stromal cells with co-culture with fibroblasts most commonly reported [149, 195, 201] and examples of combinations of fibroblasts and adipocytes also demonstrated [203, 204]. As previously discussed (Chapter 1), it has emerged that fibroblasts regulate epithelial cell invasion [205] secreting various growth factors such as MMPs [206] which have been proven through use of 3D co-cultures. Markedly, some of these effects are only evident upon culture in collagen I [207]. As previously discussed in Chapter 1, myoepithelial cells also play a key role in normal *in vivo* breast. Given their tumour suppressive nature [72, 208] and their capacity to

maintain luminal cell polarity [71], it seems apt to include these cells in normal *in vitro* models of breast, however, to date studies incorporating these cells are lacking.

It stands to reason that luminal epithelial organisation is maintained by a delicate balance between the opposing functions of fibroblasts and myoepithelial cells. It seems apt that both these cell types are included in a 3D *in vitro* model of normal breast with luminal epithelial cells to accurately reflect the *in vivo* environment. Only one such tri-culture model has been achieved previously by Holliday et al [149] but this used aberrant luminal epithelial cells thus representing DCIS. A 3D *in vitro* tri-culture model of normal breast has not been achieved and could prove valuable for cancer initiation studies and for better understanding of how different cell types within the breast interact and communicate with each other.

3.2 Aims

To develop a 3D *in vitro* model in physiologically relevant collagen I matrix that includes luminal epithelial, myoepithelial and fibroblast cell lines. The model was validated by characterising and comparing to normal breast tissue specimens. This was achieved by :-

- Stable transduction of the myoepithelial cell line Myo1089 with tGFP protein to enable tracking in culture
- Optimisation of culture conditions in collagen I with GFP Myo1089 and either HB2 or MCF10A cells
- Isolation of fibroblasts from a breast reduction mammoplasty primary sample and their stable transduction with human Telomerase Reverse Transcriptase (hTERT) to increase longevity in culture and with dsRed fluorescent reporter to enable tracking in a tri-culture model
- Characterising the phenotype and immunoprofile by IHC and compared profile to a normal breast tissue specimen

3.3 Materials and Methods

3.3.1 Immunofluorescence

Cells were trypsinised as per Chapter 2, Table 2.1 and seeded onto glass coverslips (Scientific Laboratory Supplies Ltd) which had been sterilised with 70% ethanol in water. These were left to recover in normal growth conditions until 60% confluency was reached. Cells were rinsed in PBS at 4°C and fixed in 4% paraformaldehyde in PBS for 10 minutes. Cells were permeabilised for 5 mins with 0.1% Triton X-100 (Sigma) in PBS, rinsed in PBS and processed for immunofluorescence (IF), or stored for up to 2 weeks at 4°C. Fixed cells were rinsed in PBS and blocked with 1% BSA in PBS for 30 mins. Cells were washed in PBS (3 x 5 mins) and then incubated with primary antibody diluted in blocking solution (Table 3.1) by inversion on to the solution on parafilm (M Lab supplies). Primary antibody was omitted to serve as a negative control. Following 3 x 5 mins PBS washes, secondary antibody conjugated to a fluorescent dye was applied and incubated in the dark for 40 mins. Coverslips were washed and mounted on a microscope slide (VWR International) using Vectashield hard-set mountant containing 4', 6-diamidino-2-phenylindole (DAPI) (Vector Laboratories Inc). Slides were stored at 4^{o}C in the dark until imaged. Fluorescent images were captured within 2 weeks of staining using microscopes detailed in relevant figures. Secondary antibodies used: Goat anti-mouse IgG Texas Red ®-X (Invitrogen, diluted 1:400), goat anti-rabbit IgG (H+L) Alexa Fluor® 594 (Invitrogen, diluted 1:400) and goat anti-mouse IgG FITC conjugated (Dako, diluted 1:500).

Antibody Against	Manufacturer	Clone	Type	Dilution
β4-Integrin	Millipore	3E1	Mouse Monoclonal	1:25
Cytokeratin 14	AbD Serotec	LL002	Mouse Monoclonal	1:100
Cytokeratin 5/6	Dako	D5/16 B4	Mouse Monoclonal	1.100
Cytokeratin 18	Sigma	CM-90	Mouse Monoclonal	1:500
α-Smooth Muscle Actin	Dako	1A4	Mouse Monoclonal	1:100
Vimentin	Dako	Vim 3B4	Mouse Monoclonal	1:200
Epithelial Membrane Antigen	Dako	E29	Mouse Monoclonal	1:200

Table 3.1 Details of antibodies and dilutions used for immunofluorescence

3.3.2 Lentiviral transduction for cell tracking

Lentiviral transduction was carried out as per Chapter 2. In order to produce Myo1089 cells that stably expressed green fluorescent protein, the pGIPZ-tGFP empty lentiviral expression vector was used (see Fig 3.1, Thermo Scientific). In order to produce LS11-083 hTERT fibroblast cells that stably expressed dsRed fluorescent protein, the pFURW empty lentiviral expression vector was used (unpublished, gift from Dr Mihaela Lorger, Leeds Institute of Cancer and Pathology). This expression construct was generated by Dr Mihaela Lorger by splicing out the DsRed gene from pDsRed-express1 plasmid via BamHI/HpaI restriction enzyme sites. The fragment was then blunted and ligated into the HpaI restriction site of the pFUW vector [209]. See Fig 3.2 for a plasmid map of the pFURW vector.

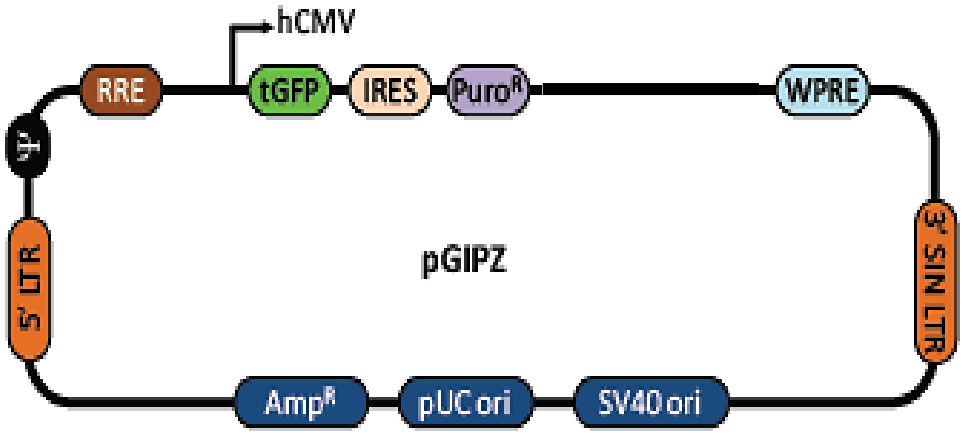

Fig 3.2 Simplified plasmid map of pGIPZ lentiviral expression plasmid

Diagram represents key elements contained within the expression plasmid used to lentivirally transduce cells with TurboGFP protein. Key elements are as follows:- Human Cytomegalovirus promoter (hCMV), TurboGFP gene (tGFP), internal ribosome entry site (IRES), Puromycin resistance gene ($Puro^R$), Woodchuck hepatitis virus post-transcription regulatory element (WPRE), 3'- self inactivating long terminal repeat (3'-SIN LTR), Simian Vacuolating Virus 40 origin of replication (SV40 Ori), pUC origin of replication (pUC), Ampicillin resistance gene (Amp^R), 5'-LTR, psi packaging sequence (ψ) and Rev Response Element (RRE). Adapted from [210].

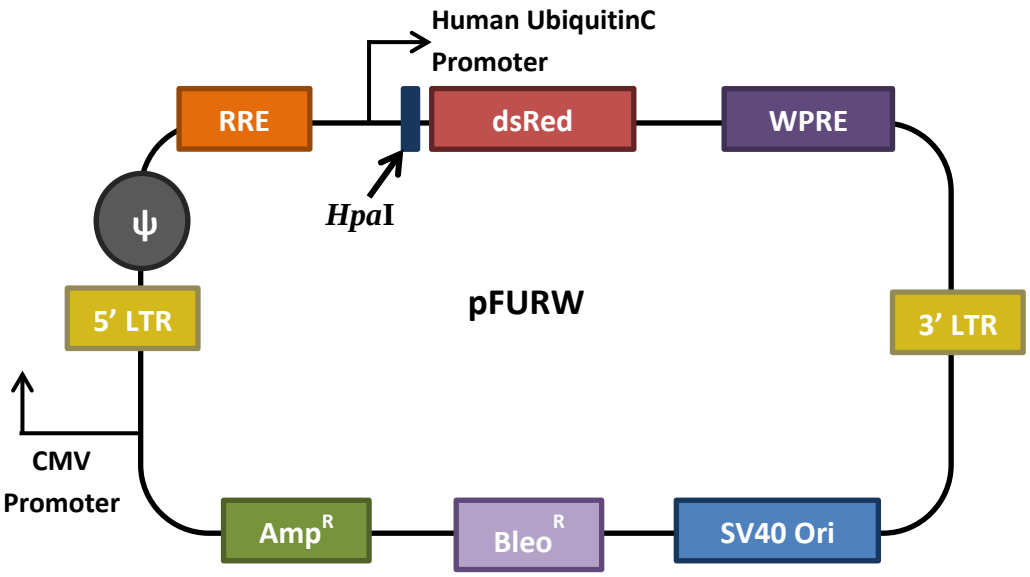

Fig 3.3 Simplified Plasmid map of pFURW lentiviral expression plasmid

Diagram represents key elements contained within the expression plasmid used to lentivirally transduce cells with dsRed protein. Key elements are as follows:- Cytomegalovirus promoter (CMV), 5'-long terminal repeats (LTR), psi packaging sequence (ψ), Rev Response Element (RRE), human ubiquitinC promoter, restriction enzyme site for HpaI, dsRed gene, Woodchuck hepatitis virus post-transcription regulatory element (WPRE), 3'-LTR, Simian Vacuolating Virus 40 origin of replication (SV40 Ori), Bleomycin resistance gene ($Bleo^R$) and Ampicillin resistance gene (Amp^R).

3.4 Results

3.4.1 Production and characterisation of a GFP positive myoepithelial cell line

The cell line Myo1089 (gift from Dr Mike Allen, Barts Cancer Institute, Queen Mary, University of London) was selected as a representative myoepithelial cell line for our study. Following recommended purification using β4-integrin coated Dynabeads, in 2D culture, these cells formed a cobblestone-like monolayer consisting of elongated stellate-shaped cells characteristic of myoepithelial cells in culture [211]. To enable the tracking of Myo1089 cells in 3D culture, Myo1089 cells were lentivirally transduced with pGIPZ-tGFP empty vector plasmid (courtesy of Dr Georgia Mavria, Leeds Institute of Cancer and Pathology). FACS courtesy of in house flow cytometry facility (Leeds Institutes of Molecular Medicine), produced a cell population which retained a stellate-shaped morphology in which >99% of cells were GFP positive (Fig 3.4). These were termed GFP Myo1089 cells throughout the study.

In order to assess GFP Myo1089 cell phenotype, immunofluorescence was carried out using a panel of antibodies containing markers of luminal and myoepithelial cell populations with representative images from three biological replicate experiments presented (Fig 3.5). While GFP Myo1089 cells stained uniformly for the myoepithelial associated markers β4-integrin and αSMA, cells were negative for the myoepithelial markers cytokeratin 14 and vimentin. Only approximately 1% of cells exhibited staining for EMA however all cells demonstrated strong cytoplasmic staining for cytokeratin 18 which are both luminal epithelial markers. This indicates that GFP Myo1089 cells may consist of a mixed population of cells.

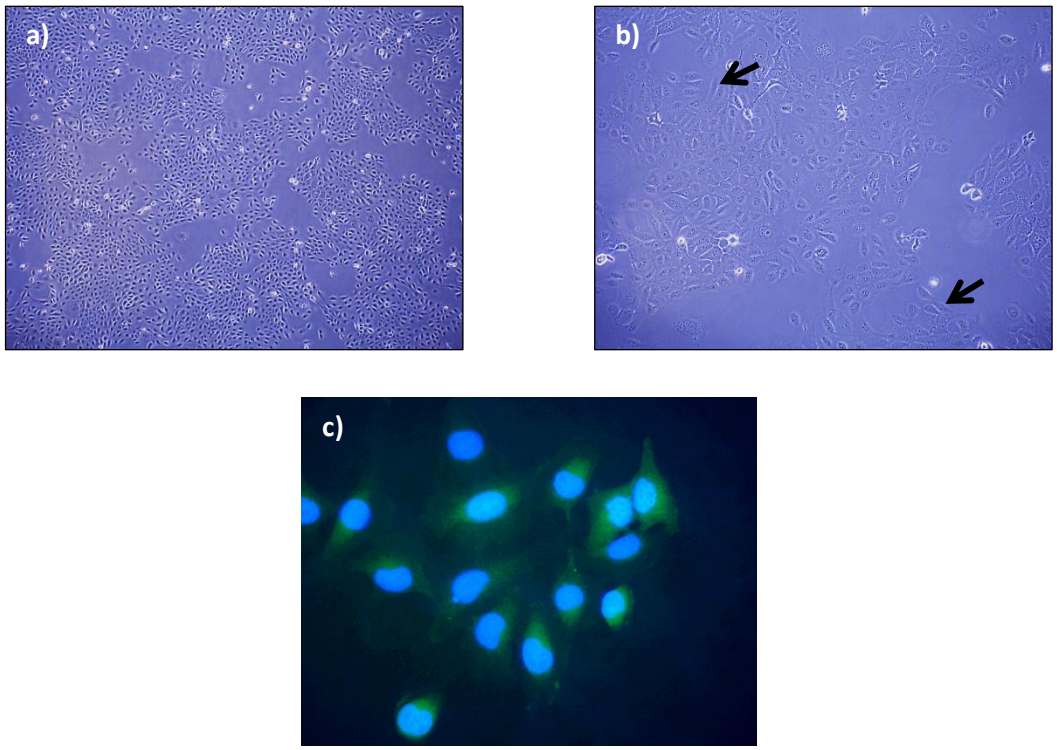

Fig 3.4 GFP Myo1089 cells imaged using phase contrast and fluorescence microscopy

Phase contrast microscopy of GFP Myo1089 cells demonstrate formation of a cobblestone monolayer (a, original magnification 4x) consisting of elongated stellate-shaped cells (b, arrows, original magnification 20x). Fluorescence microscopy shows >99% GFP positivity of GFP Myo1089 cells in green with DAPI stained nuclei in blue (c, original magnification 63x taken with a Nikon C1 confocal microscope).

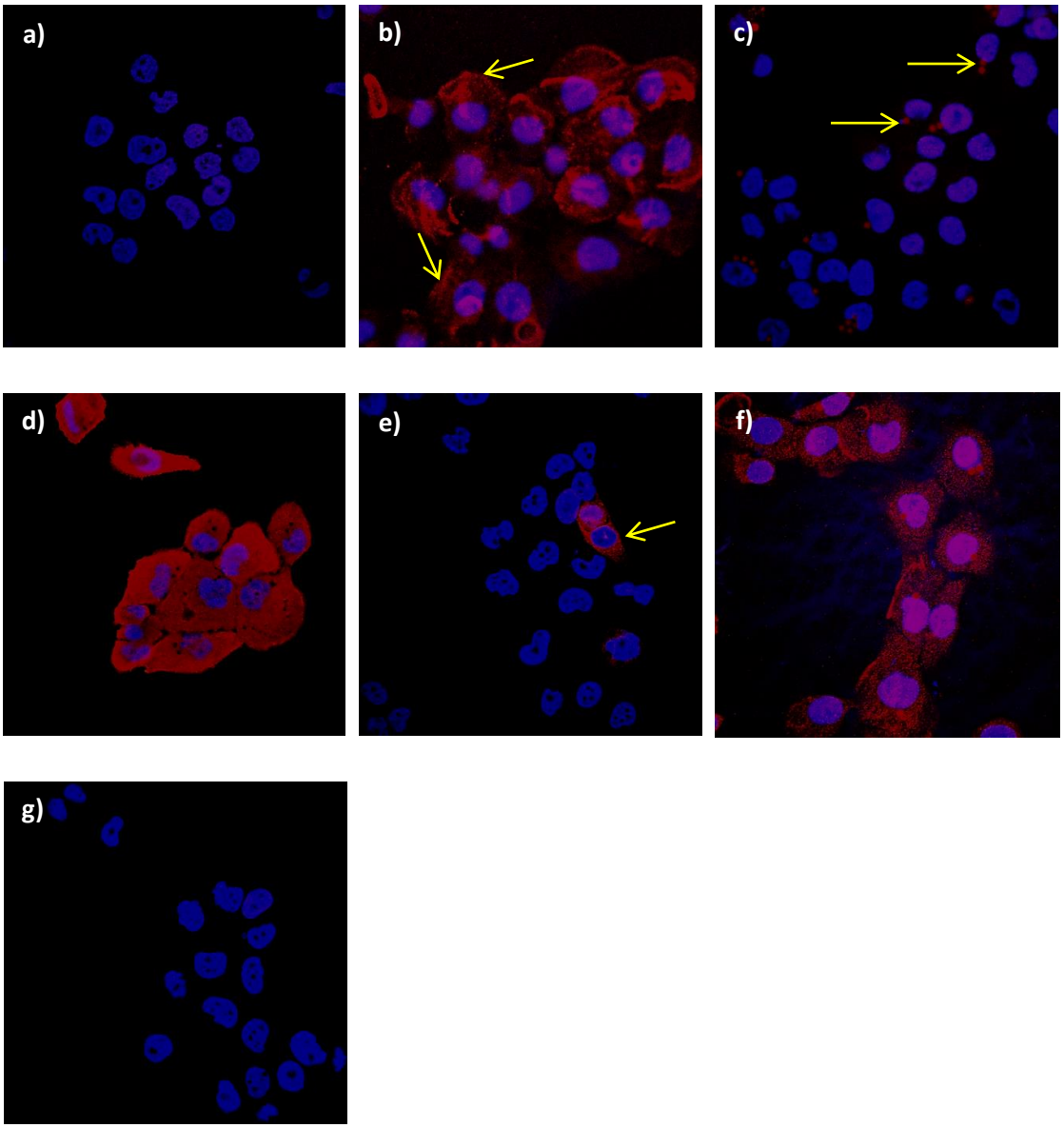

Fig 3.5 Characterisation of GFP Myo1089 cells

GFP Myo1089 cells were characterised by immunofluorescence staining with a panel of antibody markers and visualised using Texas Red (red) with nuclei visualised using DAPI (blue). Representative images from three biological replicate experiments presented. Primary antibody was omitted to serve as a negative control (a). Over 95% of GFP Myo1089 cells exhibited positive staining for β4-Integrin concentrated at cell membranes (arrows, b). Cells were negative for cytokeratin 14 but staining artefacts were detected thought to be staining of Dynabeads following purification (arrows, c). All cells exhibited strong cytoplasmic staining for cytokeratin 18 (d) while approximately 1% of cells displayed epithelial membrane antigen positivity (e). Over 95% of cells demonstrated cytoplasmic α-smooth muscle actin staining (f) while cells were negative for vimentin (g). All images taken at 63x magnification with a Nikon A1R confocal microscope.

3.4.2 Characterisation of luminal epithelial cell line MCF10A

The MCF10A cell line was assessed for its suitability as a representative luminal epithelial cell line for study (Fig 3.6). In 2D culture, MCF10A cells demonstrated varying cell morphologies. Sub-populations of MCF10A cells were detected with either an elongated spindle-shaped morphology akin to myoepithelial cells as well as smaller, rounded and cohesive cells that form a cobblestone monolayer. MCF10A cell phenotype was examined by immunofluorescence with representative images from three biological replicate experiments presented. MCF10A cells largely exhibited a myoepithelial cell phenotype with all cells displaying strong positive staining for cytokeratin 5/6 and αSMA with some positive staining for cytokeratin 14. In addition, approximately 30% of cells were positive for the myoepithelial specific marker β4-integrin and although EMA staining was detected in these cells, the majority of cells were negative.

3.4.3 Morphology and phenotype of 3D *in vitro* dual-culture models containing MCF10A cells with myoepithelial cells

Due to the apparent plasticity of MCF10A cells and basal nature of sub-populations of cells, purification with β4-integrin coated Dynabeads was attempted in order to separate basal and luminal epithelial cell populations. Original MCF10A cells were designated MCF10A wildtype (MCF10A WT), β4-integrin positive MCF10A cells were designated MCF10A basal (MCF10A Basal) and β4-integrin negative MCF10A cells were designated MCF10A luminal (MCF10A Luminal). MCF10A WT, MCF10A Basal and MCF10A Luminal were cultured in 3D collagen gels for up to 14 days with GFP Myo1089 cells in a 1:1 cell ratio with a total cell density of $4x10^5$ cells/ml of collagen gel (Fig 3.7). Representative images from three biological replicate experiments presented. Visualisation by H & E staining demonstrated that in the presence of GFP Myo1089 cells, all sub-types of MCF10A cells formed cohesive cell structures after 7 days in culture with the appearance of spindle-shaped cells loosely distributed throughout the collagen gels. MCF10A WT cells

displayed a combination of small cohesive rounded units and larger elongated units indicative of mixed populations of MCF10A structures. MCF10A Luminal cell structures were uniformly small, cohesive and rounded in comparison to MCF10A WT structures. Surprisingly, it was MCF10A Basal cells that formed structures most representative of *in vivo* breast acini which were larger with evidence of lumen formation unlike other MCF10A sub-types. After 14 days in culture, regardless of MCF10A sub-type, all cohesive structures were lost with cells loosely scattered throughout the collagen gels.

Distribution of GFP Myo1089 cells was visualised by IHC using anti-tGFP (Fig 3.8). tGFP staining was observed in cells associated around the edges of all MCF10A units and remained un-changed with different populations of MCF10A cells. This confirmed the spheroid units observed by H & E staining consisted of MCF10A cells and not GFP Myo1089 cells.

Characterisation by IHC demonstrated a mixed phenotype of MCF10A WT cells and a largely basal phenotype of MCF10A Luminal and MCF10A Basal cells regardless of segregation using β4-integrin coated beads (Fig 3.9 & 3.10, representative images from three biological replicate experiments presented). A combination of both positive and negative staining for E-cadherin (E-Cad) was detected in MCF10A WT units as well as some units proving positive for EMA while some were negative. Both MCF10A Luminal and MCF10A Basal units were uniformly positive for E-Cad at cell-cell junctions and strong cytoplasmic EMA staining was detected in all units. M30 staining was detected in centres of MCF10A WT and MCF10A Basal units only and was negative in MCF10A Luminal units suggesting only MCF10A WT and MCF10A Basal cells were capable of lumen formation. All sub-populations of MCF10A cells formed units that were positive for basal/myoepithelial markers α-SMA and vimentin (Vim) as well as accompanying GFP Myo1089 cells. All MCF10A sub-populations showed ability to produce basement membranes distributed on

the outer edges of MCF10A units as demonstrated by positive staining for collagen IV (Coll IV) and tenascin-C (TN-C). Therefore, despite attempts to separate a sub-population of MCF10A cells using β4-integrin coated beads to represent the luminal epithelium of our *in vitro* model of normal breast, all sub-populations of MCF10A cells displayed basal/myoepithelial characteristics in this culture system deeming MCF10A cells an inadequate luminal epithelial cell line for study. This highlighted a need to identify another luminal epithelial cell line for the model.

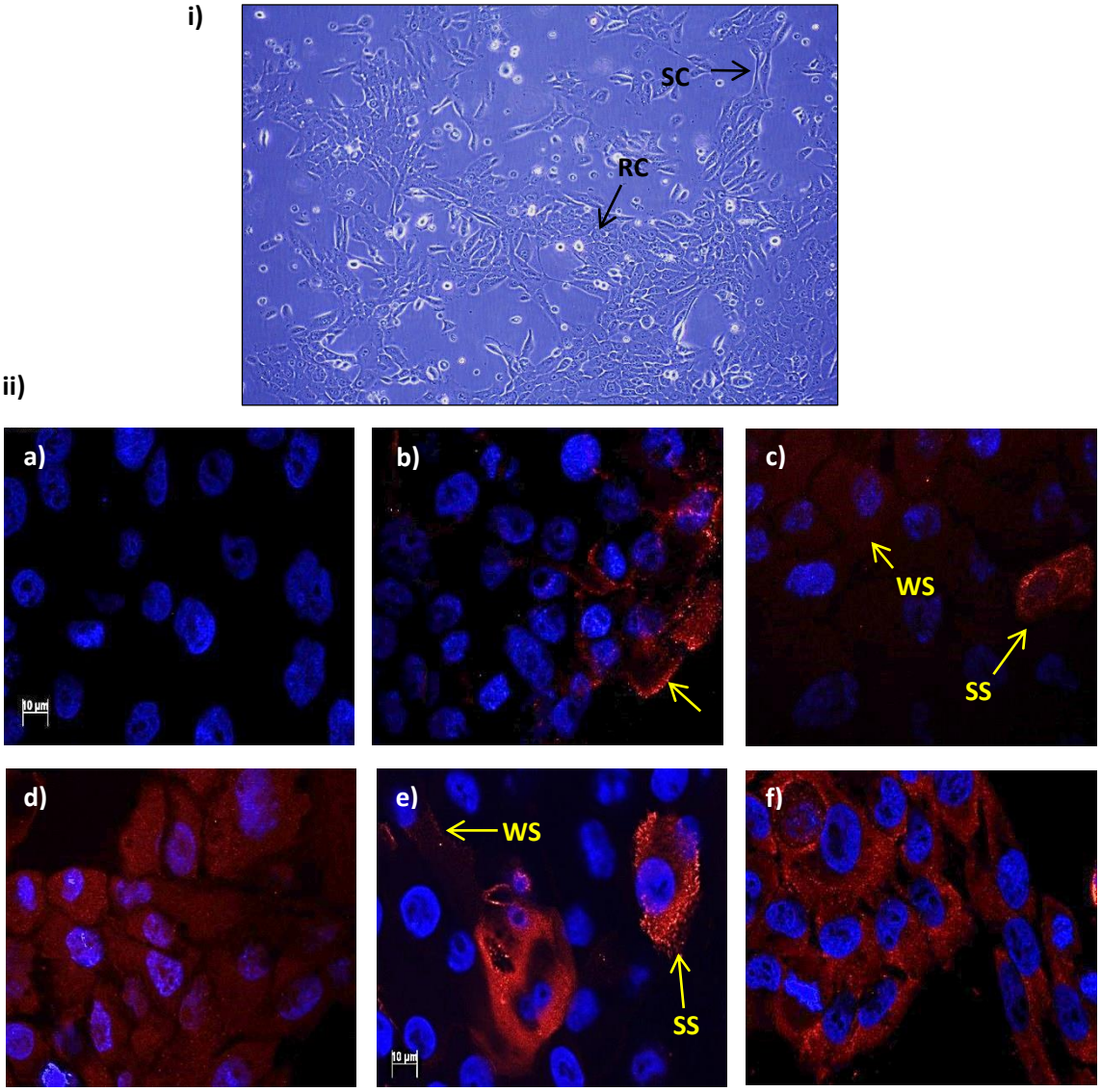

Fig 3.6 Morphology and characterisation of MCF10A cells using phase contrast microscopy and fluorescence microscopy

Phase contrast microscopy of MCF10A cells displayed a mixed population of cells consisting of longer spindle-shaped cells (SC) and cohesive rounded cells (RC) in a cobblestone monolayer (i, original magnification 20x). MCF10A cells were characterised by immunofluorescence (ii) staining with a panel of antibody markers and visualised using Texas Red (red) with nuclei visualised using DAPI (blue). Representative images from three biological replicate experiments presented. Primary antibody was omitted to serve as a negative control (a). ~30% of cells exhibited positive staining for β4-Integrin concentrated at cell membranes (arrow, b). Majority of cells displayed weak cytoplasmic cytokeratin 14 staining (WS, c) with ~1% of cells exhibiting strong staining (SS, c). All cells exhibited cytoplasmic staining for cytokeratin 5/6 (d) while a mixture of weak membranous staining (WS) and strong cytoplasmic staining (SS) was detected for epithelial membrane antigen (e). All cells displayed strong cytoplasmic staining for α-smooth muscle actin staining (f). All images taken at 63x magnification with a Zeiss AxioPlan II microscope.

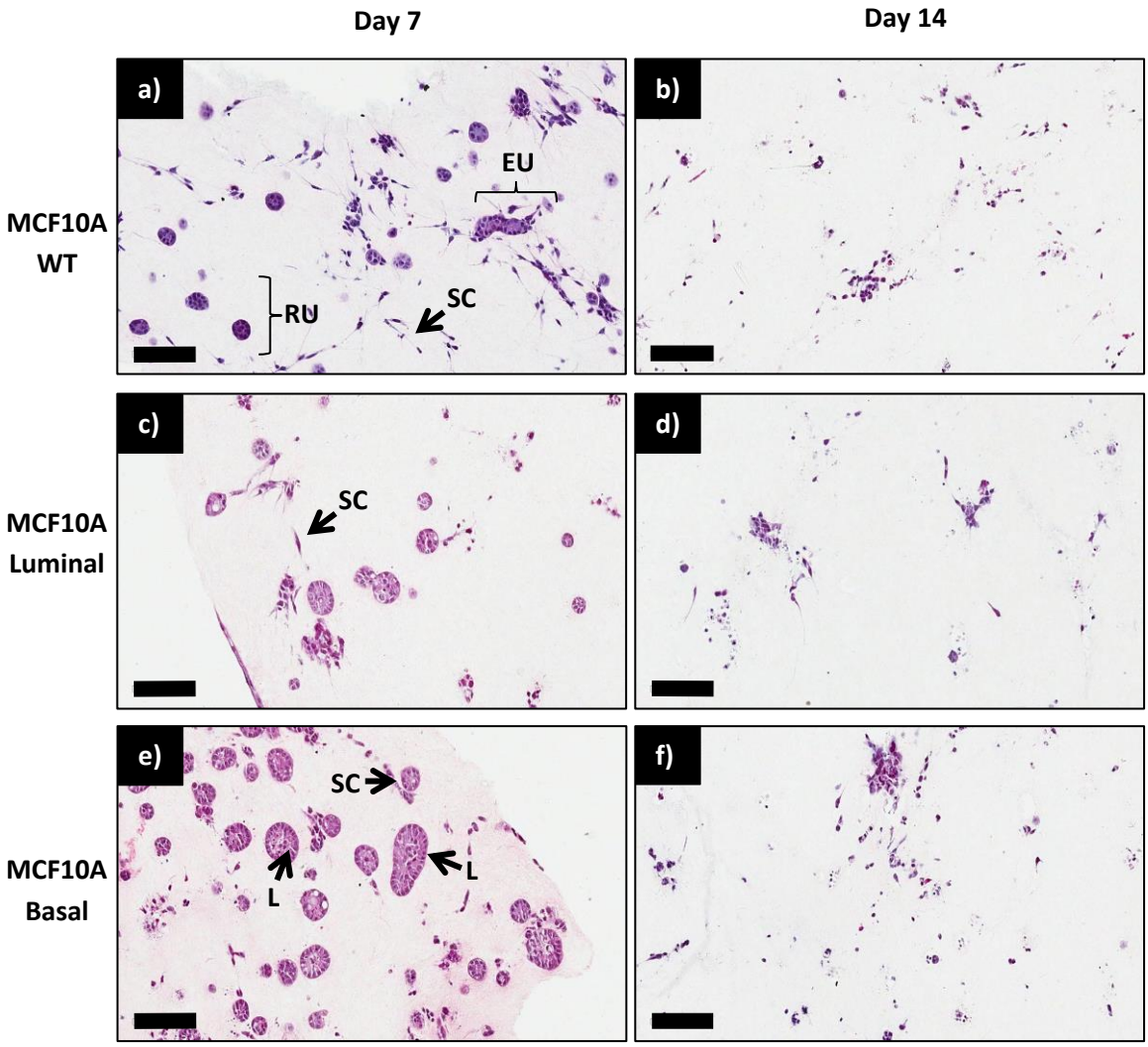

Fig 3.7 H & E staining of 3D *in vitro* dual-culture models of different populations of MCF10A cells with myoepithelial cells

Wildtype (MCF10A WT), β4-integrin negative (MCF10A Luminal) and β4-integrin positive (MCF10A Basal) MCF10A cells were cultured with GFP positive myoepithelial cells (GFP Myo1089) in 3D collagen gels for 7 and 14 days. 5µm sections of gels were stained with H & E. Representative images from three biological replicate experiments presented. After 7 days in culture, MCF10A WT (a) formed a combination of compact rounded units (RU) and more elongated units (EU). Both MCF10A Luminal cells (c) and MCF10A Basal cells (e) formed compact rounded units but these appeared larger with MCF10A Basal cells and demonstrated possible lumen formation (L) in their centres. All gels featured spindle-shaped cells (SC) loosely distributed throughout the collagen gel. After 14 days, all MCF10A structures were lost regardless of type of MCF10A cell (b, d & f). Original magnification 20x, scale bars = 100µm.

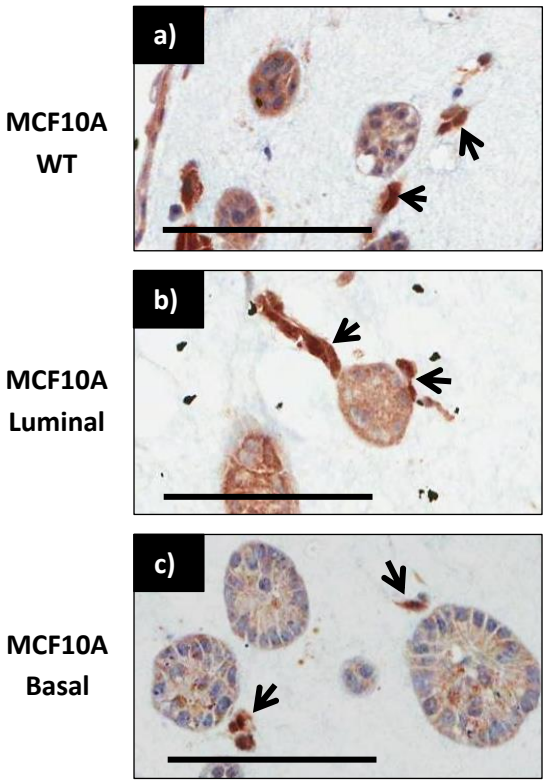

Fig 3.8 Immunohistochemical labelling of myoepithelial cells in 3D *in vitro* dual-culture model with different sub-populations of MCF10A cells

Wildtype (MCF10A WT), β4-integrin negative (MCF10A Luminal) and β4-integrin positive (MCF10A Basal) MCF10A cells were cultured with GFP positive myoepithelial cells (GFP Myo1089) in 3D collagen gels for 7 days. 5µm sections of gels were stained with anti-tGFP by IHC to visualise distribution of myoepithelial cells within gels. Representative images from three biological replicate experiments presented. All gels display positive staining for tGFP in cells distributed around the outer edges of HB2 cell units (arrows, a-c). Original magnification 20x, scale bars = 100µm.

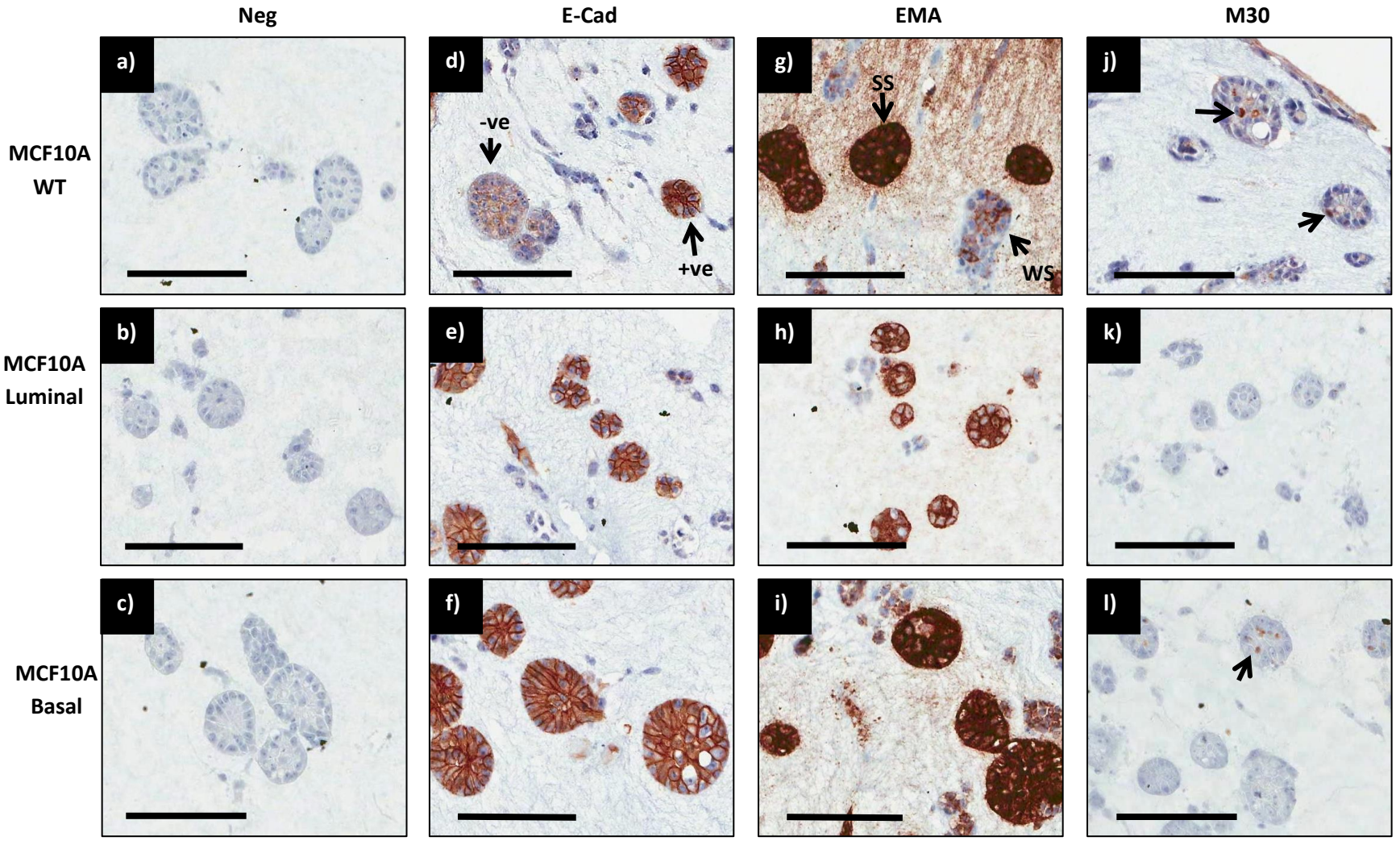
Neg
E-Cad
EMA
M30
MCF10A WT
MCF10A Luminal
MCF10A Basal
a)
b)
c)
d)
e)
f)
g)
h)
i)
j)
k)
l)
-ve
+ve
SS
WS

Fig 3.9 Immunohistochemical characterisation of 3D *in vitro* dual-culture model with different sub-populations of MCF10A cells A

In vitro dual-culture model containing GFP Myo1089 cells with MCF10A wildtype (MCF10A WT), β4-integrin negative MCF10A cells (MCF10A Luminal) or β4-integrin positive MCF10A cells (MCF10A Basal) were characterised by IHC. Representative images from three biological replicate experiments presented. Primary antibody was omitted to serve as negative (Neg) controls (a, b, & c). A combination of E-cadherin (E-Cad) positive MCF10A units (+ve) with staining between cell-cell junctions of MCF10A cells and E-Cad negative MCF10A units (-ve) were detected with MCF10A WT cells (d). All units with MCF10A Luminal and MCF10A Basal displayed strong E-Cad positivity at cell-cell junctions of MCF10A cells (e & f respectively). A combination of strong staining (SS) and weak staining (WS) for epithelial membrane antigen (EMA) was detected in units with MCF10A WT cells (g) whereas MCF10A Luminal (h) and MCF10A Basal (i) displayed strong uniform EMA staining across all units. M30 staining was detected both in the centre and in cells at the periphery of MCF10A WT units (arrows, j). MCF10A Luminal units were negative for M30 (k) and MCF10A Basal units also stained positive for M30 in the centres of units (l). Original magnification 20x, scale bars = 100µm.

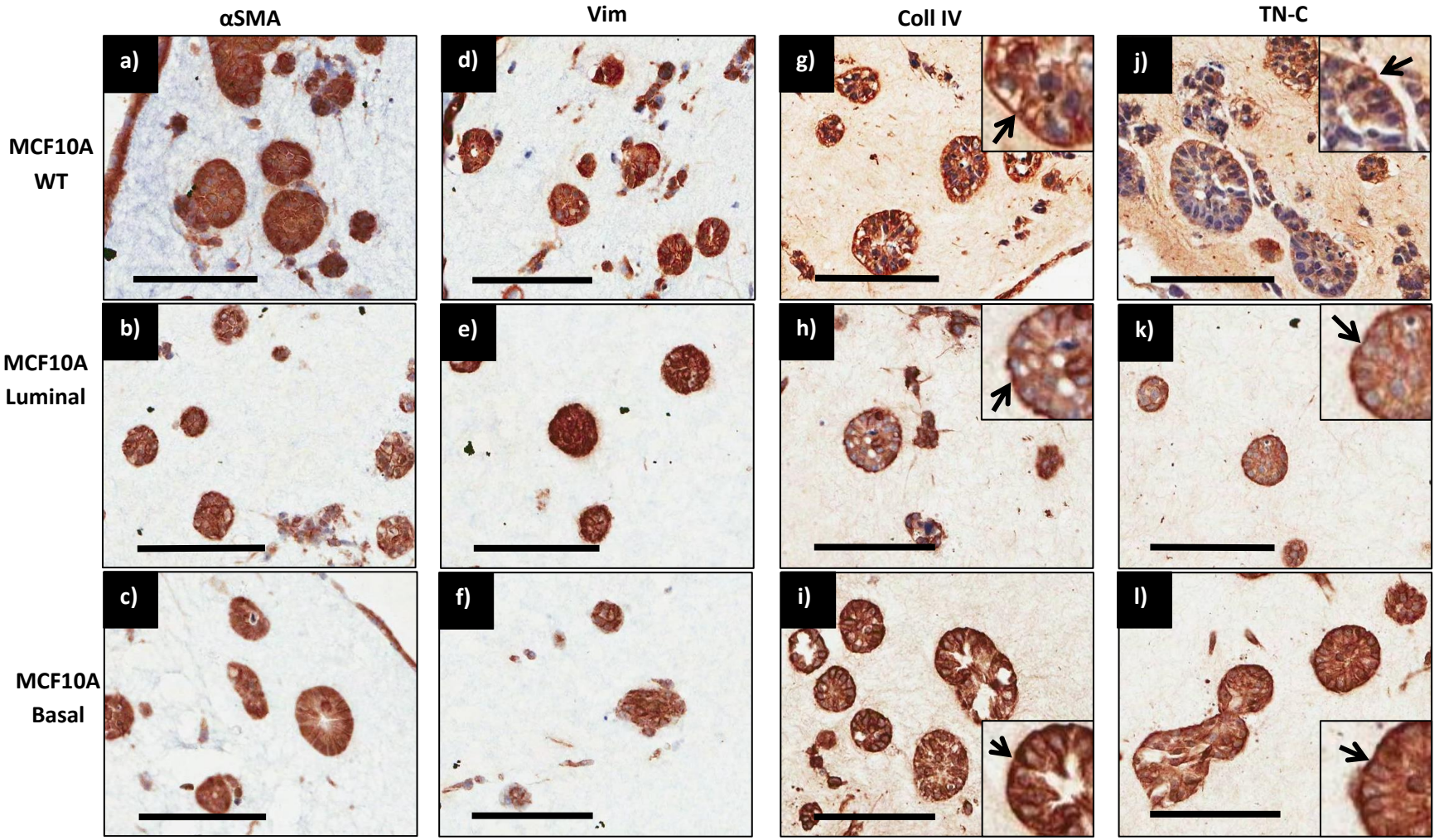
αSMA
Vim
Coll IV
TN-C
MCF10A WT
MCF10A Luminal
MCF10A Basal
a)
b)
c)
d)
e)
f)
g)
h)
i)
j)
k)
l)

Fig 3.10 Immunohistochemical characterisation of 3D *in vitro* dual-culture model with different sub-populations of MCF10A cells

In vitro dual-culture model containing GFP Myo1089 cells with MCF10A wildtype (MCF10A WT), β4-integrin negative MCF10A cells (MCF10A Luminal) or β4-integrin positive MCF10A cells (MCF10A Basal) were characterised by IHC. Representative images from three biological replicate experiments presented. All MCF10A units were uniformly positive for α-smooth muscle actin (αSMA) as well as GFP Myo1089 cells regardless of sub-population (a-c). Similarly, all MCF10A types of units were positive for vimentin (Vim) as well as GFP Myo0189 cells (d-f). Collagen IV (Coll IV) was found concentrated at the outer edges of all types of MCF10A units (arrows inset, g-i) and similarly tenascin-C (TN-C) was found at outer edges of all types of MCF10A units (arrows inset, j-l). Original magnification 20x, scale bars = 100µm.

3.4.4 Characterisation of luminal epithelial cell line HB2

As mentioned, the cell line HB2 has been used by other research groups as a representative of normal luminal breast epithelium. We therefore selected HB2 cells as an alternative to MCF10A cells and assessed their suitability to represent the luminal epithelium in the model (Fig 3.11). In 2D culture, HB2 cells demonstrated a more uniform cell morphology than MCF10A cells consisting of rounded and cohesive cells that formed clusters in a monolayer. When examined by immunofluorescence, HB2 cells exhibited a luminal epithelial cell phenotype with cells displaying strong staining for the luminal epithelial markers EMA and cytokeratin 18 and were negative for the myoepithelial markers cytokeratin 5/6 and αSMA. The myoepithelial vimentin marker was detected in these cells but was considerably weaker than the staining for luminal markers tested. Representative images from three biological replicate experiments presented.

3.4.5 Optimisation of culture media in 3D *in vitro* dual-culture model with myoepithelial and HB2 luminal cells

Though not necessary for culture using MCF10A cells due to the similarities in media requirements of MCF10A cells and GFP Myo1089 cells, composition of culture media for co-culture of HB2 cells and GFP Myo1089 cells was optimised. HB2 cells were cultured in 3D collagen gels for 7 days with GFP Myo1089 cells in a 1:1 cell ratio with a total cell density of $4x10^5$ cells/ml of collagen gel in different media conditions with representative images from three technical replicates presented (Fig 3.12). Medium 1 consisted of 100% HB2 cell specific culture medium (DMEM Glutamax + 10% FCS, 10µg/ml insulin & 5µg/ml hydrocortisone). Medium 2 consisted of 50% HB2 cell culture medium with 50% fibroblast conditioned medium (FCM, DMEM Glutamax + 10% FCS collected from normal fibroblast cell line HMFU-19 after 48 hours in culture). Medium 3 consisted of 50% GFP Myo1089 cell specific culture medium (HAMF12 Nutrient mixture + 10% FCS, 10ng/ml EGF, 10µg/ml insulin & 5µg/ml hydrocortisone) with 50% FCM. Visualisation by H & E staining

demonstrated culture in medium 1 yielded small compact cell units which were sparsely distributed throughout the collagen gel. Addition of fibroblast conditioned medium, as demonstrated by culture in medium 2, did not affect the morphology of structures which had a similar appearance to structures in medium 1. Inclusion of GFP Myo1089 specific medium in the culture system, as demonstrated by culture in medium 3, dramatically changed the morphology of structures formed as larger, compact and more numerous structures were observed with evidence of some lumen formation. Spindle-shaped cells were also detected in medium 3 loosely distributed throughout the collagen gels. Therefore, the presence of GFP Myo1089 cells specific medium was necessary to produce structures more reflective of *in vivo* breast acini.

3.4.6 Optimisation of cell ratios in 3D *in vitro* dual-culture model with myoepithelial and HB2 luminal cells

In order to yield more HB2 structures with a breast acini-like morphology, the ratio of GFP Myo1089 cells to HB2 cells was altered in order to identify an appropriate number of GFP Myo1089 cells to use in culture with representative images from three technical replicates presented (Fig 3.13). HB2 cells were cultured in 3D collagen gels for 14 days with GFP Myo1089 cells in different ratios. A ratio of 1 part GFP Myo1089 cells to 1 part HB2 cells (1:1) was compared to a ratio of 3 parts GFP Myo1089 cells to 1 part HB2 cells (3:1) with a total cell density of $4x10^5$ cells/ml of collagen gel in both cases. Visualisation by H & E staining demonstrated that a 1:1 ratio produced structures that were elongated, branched and in some cases appeared discohesive. Lumen formation was detected in a small number of these structures but was rare and therefore not shown. An excess of myoepithelial cells in a 3:1 ratio yielded structures which were more rounded and which consisted of more lumen formation than 1:1 ratio. In both cases, spindle-shaped cells were detected loosely distributed throughout collagen gels. Therefore, an excess of

myoepithelial cells produced more structures that better resemble the rounded and hollow architecture of *in vivo* breast acini.

3.4.7 Distribution of myoepithelial cells in 3D *in vitro* dual-culture model with HB2 cells

Distribution of GFP Myo1089 cells in dual-cultures with HB2 cells was visualised by IHC using anti-tGFP representative images from three technical replicates presented (Fig 3.14). tGFP staining was observed in rounded cells attached around the edges of HB2 units under optimised conditions. This confirmed the spheroid units observed by H & E staining consisted of HB2 cells and not GFP Myo1089 cells.

3.4.8 Optimisation of time in culture of 3D *in vitro* dual-culture model with myoepithelial and HB2 luminal cells

In order to determine the maximum length of time in culture that could sustain the production of HB2 acini-like structures under optimum media and cell ratio conditions described above, HB2 cells were cultured in 3D collagen gels for up to 35 days with GFP Myo1089 cells and examined at 7 day intervals (Fig 3.15). Representative images from three technical replicates presented. Visualisation by H & E staining demonstrated that after 7 days, small cohesive rounded structures were formed with no lumen formation detected. After 14 days, structures appeared larger with evidence of some lumen formation in their centres and after 21 days in culture, wide and cleared lumens were detected within structures surrounded by a thinner layer of epithelial cells. However, culture for longer than 21 days saw a loss in cohesive architecture of HB2 structures with remaining structures consisting of discohesive cells and containing large breaches. Therefore, 21 days was deemed the maximum length of time for culture and yielded structures that most resembled breast *in vivo* breast acini architecture.

To summarise, the optimal conditions for co-culture of HB2 cells with GFP Myo1089 cells in the 3D *in vitro* model determined through these experiments were as follows:-

- Culture medium: 50% GFP Myo1089 cell specific medium with 50% FCM
- Cell ratios: 3 parts GFP Myo1089 cells: 1 part HB2 cells
- Maximum length of time in culture: 21 days

3.4.9 Characterisation of 3D *in vitro* dual-culture model with HB2 cells

Characterisation of the 3D dual-culture model cultured under optimised conditions above was assessed by IHC with representative images from three technical replicates presented (Fig 3.16). Under optimal conditions, HB2 cells formed units that expressed E-Cad at cell-cell junctions and EMA was concentrated at the apical-lumen interface of HB2 cells. Cell apoptosis was limited to central lumens of HB2 units as demonstrated by M30 staining. Vim and αSMA was specific to GFP Myo1089 cells and HB2 cells remained negative. Basement membrane protein production was evident in GFP Myo1089 cells only around the outer edges of HB2 units as demonstrated by Coll IV and TN-C staining. Overall, HB2 cells exhibited a luminal epithelial phenotype and GFP Myo1089 a myoepithelial phenotype in 3D culture in collagen I.

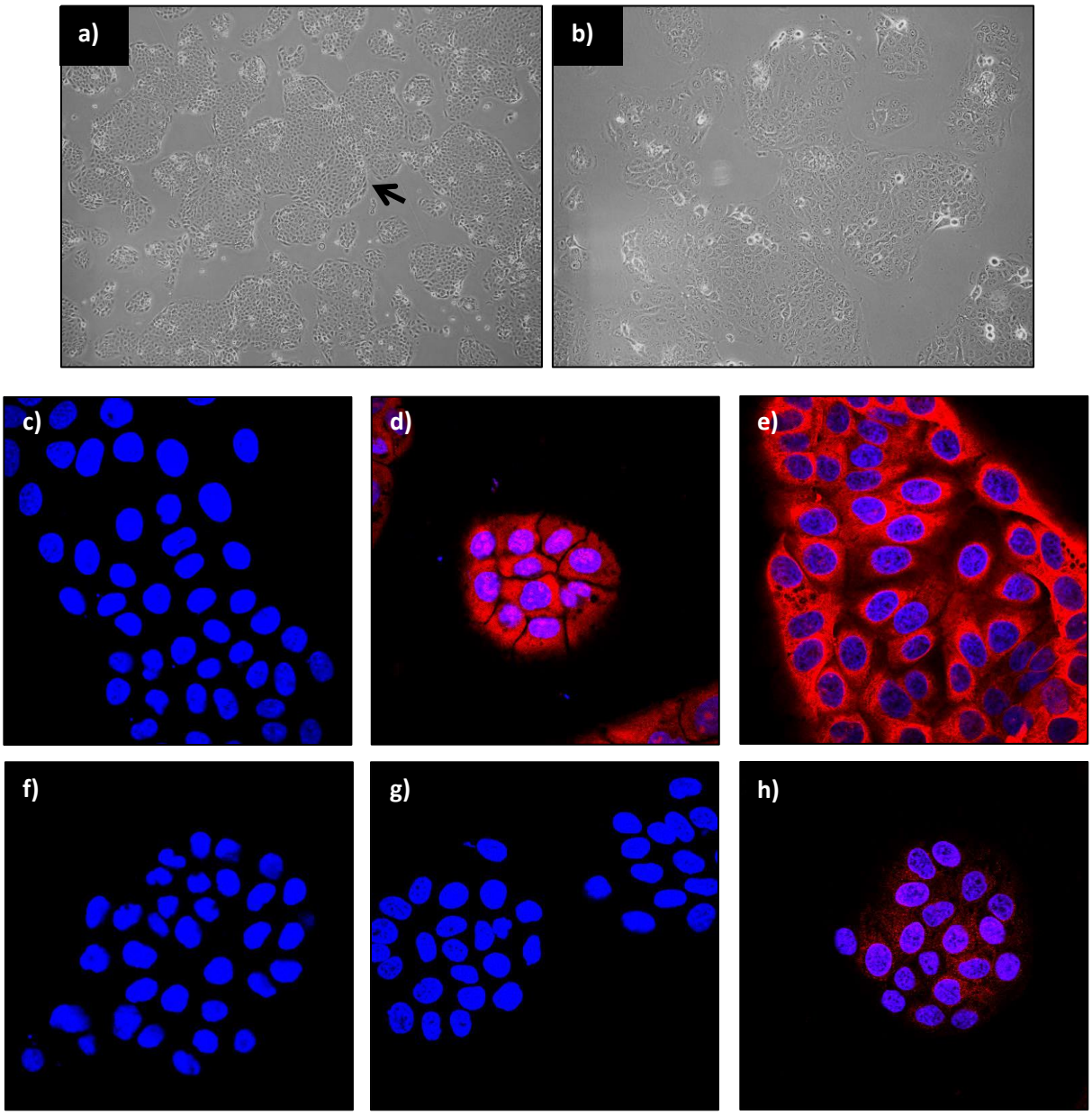

Fig 3.11 Morphology and characterisation of HB2 cells using phase contrast microscopy and fluorescence microscopy

Phase contrast microscopy of HB2 cells demonstrated formation of an adhesive cell monolayer arranged in clusters (arrow a, original magnification 4x) consisting of rounded and cohesive cells (b, arrows, original magnification 20x). HB2 cells were characterised by immunofluorescence staining with a panel of antibody markers and visualised using Texas Red (red) with nuclei visualised using DAPI (blue). Representative images from three biological replicate experiments presented. Primary antibody was omitted to serve as a negative control (a).100% of cells stained positive for the luminal epithelial markers EMA (d) and CK18 (e) and negative for the myoepithelial markers CK5/6 (f) and αSMA (g). Vim staining was detected in all cells (h) but was weaker than for the luminal markers tested. All images taken at 63x magnification.

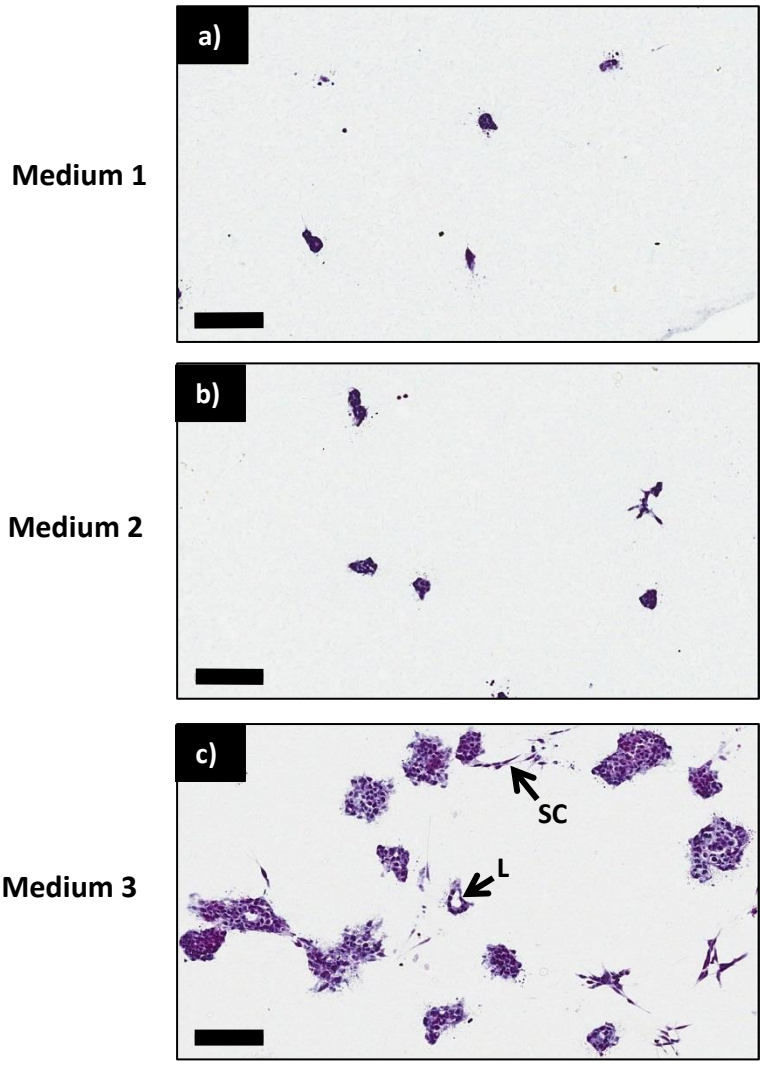

Fig 3.12 H & E staining of 3D *in vitro* dual-culture models of HB2 cells with myoepithelial cells in different cell culture media conditions

HB2 cells were cultured with GFP positive myoepithelial cells (GFP Myo1089) in 3D collagen gels for 7 days in Medium 1 (100% DMEM + 10% FCS, 10µg/ml Insulin & 5µg/ml Hydrocortisone), Medium 2 (50% Medium 1: 50% fibroblast conditioned medium) or Medium 3 (50% HAMF12 Nutrient mixture + 10% FCS, 10ng/ml EGF, 10µg/ml Insulin & 5µg/ml Hydrocortisone: 50% fibroblast conditioned medium). 5µm sections of gels were stained with H & E and representative images from three technical replicates taken. Culture in either medium 1 (a) or medium 2 (b), yielded small compact units which were sparse throughout the collagen gels. Upon culture with medium 3 (c), much larger units were detected with evidence of some lumen formation (L) and spindle-shaped cells (SC) loosely distributed throughout the collagen gel. Original magnification 20x, scale bars = 100µm.

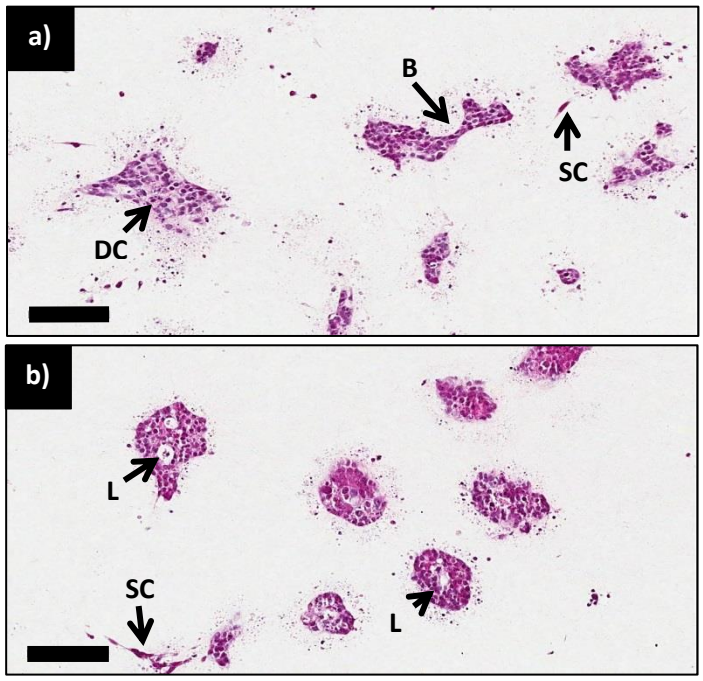

Fig 3.13 H & E staining of 3D *in vitro* dual-culture models comparing different cell ratios of HB2 cells with myoepithelial cells

HB2 cells were cultured with GFP positive myoepithelial cells (GFP Myo1089) in 3D collagen gels for 14 days in a 1:1 (1 part GFP Myo1089 cells to 1 part HB2 cells) or a 3:1 (3 parts GFP Myo1089 cells to 1 part HB2 cells) cell ratio. 5µm sections of gels were stained with H & E and representative images from three technical replicates taken. With a 1:1 cell ratio (a), large elongated units were observed consisting in some cases of discohesive cells (DC) with some evidence of branching (B). With a 3:1 cell ratio (b), cell units appeared more rounded with more evidence of lumen formation (L). Spindle-shaped cells (SC) were detected loosely distributed throughout the collagen gel in both cases. Original magnification 20x, scale bars = 100µm.

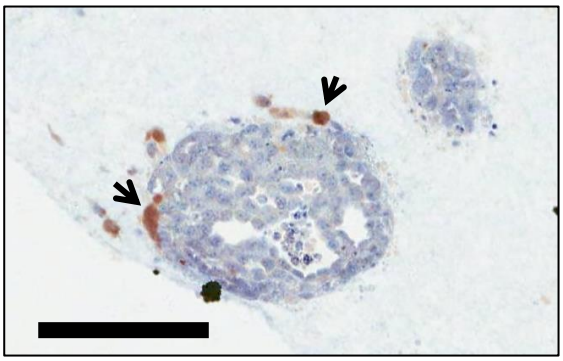

Fig 3.14 Immunohistochemical labelling of myoepithelial cells in 3D *in vitro* dual-culture model with HB2 cells under optimal conditions

HB2 cells were cultured with GFP positive myoepithelial cells (GFP Myo1089) in 3D collagen gels for 21 days. 5µm sections of gels were stained with anti-tGFP by IHC to visualise distribution of myoepithelial cells within gels. Representative images from three technical replicates presented. tGFP staining was detected in rounded cells distributed around the outer edges of HB2 cell units (arrows). Original magnification 20x, scale bars = 100µm.

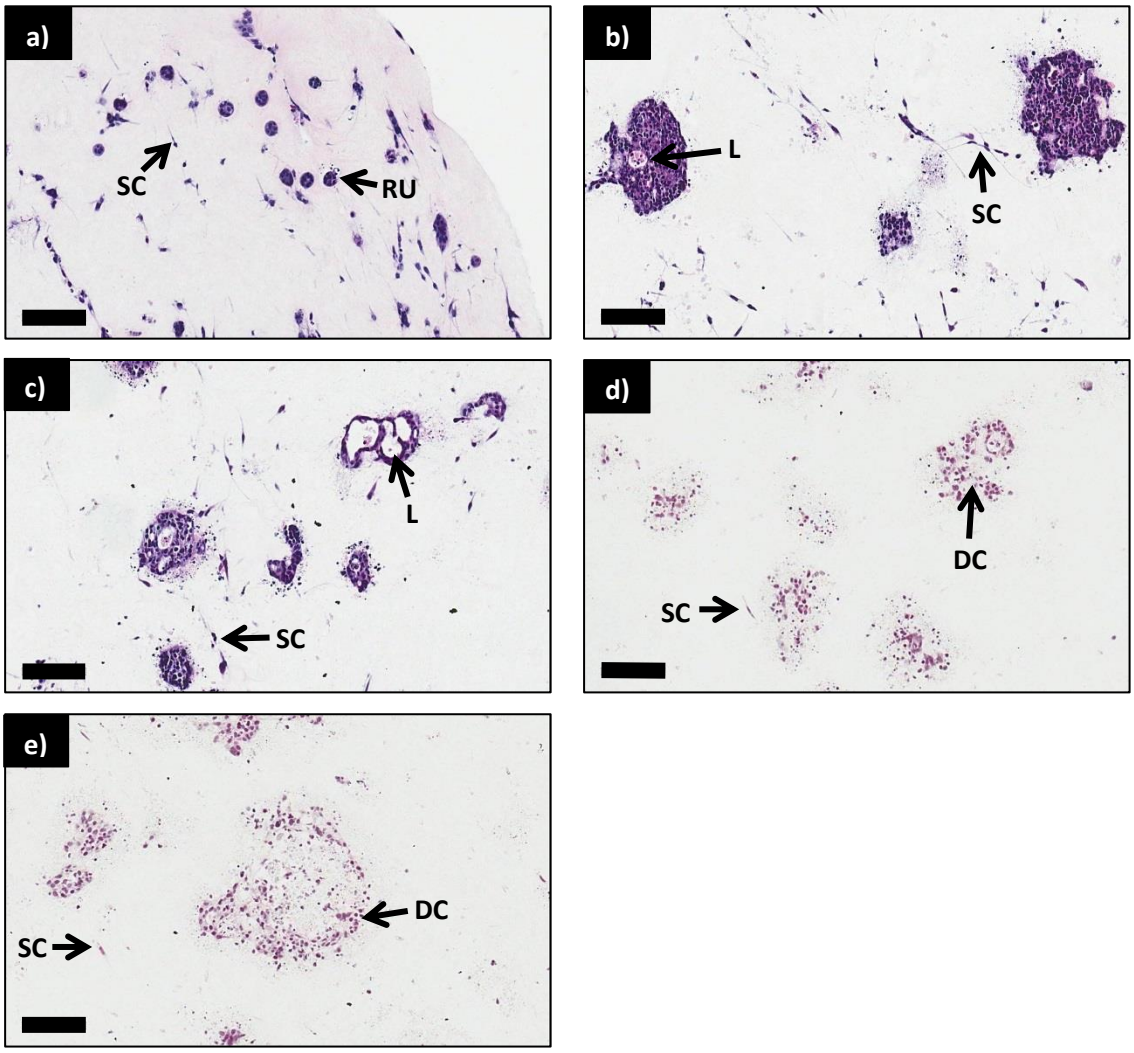

Fig 3.15 H & E staining of 3D *in vitro* dual-culture models of HB2 cells with myoepithelial cells at different time-points in culture

HB2 cells were cultured with GFP positive myoepithelial cells (GFP Myo1089) in 3D collagen gels for up to 5 weeks and examined at 1 week intervals. 5µm sections of gels were stained with H & E and representative images from three technical replicates taken. Culture for 1 week (a) yielded small cohesive rounded units (RU). After 2 weeks in culture (b), units appeared much larger with evidence of lumen formation (L). Culture for 3 weeks (c) produced units with much wider cleared lumens (L). After 4 (d) and 5 (e) weeks, units were less compact and consisted of discohesive cells (DC). Spindle-shaped cells (SC) loosely distributed throughout the collagen gels featured at all time points. Original magnification 20x, scale bars = 100µm.

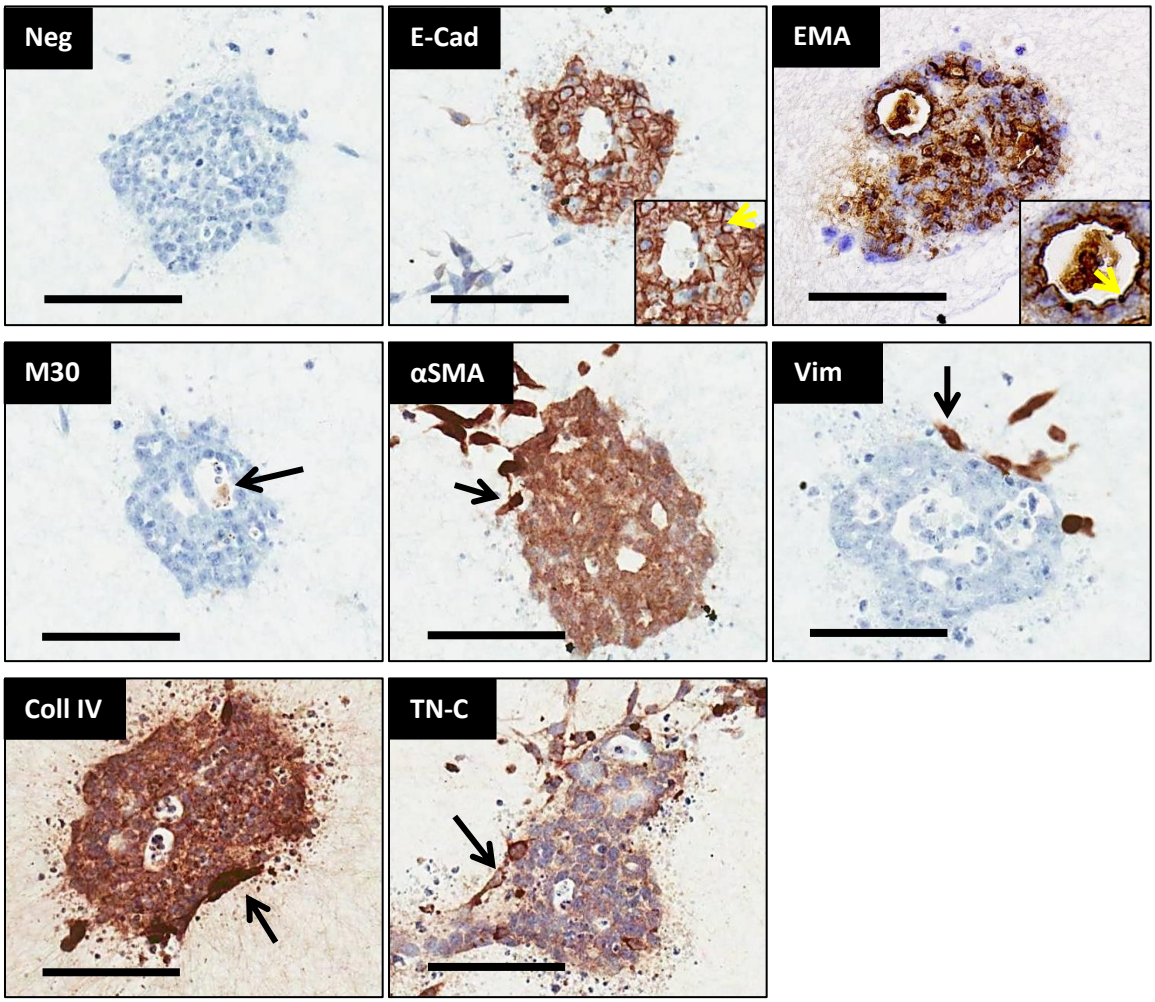

Fig 3.16 Immunohistochemical characterisation of 3D *in vitro* dual-culture model with HB2 cells

In vitro dual-culture model containing GFP Myo1089 cells with HB2 cells were characterised by IHC. Representative images from three technical replicates presented. Primary antibody was omitted to serve as a negative control (Neg). E-cadherin (yellow arrow, inset, E-Cad) staining was detected between cell-cell junctions of all HB2 units. Epithelial membrane antigen (yellow arrow, inset, EMA) staining was concentrated at the apical-lumen interface of HB2 cells and M30 staining was specific to lumens of HB2 units (arrow, M30). α-smooth muscle actin (arrow, αSMA) and vimentin (arrow, Vim) was specific to GFP Myo1089 cells. Collagen IV (arrow, Coll IV) and similarly tenascin-C (arrow, TN-C) was found concentrated at the outer edges of HB2 units. Original magnification 20x, scale bars = 100µm. Inset images for E-Cad and EMA magnified using to Microsoft Word to highlight areas of interest.

3.4.10 Characterisation of fibroblast cell line HMFU19

As discussed, a major functional component of *in vivo* breast is stromal fibroblasts and inclusion of which in our 3D *in vitro* model was deemed essential in accurately representing normal breast tissue architecture. We first considered the use of the cell line HMFU19 as a representative fibroblast component for our study and assessed their suitability via examination of their morphology and phenotype (Fig 3.17). In 2D culture, HMFU19 cells displayed an elongated spindle-shaped morphology and formed a discohesive monolayer. HMFU19 cell phenotype was examined by immunofluorescence with representative images from three biological replicate experiments presented. HMFU19 cells exhibited a mixed phenotype as all cells displayed both positive staining for epithelial-associated cytokeratins 14 and 18 and strong staining for fibroblast associated vim. Strong αSMA staining was also detected in ~25% of cells. On inspection of immunofluorescence staining it was also noted that cells exhibited a mixed morphology with some fibroblast-like elongated spindle-shaped cells and some fatter rounded cells with lamellipodia formation. Overall, it appeared that these fibroblasts represent a myofibroblast/activated cell population presenting a need to source a more appropriate fibroblast cell line for the model.

3.4.11 Isolation and hTERT transduction of fibroblasts from primary breast reduction mammoplasty tissue

Following appropriate ethical approval as described in Chapter 2, a breast reduction mammoplasty sample was selected in order to produce a normal fibroblast cell line to include in the 3D tri-culture model of normal breast. The breast reduction mammoplasty tissue was digested and processed as described in Chapter 2 and yielded a monolayer of dispersed cells with an elongated spindle-shaped morphology characteristic of breast fibroblasts (Fig 3.18). To produce a fibroblast cell population that could be cultured longer term, fibroblasts at passage 2 were engineered to overexpress hTERT via retroviral transduction with pBabe-hTERT-neo vector by Dr Euan Baxter

(Leeds Institute of Cancer and Pathology) and designated LS11-083 hTERT fibroblasts. Both primary and LS11-083 hTERT fibroblasts were cultured for 21 days to assess their longevity in culture. Over 21 days, primary fibroblasts underwent 5 passages. Following passage 5, primary fibroblasts were lost demonstrated by a lack of adherent cells and the appearance of rounded floating bodies in the culture medium. In this time, LS11-083 hTERT fibroblasts underwent 12 passages and retained an elongated spindle-shaped morphology and grew in characteristic "whorls" reminiscent of cultured breast fibroblasts.

3.4.12 Production and characterisation of a dsRed positive fibroblast cell line

To enable the tracking of LS11-083 hTERT fibroblasts in 3D tri-culture with GFP Myo1089 and HB2 cells, LS11-083 hTERT fibroblasts were lentivirally transduced with pFURW-dsRed empty vector plasmid. FACS was used to sort cells and produced a 100% dsRed positive LS11-083 hTERT fibroblast population which retained an elongated spindle-shaped morphology (Fig 3.19). These were termed LS11-083 dsRed Fibs throughout the study. 100% of LS11-083 dsRed Fibs stained uniformly for vim and were 100% negative for cytokeratin 14, cytokeratin 18 and EMA epithelial markers. LS11-083 dsRed Fibs were also negative for αSMA indicating that these fibroblasts do not represent a myofibroblast/activated fibroblast population. Representative immunofluorescence images from three biological replicate experiments presented.

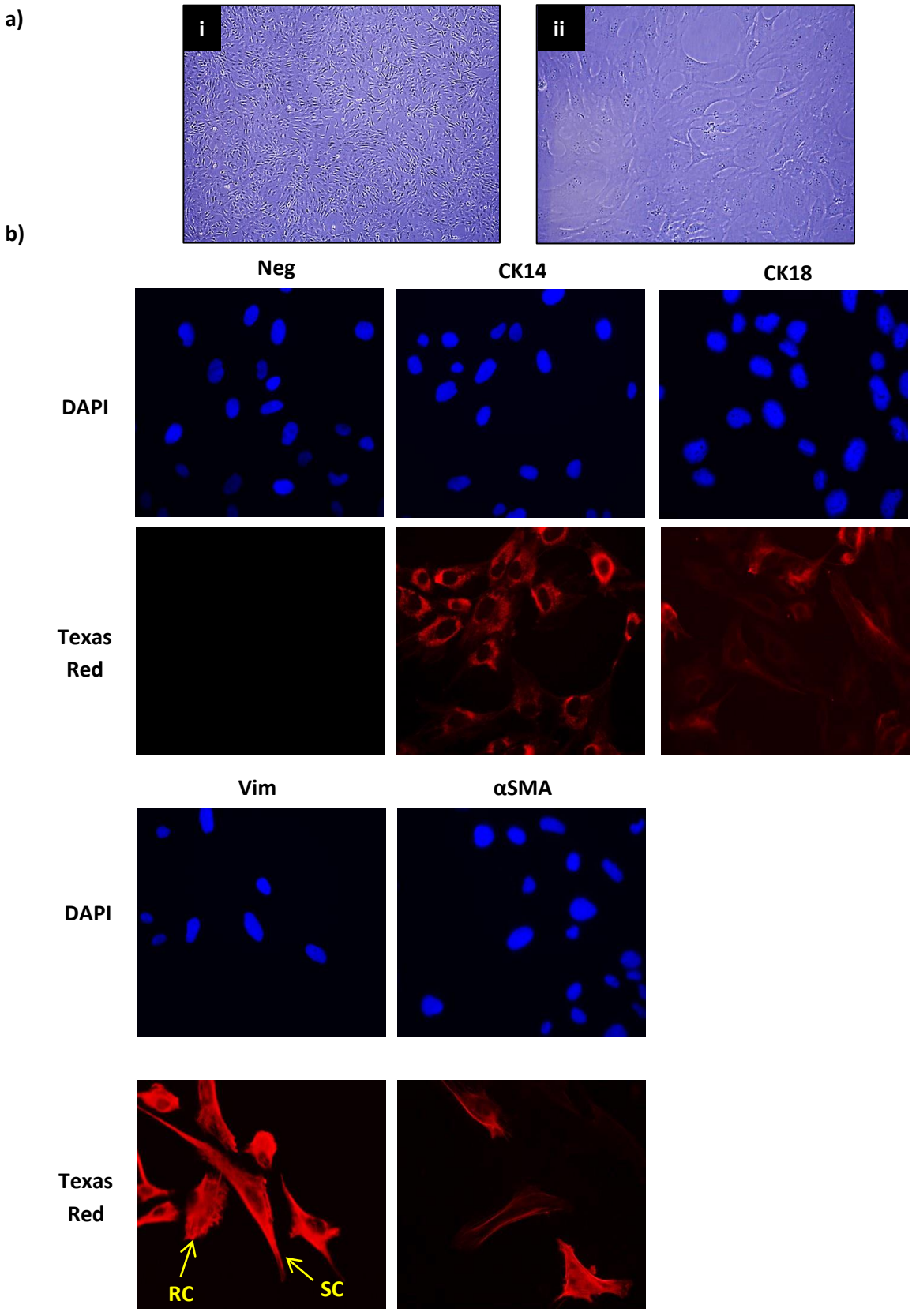
a)
i
ii
b)
Neg
CK14
CK18
DAPI
Texas Red
Vim
αSMA
DAPI
Texas Red
RC
SC

Fig 3.17 Morphology and characterisation of HMFU19 cells using phase contrast microscopy and fluorescence microscopy

Phase contrast microscopy allowed visualisation of HMFU19 cells cultured in 2D (a). HMFU19 cells grew in a discohesive monolayer (i, original magnification 4x) consisting of elongated spindle-shaped cells (ii, original magnification 20x). HMFU19 cells were characterised by immunofluorescence (b) staining with a panel of antibody markers and visualised using Texas Red (red) with nuclei visualised using DAPI (blue). Representative images from three biological replicate experiments presented. Primary antibody was omitted to serve as a negative control (Neg). 100% of cells stained positive for cytokeratin 14 (CK14) with over 90% of cells also positive for cytokeratin 18 (CK18) which are both epithelial markers. While all cells were positive for the fibroblast marker for vimentin (Vim), cells with a more rounded morphology with evidence of lamellipodia formation (RC) were detected as well as fibroblast-like spindle-shaped cells (SC). α-smooth muscle actin staining (αSMA) was detected in ~25% of cells and further demonstrated cell populations with a lack of characteristic fibroblast morphology. All immunofluorescence images taken at 63x magnification using a Nikon C1 confocal microscope.

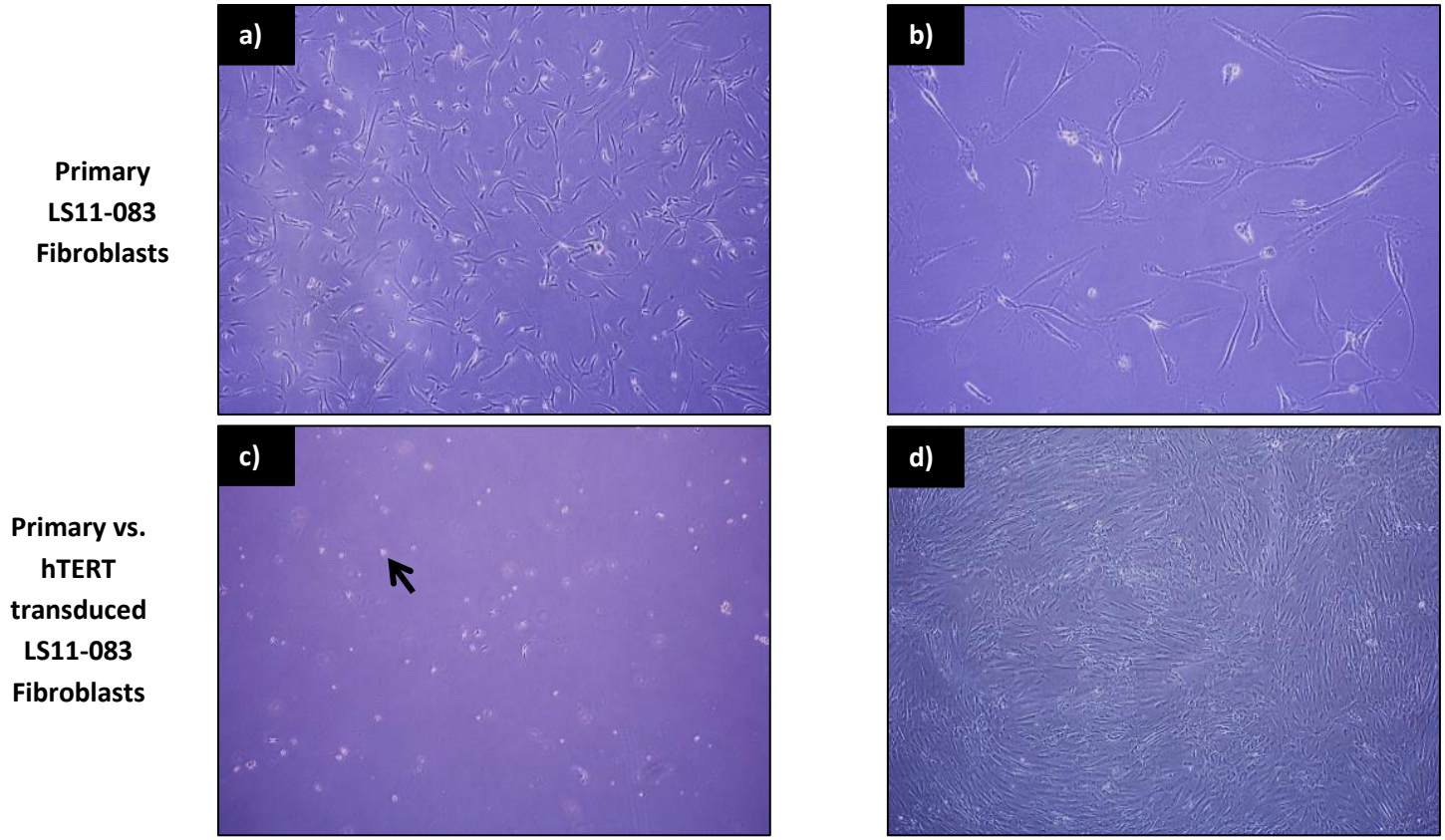

Fig 3.18 Morphology of primary fibroblasts compared to hTERT transduced fibroblasts

Phase contrast microscopy of primary fibroblasts shows a mono layer of dispersed cells (a, original magnification 4x) which consist of an elongated spindle-shaped morphology (b, original magnification 10x). Cell death of primary fibroblasts at passage 5 is demonstrated by lack of adhered cells and appearance of rounded floating bodies in the medium (arrow, c) whereas virally transduced hTERT fibroblasts at passage 12 (d) are spindle-shaped, adherent and grow in characteristic whorls typical of fibroblasts populations (original magnification of c & d, 4x).

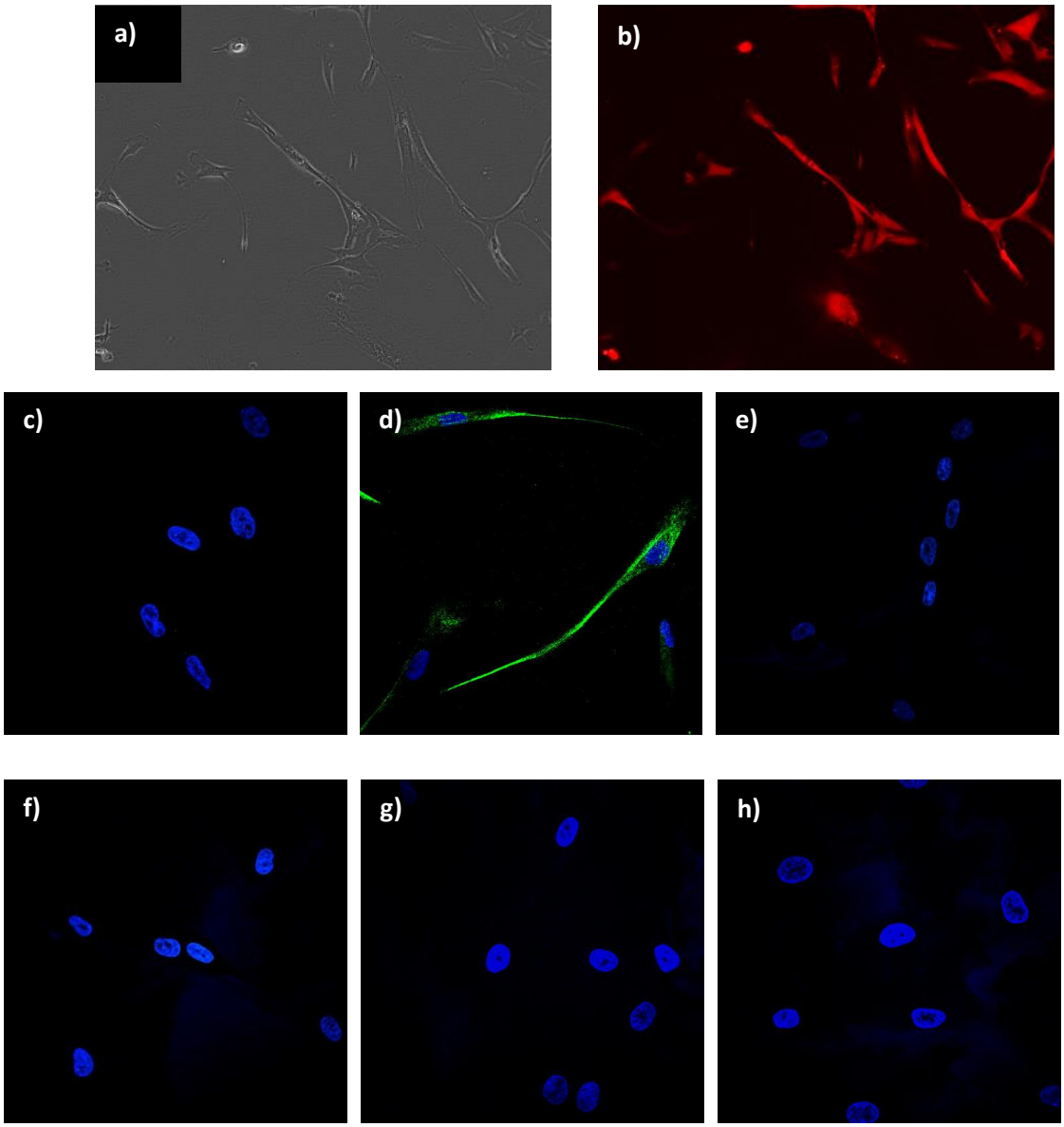

Fig 3.19 dsRed lentiviral transduction and immunofluorescence characterisation of LS11-083 hTERT fibroblasts

LS11-083 hTERT fibroblasts were lentivirally transduced with dsRed protein and FACS sorted to produce a 100% dsRed positive fibroblast population and termed LS11-083 dsRed Fibs. Phase contrast microscopy demonstrated LS11-083 dsRed Fibs retained an elongated spindle-shape morphology (a) and showed >99% positivity for dsRed with fluorescence microscopy (b). Original magnification for (a) and (b) 10x. LS11-083 dsRed Fibs were characterised by immunofluorescence staining with a panel of antibody markers and visualised using FITC (green) with nuclei visualised using DAPI (blue). Representative images from three biological replicate experiments presented. Primary antibody was omitted to serve as a negative control (c). 100% of cells exhibited positive staining for vimentin (d) demonstrating an elongated spindle-shape. All cells were negative for fibroblast activation marker α-smooth muscle actin (e), for myoepithelial marker cytokeratin 14 (f) and for luminal epithelial markers cytokeratin 18 (g) and epithelial membrane antigen (h). All images taken at 63x magnification with a Nikon A1R confocal microscope.

3.4.13 Optimisation of number of fibroblasts in 3D *in vitro* tri-culture model with myoepithelial and HB2 luminal cells

In order to determine an appropriate number of LS11-083 dsRed Fibs to co-culture in a 3D tri-culture in collagen I which does not disrupt the acini-like HB2 architecture with lumen formation, GFP Myo1089 and HB2 cells were cultured together according to previously optimised ratios with the addition of varying numbers of LS11-083 dsRed Fibs for 21 days (Fig 3.20). Representative images from three technical replicates presented. Due to the inclusion of fibroblasts in the culture system and their propensity to thrive in epithelial-associated medium, 50% HB2 medium (DMEM Glutamax + 10% FCS, 10µg/ml insulin & 5µg/ml hydrocortisone) to 50% GFP Myo1089 medium (HAMF12 Nutrient mixture + 10% FCS, 10ng/ml EGF, 10µg/ml insulin & 5µg/ml hydrocortisone) was used for the tri-culture system. FCM, included in the dual-culture system, was omitted. In all culture conditions, elongated, spindle-shaped cells were detected spread throughout collagen gels and appeared to increase with increasing numbers of LS11-083 dsRed Fibs. Culture with $0.1x10^5$ LS11-083 dsRed Fibs retained HB2 structures with lumens which consisted of cohesive cells as seen in dual-cultures. Similar results were attained upon culture with $0.25x10^5$ LS11-083 dsRed Fibs with lumen formation within HB2 units, however, units appeared less cohesive featuring discohesive cells. Culture with $0.5x10^5$, $1x10^5$ and $2x10^5$ LS11-083 dsRed Fibs resulted in disorganised and discohesive HB2 structures with little evidence of lumen formation. In addition, only culture with $1x10^5$ and $2x10^5$ LS11-083 dsRed Fibs caused extensive contraction of gels in some cases leaving gels unanalysable. Therefore, $0.1x10^5$ was considered an appropriate number of LS11-083 dsRed Fibs to include in the tri-culture model with which to retain acini-like HB2 features observed in dual-culture conditions.

3.4.14 Distribution of myoepithelial cells and fibroblasts in 3D *in vitro* tri-culture model

Distribution of GFP Myo1089 cells and LS11-083 dsRed Fibs in tri-cultures with HB2 cells was visualised by IHC using anti-tGFP and anti-dsRed respectively (Fig 3.21). Representative images from three technical replicates presented. tGFP staining was observed in rounded cells associated around the edges of HB2 units. dsRed staining was detected in long spindle-shaped cells in all HB2 gels. These were loosely distributed throughout the collagen gels and on occasions, associated with edges of HB2 units. This confirmed units observed by H & E staining still consisted predominantly of HB2 cells and not GFP Myo1089 cells or LS11-083 dsRed Fibs.

3.4.15 Characterisation of 3D *in vitro* tri-culture model and comparison to normal breast tissue

Immunohistochemical characterisation of the 3D tri-culture model optimised above demonstrated a phenotype strikingly similar to that of the normal breast (Fig 3.22 & 3.23). Representative images from three technical replicates presented. With the addition of LS11-083 dsRed Fibs, HB2 units retained a phenotype as shown in dual-culture with GFP Myo1089 cells. Briefly, E-Cad was expressed at HB2 cell-cell junctions with EMA at apical membranes. Mixtures of proliferative and non-proliferative HB2 cells were identified via Ki67 staining, with cell apoptosis detected within central lumens of units via M30 staining. αSMA was found to be specific to GFP Myo1089 cells while basement membrane production was detected around outer edges of HB2 units via Coll IV expression. Vim expression was detected in both GFP Myo1089 cells and LS11-083 dsRed Fibs. Comparison of these features to normal breast demonstrated strong similarities to breast acini. E-Cad expression was specific to luminal epithelium with EMA sequestered to the apical-lumen interface of acini. Apoptosis featured within the lumens of breast acini as demonstrated by M30 expression and αSMA staining was specific to the myoepithelial layer of breast acini. Coll IV staining was detected in basement

membranes surrounding breast acini with Vim expression seen in both myoepithelial cells and fibroblasts within the breast tissue.

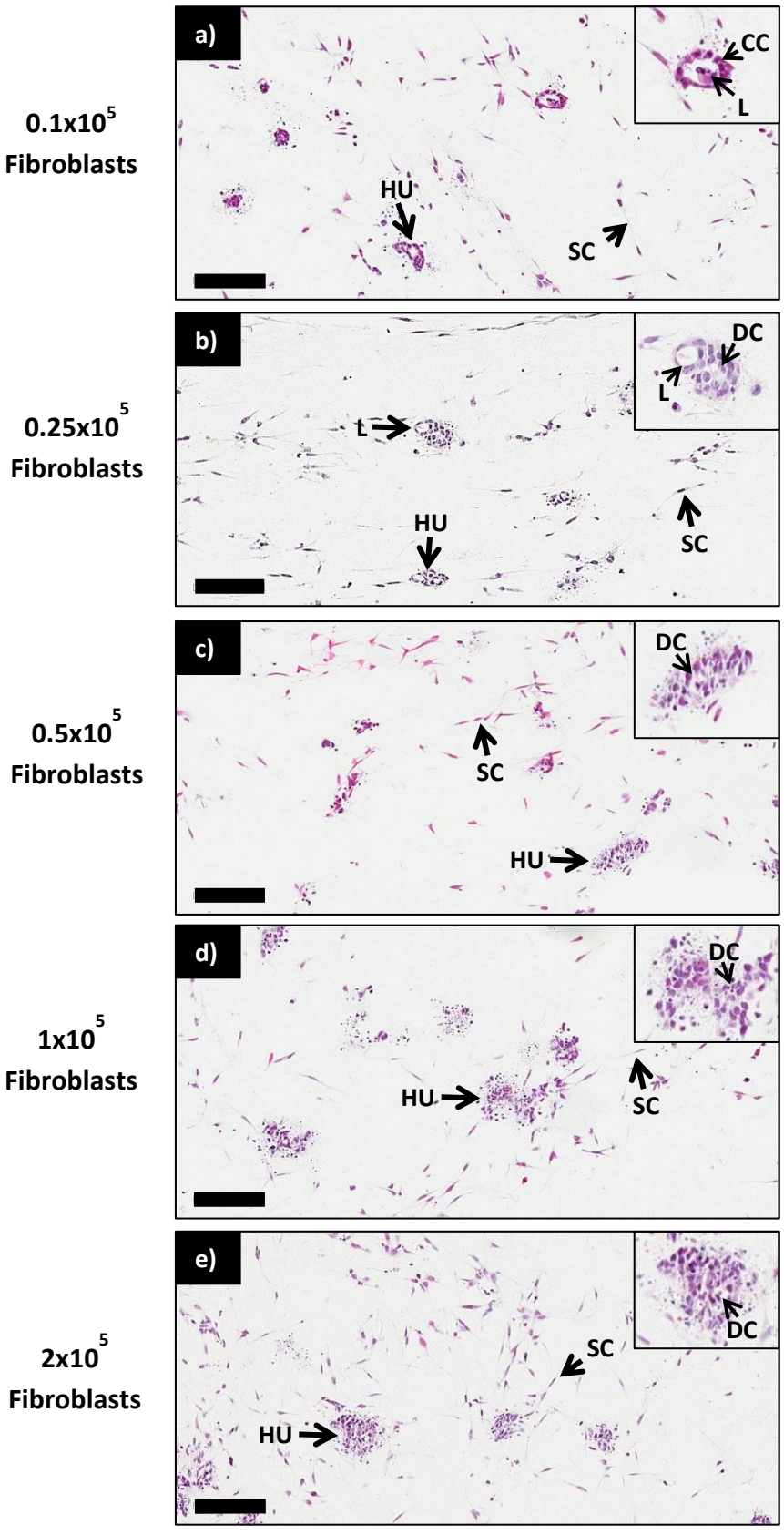
0.1x10^5 Fibroblasts
a)
CC
L
HU
SC
0.25x10^5 Fibroblasts
b)
DC
L
L
HU
SC
0.5x10^5 Fibroblasts
c)
DC
SC
HU
1x10^5 Fibroblasts
d)
DC
HU
SC
2x10^5 Fibroblasts
e)
DC
SC
HU

Fig 3.20 H & E staining of 3D *in vitro* tri-culture models of HB2 cells with myoepithelial cells and different numbers of fibroblasts

HB2 cells were cultured with GFP positive myoepithelial cells (GFP Myo1089) and dsRed positive fibroblasts (LS11-083 dsRed Fib) in 3D collagen gels for 21 days. 5µm sections of gels were stained with H & E and representative images from three technical replicates taken. Regardless of number of LS11-083 dsRed Fibs, all gels featured HB2 units (HU) and spindle-shaped cells (SC) loosely distributed throughout the collagen. Culture with $0.1x10^5$ LS11-083 dsRed Fibs (a) yielded HB2 units with lumens (L) consisting of cohesive cells (CC). HB2 units with $0.25x10^5$ LS11-083 dsRed Fibs (b) similarly contained lumens (L) but featured discohesive cells (DC) compared with $0.1x10^5$ LS11-083 dsRed Fibs. HB2 units cultured with $0.5x10^5$ (c), $1x10^5$ (d) and $2x10^5$ (e) LS11-083 dsRed Fibs all featured discohesive cells (DC) an appeared less organised with no lumen formation. Original magnification 20x, scale bars = 100µm.

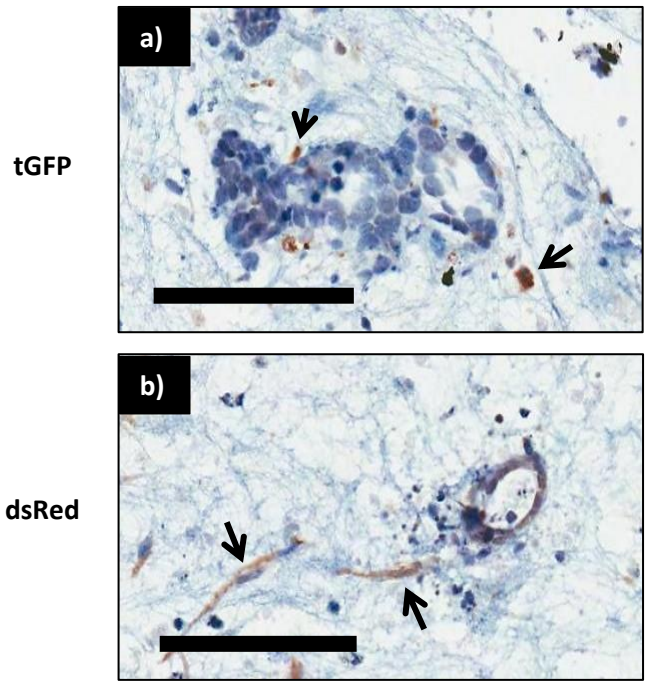

Fig 3.21 Immunohistochemical labelling of myoepithelial cells and fibroblasts in 3D *in vitro* tri-culture model

HB2 cells were co-cultured in 3D collagen gels with GFP positive myoepithelial cells (GFP Myo1089) and dsRed positive fibroblasts (LS11-083 dsRed Fibs) for 21 days. 5µm sections of gels were stained with anti-tGFP and anti-dsRed by IHC to visualise distribution of myoepithelial cells and fibroblasts within gels. Representative images from three technical replicates presented. Positive staining for tGFP was detected in GFP Myo1089 cells distributed around the outer edges of HB2 cell units (arrows, a). dsRed staining highlighted LS11-083 dsRed Fibs loosely distributed throughout collagen gels (arrows, b). Original magnification 20x, scale bars = 100µm.

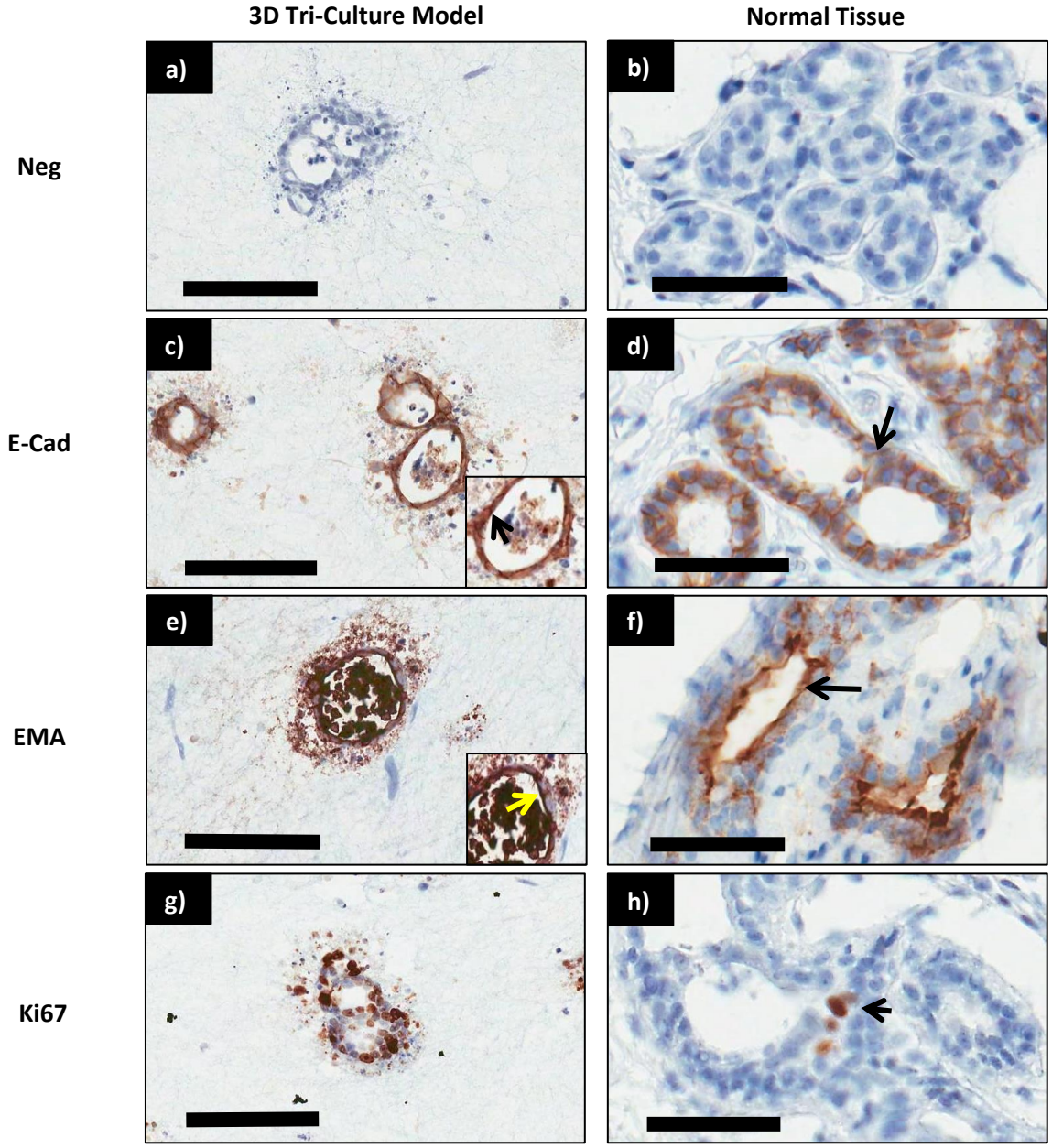

Fig 3.22 Immunohistochemical characterisation of 3D *in vitro* tri-culture model compared to normal human breast tissue A

In vitro tri-culture model containing HB2 cells, GFP Myo1089 cells and LS11-083 dsRed Fibs were characterised by IHC and compared to normal breast tissue sections. Representative images from three technical replicates presented. Primary antibody was omitted to serve as a negative control (a & b). E-cadherin (E-Cad) was expressed by HB2 cells at cell-cell junctions (arrow, c) in keeping with luminal epithelium of breast acini (arrow, d). Strong staining was concentrated at the HB2 cell-lumen interface of HB2 units (yellow arrow, e) and was specific to apical membranes of luminal epithelium of breast acini (arrow, f). The majority of cells within HB2 units were positive for Ki67 (g) while few Ki67 positive cells were detected within breast acini (arrow, h). Original magnification for tri-culture model (a, c, e & g) 20x, scale bars = 100µm. Original magnification for normal tissue (b, d, f & h) 40x, scale bars = 50µm.

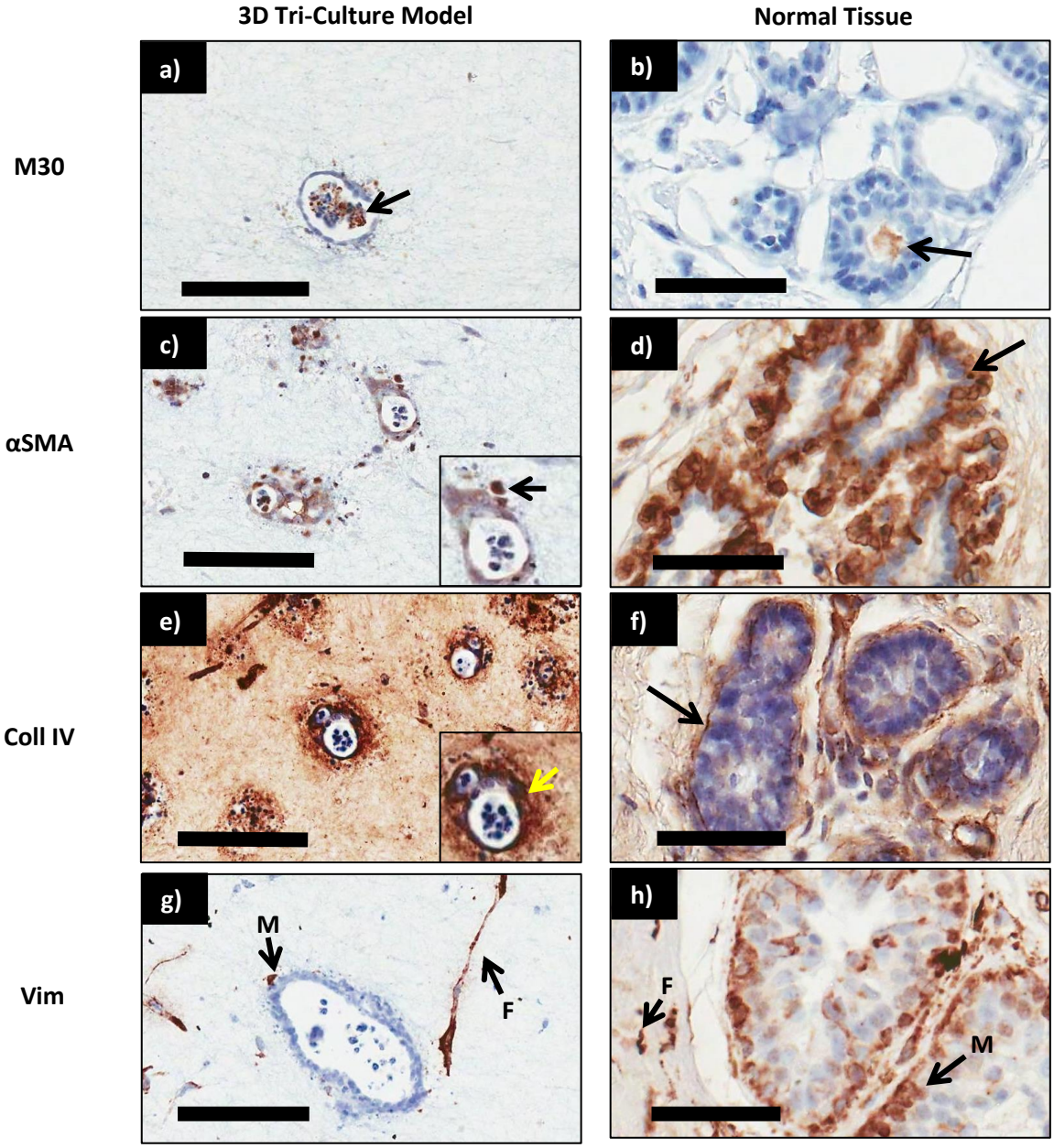

Fig 3.23 Immunohistochemical characterisation of 3D *in vitro* tri-culture model compared to normal human breast tissue B

In vitro tri-culture model containing HB2 cells, GFP Myo1089 cells and LS11-083 dsRed Fibs were characterised by IHC and compared to normal breast tissue sections. Representative images from three technical replicates presented. M30 staining was detected within lumens of HB2 units (arrow, a) comparable to M30 staining observed within lumens of breast acini (arrow, b). α-smooth muscle actin (αSMA) was observed in rounded myoepithelial cells on the outer edges of HB2 units (arrow, c) while a continuous layer of αSMA positive myoepithelial cells surround luminal epithelial cells of breast acini (arrow, d). Collagen IV (Coll IV) was concentrated around outside edges of HB2 units (yellow arrow, e) and similarly is demonstrated encapsulating breast acini (arrow, f). Vimentin (Vim) staining was detected in both rounded GFP Myo1089 cells (M) on outer edges of HB2 units and spindle-shaped LS11-083 dsRed Fibs (F) in the tri-culture model (g) analogous to Vim positivity in myoepithelial cells (M) and fibroblasts (F) in normal breast tissue (h). Original magnification for tri-culture model

(a, c, e & g) 20x, scale bars = 100µm. Original magnification for normal tissue (b, d, f & h) 40x, scale bars = 50µm.

3.4.16 Optimisation of quantification methods for number and size of HB2 units

It was considered necessary to determine a method of quantifying the co-unit structures observed in the model in order to make it a more viable model for research, and in order to elucidate any changes in structural features in a scientific manner. In order to determine whether the depth of an individual gel had an effect on the number and area of HB2 units formed and thus to determine an appropriate number of sections to use for quantification, 10 x 5µm H & E stained serial sections from a single representative 3D tri-culture gel were quantified using Aperio Imagescope software (Fig 3.24). Quantification of number of HB2 units showed variation between individual serial sections but did not systematically increase or decrease when traversing through the gel. No significant correlation between the mean number of units to the depth of gel section was observed upon calculation of the Pearson product-moment correlation coefficient using GraphPad Prism software (p= 0.1931). The coefficient of variation for number of units was calculated as a running coefficient of variation and demonstrated that quantification of one section gave a coefficient of variation from the mean of 10 sections of 13%. As serial sections were sequentially calculated this steadily decreased and dropped to 9.52% upon quantification of 10 serial sections.

Quantification of area of HB2 units (Fig 3.25) demonstrated no significant correlation between the mean area of units to the depth of gel section upon calculation of the Pearson product-moment correlation coefficient using GraphPad Prism software (p=0.0779). The coefficient of variation for area of units was calculated as a running coefficient of variation and demonstrated that quantification of one section gave a coefficient of variation from the mean of 10 sections of 11.6%. As serial sections were sequentially calculated this steadily decreased and dropped to 9.36% upon quantification of 8 serial sections but then rose to 17.2% upon quantification of 10 serial sections. This suggests sections taken from greater than 40µm contains units with areas that are not representative of the mean population. The running

mean area of HB2 units plotted against the number of units counted demonstrated that the mean area taken from 80 measurements or upwards gave a good representation of the mean taken from all 10 serial sections. Quantification of the number of units showed that the mean number of units per section was between 62 and 90 units which indicated that to get a good representation of the mean area of HB2 units from 10 serial sections, one section could be quantified.

Taken together, it was reasoned that by taking one section from the gel at a depth between 15µm and 40µm would give a sufficient representation of the mean area of HB2 units from 10 serial sections and would give a count of number of units with an error of 13% and an area of units with an error of 11.6%. Therefore, quantifying one section taken from an appropriate depth of a gel was reasoned to be a satisfactory method of quantifying area and number of HB2 units.

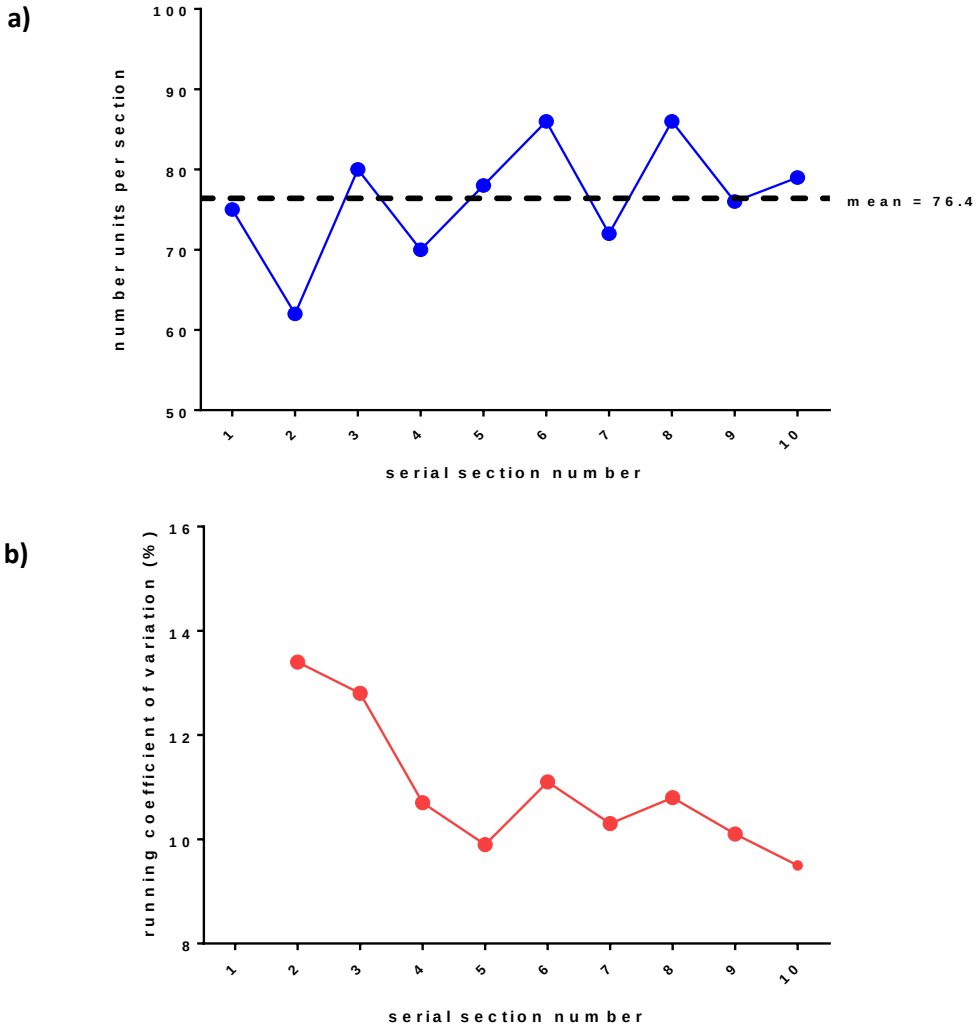

Fig 3.24 Quantification of number of HB2 units in 3D tri-culture gels from 10 H&E stained serial sections

10 x 5µm serial sections of one representative 3D tri-culture gel were stained with H&E. Number and area (µm^2) of HB2 units from each serial section were quantified with Aperio Image scope and analysed with Graph Pad Prism 6 software. (a) The total mean number of HB2 units from all 10 sections was calculated and is denoted by the dashed line. While the number of HB2 units did vary between sections, the numbers did not systematically increase or decrease when traversing through the gel as demonstrated by quantification of serial sections. Correlation analysis for number and depth of gel demonstrated no significant trend when traversing through the gel (p=0.1931, Pearsons product-moment correlation coefficient). (b) The running coefficient of variation demonstrated that taking one section gives an error of 13% to the total mean across 10 serial sections. This error falls to 9.52% upon quantification of 10 serial sections.

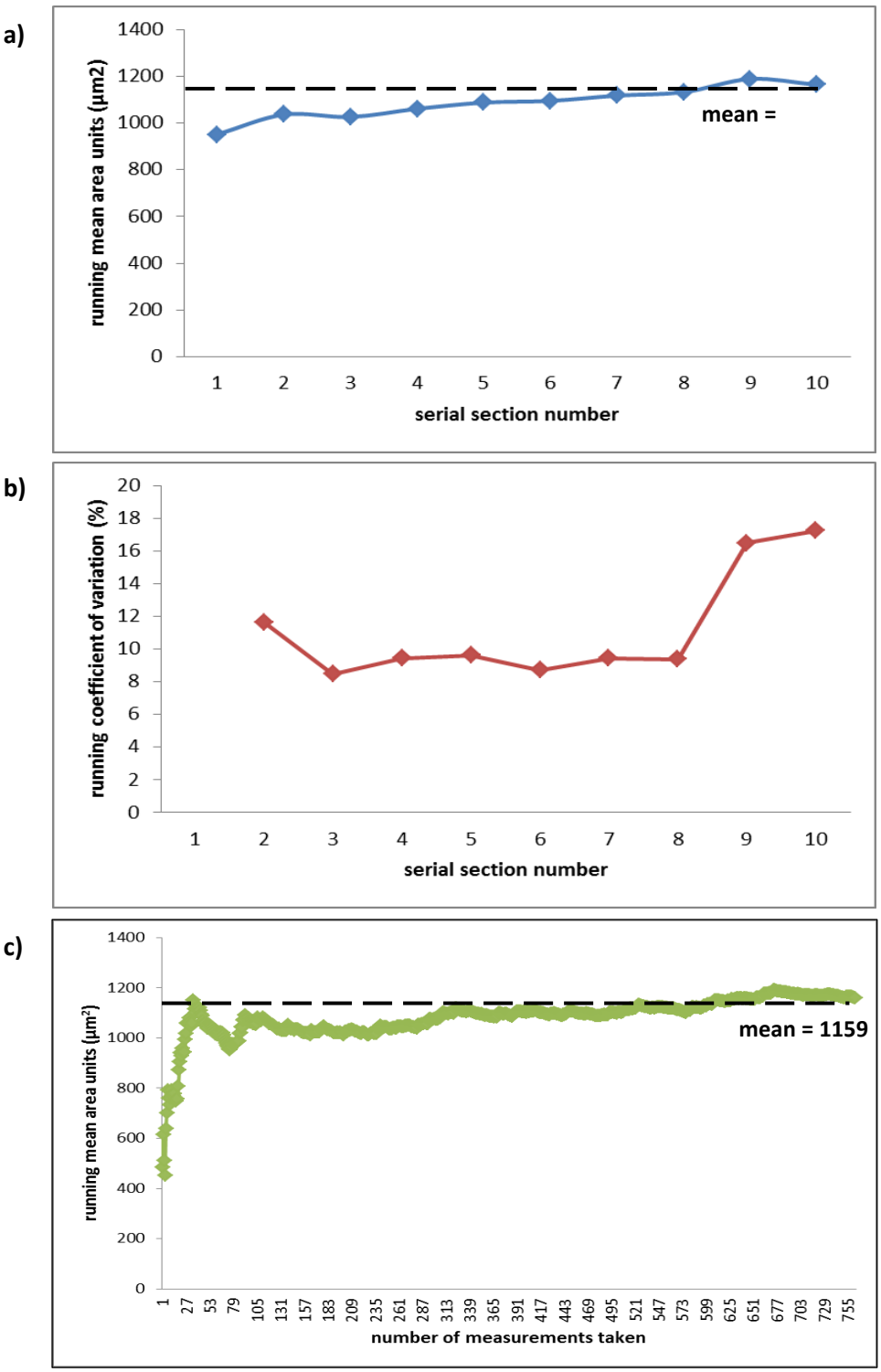

Fig 3.25 Quantification of area of HB2 units in 3D tri-culture gels from 10 H & E stained serial sections

10 x 5µm serial sections of 1 representative 3D tri-culture gel were stained with H & E. Area of HB2 units (µm^2) from each serial section were quantified with Aperio Image scope and analysed with Microsoft Excel and Graph Pad Prism 6 software. The total mean area of HB2 units from all 10 sections was calculated and is denoted by the dashed lines. (a) The running mean area of units demonstrated that size of units did not significantly increase or decrease

when traversing through the gel as demonstrated by quantification of serial sections. Correlation analysis for area and depth of gel demonstrated no significant trend when traversing through the gel ($p=0.0779$, Pearsons product-moment correlation coefficient). (b) The running coefficient of variation demonstrated that taking 1 section gives an error of 11.6% to the total mean across 10 serial sections. This error falls to 9.36% upon quantification of 8 serial sections. mean of all measurements of HB2 unit area taken across all 10 sections was calculated to determine an appropriate sample size for quantification. This demonstrated that the mean area of HB2 units calculated from approximately 80 units and upwards gives a good estimate of the mean for the whole population from 10 serial sections. (c) The running mean of all measurements of HB2 unit area taken across all 10 sections was calculated to determine an appropriate sample size for quantification. This demonstrated that the mean area of HB2 units calculated from approximately 80 units and upwards gives a good estimate of the mean for the whole population from 10 serial sections.

3.5 Discussion

Traditionally, breast cancer studies have focussed on the transition of luminal epithelial cells from a pre-invasive to an invasive state while less emphasis has been put on investigating the earlier stages of breast cancer initiation and carcinogenesis. In order to address this, an appropriate 3D model of normal breast tissue would be required that incorporates all three of the major cell types of breast and that is representative of *in vivo* breast tissue. Research groups striving to elucidate the mechanisms behind luminal epithelial transformation have relied on the use of MCF10A cells in 3D basement membrane preparations with either fibroblasts or fibroblasts with endothelial cells or adipocytes [201, 204, 212]. While these models provide a more sophisticated 3D environment in which cells can propagate, breast tissue consists predominantly of collagen I and thus would be a more appropriate matrix for an *in vitro* model of breast. In addition, myoepithelial cells have largely been neglected in these studies despite their presence in normal *in vivo* breast tissue, their loss in the transition from DCIS to invasive cancer [213] and despite evidence of their tumour suppressive nature [71, 214]. While Holliday et al produced a such a model of DCIS, analysis was costly and laborious and involved the use of cell tracker dyes which limited culture to 7 days [149].

Therefore, in this series of experiments we endeavoured to develop a longer term and easily analysable 3D *in vitro* model that included both myoepithelial cells and fibroblasts with luminal epithelial cells in the physiologically relevant matrix of collagen I. By validating against normal breast reduction mammoplasty tissue during model development, we aimed to validate that the model recapitulated the features and phenotype of *in vivo* breast acini.

To produce such a model, the gold standard would have been to use individual cell populations isolated from primary breast tissue. However, in order to optimise a model without wasting valuable material and without introducing complications such as donor variability, representative luminal and myoepithelial cell lines were used to optimise a dual-culture model

in the first instance. Both the commonly used cell line MCF10A and less commonly used cell line HB2 were used to represent luminal epithelium. The cell line Myo1089 was used to represent the myoepithelium.

One of the first hurdles to overcome in developing this model was distinguishing between luminal epithelial and myoepithelial cells in culture due to their similarities in cell morphology. Lentiviral vectors are a widely used tool to deliver exogenous genes into cells [215]. These genes can be advantageous in that they can assign a specific characteristic to a cell such as fluorescence which can be used to track cells in culture [216]. We applied this concept to track Myo1089 cells in culture via stable transduction with turbo green fluorescent protein (tGFP) using pGIPZ lentiviral vector. Production of GFP Myo1089 cells and identification of a suitable tGFP antibody for IHC allowed us to distinguish between GFP Myo1089 cells and either MCF10A cells or HB2 cells during longer term culture of these cells in 3D.

3.5.1 Choice of representative normal luminal epithelial cell for the model

Since the use of MCF10A cells as a representative of "normal" luminal epithelium is well documented, we attempted to incorporate these cells in our 3D co-culture model with GFP Myo1089 cells in collagen I. It was first noted that MCF10A cells were plastic in culture with a mixture of luminal- and basal-like cell morphologies observed as a 2D monolayer. This was confirmed through immunofluorescence characterisation which demonstrated expression of luminal markers EMA and cytokeratin 18 as well as basal/myoepithelial markers cytokeratin 14, β4-integrin and αSMA. The use of immunomagnetic beads to isolate different populations of breast epithelial cells has been previously described [183, 217]. Since β4-integrin is a transmembrane receptor which is specific to basal/myoepithelial cells of the breast [18], and was expressed by a sub-set of our MCF10A cells, we attempted to isolate sub-populations of basal-like MCF10A cells from luminal-like MCF10A cells via β4-integrin coated Dynabead separation. The two separate sub-populations were designated MCF10A Luminal (β4-integrin

negative) and MCF10A Basal (β4-integrin positive) and these along with MCF10A wildtype cells were co-cultured with GFP Myo1089 cells in collagen I in three separate 3D *in vitro* dual-culture models and compared. Since fibroblasts are proven to influence arrangement and growth of mammary epithelial cells [218] and conditioned media has been validated to serve as a substitute for using fibroblast cells in culture [219], MCF10A and GFP Myo1089 cells were cultured in 50% MCF10A specific medium and 50% HMFU19 fibroblast conditioned medium. Examination of MCF10A wildtype structures by H & E staining and IHC demonstrated variation in morphology and a mixed phenotype with only some structures positive for E-Cad and EMA reminiscent of the plasticity of these cells in 2D culture. MCF10A Luminal and MCF10A Basal were uniformly positive for these two markers. However, regardless of population of MCF10A cells, all structures were positive for basal/myoepithelial markers αSMA and vim and evidence of basement membrane production was seen in all structures. The propensity of MCF10A cells to adopt a basal phenotype has been described by several research groups [180, 220] and are reported to be highly sensitive to changes in culture conditions [221]. The inability of these cells to maintain expression of luminal epithelial markers in our culture system suggested they may not be an appropriate representative of luminal epithelium for our model. In addition, despite the successful culture of MCF10A spheroids for up to 26 days in other studies [222], MCF10A structures could not be maintained in our culture system beyond 7 days despite the presence of fibroblast conditioned medium, preventing any long term experimentation with this model. This highlighted a need to identify another cell line to better represent the luminal epithelium in our model in order to investigate cancer initiation mechanisms.

HB2 cells were selected as an alternative representative of luminal epithelium due to their proven ability to form branching duct-like structures in collagen I and for their luminal epithelial characteristics [199]. In concordance with this, immunofluorescence characterisation of these cells as a 2D monolayer demonstrated a luminal epithelial cell phenotype with positive staining for cytokeratin 18 and EMA luminal markers and no staining for the

myoepithelial markers cytokeratin 5/6 and αSMA. These were therefore considered viable as a luminal epithelial representative for our study.

It was recognised that co-culturing different cell types together each with their own specific media requirements would require optimisation of culture media conditions to ensure survival and to maintain phenotype of both GFP Myo 1089 and HB2 cells. Since luminal epithelial cells are susceptible to adopting a more basal phenotype [223] which could have been induced by using GFP Myo1089 specific medium on HB2 cells, 100% HB2 specific medium was used initially when co-culturing HB2 and GFP Myo1089 cells in 3D collagen I. Examination of HB2 structures by H & E staining demonstrated small, compact and sparse structures using HB2 specific medium with no evidence of cells with a myoepithelial-like spindle-shaped morphology. Addition of fibroblast conditioned medium had no effect on the morphology of these structures. However, the use of 50% GFP Myo1089 cell specific medium with 50% FCM produced much larger structures which were more abundant, showed evidence of lumen formation with appearance of cells with a myoepithelial-like spindle-shaped morphology distributed throughout the collagen gel. This suggested that the presence of GFP Myo1089 cell specific medium was necessary to retain GFP Myo1089 cell survival and that these cells influenced HB2 cell arrangement. We confirmed that these features were mediated by the presence of GFP Myo1089 cells in the culture system and not just through the influence of GFP Myo1089 cell specific medium through culturing HB2 cells alone in either 50% HB2 cell specific medium: 50% FCM or 50% GFP Myo1089 cells specific medium : 50% FCM. This proved that HB2 cells are unable to form large units with lumens without the presence of GFP Myo1089 cells regardless of the GFP Myo1089 cell specific medium being present.

The importance of GFP Myo1089 cells in HB2 cell arrangement was further demonstrated by increasing the number of GFP Myo1089 cells. An excess of GFP Myo1089 cells produced HB2 units which were more cohesive, rounded, contained lumens and thus more representative of

in vivo breast acini. Immunohistochemical analysis of these structures using anti-tGFP antibody demonstrated GFP Myo1089 cell distribution around outer edges of HB2 units making physical contacts with HB2 cells reminiscent of *in vivo* breast acini. This indicated that HB2 cells and GFP Myo1089 cells could be co-cultured together in 3D collagen I and produce structures that were comparable to *in vivo* breast acini. Furthermore, the quality of these structures were retained and even enhanced noted by production of larger "cleared" lumens through prolonged culture for up to three weeks allowing this model to be used for longer term experimentation.

It has been previously reported that inclusion of myoepithelial cells with luminal epithelial cells in 3D collagen I matrix can abrogate the need for basement membrane preparations such as Matrigel™ [71] due to their ability to produce proteins required for basement membrane formation [72]. Immunohistochemical characterisation of our dual-culture model of HB2 and GFP Myo1089 cells demonstrated such basement membrane deposition around the outer edges of HB2 units through coll IV and TN-C expression. All HB2 cell units displayed E-Cad expression between HB2 cell junctions indicating these cells did not undergo EMT and all units were polarised with EMA situated at the apical-luminal interface of HB2 cells. Furthermore, unlike MCF10A dual-cultures, HB2 cells retained a luminal epithelial phenotype with αSMA and vim staining restricted to GFP Myo1089 cells. Lumen formation was evidenced through apoptosis in the centres of HB2 units. The morphology and phenotype of these structures provided confidence that, under the right conditions, HB2 cells in co-culture with GFP Myo1089 in 3D collagen I were a better representative of breast acini than MCF10A cells and could be cultured for up to three weeks providing a better platform for experimentation of cancer initiation events.

3.5.2 Developing a tri-culture model by incorporation of fibroblasts

Having successfully established a heterotypic 3D *in vitro* dual-culture model of normal human breast, we endeavoured to introduce a stromal fibroblast component to the model to better represent the *in vivo* breast microenvironment.

Collagen I is a major synthetic product of fibroblasts thus fibroblasts form the structural framework for the majority of connective tissues and serve to maintain the ECM environment through secretion of factors such as MMPs [206]. Quiescent fibroblasts have the capacity to become "activated" during wound healing and fibrosis, synthesise collagen I [224] and characteristically acquire contractile stress fibres and express αSMA [225]. Fibroblast influence on breast epithelial architecture is well documented [205, 226, 227] and is specifically enhanced by culture in 3D in response to an ECM environment [228].

HMFU19 cells are a breast fibroblast cell line originally isolated from breast reduction mammoplasty samples [181]. While these were originally considered for use as the fibroblast component of our tri-culture model, characterisation of these cells by immunofluorescence demonstrated a loss of a "normal" fibroblast phenotype through expression of αSMA suggestive of a myofibroblast phenotype and expression of epithelial-associated cytokeratins 14 and 18. These cells were therefore deemed an inadequate representative of normal fibroblasts and presented a need to obtain a new normal fibroblast cell line.

Due to lack of commercially available normal fibroblast cell lines, we isolated fibroblasts from breast reduction mammoplasty samples to produce a normal primary fibroblast cell population. This was based on a technique by Holliday et al [149] whereby digestion of primary tissue with collagenase I yielded a fibroblast-rich supernatant fraction from which adherence and outgrowth of a cell population with an elongated spindle-shaped morphology was achieved. These grew in whorl patterns characteristic of fibroblast monolayer cultures.

However, primary cell cultures have a finite life span [229] limiting use of these cells to short term experiments and presenting issues with reproducibility. hTERT is the catalytic subunit of the telomerase enzyme and catalyses the addition of nucleotides to chromosome telomeres. This prevents degradation of chromosome ends and allows multiple rounds of DNA replication and thus proliferation and immortalisation of cells [230, 231]. It was reasoned that this technique could be applied to our primary fibroblasts to prolong their culture life span sufficiently for use throughout our study. Primary fibroblasts were retrovirally transduced with pBABE-hTERT-neo vector and compared to non-transduced cells. Previous cultures of primary fibroblasts in our laboratory have proven to senesce and apoptose following five passages (Dr Deborah Holliday, personal communication). It was therefore deemed unnecessary to select hTERT transduced fibroblasts with geneticin as if hTERT transduction was not successful; hTERT transduced fibroblasts would also have a finite life span in culture with little cell survival past five passages. As expected, un-transduced primary fibroblasts did not survive more than five passages over three weeks while hTERT transduced fibroblasts underwent 12 passages in the same time while retaining an elongated spindle-shaped morphology. These also did not show evidence of becoming larger and fatter which are phenotypic changes associated with fibroblast senescence [232]. All subsequent experiments using these fibroblasts were done so with hTERT transduced fibroblasts between passages 12 and 20. hTERT transduced fibroblast morphology did not change upon 20 passages suggesting these cells may be immortalised but would require further experimentation to confirm this. Satisfied with a representative fibroblast population that could be cultured in excess of three weeks and therefore sufficient for our experiments, LS11-083 hTERT fibroblasts were lentivirally transduced with pFURW-dsRed vector to allow tracking in 3D tri-culture. Following FACS, these retained constitutive expression of dsRed protein in 100% of the cells with an elongated spindle-shaped morphology and were termed LS11-083 dsRed Fibs. Furthermore, characterisation of LS11-083 dsRed Fibs by immunofluorescence demonstrated a normal fibroblast phenotype with 100% positivity for

vim and lack of luminal and myoepithelial cell markers in all cells. These were also confirmed to be non-activated through lack of αSMA expression. LS11-083 dsRed Fibs were therefore considered a robust, traceable cell population to represent the normal fibroblast component in our model.

Due to the propensity of fibroblasts to dominate primary cultures [233], their basic media requirements to thrive and their ability to maintain their fibroblast phenotype regardless of culture in epithelial specific media, we anticipated that LS11-083 dsRed Fibs would flourish in both HB2 and GFP Myo1089 medium in a tri-culture model. The introduction of LS11-083 dsRed Fibs into the tri-culture model negated the need for fibroblast conditioned medium in the culture system as previously optimised with HB2 and GFP Myo1089 dual-culture. Since we were conscious of inducing a luminal-myoepithelial transition of HB2 cells by using an excess of GFP Myo1089 cell specific medium and had also proved 50% GFP Myo1089 cell specific medium was sufficient for GFP Myo1089 cell survival, 50% HB2 cell specific medium: 50% GFP Myo1089 cell specific medium was used for the tri-culture model. Varying numbers of LS11-083 dsRed Fibs were incorporated into the culture system with the previously optimised ratio of HB2 to GFP Myo1089 cells and assessed through visualisation with H & E. An optimal number of $0.1x10^5$/ml of LS11-083 dsRed Fibs was identified that successfully retained the acini-like structures seen in the dual-culture system with hollow HB2 units, GFP Myo1089 cells associated around outside edges and LS11-083 dsRed Fibs loosely distributed throughout the collagen gel. These structures were examined by a consultant breast pathologist (Dr Rebecca Millican-Slater) who confirmed that the proportion of each of these three cell types and the structures they formed were a good representation of normal *in vivo* breast. In these conditions, a maximum culture period of three weeks was established through time course experiments with structural degradation noted after weeks four, five and six.

Immunohistochemical analysis of the tri-culture model phenotype under optimised culture conditions revealed a strikingly similar staining pattern to breast acini providing confidence that this is a robust model of normal breast tissue. Through culture of HB2 cells in the presence of both a myoepithelial and a fibroblast component, we have demonstrated the production of a basement membrane through coll IV and TN-C expression, the polarisation of HB2 cells through EMA and E-cad expression and the presence of lumens cleared via apoptosis through M30 expression without the need for Matrigel^{TM}. In addition, we have proved that each individual cell type retains a phenotype representative of their corresponding cell type in normal breast tissue with vimentin expression detected in GFP Myo1089 and LS11-083 dsRed Fibs cells and αSMA found in GFP Myo1089 cells only.

3.5.3 Quantification Technique

Having established a model that we were confident was representative of normal breast tissue, we reasoned that this model could be a useful tool for cancer initiation studies through manipulation of individual cells prior to culture. In order to analyse and interpret differences in structure formation/architecture scientifically upon cell manipulation in future experiments, we deemed it necessary to determine a technique of quantifying our observations obtained from histological methods. Through collaboration with the Leeds Digital Pathology Team, a method of quantifying size and number of HB2 units was developed by annotating digitally scanned H & E stained slides using Aperio Image Scope software. Due to the 3D nature of the model, it was anticipated that the depth of gel may affect the size and number of HB2 units. With this in mind, 10 x 5µm serial sections from one tri-culture gel were taken, H & E stained, digitally scanned, annotated and size and number of HB2 units compared. We found that the number of HB2 units did not systematically increase or decrease when traversing through the gel suggesting that HB2 units were evenly distributed throughout the gel. We demonstrated that quantifying one section gave a good estimate of the mean number of HB2 units throughout the whole population from 10 sections with an error of 13%.

Similarly, no significant differences were seen between sections two to eight from the mean area of HB2 units from the whole population. Since the quantification of area of approximately 80 HB2 units gave a good representation of the mean from the whole population and the mean number of units per section was between 62 and 90 units, we reasoned that quantifying one section, providing it was taken from a depth of between 15 to 40µm, was an acceptable method of quantification of area and number of HB2 units.

Conscious of the fact that there may be variation in diameter and therefore sections between gel replicates or gels cultured in different conditions that could influence the number and size

of HB2 units, we reasoned that area and number of HB2 units would be expressed as a ratio of the total area of the gel section in future experiments.

3.5.4 Summary

Current available 3D *in vitro* models of breast typically incorporate one or two cell types, such as MCF10A cells and fibroblasts [149, 195, 201]. Presented here for the first time is a 3D *in vitro* model of normal breast tissue that not only incorporated luminal epithelial cells and fibroblasts, but also included myoepithelial cells which are often neglected from other 3D *in vitro* cultures of breast. In addition, unlike other 3D *in vitro* models of breast which are often cultured in basement membrane preparations such as Matrigel™ [190], this model was cultured in the more physiologically relevant matrix of collagen I. Using cells engineered to express red and green fluorescent proteins we proved individual cell populations could be co-cultured and tracked in 3D. Culture in this manner yielded polarised structures with lumens that mimic breast acini and that produced basement membrane proteins at their periphery, replicating features achieved with other available 3D *in vitro* models of breast in the literature [154, 190]. However, unlike other models, this was achieved by incorporating myoepithelial cells and without the need for Matrigel™ and also made the model more representative of normal *in vivo* breast tissue than other available models. This was proven by comparing morphology and phenotype to normal *in vivo* breast. This demonstrated that each individual cell type retained an *in vivo* phenotype and, that combined, shared morphology and phenotype with normal breast acini.

Therefore this model is robust and a good representative model of normal human breast tissue. Furthermore, while mimicking features of acini *in vivo* and replicating key features of other available 3D models, our model offers the opportunity to study the role of myoepithelial cells in 3D luminal epithelial architecture and the co-operation of these with fibroblasts in this process which have not been possible before.

However, it is recognised that although our model may be a good representation of normal breast acini, it does lack the complete cellular heterogeneity found in *in vivo* breast tissue. Other stromal components such as endothelial cells [234-236], immune cells [237, 238] and adipocytes [239] all play key roles in breast cancer progression through release of tumour promoting cytokines and growth factors. 3D co-culture models have been achieved which include endothelial cells [240] or adipocytes [204, 212] with epithelial cells and fibroblasts but neglect the myoepithelial cell component of breast. In order to provide a comprehensive model of human breast tissue, cells such as these would need to be incorporated into our model. However, tracking cells in a multicellular model such as this may prove challenging. This could perhaps be overcome to certain degree by use of cell conditioned media but applications of the model would be limited.

Nevertheless, since our model provided an adequate stromal component, could be analysed through standard laboratory techniques and was quantifiable, we feel it has the potential to be used as a tool for cancer initiation studies and could be built upon in the future to include other aspects of *in vivo* breast architecture.

4 Chapter 4: Assessing the suitability of the model for cancer initiation studies via overexpression of HER proteins

4.1 Introduction

Having produced a 3D *in vitro* tri-culture model that accurately recapitulates the normal breast environment, we then sought to determine if the model could be used as a tool to study cancer initiation processes. By genetic manipulation of the luminal epithelium in the model which as discussed in Chapter 1 are the source for the majority of breast cancers, we aimed to disrupt the normal architecture of the model to produce a morphology and phenotype akin to early stages of breast cancers. To do this we selected HER proteins as a candidate to overexpress in HB2 cells.

4.1.1 HER2

Human epidermal growth factor receptor-2 (HER2/Neu, c-erbB2) is a member of a family of receptor tyrosine kinases (RTKs) known as HERs/ErbBs. The HER family contains three other members, epidermal growth factor receptor (HER1/ErbB1/EGFR), HER3 (ErbB3) and HER4 (ErbB4). Like other RTKs, HER proteins are transmembrane spanning receptors usually consisting of a cysteine rich extracellular domain designed for ligand binding, and an intracellular kinase domain rich in tyrosine autophosphorylation sites [241]. HER receptors exist in a monomeric form until stimulation from ligand binding where dimerization occurs forming homodimers or heterodimers with other HER receptors [242]. Heterodimerisation is the key to the signal amplification and diversification of HER receptors and is summarised in Fig 4.1. Investigation into the extracellular and intracellular domains of HER receptors has revealed that HER2 proteins are incapable of binding ligands [243] while HER3 receptors have weaker intrinsic tyrosine kinase activity in comparison to other HER receptors [244]. Without heterodimerisation with other receptors, these HER members remain inactive. Since HER2 exists in an open confirmation [245], it is the preferred heterodimerisation partner for other

HER family members. HER2 reduces the dissociation rate of its heterologous ligands [246] and can prevent internalisation and thus down-regulation of its binding partners [247]. This results in prolonged and more potent signalling, making HER2 containing heterodimers the most catalytic heterodimer combinations of the HER family. Due to the ability of HER3 to bind multiple PI3K protein substrates at a time [248] and the ability of HER2 to sustain ligand-HER3 interactions, the HER2-HER3 heterodimer is the most potent and mitogenic heterodimer of the HER family. The potential of the HER2-HER3 heterodimer to activate PI3K [249],the ability of HER2 to activate the MAPK pathway [250, 251] and Stat transcription factors [252, 253] makes HER2 a key regulator of a variety of cell responses such as proliferation, apoptosis and differentiation. It could therefore be expected that HER2 would play a role in normal mammary development and maintenance of normal breast physiology.

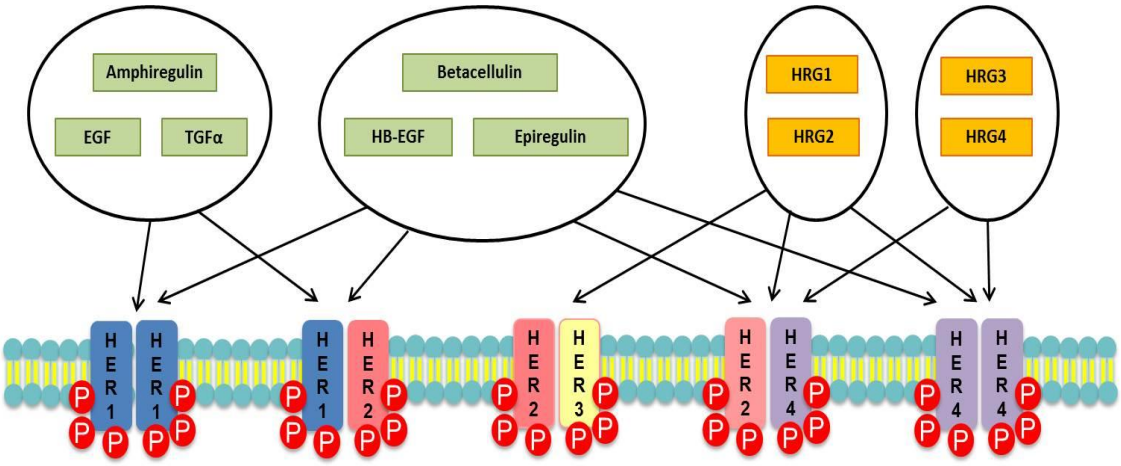

Fig 4.1 Diagrammatic representation of HER dimerization combinations and their corresponding ligands

Ligand binding to HER receptors induces formation of homodimers (HER1 and HER4 only) or heterodimers leading to activation and phosphorylation (P) of tyrosine residues within the intracellular domains. HER ligands belong to the epidermal growth factor family (EGF) and over 16 different ligands have been identified, selections of which are displayed. These can be grouped into three main categories. HER1 binding ligands such as EGF, amphiregulin and transforming growth factor α (TGFα), HER1 and HER4 binding ligands such as betacellulin, heparin-binding EGF (HB-EGF) and epiregulin, and, the heregulin family (HRG). HRG1 and HRG2 bind HER2-HER3, HER2-HER4 and HER4-HER4 dimers while HRG3 and HRG4 are HER4 binding ligands. The ability of HER receptors to heterodimerize allows the activation of a variety of different as well as overlapping downstream signalling pathways from the same the ligand making the HER signalling network diverse and complex.

However, perhaps due to the variety of signalling pathways that HER2 regulates coupled with the lethality of knocking out the HER2 gene in mouse models, the role HER2 plays in mammary development remains unclear. Due to overlapping functions of all four HER receptors, and the fact that more than one HER receptor has the capacity to respond to the same ligand [reviewed in 254], clarifying the role of individual receptors in mammary development is challenging. Furthermore, research on this topic to date has been limited to studies with murine models which may not be conserved in humans due to physiological differences between mice and humans [255]. However, studies in mice and rats have demonstrated a need for HER2 in several stages of mammary development. HER2 has proven necessary for terminal end bud formation [256], for lactation at parturition [257] and plays a role in hormonally controlled pubertal development [258]. The roles of HER2 in these processes are largely linked to epithelial cell proliferation and invasion which are key events in breast tumorigenesis. Therefore it is logical that this receptor would have oncogenic potential and could play a key part in breast cancer progression.

4.1.2 HER2 and breast cancer

With this in mind, it is not surprising that HER2 gene amplification and protein overexpression is found in approximately 16% of breast cancers [259] with breast cancer cells demonstrating as many as 50 copies of the HER2 gene [260]. Overexpression of HER2 is associated with a poor prognosis and survival in breast cancer patients and correlates with more invasive tumours [261]. The fact that HER2 overexpression also occurs in up to 50% of DCIS [97] suggests a role for HER2 in early events of cancer initiation and tumorigenesis. Studies in mice have shown HER2 overexpression alone is sufficient to induce transformation of mammary epithelium in a single step [262, 263] demonstrating the potency of HER2 as an oncogene. In addition to its mitogenic properties, HER2 has been linked to an increase in cancer stem cell populations in breast [264] suggesting this receptor may initiate breast tumour formation through a variety of mechanisms.

The mechanism behind how HER2 can promote cancer initiation still remains unclear. *In vitro* studies using cell lines has provided some insight into the effect HER2 signalling has on already established tumorigenic breast cancer cells. Early *in vitro* studies demonstrate a decrease in apoptosis [265], an increase in proliferation [266] as well as an increase in migration [267-269] and invasion [270] in breast cancer cell lines in response to HER2. However, this does not address the transforming ability of HER2. Limited studies using non-tumorigenic breast epithelial cell lines in more sophisticated 3D models have given clues as to how this may occur. Studies using the non-tumorigenic breast cell lines HB2 in 3D collagen matrix have demonstrated increased branching [271] and MCF10A in 3D Matrigel have demonstrated disrupted and invasive structures in response to HER2 overexpression. This suggests a role for HER2 in increasing normal mammary epithelial cell migration and inducing an EMT phenotype. In addition, increased cell proliferation in luminal spaces of 3D MCF10A acini structures in response to HER2 overexpression suggests HER2 may promote a DCIS-like phenotype [165]. Although promising, these *in vitro* models do not take into account the influence of surrounding stromal cells on these processes. A more representative model of normal breast tissue is needed to investigate the effects of HER2 on normal mammary epithelial cell phenotype in the presence of stromal signals to get a more accurate picture of how HER2 functions *in vivo* breast.

4.2 Aims

The aim of this series of experiments was to investigate the ability of HER2 and HER3 both alone and combined to induce changes in phenotype and morphology of normal luminal breast epithelial cells in a physiologically relevant 3D tri-culture *in vitro* model of normal breast tissue described in Chapter 3. In parallel to this we sought to validate the appropriateness of using our 3D *in vitro* model for breast cancer initiation studies. This was addressed by :-

- Comparing the phenotype of HER2, HER3 and both HER2 and HER3 overexpressing HB2 cells to wildtype HB2 cells in a 3D collagen mono-culture model
- Investigating the effect of adding either myoepithelial cells or fibroblasts to wildtype and HER overexpressing HB2 cells in a 3D collagen dual-culture model
- Investigating the effect of adding a combination of myoepithelial cells and fibroblasts on wildtype and HER overexpressing HB2 cells in a 3D tri-culture model
- Quantifying differences in morphology of HB2 units by measuring area, number and lumen formation from sections of 3D gels stained with H & E
- Characterising the phenotype by IHC

4.3 Materials and Methods

HB2 cells that overexpressed HER2 and HER3 proteins were a gift courtesy of Dr Fedor Berditchevsky (University of Birmingham) and were maintained as per Table 2.1 Chapter 2. To generate HER2 overexpressing (HB2 HER2OE) and HER3 overexpressing HB2 cells (HB2 HER3OE), HB2 wildtype cells (HB2 WT) were retrovirally transduced with HER2 and HER3 using two separate pSV2-neo plasmids containing HER2 and HER3 genes as previously described [272] and FACS was performed to isolate cell populations which were >95% positive for either HER2 or HER3. To generate both HER2 and HER3 overexpressing HB2 cells (HB2 HER2/3OE), HB2 HER2OE cells were retrovirally transduced with a pSV2-neo plasmid containing the HER3 gene and double-staining flow cytometry was performed to isolate cell populations which were >95% positive for both transgenes.

4.4 Results

4.4.1 Confirmation of the overexpression of HER2 and HER3 in HB2 cell lines

HER2 and HER3 protein expression was assessed in HB2 WT, HB2 HER2OE, HB2 HER3OE and HB2 HER2/3OE using western blotting. Fig 4.2 represents results from three biological replicates and showed that HER2 protein expression was increased in HB2 HER2OE and HB2 HER2/3OE cells and HER3 protein expression was increased in HB2 HER3OE and HB2 HER2/3OE cells. Quantification data is presented as expression fold difference to HB2 WT for both proteins and confirmed a 40-fold increase in HER2 expression in HB2 HER2OE cells and a 13-fold increase in HB2 HER2/3OE cells. HER3 was increased by 10-fold in HB2 HER3OE cells and by 17-fold in HB2 HER2/3OE cells. This confirmed that HB2 cells retained the overexpressed of HER2 and HER3 proteins as expected.

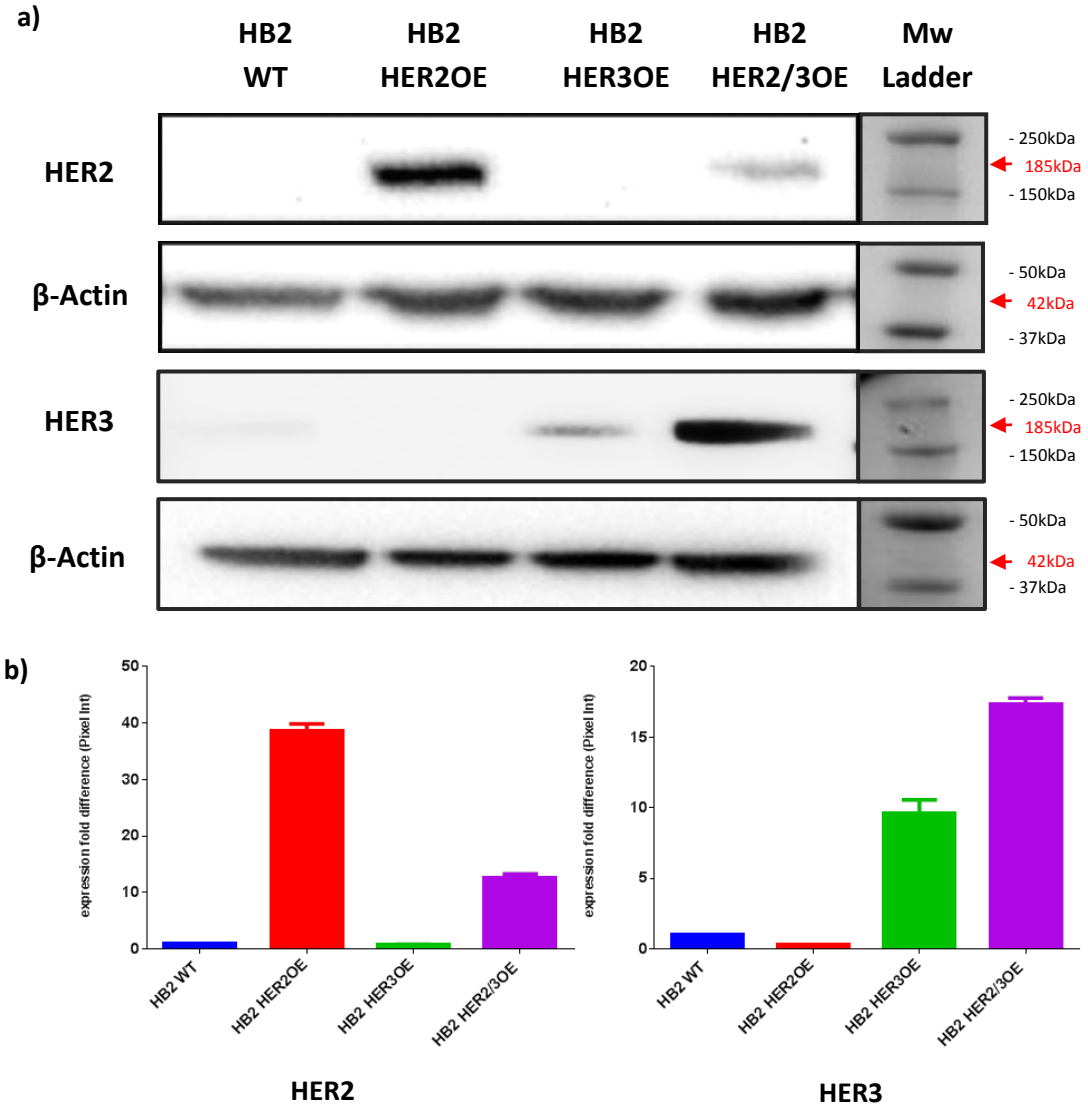

Fig 4.2 Western blot for HER2 and HER3 in HB2 cells transduced with HER2, HER3 or both HER2 and HER3 expression plasmids in comparison to HB2 wildtype cells.

a) Anti-HER2 IgG was used to detect total HER2 protein in HB2 wildtype cells (HB2 WT), HB2 cells overexpressing HER2 (HB2 HER2OE), HB2 cells overexpressing HER3 (HB2 HER3OE) and HB2 cells overexpressing both HER2 and HER3 (HB2 HER2/3OE). Bands of ~185kDa were observed in HB2 HER2OE and HB2 HER2/3OE cells with HB2 HER2OE displaying a more intense band than HB2 HER2/3OE. No bands were detected in HB2 WT and HB2 HER3OE cells. Anti-HER3 IgG was used to detect total HER3 protein for which bands of ~185kDa were observed in HB2 HER3OE and HB2 HER2/3OE cells with HB2 HER2/3OE displaying a more intense band than HB2 HER3OE. No bands were detected in HB2 WT and HB2 HER2OE cells. Anti-β-Actin IgG was used as a loading control for which bands were observed in all samples at ~42kDa.
b) Histograms show quantification of HER2 and HER3 expression following densitometry analysis using BioRad Image Lab 4.1 software. Expression was calculated as fold difference to HB2 WT after normalization to β-Actin for each cell type. Bars denote mean from three biological replicates and error bars the standard error of the mean (SEM).

4.4.2 The effect of HER protein overexpression on the morphology and phenotype of 3D *in vitro* tri-culture model of normal breast

In order to determine the effect of HER protein overexpression in HB2 cells in our model, morphology of morphology of HB2 WT, HB2 HER2OE, HB2 HER3OE and HB2 HER2/3OE tri-cultures with LS11-083 dsRed Fibs and GFP Myo1089 cells was assessed by H & E. These were analysed following 21 days in culture as it was demonstrated in Chapter 3 that 21 days was the optimal culture period for production of representative acini-like structures in our HB2 WT control cells. Results presented are representative images from three technical replicates (Fig 4.3). This demonstrated that as in Chapter 3, HB2 WT cells formed small rounded units with clear lumen formation with spindle-shaped cells loosely distributed throughout the collagen gel. Upon HER2 overexpression, HB2 cells appeared to form much larger, elongated units which featured distorted lumens and appearance of protrusions from outer edges of units. HER3 overexpressing cells also appeared to form larger units containing distorted lumens but these remained more rounded. HB2 cells overexpressing both HER2 and HER3 appeared to form a combination of smaller rounded units and larger elongated units that were larger than HB2 WT and also featured distorted lumens. Quantification of these structures (Fig 4.4) supported these observations. A significant increase in size of HB2 units was demonstrated upon HER2 and both HER2 and HER3 overexpression compared to HB2 WT units ($p=<0.05$, unpaired t-test). Only overexpression of HER3 alone induced a difference in number of units formed showing a significant decrease ($p=0.0442$, unpaired t-test). Overexpression of HER2, HER3 and a combination of HER2 and HER3 caused a decrease in lumen formation compared to HB2 WT ($p=<0.05$, unpaired t-test).

Distribution of GFP Myo1089 cells and LS11-083 dsRed Fibs in tri-cultures with HER overexpressing HB2 cells was visualised by IHC using anti-tGFP and anti-dsRed respectively with representative images from three technical replicates presented (Fig 4.5). As per Chapter 3, GFP Myo1089 cells were observed around outer edges of all HB2 units, and LS11-083 dsRed

Fibs were detected loosely distributed throughout all collagen gels and remained un-changed upon overexpression of HER2 and HER3. Association of LS11-083 dsRed Fibs with edges of HB2 HER3OE units was also noted. This confirmed units observed and quantified by H & E staining still consisted predominantly of HB2 cells and not GFP Myo1089 cells or LS11-083 dsRed Fibs regardless of HER protein overexpression.

Characterisation of phenotype of HB2 WT, HB2 HER2OE, HB2 HER3OE and HB2 HER2/3OE 3D tri-cultures by IHC with representative images from three technical replicates presented (Fig 4.6 & 4.7) demonstrated that in the presence of both GFP Myo1089 and LS11-083 dsRed Fibs, E-Cad expression was observed at cell-cell junctions within all HB2 units regardless of HER2 or HER3 overexpression. However, this staining did appear weaker in HB2 HER2/3OE units. Strong EMA staining was detected in the single monolayer of cells surrounding a central lumen in HB2 WT units, and across the entirety of HB2 HER2OE and HB2 HER3OE units. EMA staining appeared weaker in HB2 HER2/3OE units but distributed at the cell-lumen interface. Strong Ki67 expression was observed largely across the entirety of all HB2 units, however, areas of Ki67 negativity were detected within central luminal spaces of HB2 HER2/3OE units. No M30 expression was detected within HB2 WT units but weak staining was detected in cells loosely distributed throughout collagen gel. HB2 HER2OE units contained no M30 expression while HB2 HER3OE and HB2 HER2/3OE showed speckles of M30 expression within centre of HB2 units. Strong coll IV expression was detected neatly distributed around the edges of HB2 units regardless of HER2 or HER3 overexpression.

4.4.3 HER2 overexpressing HB2 tri-cultures resemble DCIS *in vivo*

In order to validate whether our HER2 overexpressing tri-culture models were representative of *in vivo* DCIS, we compared H & E stained sections of HB2 HER2OE tri-cultures with a cross section of a human *in vivo* breast tissue specimen that contained areas of both DCIS and normal adjacent acini to compare to our HB2 WT controls (Fig 4.8). As per Chapter 3, HB2 WT

units were small, rounded and contained clear lumens and were therefore strikingly similar to normal breast acini *in vivo*. Areas of DCIS *in vivo* featured large elongated ducts and contained distorted lumens with necrotic tissue. These also featured enlarged and discohesive cells. HB2 HER2OE units similarly were elongated in shape and contained discohesive cells and distorted luminal spaces thought to be a product of necrosis. This not only confirmed that the normal tri-culture model was robust and retained features of normal breast acini, but this also confirmed that we could accurately recapitulate features of DCIS through overexpression of HER2 in our model.

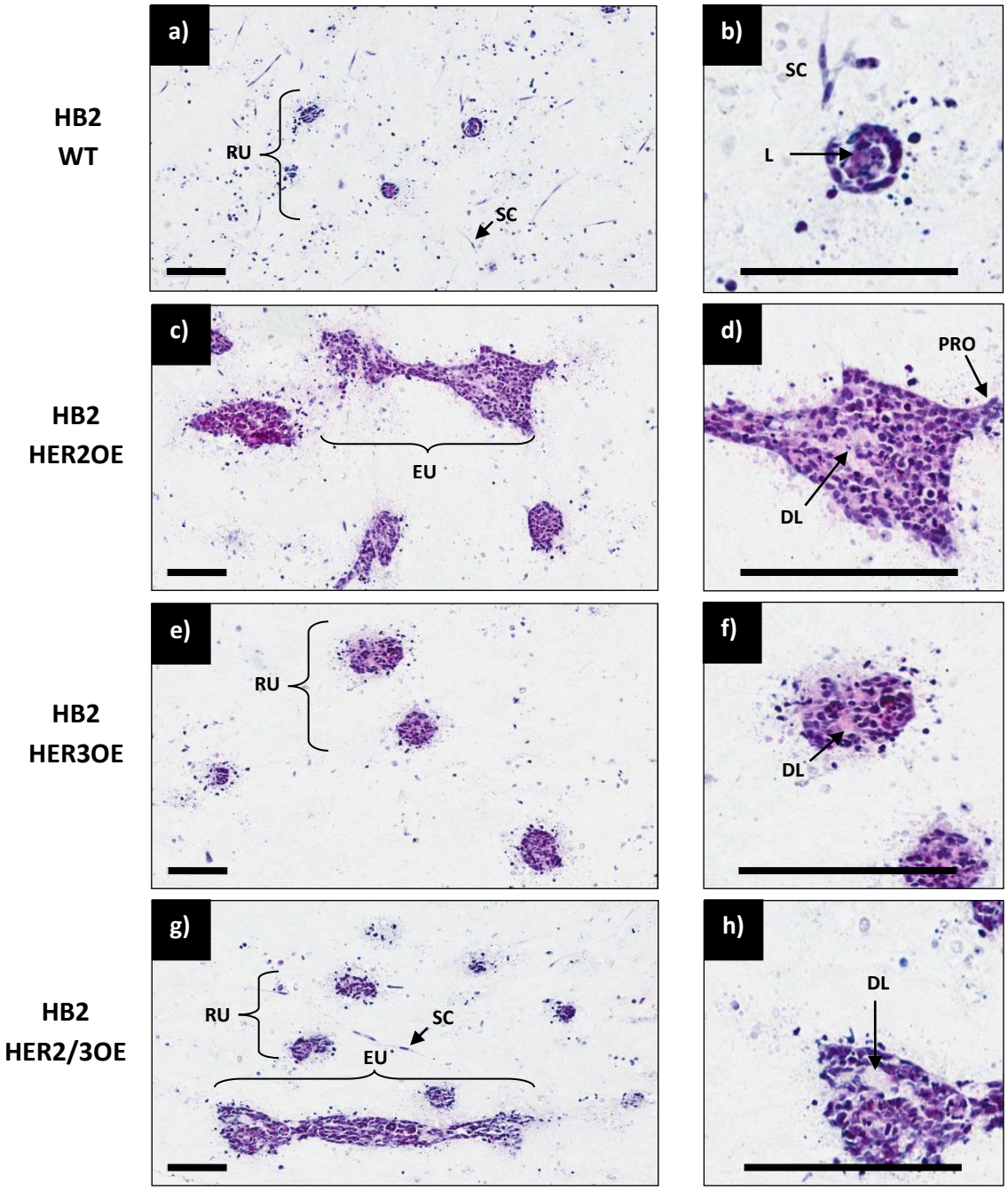

Fig 4.3 H & E staining of 3D *in vitro* tri-culture models containing HER overexpressing HB2 cells

Wildtype (HB2 WT), HER2 overexpressing (HB2 HER2OE), HER3 overexpressing (HB2 HER3OE) and both HER2 and HER3 overexpressing (HB2 HER2/3OE) HB2 cells were co-cultured in 3D collagen gels with GFP positive myoepithelial cells (GFP Myo1089) and dsRed positive fibroblast cells (LS11-083 dsRed Fib) for 21 days. 5µm sections of gels were stained with H & E and representative images from three technical replicates are presented. HB2 WT cells (a & b) formed cohesive rounded units (RU) with lumens (L) and gels featured spindle shaped cells (SC) loosely distributed throughout collagen matrix. HB2 HER2OE cells (c & d) formed much larger more elongated units (EU) with distorted lumens (DL) and featured protrusions (PRO) at edges. HB2 HER3OE cells (e & f) formed larger rounded units with distorted lumens. HB2 HER2/3OE cells (g & h) formed a combination of large rounded and elongated units with distorted lumens

and gels featured spindle shaped cells loosely distributed in surrounding collagen matrix. Original magnification 20x, scale bars = 100µm.

a)

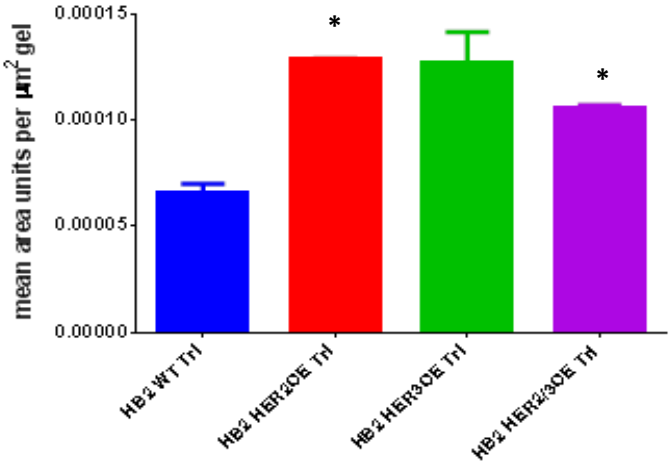

b)

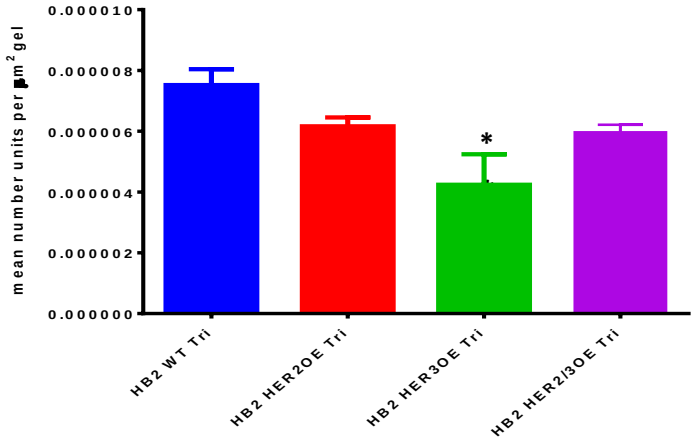

c)

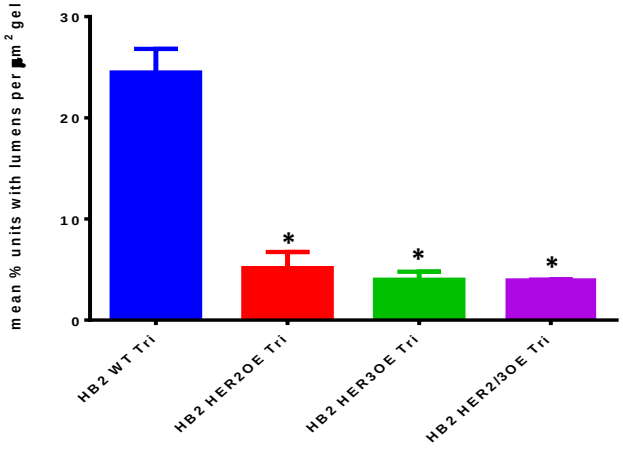

Fig 4.4 Quantification of area, number and lumen formation of HER overexpressing HB2 units in 3D tri-culture gels from H & E stained sections

Size, number and lumen formation of wildtype (HB2 WT Tri), HER2 overexpressing (HB2 HER2OE Tri), HER3 overexpressing (HB2 HER3OE Tri) and both HER2 and HER3 overexpressing (HB2 HER2/3OE Tri) HB2 cell units cultured with both GFP Myo1089 and LS11-083 dsRed Fibs

were quantified with Aperio Image scope, analysed with Graph Pad Prism 6 and normalized to total size of each respective collagen gel section. (a) Overexpression of HER2 and HER2/3 in HB2 cells significantly increased the size of HB2 units formed. (b) Number of HB2 HER3OE units was significantly decreased only with no significant difference seen with HB2 HER2OE and HB2 HER2/3OE. (c) Overexpression of HER2, HER3 and HER2/3 in HB2 cells significantly decreased lumen formation. Bars denote mean from three technical replicates and error bars standard error of the mean (SEM). * indicates significant difference to HB2 WT following unpaired t-test ($p=<0.05$).

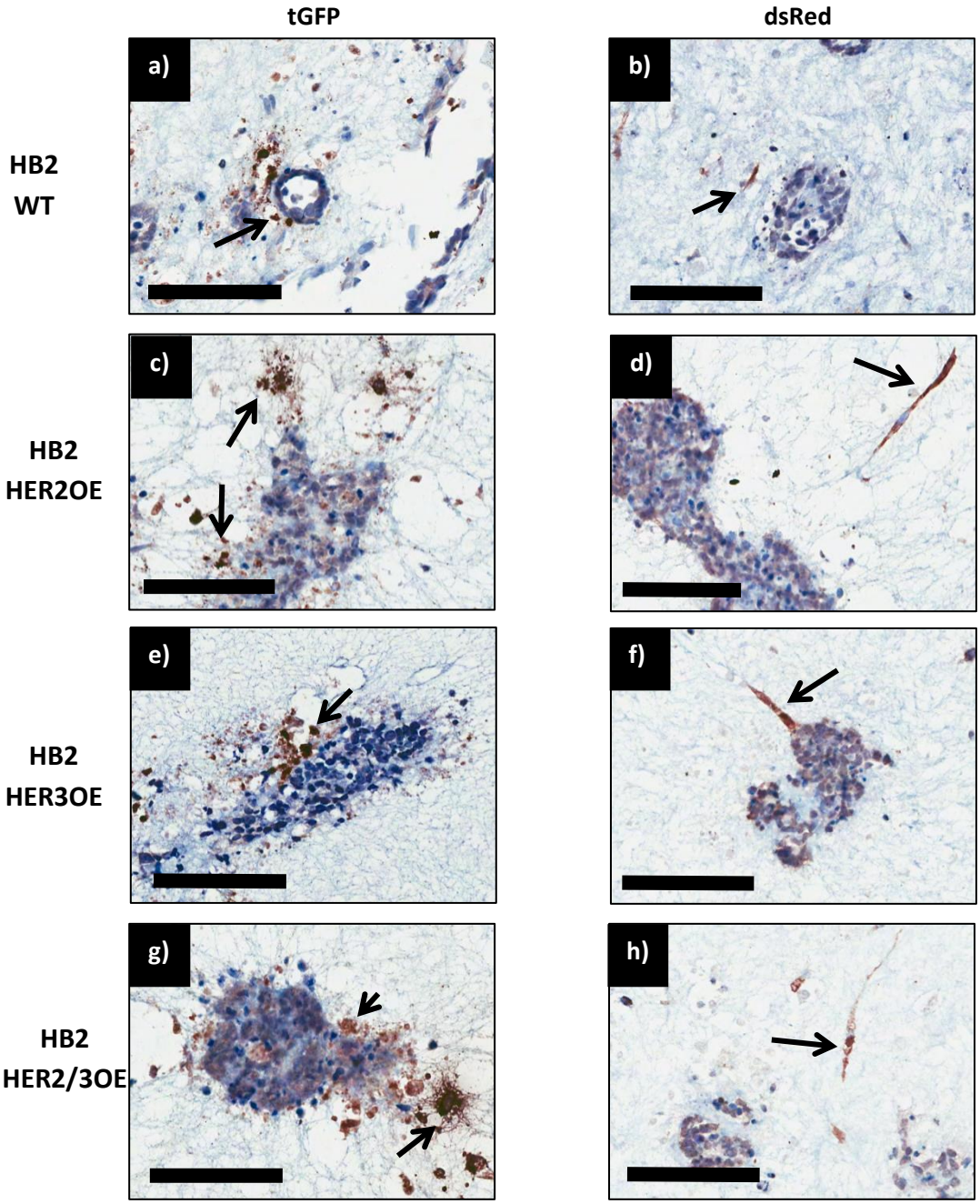

Fig 4.5 Immunohistochemical labelling of myoepithelial cells and fibroblasts in 3D *in vitro* tri-culture model

Wildtype (HB2 WT), HER2 overexpressing (HB2 HER2OE), HER3 overexpressing (HB2 HER3OE) and both HER2 and HER3 overexpressing (HB2 HER2/3OE) HB2 cells were co-cultured in 3D collagen gels with GFP positive myoepithelial cells (GFP Myo1089) and dsRed positive fibroblasts (dsRed Fibs) for 21 days. 5µm sections of gels were stained with anti-tGFP and anti-dsRed by IHC to visualise distribution of myoepithelial cells and fibroblasts within gels and representative images from three technical replicates are presented. All gels were positive for tGFP in cells distributed around the outer edges of HB2 cell units (arrows, a, c, e & g). HB2 WT, HB2 HER2OE and HB2 HER2/3OE were positive for dsRed in cells loosely distributed throughout collagen gels (arrows, b, d & h respectively). HB2 HER3OE were positive for dsRed in cells loosely associated around outer edges of HB2 units (arrow, f). Original magnification 20x, scale bars = 100µm.

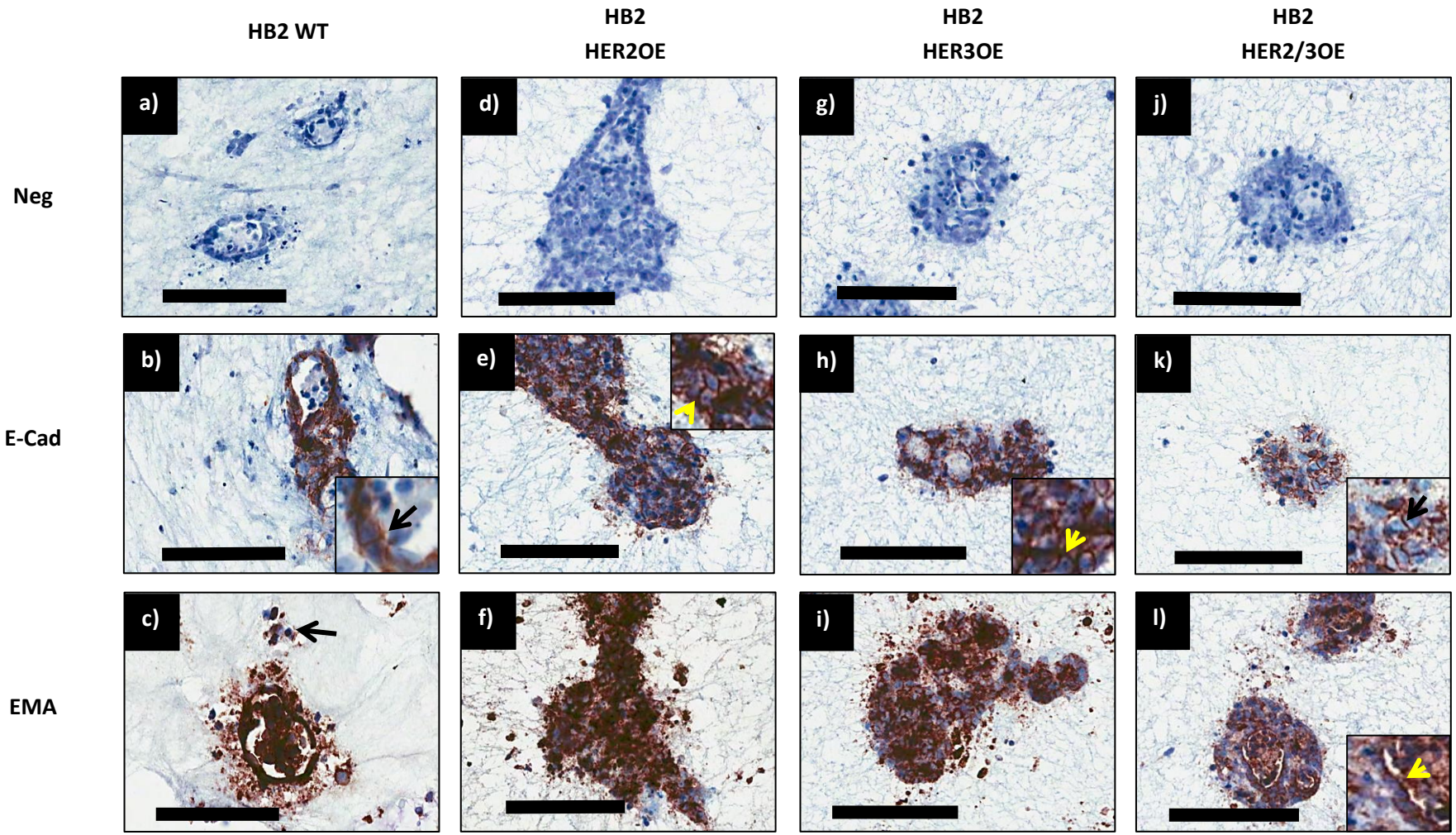
HB2 WT
HB2
HER2OE
HB2
HER3OE
HB2
HER2/3OE
Neg
E-Cad
EMA
a)
b)
c)
d)
e)
f)
g)
h)
i)
j)
k)
l)

Fig 4.6 IHC characterisation of 3D *in vitro* tri-culture models containing HER overexpressing HB2 cells A

HB2 wildtype (HB2 WT), HB2 HER2 overexpressing (HB2 HER2OE), HB2 HER3 overexpressing (HB2 HER3OE) and HB2 HER2 and HER3 overexpressing (HB2 HER2/3OE) cell unit phenotype were characterised by IHC to assess cell adhesion and polarisation and representative images from three technical replicates are presented. All HB2 units showed E-cadherin (E-Cad) staining localised between HB2 cell junctions (yellow arrows, b, e, h & k). Epithelial Membrane Antigen (EMA) staining was observed in a single monolayer of HB2 cells surrounding a central lumen with EMA negative cells (arrow) loosely associated with the edge of HB2 WT units (c). HB2 HER2OE and HB2 HER3OE units showed less organised distribution of EMA with no central areas of strong staining (f & i respectively). HB2 HER2/3OE cell units showed areas of strong EMA staining which appeared at the cell-lumen interface not localised to centre of units (yellow arrow, l). Primary antibody was omitted to serve as negative (Neg) controls (a, d, g & j). Original magnification, 20x, scale bars = 100µm.

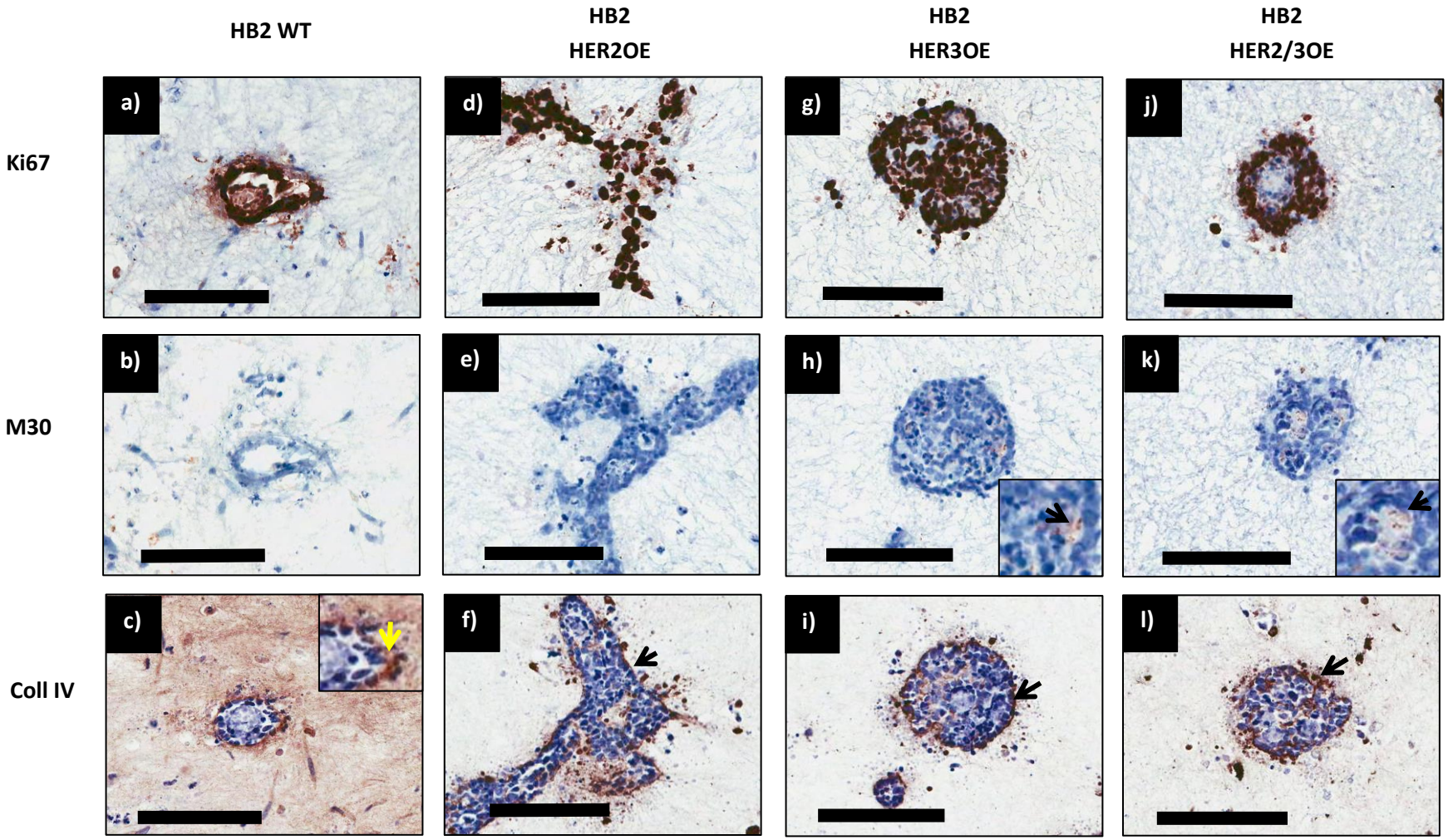
HB2 WT
HB2
HER2OE
HB2
HER3OE
HB2
HER2/3OE
Ki67
M30
Coll IV
a)
b)
c)
d)
e)
f)
g)
h)
i)
j)
k)
l)

Fig 4.7 IHC characterisation of 3D *in vitro* tri-culture models containing HER overexpressing HB2 cells B

HB2 wildtype (HB2 WT), HB2 HER2 overexpressing (HB2 HER2OE), HB2 HER3 overexpressing (HB2 HER3OE) and HB2 HER2 and HER3 overexpressing (HB2 HER2/3OE) cell unit phenotype were characterised by IHC to assess proliferation, apoptosis and basement membrane production and representative images from three technical replicates are presented. Strong Ki67 staining was observed in all cells within HB2 WT, HB2 HER2OE and HB2 HER3OE units (a, d & g respectively). HB2 HER2/3OE units also featured Ki67 positive cells but contained negative areas in the centre of units (j). While all HB2 units remained largely negative for M30 staining, speckles of weak staining was observed in cells outside of HB2 WT units (arrow, b), and within HB2 HER3OE and HB2 HER2/3OE units (yellow arrows, h & k). HB2 WT (b), HB2 HER3OE (h) and HB2 HER2/3OE (k) units were negative for M30 staining while low levels of M30 expression was detected around the edges of HB2 HER2OE units (arrow, e). Collagen IV (Coll IV) expression was detected in all gels neatly distributed around outer edges of HB2 units (arrows, c, f, i & l). Original magnification 20x, scale bars = 100µm.

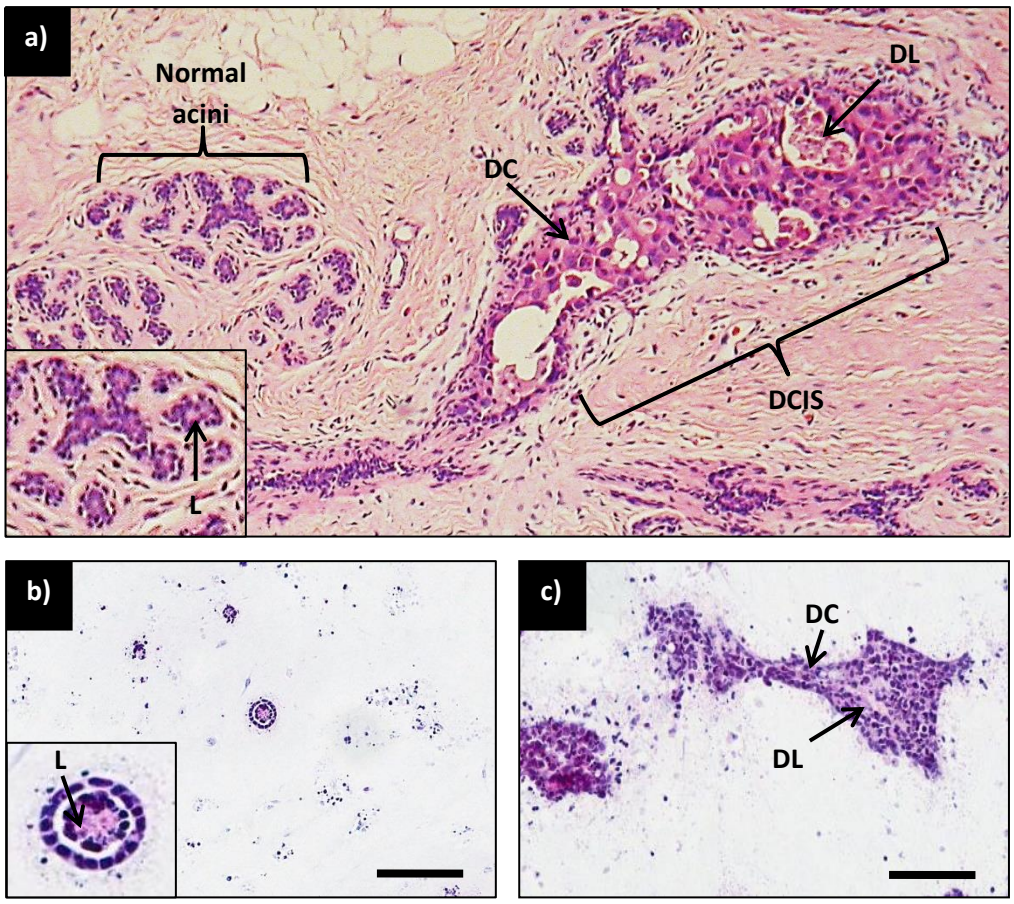

Fig 4.8 Comparison of HB2 wildtype and HB2 HER2 overexpressing tri-culture model to normal acini and DCIS *in vivo*

a) H & E stained cross section of *in vivo* breast tissue specimen containing normal acini and adjacent DCIS. Normal acini (left) appeared small and rounded in shape and contained a central cleared lumen (L, inset). Areas of DCIS consisted of enlarged, discohesive cells (DC) and featured distorted lumens containing necrotic cells (DL). Image courtesy of Prof Andrew Hanby (Leeds Institute of Cancer and Pathology). Original magnification 10x.

b) HB2 wildtype units of the tri-culture model were also small, rounded and featured central lumens (L) and therefore strongly resembled normal *in vivo* acini. Original magnification, 20x, scale bars = 100µm.

c) HER2 overexpressing HB2 units strongly resembled DCIS in both their elongated branched shape, the appearance of distorted lumens with possible necrosis (DL) and also consisted of discohesive cells (DC) akin to DCIS *in vivo*. Original magnification, 20x, scale bars = 100µm.

4.4.4 Morphology and phenotype of wildtype and HER overexpressing HB2 cells cultured in 3D *in vitro* mono-culture

In order to validate that HER protein overexpression affected HB2 architecture in a similar manner to other published studies, the morphologies of HER overexpressing HB2 cells in 3D mono-cultures were examined by H & E with representative images of three technical replicates presented (Fig 4.9). This demonstrated that while overexpression of HER2 or HER3 changed the morphology of the units, HER3 overexpression had the most disruptive effect. Although HB2 HER2OE cell units appeared larger, more elongated and less cohesive than HB2 WT units, overexpression of HER3 alone or in combination with HER2 induced cells to form units which appeared larger and more branching than HB2 WT and HB2 HER2OE units. These units also featured distorted luminal spaces. Quantification of three technical replicates (Fig 4.10) supported these observations demonstrating the most significant increase in size of HB2 units upon HER3 overexpression ($p=<0.0001$, unpaired t-test). Overexpression of HER3 alone or with HER2 also lead to a significant increase in number of units and lumens formed ($p=<0.01$ unpaired t-test).

To determine if these observations were attributed to a change in phenotype, HB2 units were characterised by IHC with representative images from three technical replicates presented (Fig 4.11 & 4.12). HB2 WT units showed the least amount of E-Cad expression suggestive of an EMT phenotype but this was not reflected by their morphology. HB2 HER2OE units contained areas of no expression or weak expression of E-Cad at cell-cell junctions. HB2 HER3OE displayed strong expression of E-Cad at cell-cell junctions while HB2 HER2/3OE units showed very strong expression of E-Cad in the cytoplasm of HB2 cells. HB2 WT units showed strong expression of EMA in their centre and cells on outer edges of units remained largely negative. Overexpression of HER2, HER3, or both HER2 and HER3 caused a loss of organised EMA expression in the centre of units with strong EMA expression seen both within and at edges of units. HB2 WT units contained a mixture of proliferative and non-proliferative cells which were

randomly distributed throughout units as indicated by Ki67 staining. Overexpression of HER2, HER3 and HER2 and HER3 caused an increase in proliferative cells with nearly all cells within units positive for Ki67 expression. Little evidence of HB2 cell apoptosis was observed in any of the units, demonstrated by lack of M30 staining, although speckles of weak staining were observed around the outer edges of HB2 HER2OE units. Weak expression of the basement membrane marker coll IV was observed in HB2 WT and HB2 HER2OE units and was found within units rather than surrounding outer edges. Stronger staining was detected in HB2 HER3OE and HB2 HER2/3OE units with some distribution noted at the outer edges.

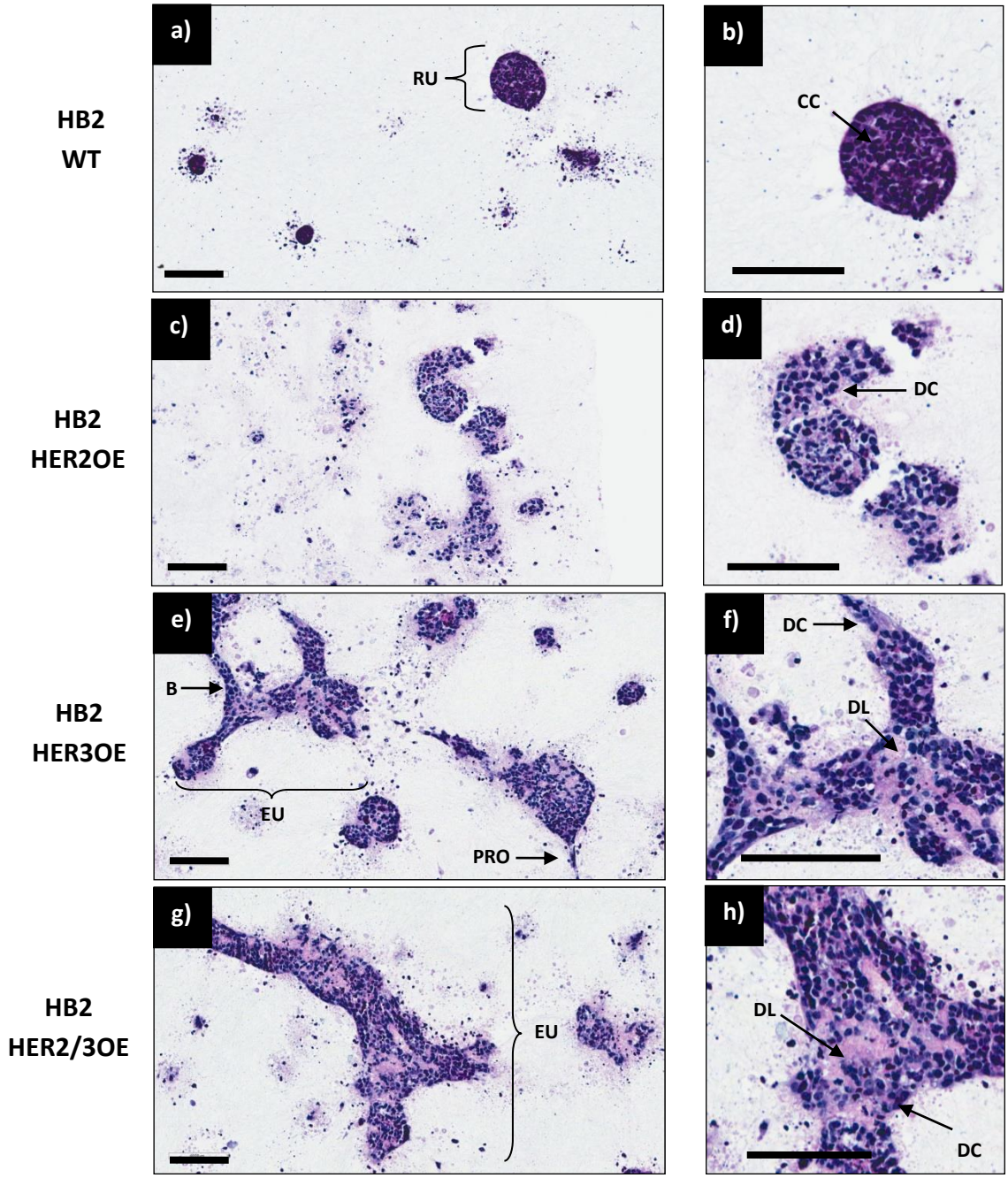

Fig 4.9 H & E staining of 3D *in vitro* mono-culture models of HER overexpressing HB2 cells

Wildtype (HB2 WT), HER2 overexpressing (HB2 HER2OE), HER3 overexpressing (HB2 HER3OE) and both HER2 and HER3 overexpressing (HB2 HER2/3OE) HB2 cells were cultured in 3D collagen gels for 21 days. 5µm sections of gels were stained with H & E with representative images from three technical replicates presented. HB2 WT cells (a & b) formed compact rounded units (RU) and contained highly cohesive cells (CC). HB2 HER2OE units (c & d) were larger less compact and less rounded containing discohesive cells (DC). HB2 HER3OE units (e & f) were much larger, elongated (EU), branched (B) and featured protrusions (PRO) at edges. These contained discohesive cells with distorted lumens (DL). HB2 HER2/3OE units (g & h) were also larger and elongated and contained discohesive cells and distorted lumens. Original magnification 20x, scale bars = 100µm.

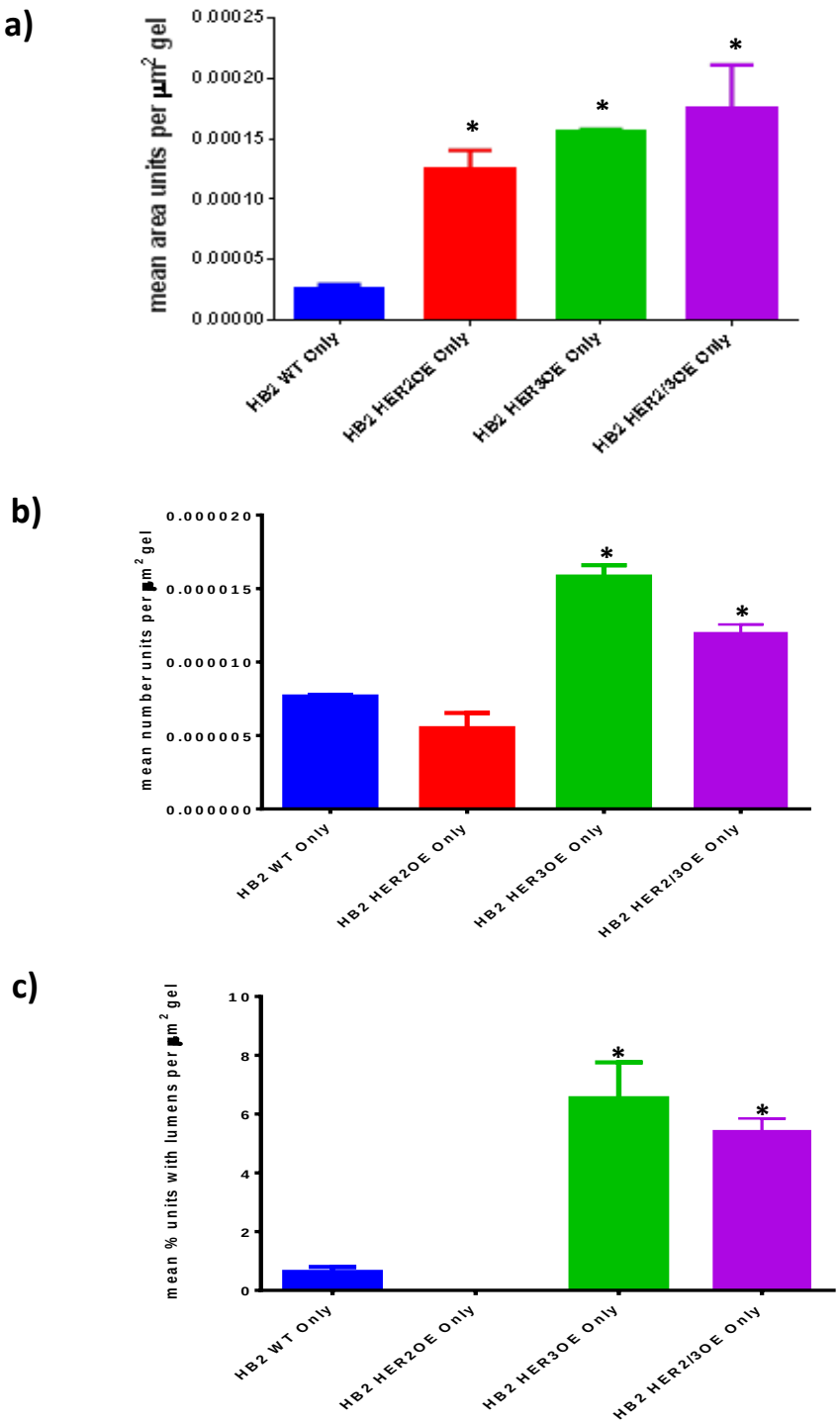

Fig 4.10 Quantification of area, number and lumen formation of HER overexpressing HB2 cell units in 3D mono-culture gels from H & E stained sections

Size, number and lumen formation of wildtype (HB2 WT), HER2 overexpressing (HB2 HER2OE), HER3 overexpressing (HB2 HER3OE) and both HER2 and HER3 overexpressing (HB2 HER2/3OE) HB2 cell units cultured alone were quantified with Aperio Image scope, analysed with Graph Pad Prism 6 and normalized to total size of each respective collagen gel section. (a) Overexpression of HER2, HER3 and HER2/3 in HB2 cells significantly increased size of HB2 units formed. (b) Number of HB2 HER3OE and HB2 HER2/3OE units were significantly decreased with no significant difference seen with HB2 HER2OE. (c) Overexpression of HER3 and both

HER2 and HER3 in HB2 cells significantly decreased lumen formation but not overexpression of HER2 only. Bars denote mean from three technical replicates and error bars standard error of the mean (SEM). * indicates significant difference to HB2 WT following unpaired t-test ($p=<0.05$).

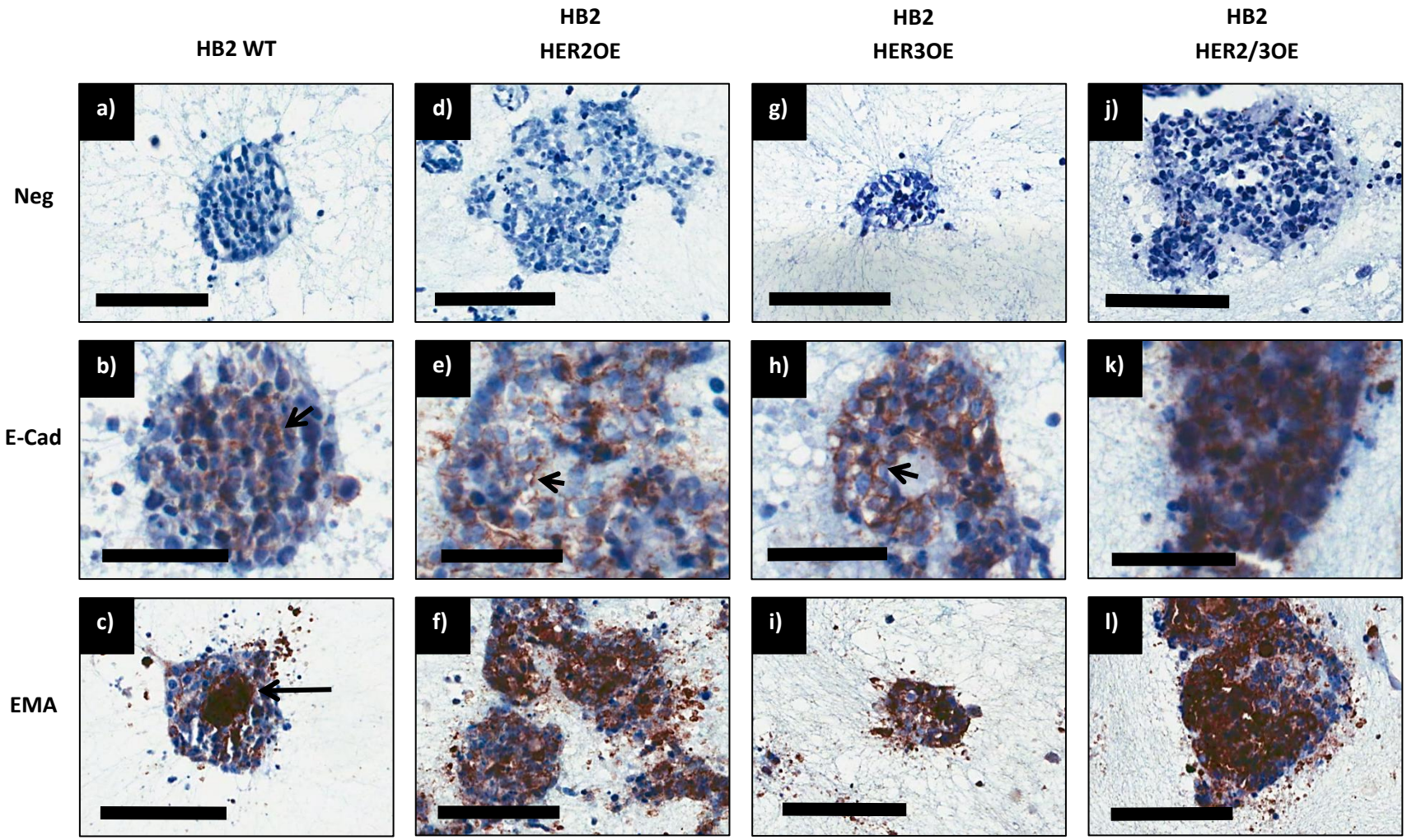
HB2 WT
HB2 HER2OE
HB2 HER3OE
HB2 HER2/3OE
Neg
E-Cad
EMA
a)
b)
c)
d)
e)
f)
g)
h)
i)
j)
k)
l)

Fig 4.11 IHC characterisation of 3D *in vitro* mono-culture models of HER overexpressing HB2 cells A

HB2 wildtype (HB2 WT), HB2 HER2 overexpressing (HB2 HER2OE), HB2 HER3 overexpressing (HB2 HER3OE) and HB2 HER2 and HER3 overexpressing (HB2 HER2/3OE) cell unit phenotypes were characterised by IHC to assess cell adhesion and polarisation with representative images from three technical replicates presented. While all HB2 units were positive for E-Cadherin (E-Cad) staining, differences in E-Cad distribution within units was detected upon HER2 and HER3 expression. HB2 WT cells expressed E-Cad in localised pockets inside units (yellow arrow, b). HB2 HER2OE cell showed patchy distribution of E-Cad staining within units localised at cell membranes (arrow, e). HB2 HER3OE cells displayed more uniform expression of E-Cad between cell junctions (arrow, h). HB2 HER2/3OE cells showed very strong uniform expression of E-Cad within units in both cell membranes and cytoplasm (k). Epithelial Membrane Antigen (EMA) staining demonstrated that only HB2 WT units showed a degree of polarisation with strong staining localised in the centre of units (arrow, c). HB2 HER2OE and HB2 HER3OE units showed less organised distribution of EMA with no central areas of strong staining (f & i respectively). HB2 HER2/3OE cell units showed areas of strong EMA staining which were not localised to centre of units (black arrow, l) but some cells remained negative at the outer edges (yellow arrow, l). Primary antibody was omitted to serve as negative (Neg) controls (a, d, g & j). Original magnification b, e, h & k, 40x, scale bars = 50µm. Original magnification of all others, 20x, scale bars = 100µm.

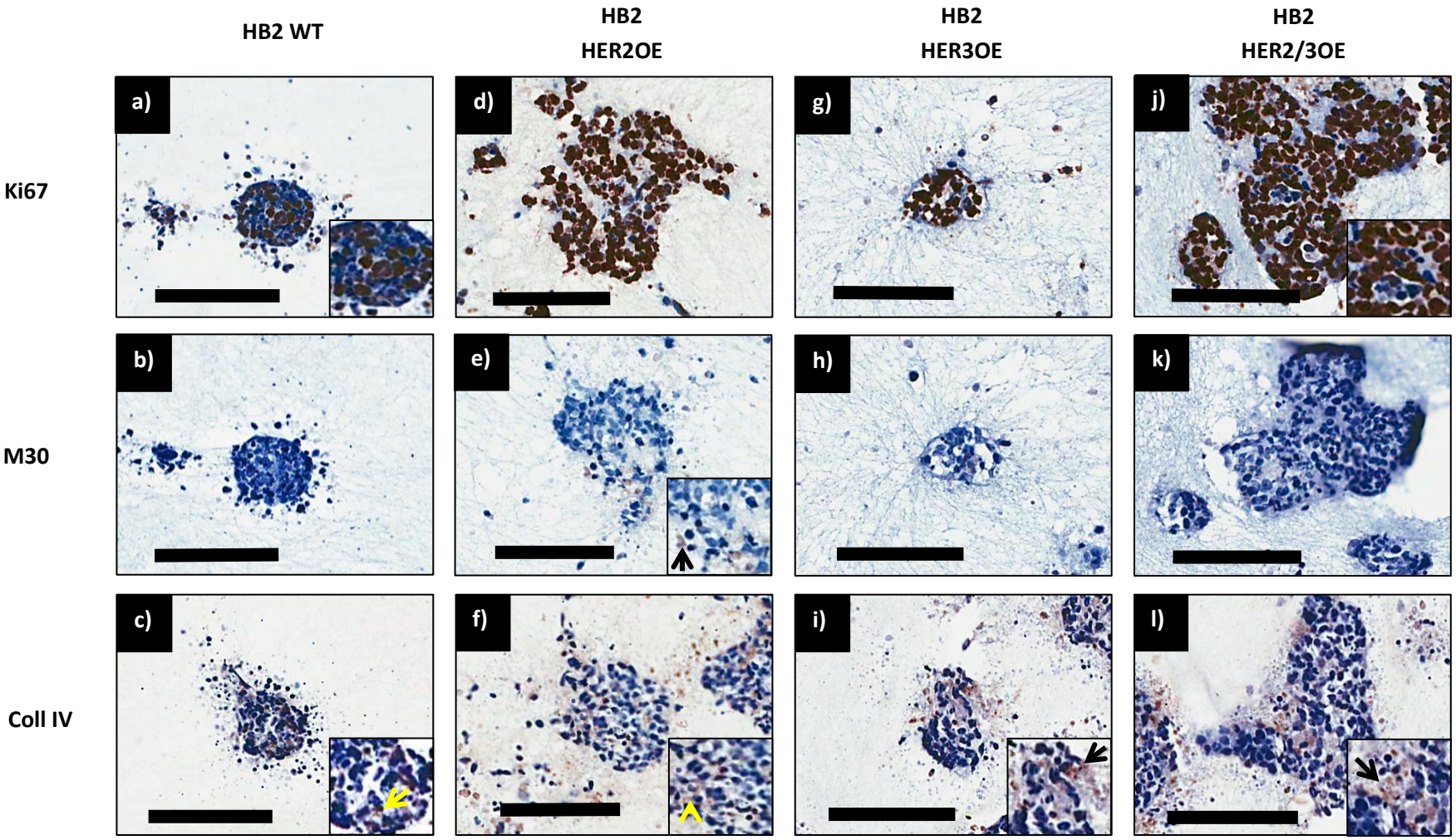
HB2 WT
HB2 HER2OE
HB2 HER3OE
HB2 HER2/3OE
Ki67
M30
Coll IV
a)
b)
c)
d)
e)
f)
g)
h)
i)
j)
k)
l)

Fig 4.12 IHC characterisation of 3D *in vitro* mono-culture models of HER overexpressing HB2 cells B

HB2 wildtype (HB2 WT), HB2 HER2 overexpressing (HB2 HER2OE), HB2 HER3 overexpressing (HB2 HER3OE) and HB2 HER2 and HER3 overexpressing (HB2 HER2/3OE) cell unit phenotype were characterised by IHC to assess proliferation, apoptosis and basement membrane production with representative images from three technical replicates presented. HB2 WT cells expressed Ki67 in patches within units (a) whereas all cells within HER2OE and HER3OE units were positive for Ki67 (d & g). HB2 HER2/3OE units contained areas which were negative for Ki67 but the majority of cells were positive (inset j). HB2 WT (b), HB2 HER3OE (h) and HB2 HER2/3OE (k) units were negative for M30 staining while low levels of M30 expression was detected around the edges of HB2 HER2OE units (arrow, e). Collagen IV (Coll IV) expression was detected in all HB2 units with HB2 WT and HB2 HER2OE units showing expression within units (yellow arrows, c & f respectively), while HB2 HER3OE and HB2 HER2/3OE expressed Coll IV on outer edges of units (arrows, i & l respectively). Original magnification 20x, scale bars = 100µm.

4.4.5 The effect of myoepithelial cells on the morphology and phenotype of wildtype and HER overexpressing HB2 cells in a 3D *in vitro* dual-culture model

In order to determine if myoepithelial cells had an effect on the formation of wildtype and HER overexpressing HB2 units, we assessed the morphology of HB2 dual-cultures and demonstrated that GFP Myo1089 cells induced all HB2 cells to form cohesive rounded units regardless of HER overexpression (Fig 4.13) with representative images from three technical replicates presented. GFP Myo1089 cells also induced clear lumen formation in HB2 WT units and distorted lumen formation in HB2 units with HER3 overexpression, either alone or with HER2. In all cases, cells which were loosely distributed throughout the collagen matrix were detected and were thought to be GFP Myo1089 cells. Quantification of units from three technical replicates (Fig 4.14) demonstrated HER2 and HER3 overexpression still significantly increased the size of HB2 units regardless of presence of GFP Myo1089 cells ($p=<0.05$, unpaired t-test). Unlike with mono- and tri-cultures whereby numbers were increased, the number of HB2 HER2/3OE units was significantly decreased compared with HB2 WT in the presence of GFP Myo1089 cells ($p=0.0016$, unpaired t-test). Quantification of lumen formation reflected observations with only overexpression of HER2 inducing a significantly decreased amount of lumen formation compared to HB2 WT in the presence of GFP Myo1089 cells ($p=0.0017$, unpaired t-test).

Analysis by IHC using anti-tGFP showed an association of GFP Myo1089 cells around the edges of all HB2 units as well as distributed throughout the collagen gel which remained un-changed upon overexpression of HER proteins (Fig 4.15). Representative images from three technical replicates are presented. This confirmed units observed and quantified by H & E staining consisted predominantly of HB2 cells and not GFP Myo1089 cells.

Characterisation of HB2 unit phenotype by IHC with representative images from three technical replicates presented (Fig 4.16 & 4.17) in response to GFP Myo1089 cells demonstrated an increase in E-Cad expression between HB2 cell junctions within HB2 WT units and a loss of E-Cad expression in HER overexpressing HB2 units. HB2 WT units retained strong expression of EMA in their centre with no staining detected in cells on outer edges of units. However, with HER3 overexpression alone, strong EMA expression was seen both within and at edges of units. GFP Myo1089 cells did not appear to alter proliferation as HB2 WT, HB2 HER2OE and HB2 HER3OE units contained a mixture of proliferative and non-proliferative cells although the majority of the cells within HB2 HER2/3OE units appeared to express Ki67. Apoptosis was also largely unaffected with HB2 WT, HB2 HER2OE and HB2 HER3OE units negative for M30 staining. However, GFP Myo1089 cells did induce apoptosis within central luminal spaces of HB2 HER2/3OE units. GFP Myo1089 cells affected basement membrane production in HB2 WT and HB2 HER2OE units only with strong coll IV staining detected around outer edges of units while coll IV expression within invaginations and in the centre HB2 HER3OE and HB2 HER2/3OE units was retained as with mono-cultures.

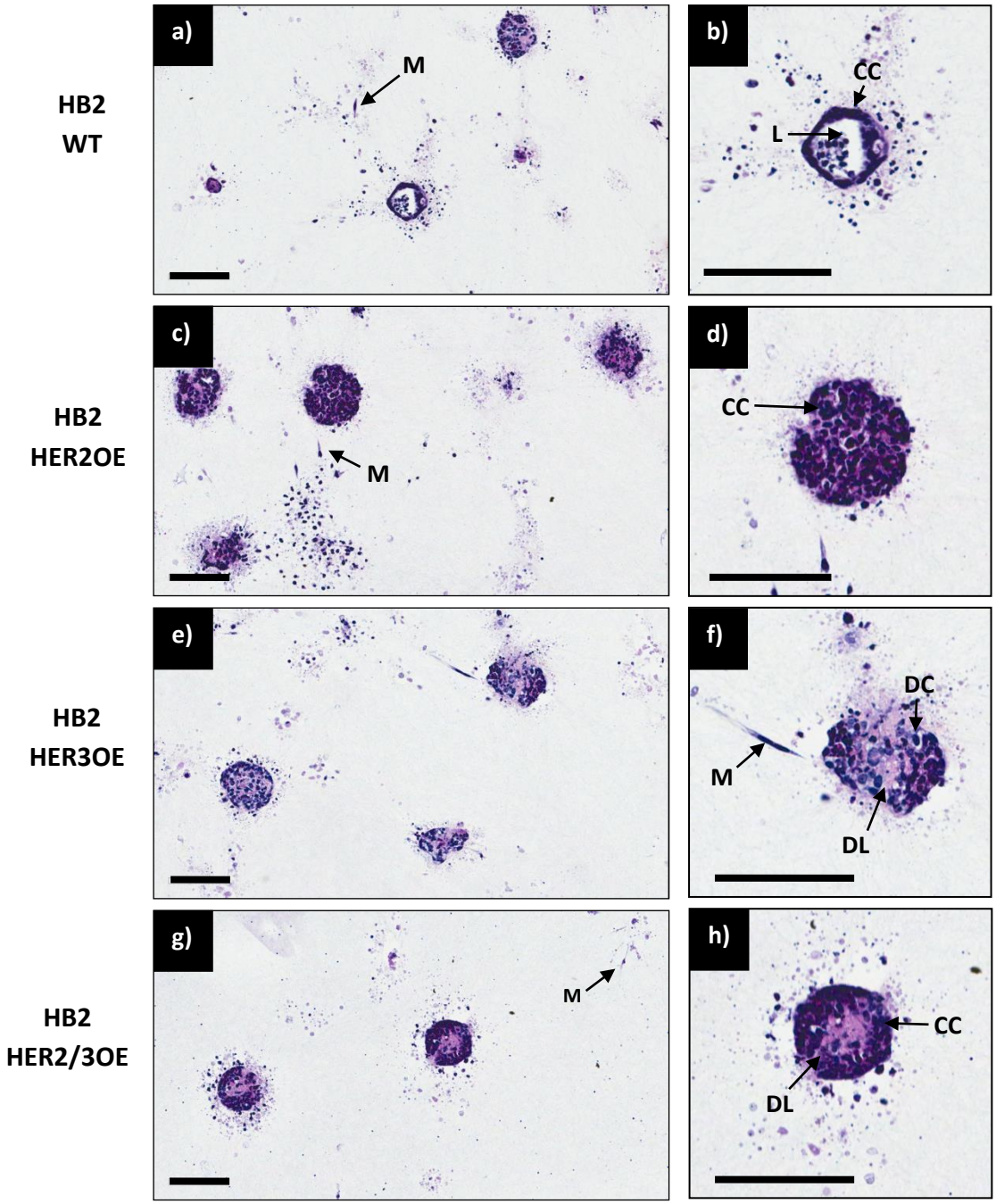

Fig 4.13 H & E staining of 3D *in vitro* dual-culture models of HER overexpressing HB2 cells with myoepithelial cells

Wildtype (HB2 WT), HER2 overexpressing (HB2 HER2OE), HER3 overexpressing (HB2 HER3OE) and both HER2 and HER3 overexpressing (HB2 HER2/3OE) HB2 cells were cultured with GFP positive myoepithelial cells (GFP Myo1089) in 3D collagen gels for 21 days. 5µm sections of gels were stained with H & E with representative images from three technical replicates presented. All types of HB2 cells formed rounded units with gels featuring spindle shaped GFP Myo1089 cells (M) loosely distributed throughout the collagen matrix. HB2 WT units (a) contained lumens (L) surrounded by a cohesive cell (CC) layer. HB2 HER2OE units (b) did not contain lumens but consisted of cohesive cells. HB2 HER3OE units (c) contained discohesive cells (DC) and distorted lumens (DL) while HB2 HER2/3OE units (d) consisted of cohesive cells but contained distorted lumens. Original magnification 20x, scale bars = 100µm.

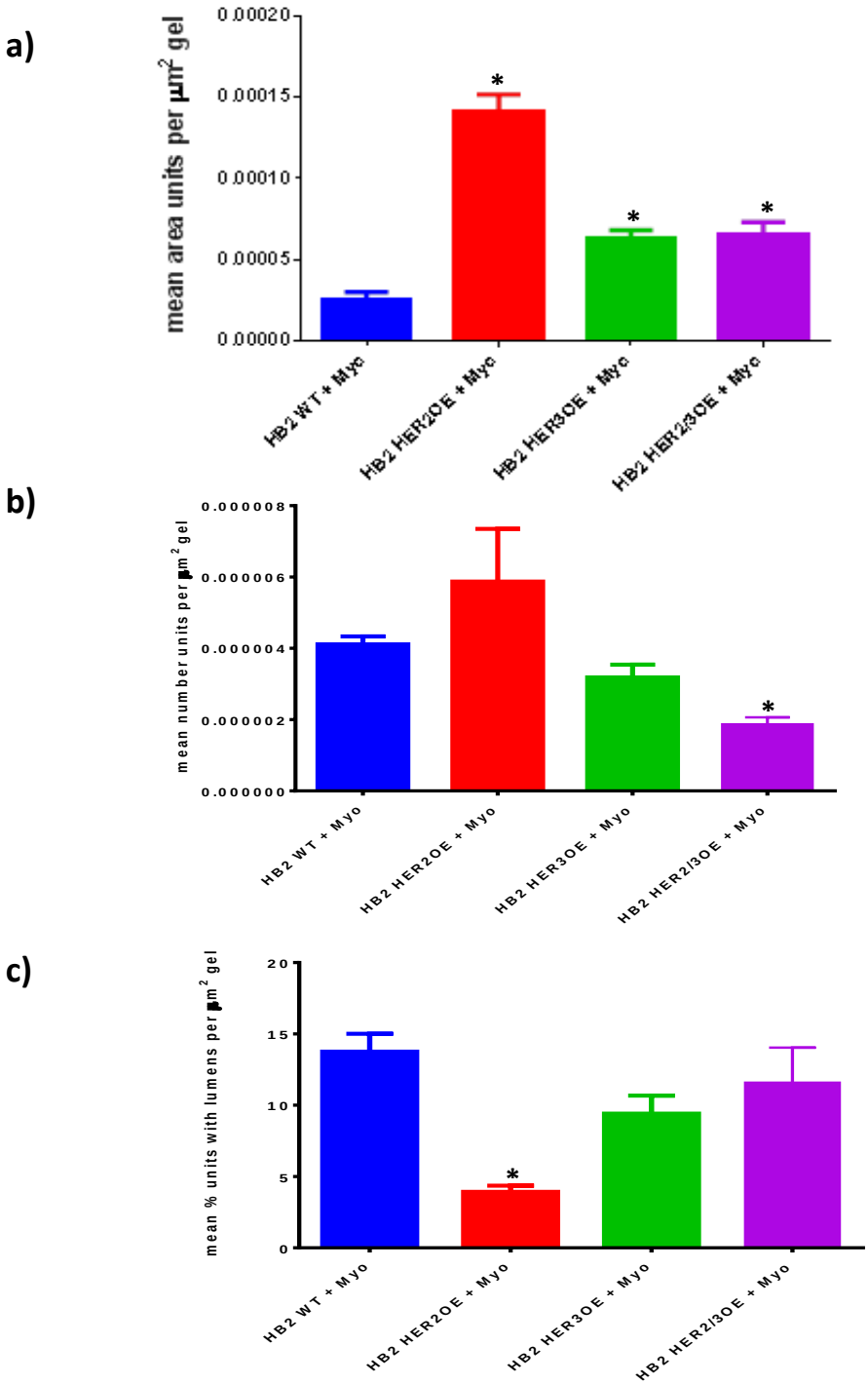

Fig 4.14 Quantification of area, number and lumen formation of HER overexpressing HB2 cell units in 3D dual-culture gels with myoepithelial cells from H & E stained sections

Size, number and lumen formation of wildtype (HB2 WT), HER2 overexpressing (HB2 HER2OE), HER3 overexpressing (HB2 HER3OE) and both HER2 and HER3 overexpressing (HB2 HER2/3OE) HB2 cell units cultured with GFP Myo1089 (Myo) was quantified with Aperio Image scope, analysed with Graph Pad Prism 6 and normalized to total size of each respective collagen gel section. (a) Overexpression of HER2, HER3 and HER2/3 in HB2 cells significantly increased size of HB2 units formed. (b) Number of units was only significantly decreased with HER2 and HER3 overexpression with no significant difference seen with HB2 HER2OE or HB2 HER3OE. (c) Overexpression of HER2 only in HB2 cells significantly decreased lumen formation. Bars denote

mean from three technical replicates and error bars standard error of the mean (SEM). * indicates significant difference to HB2 WT + Myo following unpaired t-test ($p=<0.01$).

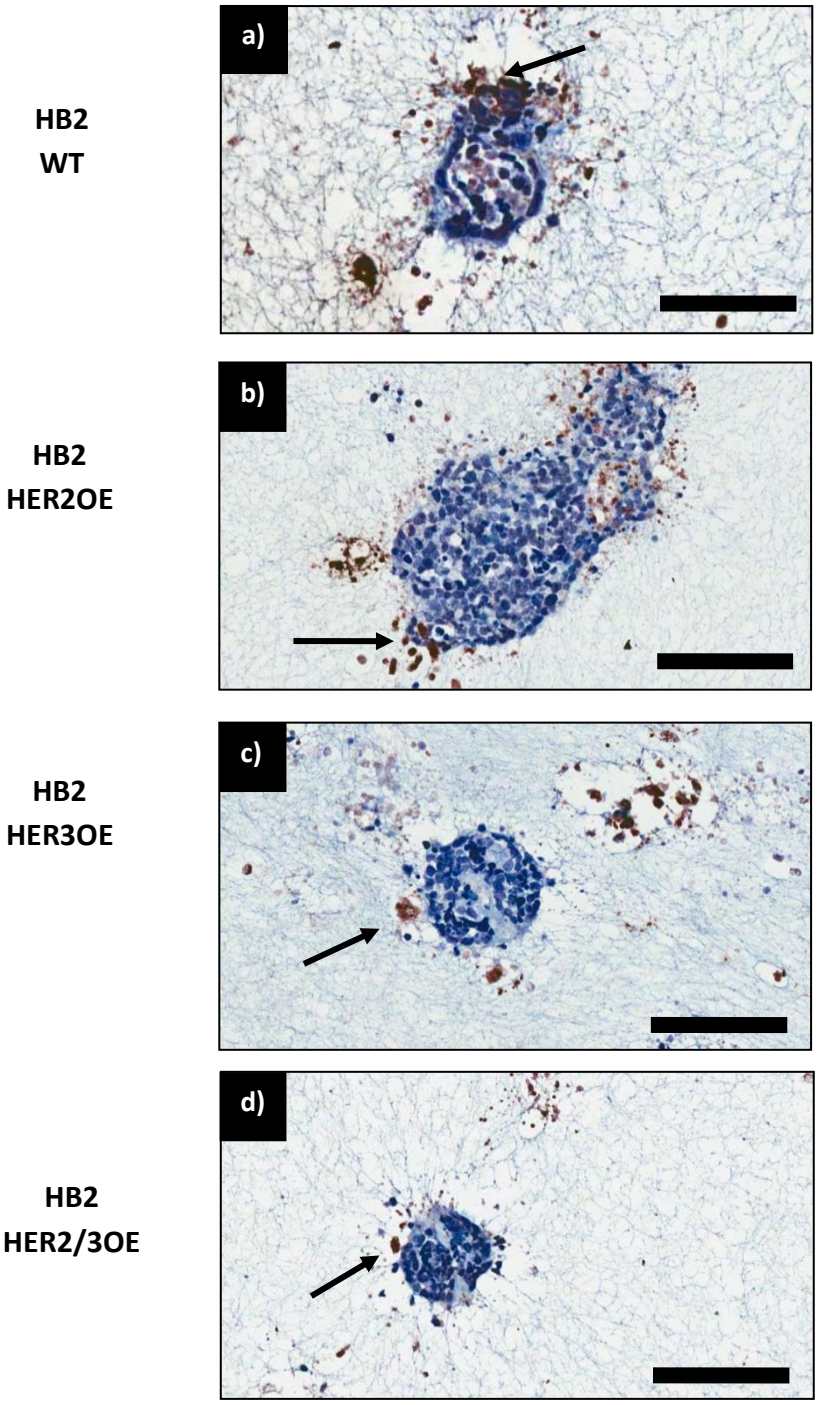

Fig 4.15 Immunohistochemical labelling of myoepithelial cells in 3D *in vitro* dual-culture model

Wildtype (HB2 WT), HER2 overexpressing (HB2 HER2OE), HER3 overexpressing (HB2 HER3OE) and both HER2 and HER3 overexpressing (HB2 HER2/3OE) HB2 cells were co-cultured in 3D collagen gels with GFP positive myoepithelial cells (GFP Myo1089) for 21 days. 5µm sections of gels were stained with anti-tGFP by IHC to visualise distribution of myoepithelial cells within gels with representative images from three technical replicates presented. All gels displayed positive staining for tGFP in cells distributed around the outer edges of HB2 cell units (arrows, a-d). Original magnification 20x, scale bars = 100µm.

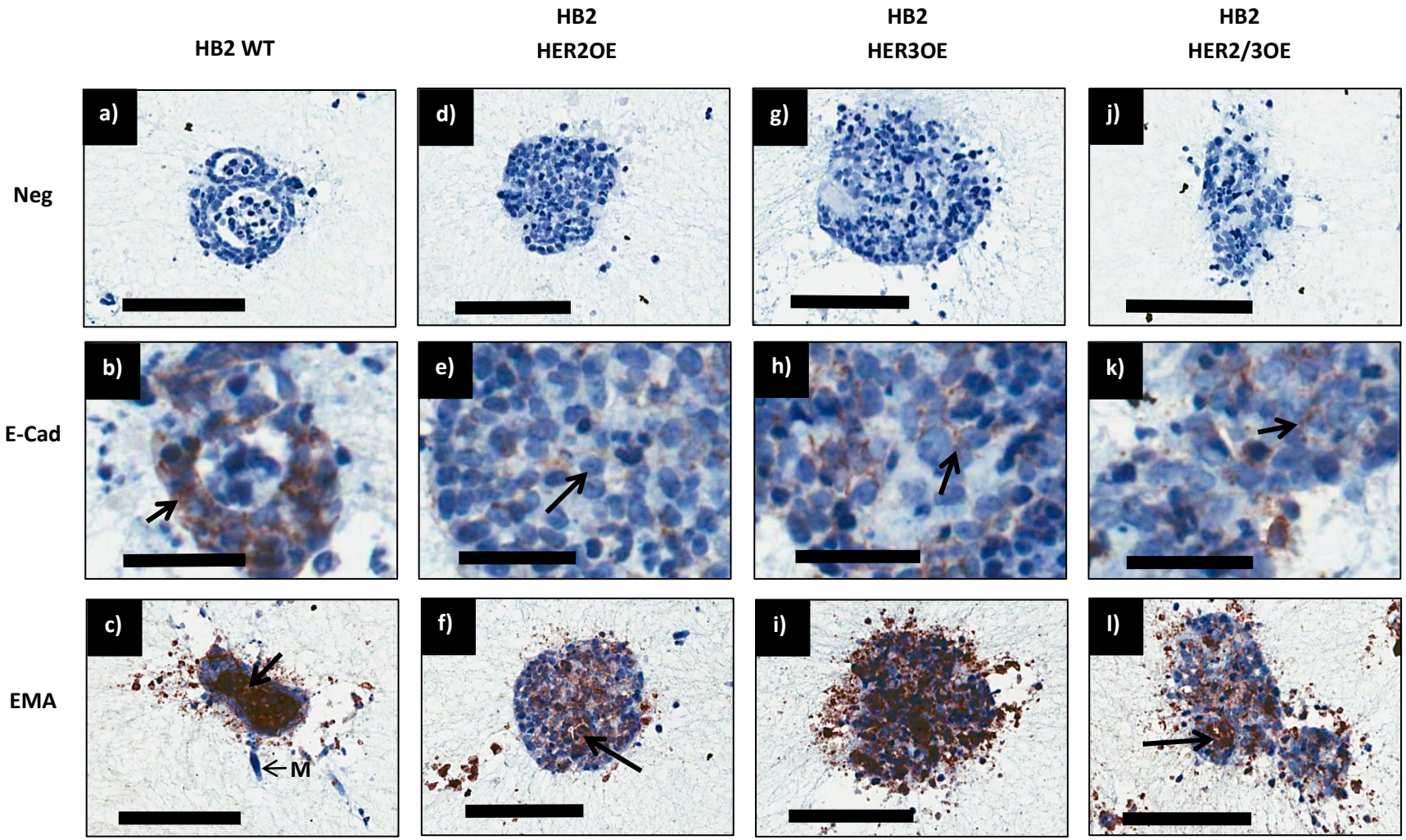
HB2 WT
HB2 HER2OE
HB2 HER3OE
HB2 HER2/3OE
Neg
E-Cad
EMA
a)
b)
c)
d)
e)
f)
g)
h)
i)
j)
k)
l)
M

Fig 4.16 IHC characterisation of 3D *in vitro* dual-culture models of HER overexpressing HB2 cells with myoepithelial cells A

HB2 wildtype (HB2 WT), HB2 HER2 overexpressing (HB2 HER2OE), HB2 HER3 overexpressing (HB2 HER3OE) and HB2 HER2 and HER3 overexpressing (HB2 HER2/3OE) cell unit phenotype in the presence of GFP Myo1089 cells (M) were characterised by IHC to assess cell adhesion and polarisation with representative images from three technical replicates presented. HER2 and HER3 overexpression reduced E-Cadherin (E-Cad) expression in HB2 units in the presence of GFP Myo1089 cells. HB2 WT units displayed strong expression of E-Cad between cell junctions surrounding a central lumen (arrow, b). There was a marked decrease in E-Cad expression in HB2 HER2OE, HB2 HER3OE and HB2 HER2/3OE units. HB2 HER3OE and HB2 HER3OE units had low levels of E-Cad expression within units (yellow arrows, e & h respectively) while HB2 HER2/3OE units (k) contain low levels of E-Cad expression both on the edge of units (black arrow) and within units (yellow arrow). Strong expression of Epithelial Membrane Antigen (EMA) was detected in the centre of HB2 WT units (arrow, c) and was negative for cells on the outer edge of the units. Expression of EMA was also detected within the middle of HB2 HER2OE (arrow, f) and HB2 HER2/3OE (arrow, l) units although this was weaker than in HB2 WT units. Strong but less organised EMA expression was detected across HB2 HER3OE units (i). Primary antibody was omitted to serve as negative (Neg) controls (a, d, g & j). Original magnification b, e, h & k, 40x, scale bars = 50µm. Original magnification of all others, 20x, scale bars = 100µm.

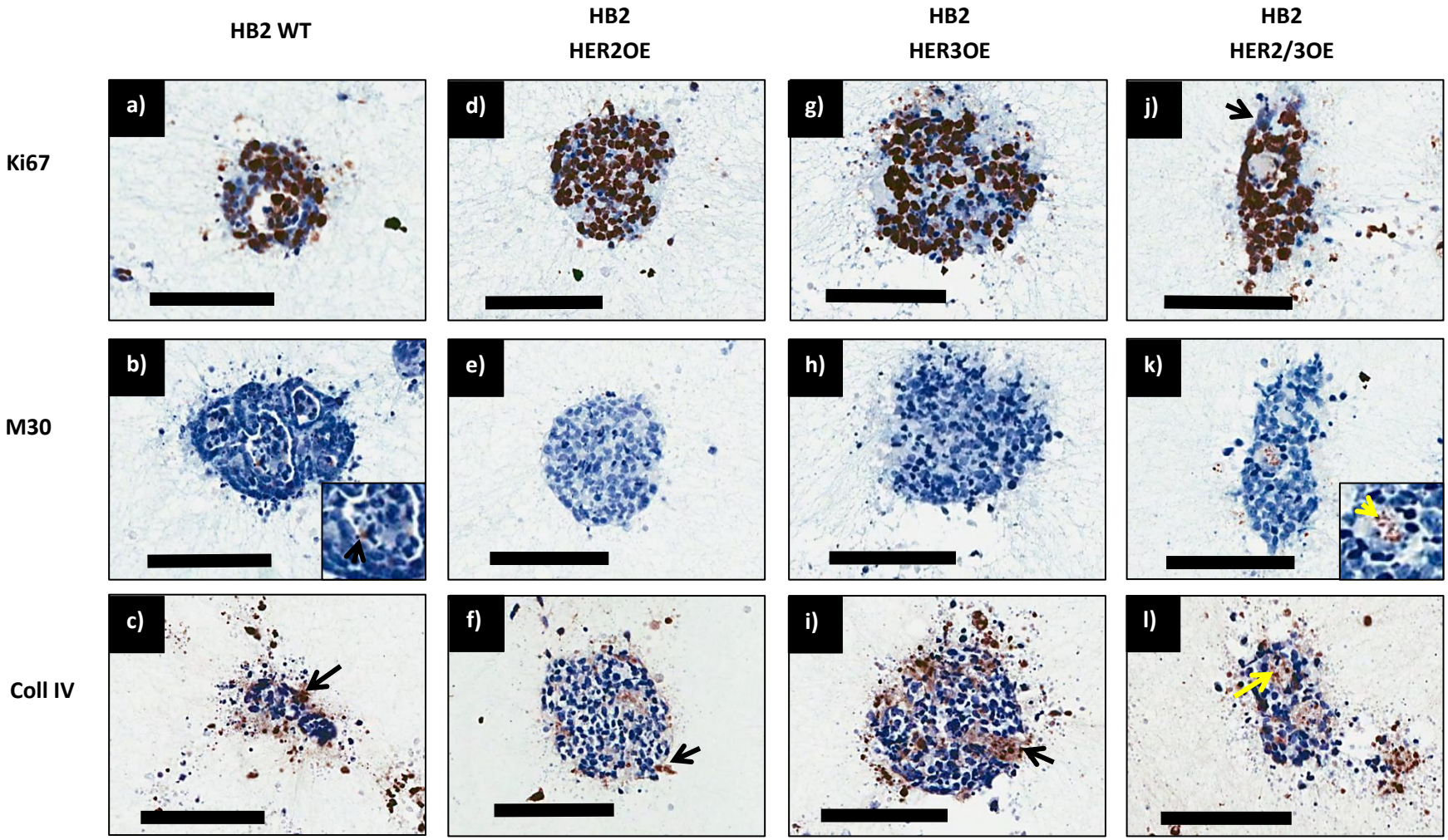
HB2 WT
HB2
HER2OE
HB2
HER3OE
HB2
HER2/3OE
Ki67
M30
Coll IV
a)
b)
c)
d)
e)
f)
g)
h)
i)
j)
k)
l)

Fig 4.17 IHC characterisation of 3D *in vitro* dual-culture models of HER overexpressing HB2 cells with myoepithelial cells B

HB2 wildtype (HB2 WT), HB2 HER2 overexpressing (HB2 HER2OE), HB2 HER3 overexpressing (HB2 HER3OE) and HB2 HER2 and HER3 overexpressing (HB2 HER2/3OE) cell unit phenotype with GFP Myo1089 cells were characterised by IHC to assess proliferation, apoptosis and basement membrane production with representative images from three technical replicates presented. HB2 WT, HB2 HER2OE and HB2 HER3OE cells expressed Ki67 in patches within units (a, d & g respectively) whereas all cells within HB2 HER2/3OE were positive for Ki67 (j). HB2 WT were largely negative for M30 expression but contained points of positivity within units (arrow, b). HB2 HER2OE (e) and HB2 HER3OE (h) units were negative for M30 staining while expression was clearly detected within lumens of HB2 HER2/3OE units (arrow, k). Collagen IV (Coll IV) expression was detected in all HB2 units with HB2 WT and HB2 HER2OE units showing expression on outer edges of units (arrows, c & f respectively), and HB2 HER3OE displaying expression in invaginations from the edges of units (arrow, i). HB2 HER2/3OE displayed expression within units (arrow l). Original magnification 20x, scale bars = 100µm.

4.4.6 The effect of fibroblasts on the morphology and phenotype of wildtype and HER overexpressing HB2 cells in 3D *in vitro* dual-culture

The determine the effect of fibroblasts on the formation of wildtype and HER overexpressing HB2 units, we assessed the morphology of HB2 dual cultures with representative images from three technical replicates presented (Fig 4.18) and demonstrated that in the presence of LS11-083 dsRed Fib, HB2 WT units remained small, rounded and cohesive but with less lumen formation than with GFP Myo1089 cells while with HER2 or HER3 overexpression alone, HB2 units appeared much larger and discohesive with the appearance of spindle-shaped cells around edges and no lumens which were features not observed with mono-, and dual-cultures with GFP Myo1089 cells. The effects of LS11-083 dsRed Fibs on HB2 HER2/3OE units were less pronounced with elongated and discohesive HB2 units observed which appeared smaller than with mono-culture. Quantification of units from three technical replicates (Fig 4.19) supported these observations with a significant increase in size of HB2 units with either HER2 or HER3 overexpression alone ($p=<0.05$, unpaired t-test). Only overexpression of either HER2 or HER3 in the presence of LS11-083 dsRed Fibs induced a change in number of units with a significant decrease to HB2 WT ($p=<0.01$, unpaired t-test). Only overexpression of HER2 demonstrated a significant loss of lumen formation compared to HB2 WT ($p=0.0210$, unpaired t-test).

Analysis by IHC using anti-dsRed (Fig 4.20) showed LS11-083 dsRed Fibs loosely distributed throughout collagen gels in HB2 WT and HB2 HER2/3OE gels only with no staining observed in HB2 HER2OE and HB2 HER3OE gels. Representative images from three technical replicates are presented. This confirmed units observed and quantified by H & E staining consisted predominantly of HB2 cells and not LS11-083 dsRed Fibs.

Characterisation of HB2 unit phenotype by IHC with representative images from three technical replicates presented (Fig 4.21 & 4.22) in response to LS11-083 dsRed Fibs demonstrated weaker E-cad expression within HB2 WT and HB2 HER3OE units, patchy

expression in HB2 HER2OE units and a loss of expression in HB2 HER2/3OE units. LS11-083 dsRed Fibs altered EMA expression with concentrated expression on the outer edges of HB2 WT units, and strong cytoplasmic staining observed across entirety of HER overexpressing HB2 units. Proliferation was increased with LS11-083 dsRed Fibs with strong Ki67 expression observed largely across the entirety of all HB2 units. Apoptosis was unaffected by LS11-083 dsRed Fibs as HB2 WT and HB2 HER2/3OE units were negative for M30 expression but an increase of apoptotic cells was detected in HB2 HER2OE and HB2 HER3OE units. Deposition of coll IV in all HB2 units was unaffected by LS11-083 dsRed Fibs exhibiting a similar profile to GFP Myo1089 dual-cultures.

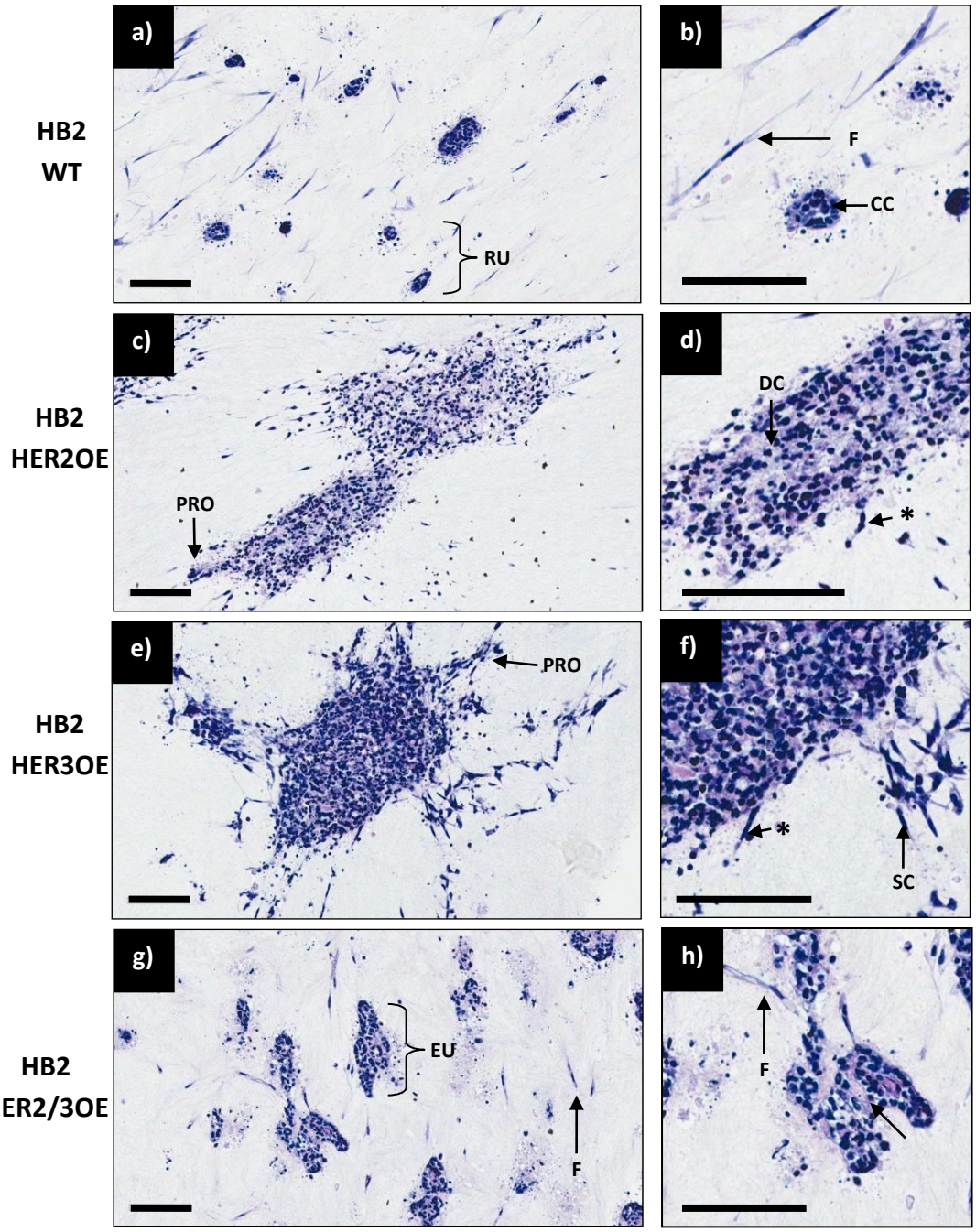

Fig 4.18 H & E staining of 3D *in vitro* dual-culture models of HER overexpressing HB2 cells with fibroblasts

Wildtype (HB2 WT), HER2 overexpressing (HB2 HER2OE), HER3 overexpressing (HB2 HER3OE) and both HER2 and HER3 overexpressing (HB2 HER2/3OE) HB2 cells were cultured with dsRed positive fibroblasts (dsRed fib) in 3D collagen gels for 21 days. 5µm sections of gels were stained with H & E with representative images from three technical replicates presented. HB2 WT cells (a) formed compact, rounded units (RU) containing cohesive cells (CC) with spindle-shaped fibroblasts (F) loosely distributed throughout the collagen gel. HB2 HER2OE cells (b) formed much larger less compact units containing discohesive cells (DC) that featured protrusions (PRO) and short spindle-shaped cells (*) loosely associated around the edge of the units. Similarly, HB2 HER3OE cells (c) formed large units that featured protrusions and short spindle-shaped cells loosely associated around the edge of the units but these were more

cohesive than HB2 HER2OE units. These also contained longer spindle-shaped cells (SC) loosely distributed around the gels. HB2 HER2/3OE cells (d) formed elongated units (EU) which contained discohesive cells but similar to HB2 WT featured fibroblasts loosely distributed throughout the collagen gel. Original magnification 20x, scale bars = 100µm.

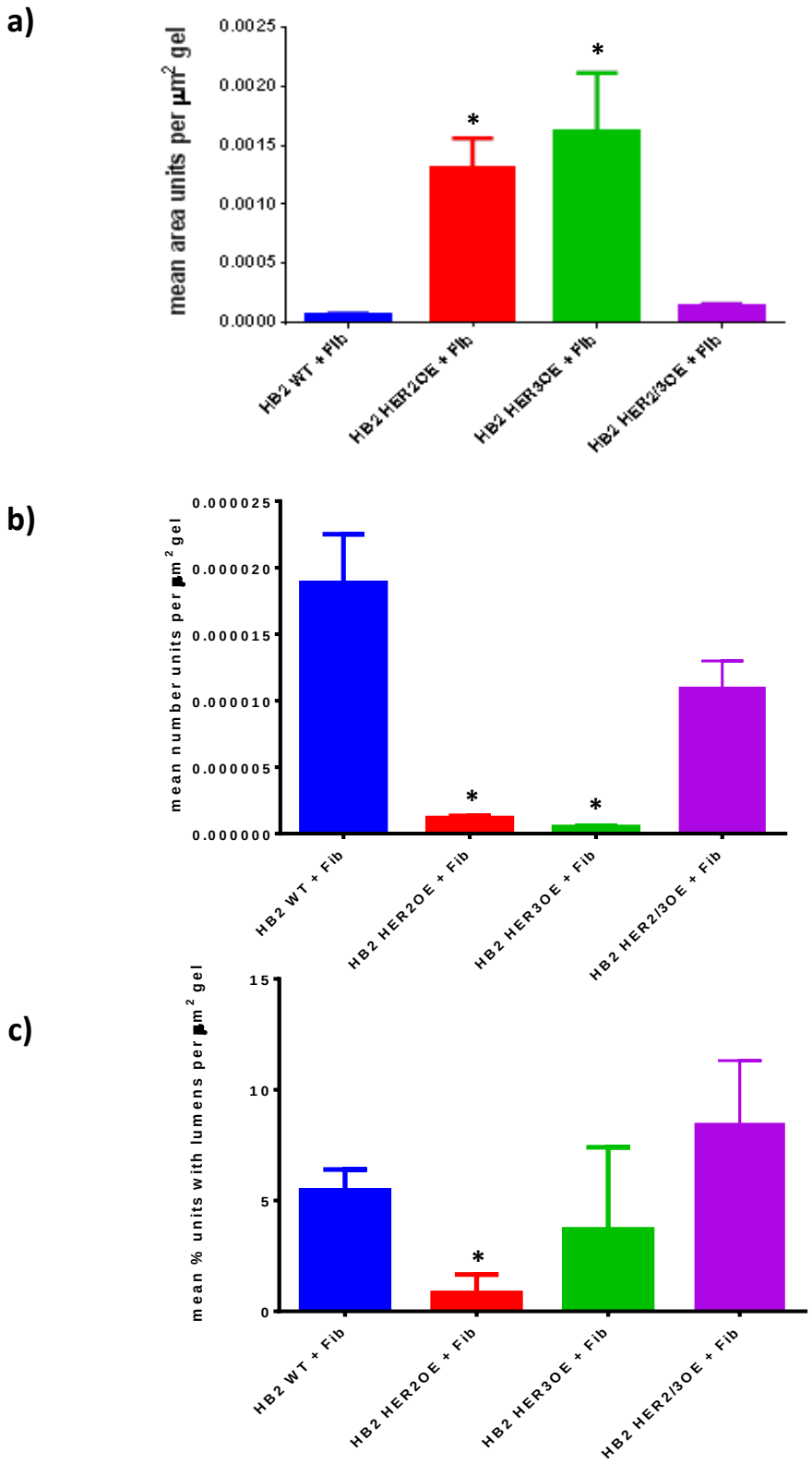

Fig 4.19 Quantification of area, number and lumen formation of HER overexpressing HB2 cell units in 3D dual-culture gels with fibroblasts from H & E stained sections

Size, number and lumen formation of wildtype (HB2 WT), HER2 overexpressing (HB2 HER2OE), HER3 overexpressing (HB2 HER3OE) and both HER2 and HER3 overexpressing (HB2 HER2/3OE) HB2 cell units cultured with dsRed Fibs was quantified with Aperio Image scope, analysed with

Graph Pad Prism 6 and normalized to total size of each respective collagen gel section. (a) Overexpression of HER2, HER3 and HER2/3 in HB2 cells significantly increased size of HB2 units formed. (b) Unlike other mono- and co-cultures, number of HB2 HER2OE and HB2 HER3OE units was significantly decreased with no significant difference seen with HB2 HER2/3OE. (c) Overexpression of HER2 only in HB2 cells significantly decreased lumen formation. Bars denote mean from three technical replicates and error bars standard error of the mean (SEM). * indicates significant difference to HB2 WT following unpaired t-test ($p=<0.05$).

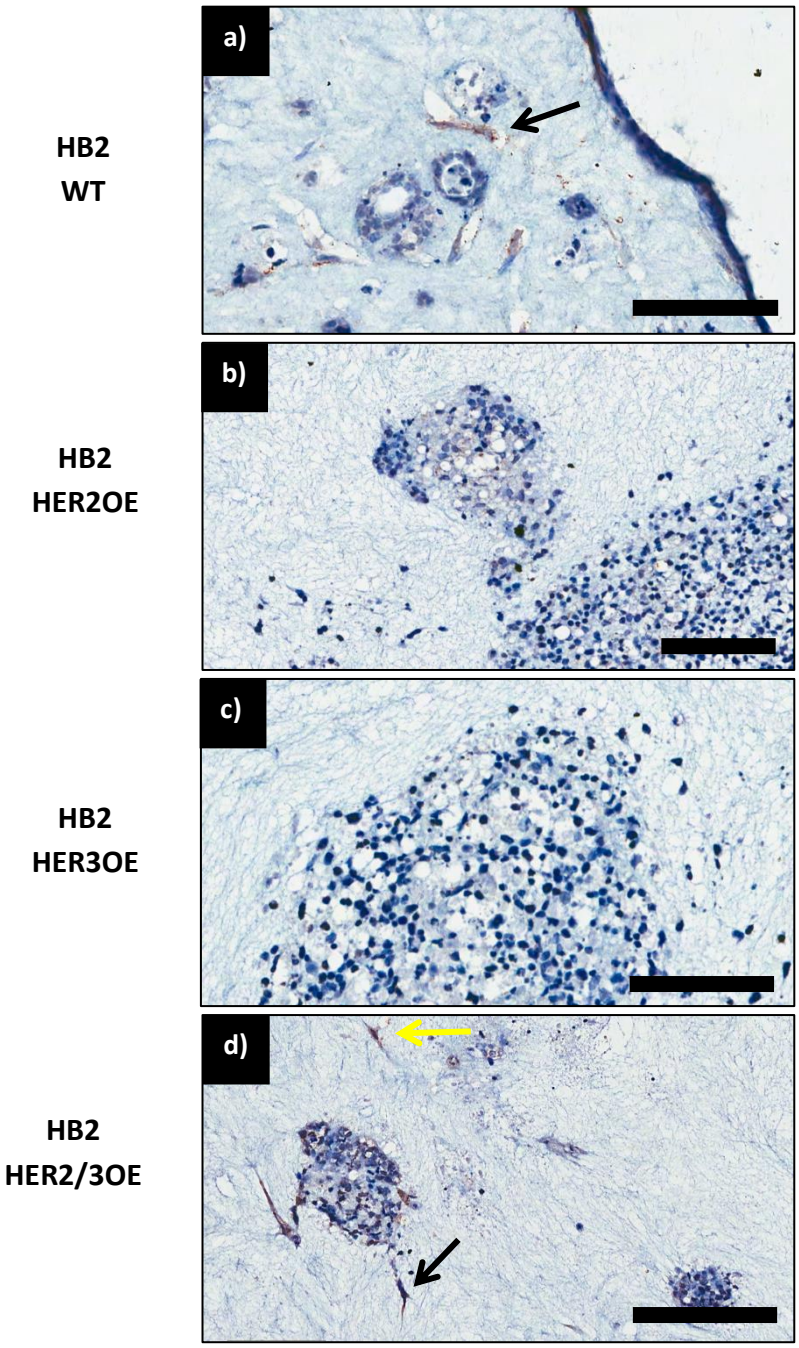

Fig 4.20 IHC labelling of fibroblasts in 3D *in vitro* dual-culture model

Wildtype (HB2 WT), HER2 overexpressing (HB2 HER2OE), HER3 overexpressing (HB2 HER3OE) and both HER2 and HER3 overexpressing (HB2 HER2/3OE) HB2 cells were co-cultured in 3D collagen gels with LS11-083 dsRed positive fibroblasts (LS11-083 dsRed Fibs) for 21 days. 5µm sections of gels were stained with anti-dsRed by IHC to visualise distribution of fibroblasts within gels with representative images from three technical replicates presented. HB2 WT and HB2 HER2/3OE gels displayed positive staining for dsRed Fibs. HB2 WT gels showed distribution of LS11-083 dsRed Fibs loosely associated with the edges of HB2 WT units (arrow, a). HB2 HER2/3OE gels also showed distribution of LS11-083 dsRed Fibs around edges of units (black arrow, d) as well as loosely distributed throughout the collagen gel (yellow arrow, d). No dsRed staining was observed in HB2 HER2OE (b) or HB2 HER3OE (c) gels. Original magnification 20x, scale bars = 100µm.

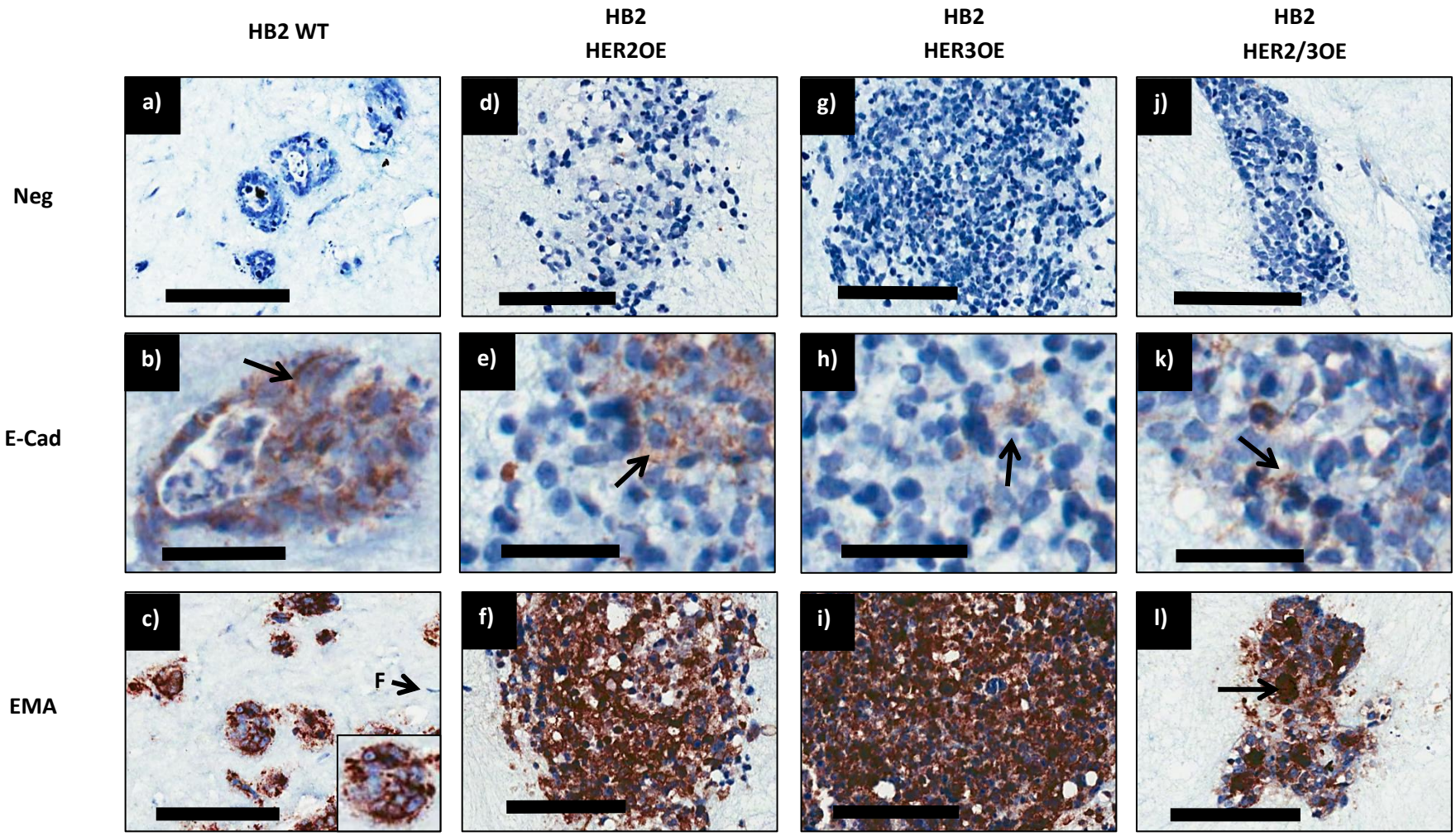
HB2 WT
HB2 HER2OE
HB2 HER3OE
HB2 HER2/3OE
Neg
E-Cad
EMA
a)
b)
c)
d)
e)
f)
g)
h)
i)
j)
k)
l)
F

Fig 4.21 IHC characterisation of 3D *in vitro* dual-culture models of HER overexpressing HB2 cells with fibroblasts A

HB2 wildtype (HB2 WT), HB2 HER2 overexpressing (HB2 HER2OE), HB2 HER3 overexpressing (HB2 HER3OE) and HB2 HER2 and HER3 overexpressing (HB2 HER2/3OE) cell unit phenotype with LS11-083 dsRed fibs (F) were characterised by IHC to assess cell adhesion and polarisation with representative images from three technical replicates presented. While all HB2 units were positive for E-Cadherin (E-Cad), E-Cad distribution within units differed upon HER2 and HER3 expression. HB2 WT cells displayed strong expression of E-Cad localised between cell junctions (arrow, b). HB2 HER2OE, HB2 HER3OE and HB2 HER2/3OE cells showed weaker patchy distribution of E-Cad staining within units (arrows, e, h & k respectively). Strong Epithelial Membrane Antigen (EMA) expression was detected within the whole of HB2 WT units (c). HB2 HER2OE and HB2 HER3OE units also showed strong expression of EMA throughout the whole of the units (f & i respectively). HER2/3OE cell units showed areas of strong EMA staining localised within centre of units (arrow, l). Primary antibody was omitted to serve as negative (Neg) controls (a, d, g & j). Original magnification b, e, h & k, 40x, scale bars = 50µm. Original magnification of all others, 20x, scale bars = 100µm.

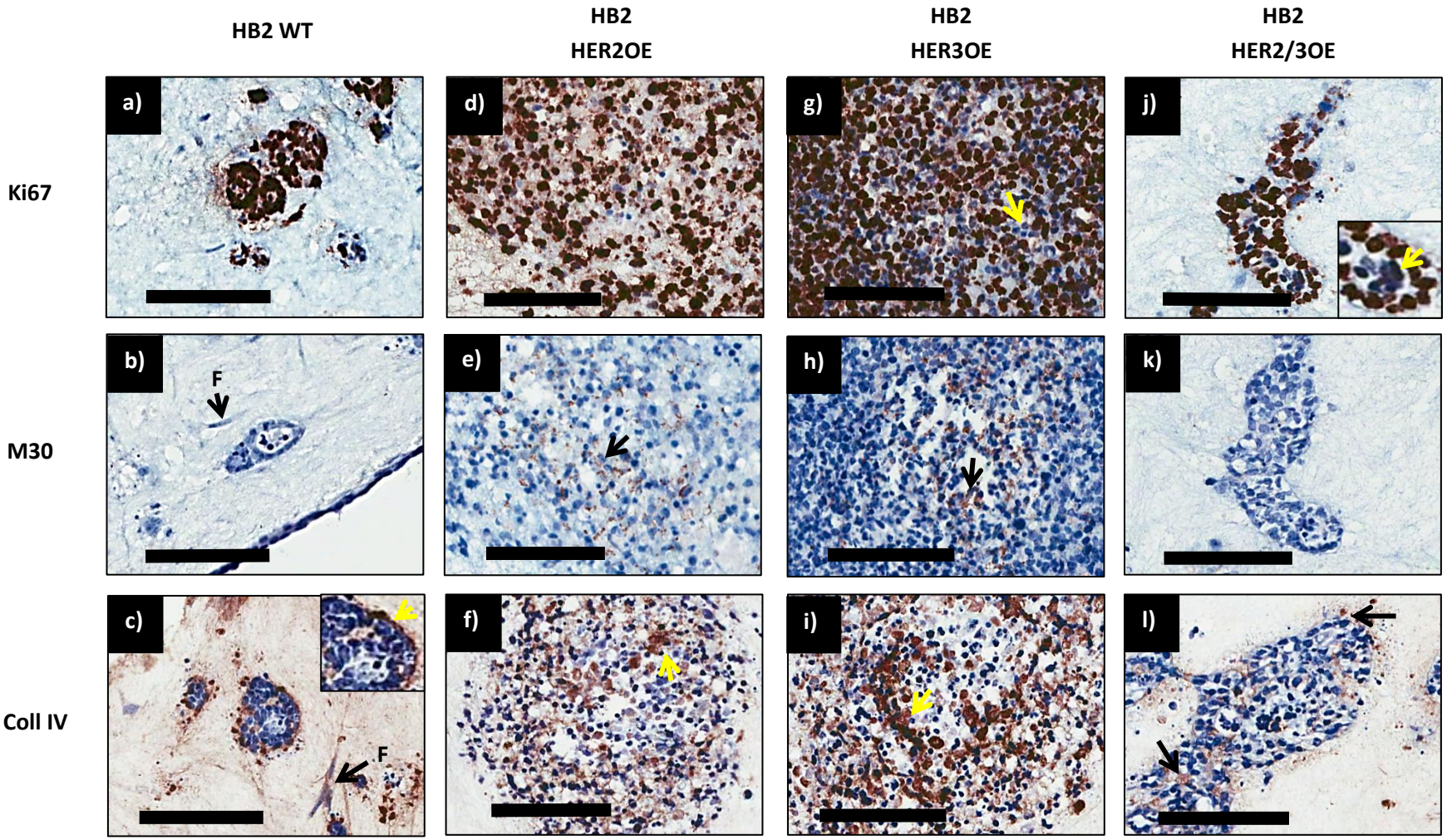
HB2 WT
HB2 HER2OE
HB2 HER3OE
HB2 HER2/3OE
Ki67
M30
Coll IV
a)
b)
c)
d)
e)
f)
g)
h)
i)
j)
k)
l)
F
F

Fig 4.22 IHC characterisation of 3D *in vitro* dual-culture models of HER overexpressing HB2 cells with fibroblasts A

HB2 wildtype (HB2 WT), HB2 HER2 overexpressing (HB2 HER2OE), HB2 HER3 overexpressing (HB2 HER3OE) and HB2 HER2 and HER3 overexpressing (HB2 HER2/3OE) cell unit phenotype with dsRed Fib (F) were characterised by IHC to assess proliferation, apoptosis and basement membrane production with representative images from three technical replicates presented. All cells within HB2 WT and HB2 HER2OE units displayed strong Ki67 expression (a & d respectively). HB2 HER3OE and HB2 HER2/3OE units also contained areas of Ki67 negativity (yellow arrows, g & j). HB2 WT and HB2 HER2/3OE were negative for M30 expression (b & k respectively), while HB2 HER2OE and HB2 HER3OE units contained positive areas in their centre (arrows, e & h respectively). Collagen IV (Coll IV) expression was detected only on outer edges of HB2 WT units (yellow arrow, c), while HB2 HER2OE and HB2 HER3OE units showed positive staining in their centres (arrows, f & i respectively). HB2 HER2/3OE units displayed Coll4 expression both within and around edges (arrows, l). Original magnification 20x, scale bars = 100µm.

4.4.7 Comparison of mono-, dual- and tri-cultures of HER protein overexpressing HB2 cells

To assess if the effects of HER protein overexpression in HB2 cells is affected by the 3D *in vitro* culture context, the representative H&E images from the HER overexpressing HB2 mono-, dual- and tri-cultures presented and discussed above were compared (Fig 4.23). This demonstrated that the co-culture of GFP Myo1089 cells, LS11-083 dsRed Fibs or both affected the morphology of HER overexpressing HB2 units. In tri-culture, HER2 overexpression induced the largest, most elongated and irregular HB2 unit morphology whereas in mono-culture, HER2, HER3 and both HER2 and HER3 overexpression all induced the formation of large, elongated, branched and discohesive HB2 units. Dual-culture with GFP Myo1089 cells had an organisational effect inducing the formation of rounded and cohesive HB2 units regardless of HER2 or HER3 protein overexpression. Dual-culture with LS11-083 dsRed Fibs had opposing effects to GFP Myo1089 cells with HB2 HER2OE, HB2 HER3OE and HB2 HER2/3OE units appearing much larger, discohesive and disorganised. Quantification of units from three technical replicates for each culture condition (Fig 4.24) supported these observations with a significant increase in size of HB2 WT, HB2 HER2OE and HB2 HER3OE units in dual-culture with LS11-083 dsRed Fibs ($p=<0.05$, unpaired t-test. The size of HB2 HER2/3OE units remained unchanged in mono-culture, dual-culture with LS11-083 dsRed Fibs and in tri-culture but was significantly decreased in dual-culture with GFP Myo1089 cells ($p=<0.0001$, unpaired t-test). This demonstrated that the effects of HER protein overexpression is context dependent suggesting a tumour suppressive role for GFP Myo1089 cells and a tumour promoting role for LS11-083 dsRed Fibs.

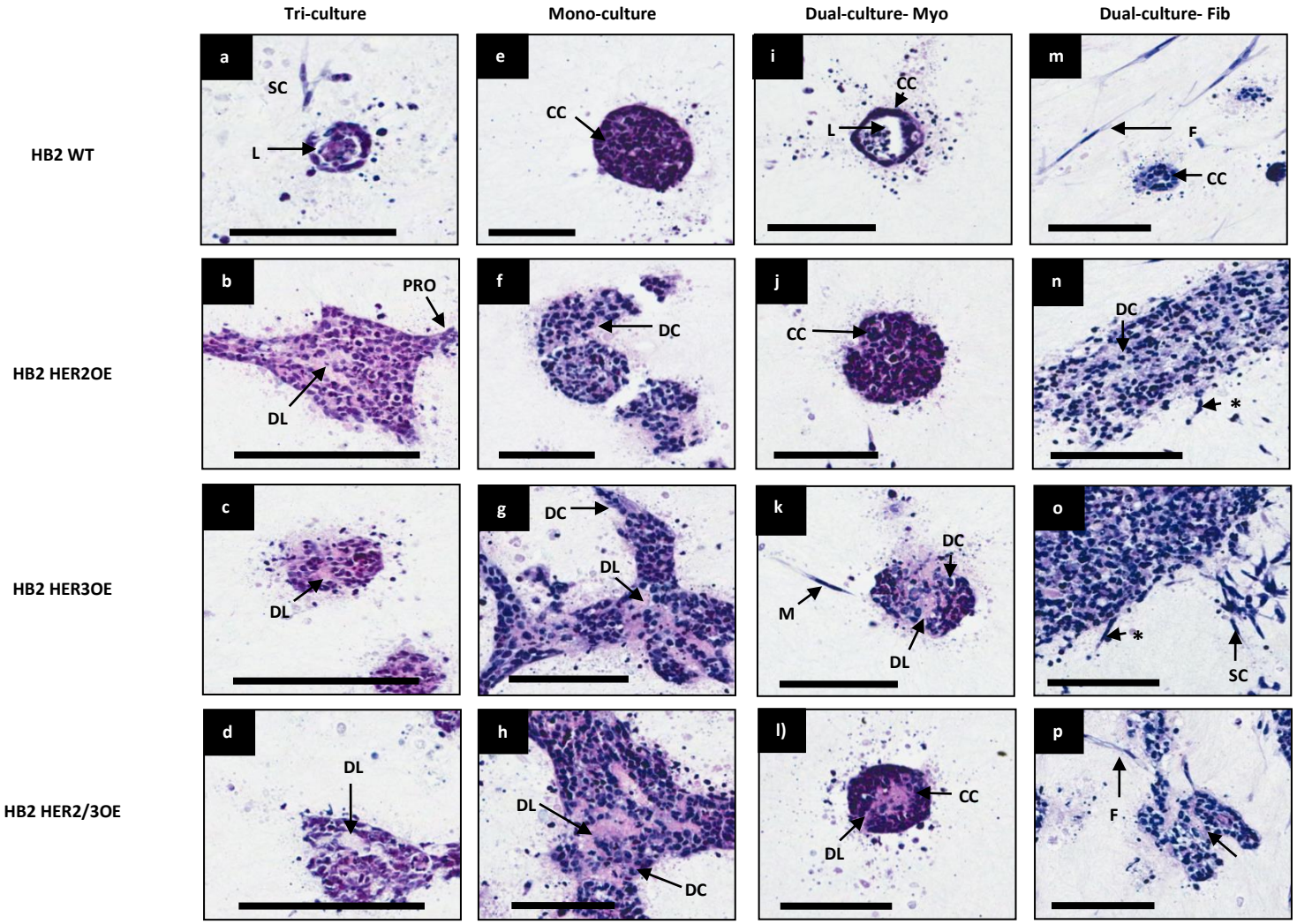
Tri-culture
Mono-culture
Dual-culture- Myo
Dual-culture- Fib
HB2 WT
HB2 HER2OE
HB2 HER3OE
HB2 HER2/3OE
a
SC
L
e
CC
i
CC
L
m
F
CC
b
PRO
DL
f
DC
j
CC
n
DC
*
c
DL
g
DC
DL
k
DC
M
DL
o
*
SC
d
DL
h
DL
DC
l)
CC
DL
p
F

Fig 4.23 Comparison of the morphological effects of HER protein overexpression on HB2 cells in different co-culture contexts

Representative H&E images from three technical replicates for HB2 WT, HB2 HER2OE, HB2 HER3OE and HB2 HER2/3OE units in tri-culture, in mono-culture and in dual-culture with either GFP Myo1089 cells (Dual-culture- Myo) or LS11-083 dsRed Fibs (Dual-culture- Fibs) are presented to compare morphological changes in response to HER overexpression in different co-culture contexts. It is apparent that HER overexpression had different effects on HB2 unit phenotype dependent on the co-culture context. On the whole, GFP Myo1089 cells had an organisational effect on HB2 units inducing formation of rounded and cohesive units regardless of HER protein overexpression (i-l). LS11-083 dsRed Fibs had opposing effects on HER overexpressing HB2 units as units appeared much larger, discohesive and disorganised (m-p). While HER2 overexpression appeared to have the most disruptive effects in the tri-culture context (a-d), it was HER3 overexpression that had the most effect on HB2 unit morphology in mono-cultures (e-h). Abbreviations :- SC = Spindle cell, L = Lumen, DL = Distorted Lumen, CC = Cohesive Cells, DC = Discohesive cells, M = Myoepithelial and F = Fibroblast. Original magnification, 20x, scale bars = 100µm.

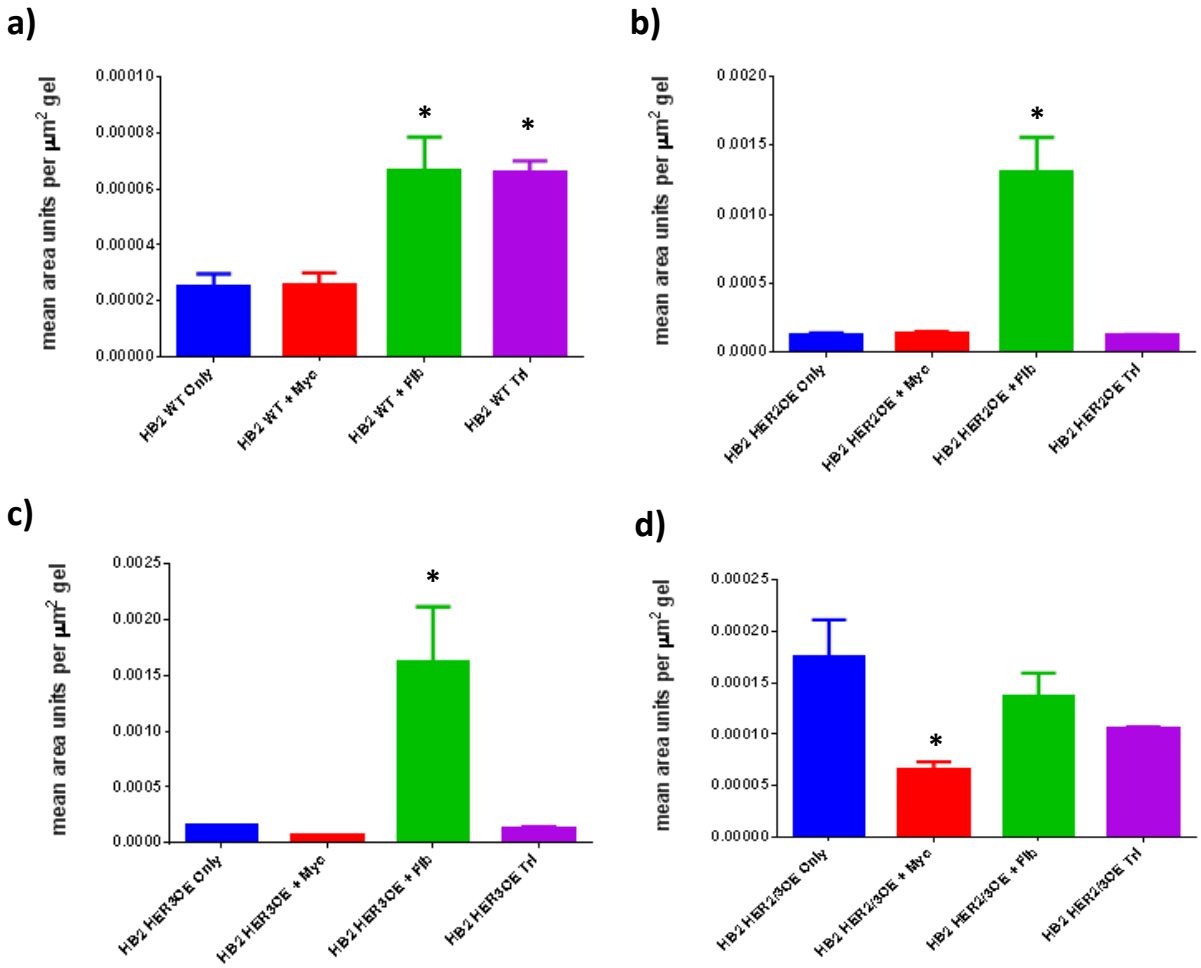

Fig 4.24 Quantification of area of HER overexpressing HB2 units in 3D mono-, dual- and tri-culture gels from H & E stained sections

Size of wildtype (HB2 WT), HER2 overexpressing (HB2 HER2OE), HER3 overexpressing (HB2 HER3OE) and both HER2 and HER3 overexpressing (HB2 HER2/3OE) HB2 cell units cultured as mono-culture (HB2 only), in dual culture with GFP Myo1089 (HB2 + Myo), in dual-culture with LS11-083 dsRed Fibs (HB2 + Fib) and in tri-culture with both GFP Myo1089 and LS11-083 dsRed Fib (HB2 Tri) was quantified with Aperio Image scope, analysed with Graph Pad Prism 6 and normalized to total size of each respective collagen gel section. (a) Dual-culture of HB2 WT cells with LS11-083 dsRed Fibs and in tri-culture significantly increased the size of HB2 units formed whereas dual-culture with GFP Myo1089 cells had no significant effect compared to HB2 WT mono-cultures. The size of HB2 HER2OE (b) and HB2 HER3OE cells (c) was significantly increased in dual-culture with LS11-083 dsRed Fibs only in comparison to mono-cultures. The size of HB2 HER2/3OE units (d) remained unchanged in dual-culture with LS11-083 dsRed Fibs and in tri-culture whereas dual-culture with GFP Myo1089 cells significantly decreased the size of HB2 units formed. Bars denote mean from three technical replicates and error bars standard error of the mean (SEM). * indicates significant difference to respective mono-cultures following unpaired t-test ($p=<0.05$).

4.5 Discussion

HER2 is a well characterised oncogene thought to be involved in breast tumorigenesis. However, despite the wealth of data available on HER2, the mechanisms behind how its overexpression affects normal mammary epithelium and breast cancer initiation is unclear. 3D models of HER protein overexpression in non-tumorigenic mammary epithelial cells usually consist of mono-cultures of MCF10A cells in reconstituted basement membrane preparations. These studies demonstrate a role for HER2 and HER3 in lumen filling, akin to features of DCIS, and invasion of non-tumorigenic mammary epithelial cells [273-275]. Possibly due to the scarcity of available cell lines, there have been few studies validating these features in other non-tumorigenic mammary epithelial cell types. Though not using HER2 overexpressing cells, the effects of HER2 and HER3 signalling have been investigated using the HB2 cell line cultured in collagen. Stimulation of HER2 signalling induced morphological changes such as increased branching of HB2 structures as well as increased cell proliferation [271] but lumen filling could not be addressed with this model. Though these studies go some way to investigating the transforming potential of HER2 and do so in a 3D context, they are still inadequate models of normal *in vivo* breast as they do not contain a stromal component.

This made HER2 a good candidate to focus on when assessing if the model was amenable to genetic manipulation and thus suitable for breast cancer initiation studies. We incorporated HER2 and HER3 overexpressing HB2 cells in our 3D tri-culture *in vitro* model of normal breast, providing a more *in vivo*-like microenvironment. To highlight the importance of culturing cells in an appropriate microenvironment, we also cultured HER overexpressing HB2 cells either alone, in co-culture with myoepithelial cells only or with fibroblasts only and compared to our tri-culture models with the aim of elucidating whether the effects of HER protein on luminal epithelial cells were context dependent.

4.5.1 The effects of HER protein overexpression in HB2 cells in the 3D tri-culture model

First, we sought to assess the effects of HER2 and HER3 overexpression in the luminal epithelium in the tri-culture model of normal breast. Through culture of HB2 WT cells with GFP Myo1089 cells and LS11-083 dsRed Fibs, we were able to recapitulate features seen in Chapter 3 with small rounded units formed containing lumens as well as a similar phenotype upon IHC characterisation proving that the model was robust and reproducible. It appeared HER2 overexpression in HB2 cells alone had the most dramatic effect on the architecture of HB2 units. HB2 HER2OE units were much larger, more elongated, featured protrusions and were remarkably similar to DCIS. We quantified lumen formation within HB2 units and defined a lumen as a space within units surrounded by a continuous layer of HB2 cells. We found that HER protein overexpression significantly reduced lumen formation within HB2 units. This correlated with reports in the literature which suggested HER2 and HER3 protein overexpression increased proliferation and lumen filling in MCF10A cells [273-275]. However, these features were less pronounced with HER3 overexpression alone or with a combination of HER2 and HER3 overexpression suggesting that the HER2-HER3 heterodimer was not the most potent inducer of aberrant epithelial architecture in our tri-culture model. This indicated that in the tri-culture model, HER2 overexpression elicited a DCIS-like phenotype of HB2 cells mediated not through dimerization with HER3 but perhaps with another HER receptor. Although this contradicts studies discussed which suggested the HER2-HER3 heterodimer is the most mitogenic HER receptor combination, dimerization of HER2 with other HER proteins such as EGFR [276] has also been proven to be strongly mitogenic which could account for the larger HB2 HER2OE units.

Another theory is that the larger HB2 HER2OE units were produced via cell migration and then subsequent adhesion rather than via increased proliferation. The HER2-EGFR heterodimer can drive cell migration in HER2 overexpressing cells [277]. This would account for the appearance

of protrusions at the edges of these units as well as the little change observed in Ki67. However, loss of E-cad expression is a feature of EMT [278] which was not observed in our study. This could be explained by the fact that E-cad can aid HER2-EGFR signalling [279] and has been shown to stabilise the HER2-HER3 heterodimer [280] and thus may not be a robust marker for EMT in the context of HER protein manipulation. The retention of E-cad in HB2 units correlates with research by Aceto et al [275] who showed increased migration of MCF10A cells upon HER2 overexpression with no change in E-cad expression. This group examined markers such as N-Cadherin and Fibronectin-1 which were not analysed in our study meaning it is feasible that HER overexpressing HB2 cells in our study did undergo EMT.

Given that coll IV expression surrounding HB2 units was unchanged by HER overexpression, and considering the theory that HER2 overexpression induces larger HB2 units due to cell migration, it could be that these structures are formed by groups of cells migrating together early on in the culture process and that this migration is enhanced by HER2 overexpression. Following a period in culture, GFP Myo1089 cells and LS11-083 dsRed Fibs may induce organisation of HB2 units and subsequently stimulate basement membrane production. However, the loss of organised EMA staining in these units would indicate that the ability of HB2 HER2OE cells to resume normal polarisation and architecture is still impaired. Distribution of EMA has been proven to be disrupted via HER2 expression and is thought to contribute to increased mitogenic activity [Reviewed in 281] perhaps explaining this aberrant staining pattern. While not investigated in our study, analysis of structures formed at earlier time points in culture, IHC with specific cell motility markers, and/or time-lapse microscopy could determine whether the aberrant architecture of HB2 units upon HER overexpression is due to cell migration or other mechanisms.

It was clear from this experiment that although HER2 overexpression in the tri-culture model produced a DCIS-like phenotype, the overexpression of both HER2 and HER3 had less of a

detrimental effect on HB2 unit architecture contradicting what has been suggested in the literature. One limitation here is that the confirmation of HER2 and HER3 protein overexpression was only assessed by western blot and not confirmed by dual-stain immunofluorescence for both HER2 and HER3 in HB2 HER2/3OE cells. This coupled with the fact that these cells were generated through transduction of HER2 and HER3 genes on two separate plasmids on two separate occasions means it is therefore possible that this cell line consists of a mixed population of cells that overexpress just HER2 and cells that overexpress both HER2 and HER3. This would support the observation of a mixed morphology of HB2 units in the tri-culture model. However, this is unlikely due to the fact that the cell line was purified by dual-staining FACS to produce cell populations which were over 95% positive for both transgenes. In addition, it could be expected that cells containing both transgenes would confer a growth advantage over those that express HER2 only due to strong evidence of the ability of the HER2-HER3 heterodimer to increase PI3K and MAPK signalling [249-251] and would therefore represent the majority of the cell population. Nevertheless, further examination of this cell line by dual-stain immunofluorescence for HER2 and HER3 would be required to definitively prove this.

However, since the effects of HER protein overexpression on luminal epithelial architecture has not been studied in the presence of both myoepithelial cells and fibroblast before, we hypothesised that the unexpected response from HB2 HER2/3OE cells in the tri-culture model was due to the difference in the luminal cell microenvironment and that the effects of HER overexpression are context dependent. We therefore examined the effects of HER overexpression in HB2 cells in different co-culture conditions to address this.

4.5.2 The importance of the stromal microenvironment on the effects of HER protein overexpression in HB2 cells

The mono-culture of HER overexpressing cells resulted in different morphologies and phenotypes to those observed in tri-culture. We found that HB2 WT units were unable to form lumens without myoepithelial cells or fibroblasts. However, interestingly, lumen formation increased upon overexpression of HER3 and HER2 and HER3 in HB2 cells. Since HER2-HER3 heterodimer signalling is proven to increase cell proliferation in HB2 cells [271], a decrease in lumen formation in these units might be expected. However, examination of these lumens by H & E staining suggests they were a product of necrosis rather than HB2 cell polarisation and rearrangement. This is supported by a lack of M30 expression within these units suggesting lumens were not formed by programmed cell death. It has been demonstrated that tumours *in vivo* above 200mm^3 undergo necrosis in their centres due to lack of nutrient penetration [282]. Since HB2 units were much larger upon HER3 and both HER2 and HER3 overexpression, it could be reasoned that necrosis was triggered by a lack of nutrient penetration into these structures due to their size. However, HB2 HER2OE units were similarly much larger than HB2 WT units but necrosis was not observed suggesting this is not the case. Central necrosis following lumen filling within breast ducts is a feature of high grade DCIS [283]. HER2 amplification is found in approximately 90% of high grade DCIS lesions [284]. It was surprising that in our study, HER3 overexpression seemed to drive development of these DCIS-like features as well as increased branching. However, since these features were conserved in HB2 HER2/3OE units, we can speculate that HER3 effects were dependent on the dimerization with HER2. The abundance of HER3 protein in DCIS has not been documented so it is possible that HER3 is required for HER2 induced DCIS features *in vivo*.

The mono-culture of HER overexpressing HB2 cells produced a phenotype that largely correlated with results from tri-culture. EMA localisation to the centre of HB2 WT units was observed and was lost in response to HER2 and HER3 overexpression and all HB2 unit types

remained proliferative. One difference observed in all mono-cultures was a lack of strong and organised collagen IV staining around the outer edges of the units suggesting inadequate formation of a basement membrane. This could be due to a lack of an appropriate microenvironment in this system.

Though HER protein overexpression in HB2 cells in mono-culture better recapitulated features seen in the literature than what was observed in the tri-culture model, this agreed with our hypothesis that myoepithelial cells and fibroblasts influence the effect of HER protein overexpression in HB2 cells. We investigated this further by examining the morphology and phenotype of HER protein overexpressing HB2 cells in dual-culture with either GFP Myo1089 cells or LS11-083 dsRed Fibs.

4.5.3 Myoepithelial cells suppress the tumorigenic effects of HER overexpression in HB2 cells

Consistent with research by Gudjonsson et al [285] who demonstrated myoepithelial cells have the capacity to induce organisation and lumen formation of luminal epithelial cells, co-culture with GFP Myo1089 cells induced lumen formation in HB2 WT cells and dramatically altered structures of HER overexpressing HB2 units in comparison to mono-cultures. Branching of HER overexpressing HB2 units was diminished and these appeared cohesive and rounded akin to HB2 WT units. However, overall size did not appear to be affected with no significant difference in size demonstrated to mono-cultures apart from with HB2 HER2/3OE units.

IHC characterisation of the units provided insight into the mechanisms behind the "containment" effect of GFP Myo1089 cells. GFP Myo1089 cells appeared to increase polarisation of HER overexpressing HB2 units. GFP Myo1089 cells caused increased distribution of EMA to the centre of HB2 HER2OE and HB2 HER2/3OE units with less ubiquitous cytoplasmic staining as observed in mono-cultures. Since this was not observed in HB2 HER3OE cultures, one theory is that HER2 mediates this process as it has been proven to interact with

EMA at cell membranes [Reviewed in 281], and that dimerization with another HER partner by HER3 interfered with GFP Myo1089 induced polarisation of HB2 cells.

GFP Myo1089 cells also appeared to have pro-apoptotic effects on HER overexpressing units. M30 expression was detected in the centre of HB2 HER2/3OE units suggesting lumens may be formed by programmed cell death and was a feature not observed in mono-cultures. Myoepithelial cells have been proven to induce apoptosis in tumour cells [286]. However, this was not observed in HB2 HER2OE and HB2 HER3OE units. It could be that GFP Myo1089 cells have a pro-apoptotic effect on HB2 cells and that this effect is overcome by overexpression of HER2 or HER3 alone but not both. It is conceivable that heterodimerisation with other HER receptors in HB2 HER2OE and HB2 HER3OE cells triggers a more potent anti-apoptotic signalling cascade than the HER2-HER3 heterodimer and that this is more efficient in counteracting the pro-apoptotic signals of GFP Myo1089 cells.

Lack of organised staining of collagen IV around edges of HB2 HER2OE, HER3OE and HER2/3OE units suggests that the “containment” effect of GFP Myo1089 cells have on these structures is not mediated by laying down a collagen IV-rich basement membrane protein layer. While coll IV is a major component of basement membrane [287], it is feasible that the containment effect of GFP Myo1089 cells is mediated by production of other basement membrane proteins. For example, myoepithelial cells secrete Laminin-1 which induces organisation of luminal epithelial cells in culture [71] and could be expressed in our dual-culture model. Myoepithelial cells also release a variety of paracrine factors such as TIMP-1, Protease Nexin 2, alpha-1 antitrypsin and Maspin [288] that reduce tumour cell invasion and could also account for the containment effect of HB2 cells in the model.

4.5.4 Fibroblasts promote the tumorigenic effects of HER overexpression in HB2 cells

Co-culture of HER overexpressing HB2 cells with LS11-083 dsRed Fibs had dramatically different effects compared to mono-culture, tri-culture or co-culture with myoepithelial cells. Consistent with evidence that CAFs promote proliferation and invasion of tumour epithelial cells through paracrine factors [Reviewed in 33, 289, 290] and that CAFs have no [291] or little effect [292] on the proliferation on normal MCF10A epithelial cells, LS11-083 dsRed Fibs had little morphological effect on HB2 WT units but dramatically disrupted the architecture of HB2 HER2OE and HB2 HER3OE units. These were over 13 times larger and consisted of discohesive spindle-shaped cells.

IHC characterisation did not show any change in Ki67 staining which suggested that LS11-083 dsRed Fibs did not mediate their effects via increasing proliferation of HB2 cells. This is despite evidence that fibroblasts can stimulate epithelial cell proliferation [293] via release of HGF [294] and cause a DCIS-like phenotype in 3D culture [295]. However, a loss of E-cad expression in HB2 HER3OE and HB2 HER2/3OE was observed so it is possible that LS11-083 dsRed Fibs mediated their effects through promoting an EMT transition in these cells. Since this was only evident upon HER3 overexpression, it is conceivable that this was facilitated through production of the HER2-HER3 ligand heregulin which has been reported to be secreted by fibroblasts [296] and stimulates the PI3K-Akt pathway, down-regulating E-cad [297]. An increase in cell migration could explain the increase in size of these units perhaps indicating HB2 cells moved together to form large structures perhaps accounting for the significant reduction in number of units observed. However, E-cad expression was not lost in HB2 HER2OE units meaning LS11-083 dsRed Fibs must mediate the same effects on these cells via a different unknown mechanism.

This theory of an increased invasive phenotype is also supported by the loss of coll IV surrounding HER overexpressing HB2 units [298, 299] which could be explained by the capacity of fibroblasts to not only secrete growth and pro-migratory factors, but also their ability to secrete collagenase IV [300]. Although the production of coll IV in HB2 WT cultures is indicative that these cells had a less invasive phenotype as expected, it was surprising that this was not evident in dual-culture with GFP Myo1089 cells. While fibroblasts are known to produce collagen I [301], the literature states it is myoepithelial cells that produce coll IV [71]. The production of coll IV by fibroblasts in breast has not been documented. Since in breast, coll IV is secreted by myoepithelial cells, perhaps in this situation LS11-083 dsRed Fibs stimulate HB2 cells to become myoepithelial-like which is a process proven possible in the literature [302] via EMT through expression of CXCL12 [303]. It is possible HB2 cells produced coll IV themselves through release of TGF-β by LS11-083 dsRed Fibs [304] which is known to induce coll IV production by epithelial cells in other tissue types [305]. Since myoepithelial cells in other tissues produce coll IV in response to TGF-β signalling [306], it is feasible that GFP Myo1089 cells in our system need growth factors produced by LS11-083 dsRed Fibs to lay down basement membrane proteins, which is supported by the detection of collagen IV in our tri-culture model. TGF-β signalling in mammary epithelia is complex however; it is proven that TGF-β is tumour suppressive in normal mammary epithelia but tumour promoting in mammary epithelia that have undergone an oncogenic event [307]. It is conceivable that in our system, LS11-083 dsRed Fibs secrete TGF-β which promotes coll IV production by normal HB2 cells but invasion and migration of HB2 HER2OE and HER3OE cells.

Given the disruption caused by the addition of LS11-083 dsRed Fibs to the HB2 unit architecture, it was surprising that IHC with anti-dsRed demonstrated a loss of fibroblasts in these cultures. This could be explained by a “Reverse Warburg” effect. It is documented that breast cancer cells can induce aerobic glycolysis in neighbouring fibroblast cells [308]. It is therefore plausible that in our study, HER2 or HER3 overexpression induces a tumorigenic

phenotype in HB2 cells; these subsequently induce aerobic glycolysis and thus mitochondrial dysfunction in the LS11-083 dsRed Fibs which “feeds” the HB2 cells and leads to increased proliferation or motility but ultimately resulting in LS11-083 dsRed Fib death. Although not examined in our study, this could be confirmed by IHC for monocarboxylate transporter-1 and monocarboxylate transporter-4 thereby monitoring lactate influx and efflux in these cells [309].

4.5.5 Summary

Through the overexpression of HER proteins within HB2 cells in our study, we have demonstrated that the model is amenable to genetic manipulation and thus suitable for cancer initiation studies in a more *in-vivo* like context. By recapitulating features from Chapter 3, we have also proved the model is robust, is quantifiable and can be easily analysed through standard laboratory techniques such as IHC. Furthermore, we have proved through overexpression of HER2 that formation of structures that accurately reflect DCIS *in vivo* can be achieved (confirmed by a consultant breast pathologist, Dr Rebecca Millican-Slater) further validating the suitability of the model for cancer initiation studies.

In addition, we have provided evidence that the ability of HER2 and HER3 overexpression to induce changes in HB2 luminal epithelial architecture is altered in the presence of both myoepithelial cells and fibroblasts. It was clear that unlike the mono-cultures, the effects of HER overexpression in the tri-cultures were not consistent with studies in the literature. It is probable that co-culture of luminal cells with myoepithelial cells or fibroblasts changes the ligand availability to HER receptors and can therefore influence which heterodimers are formed, which in turn affects downstream signalling and phenotype of these cells. Wolf-Yadlin and colleagues [276] found that regardless of HER2 overexpression, it is the ligand that determines HER heterodimerisation and thus signalling outcome of epithelial cells. Since heregulin stimulates the HER2-HER3 heterodimer, a deficiency in heregulin upon co-culture

with GFP Myo1089 cells and LS11-083 dsRed Fibs could explain the lack of a significant response upon HER2 and HER3 overexpression together in the dual- and tri-culture models. This will be addressed in Chapter 5. It is apparent that the stroma influences the potency of oncogenic events in the luminal epithelium and perhaps caution should be taken when interpreting results from studies that lack these components.

5 Chapter 5: Effect of Heregulin on normal and HER overexpressing tri-culture models

5.1 Introduction

While Chapter 4 proved that overexpression of HER2 and HER3 proteins together in HB2 cells increased the size and disrupted the shape of HB2 WT units in 3D tri-culture, these changes appeared less pronounced than with either HER2 or HER3 overexpression alone. This contradicted the notion in the literature whereby the HER2-HER3 heterodimer is considered the most potent [310, 311]. We therefore sought to prove HB2 HER2/3OE cells were able to respond to HER2-HER3 ligand by examining the morphological effects of ligand stimulation in 3D tri-culture as well as the capacity to stimulate known downstream signalling proteins intracellularly. We hypothesised that HB2 HER2/3OE cells had the capacity to induce the morphological features described in the literature as well as those seen in Chapter 4 with HER2 or HER3 overexpression alone but that in the 3D novel tri-culture environment, the endogenous levels of the HER2-HER3 ligand were not sufficient to facilitate this and that the HB2 HER2/3OE cells were not deficient in their HER2-HER3 signalling capacity.

5.1.1 HER ligands: Neuregulins

Neuregulins (also known as Heregulins) are a family of structurally related proteins that mediate intercellular signalling interactions. The neuregulin gene family consists of four members, NRG1, NRG2, NRG3 and NRG4 (also known as HRG1-4). Less is known about the functions of NRG2-4 with NRG1 receiving the most research attention over the last few decades [312]. Through post-transcriptional modification, over 15 different precursor isoforms are synthesised from the NRG1 gene [313]. These isoforms are classified as Type I, Type II or Type III determined by their differing N-terminal sequences. The structure of neuregulin-1 isoforms are show in Fig 5.1. Type I and II neuregulins contain immunoglobulin-like domains (Ig domains) and only differ in their N-terminal sequences whereas Type III neuregulins do not

contain Ig domains but do contain cysteine-rich domains within their N-terminal sequences. All bioactive neuregulins contain either an α or β EGF-like domain which alone has proved sufficient to activate HER receptor dimers [314]. Type I precursors contain hydrophobic transmembrane spanning domains and thus are expressed at cell membranes. As shown in Fig 5.2, these are orientated with N-terminal region, Ig-domains and EGF-like domains situated extracellularly and cytoplasmic tail situated intracellularly. Extracellular cleavage of proproteins via ADAM17 and ADAM 19 [315, 316] at the stalk region releases an ectodomain fragment that is bioactive serving as a ligand for HER dimers in a paracrine manner.

5.1.2 Heregulin

Heregulin (HRG) is a type I NRG and is further sub classified as HRG-α and HRG-β dependent on the nature of the EGF-like domain [314]. Both these HRG isoforms are proven to have the same binding specificity to HER2/HER3 and HER2/HER4 heterodimers [317-319]. HRG-α has been demonstrated to be the dominant isoform in regulating breast development and ductal branching in pre-clinical mouse models [320]. However, other reports have suggested HRG-β can elicit these same effects in a context dependent manner requiring the presence of estradiol and progesterone [321]. It remains unclear why HRG-α has proven more critical for breast development. Most studies using human breast cells *in vitro* and biochemical assays have reported HRG-β to be up to 100 times more potent than HRG-α in the binding affinity for HER receptors [317, 319, 322] making HRG-β the preferred isoform for subsequent *in vitro* studies. These conflicting results could be attributed to the difference in physiology between mice and humans as there is no data available on the expression of HRG isoforms in during human development.

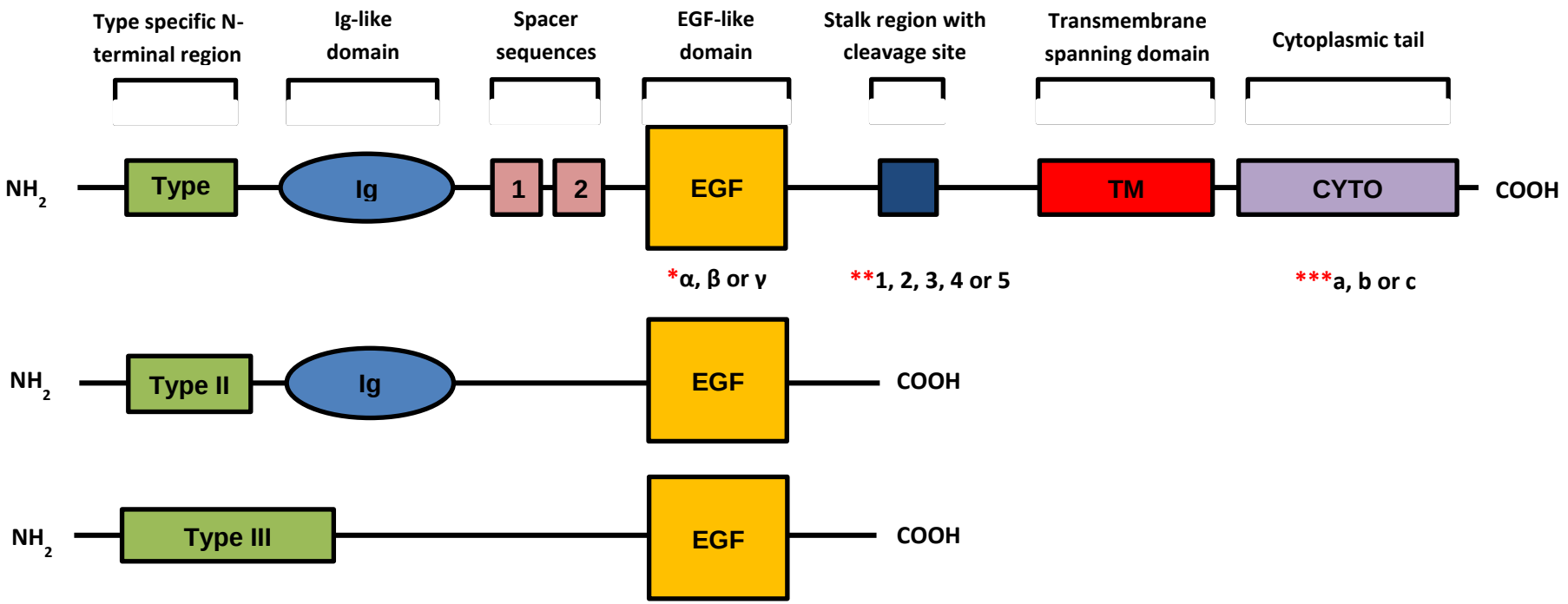

Fig 5.1 Schematic representation of the structures of neuregulin-1 isoforms

Neuregulin-1 isoforms differ in their N-terminal sequences (green) due to initiation from different promoters generating Type I, Type II and Type III NRG1. Type I, II and III NRG1 all contain an EGF-like domain (yellow) which differs following alternative splicing to give α, β or γ variants (*). Only Type I and II NRG1 contain an immunoglobulin-like domain (Ig-like domain, light blue). Domains specific to Type I NRG1 include: Spacer sequences containing glycosylation sites (pink, 1 & 2), a juxtamembrane stalk region which differs following alternative splicing to give 1, 2, 3, 4 or 5 variants (**) and that provides a cleavage site (dark blue), a transmembrane spanning domain (red) and an intracellular cytoplasmic tail (lilac) which differs following alternative splicing to give a, b or c variants (***). Type I NRG1 is the only isoform of NRG1 capable of existing as a transmembrane spanning protein due to it being the only NRG1 with a transmembrane spanning domain.

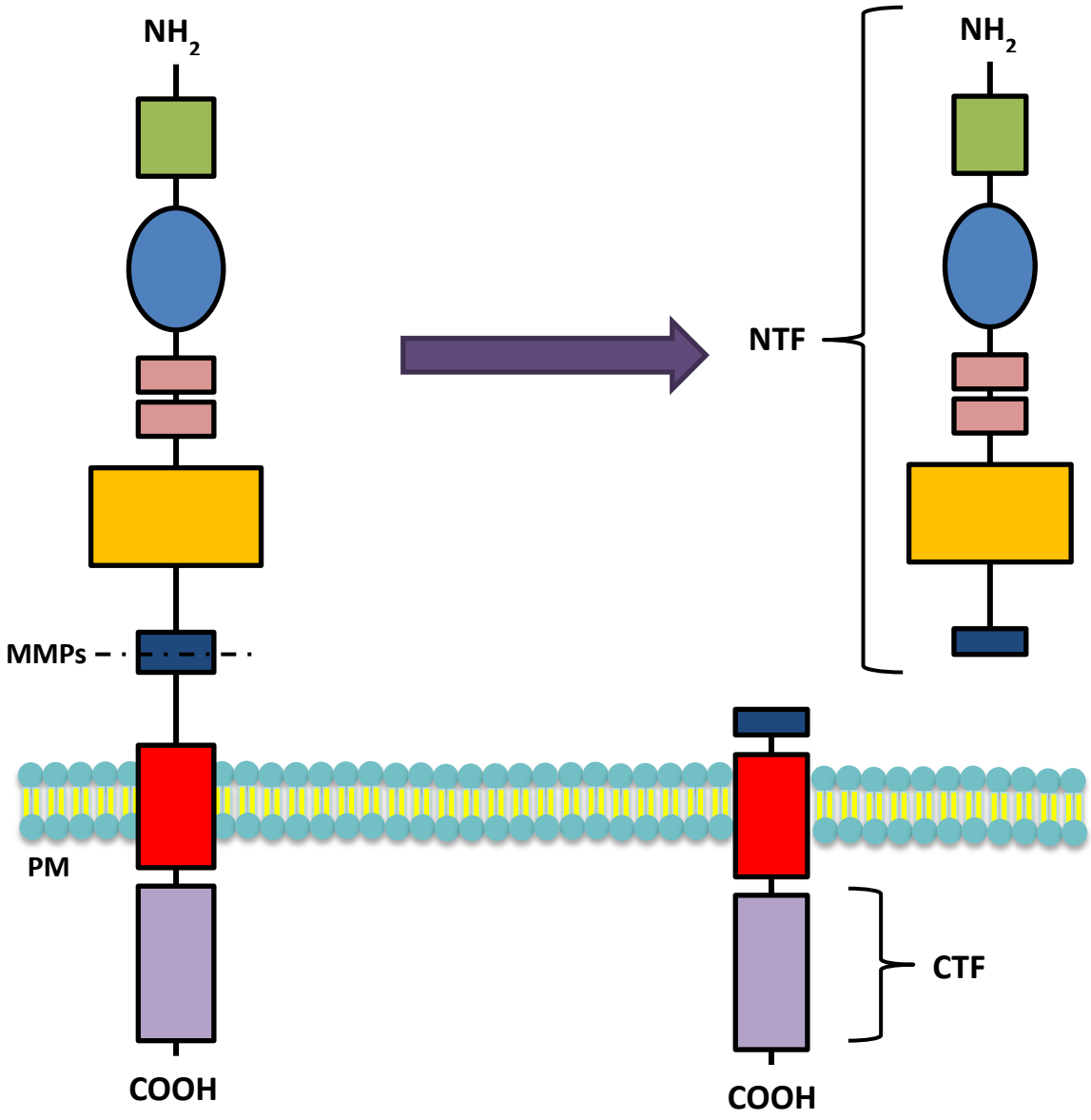

Fig 5.2 Schematic representation of proteolytic processing of Type I NRG1.

Type I NRG1 precursors are localised to the plasma membrane (PM) and cleaved in the stalk region (dashed line) by matrix metalloproteinases (MMPs). This releases an extracellular N-terminal fragment (NTF) and an inactive intracellular C-terminal fragment (CTF). The NTF contains the EGF-like domain which is bioactive and serves as a ligand both in an autocrine and paracrine manner. Type specific N-terminal sequence (green), Ig-like domain (light blue), spacer sequences (pink), EGF-like domain (yellow), stalk region (dark blue), transmembrane spanning domain (red) and cytoplasmic tail (lilac).

5.1.3 Function of Heregulin

Increasing evidence suggests a role for HRG in breast cancer progression. Pre-clinical *in vivo* studies have reported HRG-β overexpression is sufficient for mammary tumorigenesis [323, 324] and can do so independent of estradiol stimulation [325]. In addition, *in vitro* studies have demonstrated HRG to be a potent mitogenic factor in a variety of different sub-types of breast cancer cell lines with or without HER2 overexpression [314, 326-328]. Several studies have investigated the expression of HRG in human breast cancer samples. Possibly due to lack of sufficiently characterised antibodies, a variety of different levels of HRG have been reported in human breast cancers with specific isoform data not readily available. These are summarised in Table 5.1. However, it is clear that HRG was expressed in at least 25% of breast cancers regardless of the sub-group and sample size examined further indicating the prominent role HRG plays in the progression of human breast tumours.

Type of breast sample (if specified)	Type of assay used	Sample size	% HRG expression	Reference
Invasive carcinomas	Immunohistochemistry	189	30	[329]
Early stage and metastatic carcinomas	Immunohistochemistry	151	50	[330]
Carcinomas	Western Blotting	60	25	[331]
Stage II primary carcinomas	Immunohistochemistry	35	48	[332]
Ductal carcinoma in situ (various grades)	Immunohistochemistry	60	60-95	[333]
HER2 low/negative carcinomas	Immunohistochemistry	171	25	[334]
Invasive ductal and lobular carcinomas of varying grades	Immunohistochemistry	201	47 HRG-α 63 HRG-β	[335]

Table 5.1 Summary of heregulin expression in breast tumours

5.1.4 Signal transduction by Heregulin

Three major "hallmarks" of tumorigenesis and cancer progression are increased cellular proliferation, avoidance of apoptosis and tumour cell invasion [336], all of which are induced by HRG via the HER2/HER3 heterodimer. Binding of HRG to HER3 causes heterodimerization with HER2 and initiates autophosphorylation of specific tyrosine residues activating a variety of key signalling cascades (summarised in Figure 5.3). Upon activation from HRG, HER2 provides docking sites for proteins such as Grb2 and Shc [337] which activates Ras via Sos stimulating a linear signalling cascade culminating in MAPK/Erk activation. Erk activates transcription factors such as Jun/Fos and Myc resulting in cell cycle progression via Cyclin D1 [338]. Simultaneously, activated HER3 is a potent activator for PI3K. HER3 provides six docking sites for the p85 subunit of PI3K [248] which leads to activation of PI3K resulting in the production of phosphatidylinositol-3,4,5-triphosphate (PIP_3). This leads to Akt phosphorylation by PDK1 and initiates pro-survival and anti-apoptotic signalling through inhibition of proteins such as GSK3 and Bad [339]. In addition, activated HER2/HER3 heterodimers stimulate phospholipase-Cγ

(PLCγ) signalling [340, 341] which can also activate Jun/Fos, as well as Janus kinase-STAT (Jak-STAT) pathways [342] both of which regulate cell cycle progression. HRG signalling through HER2/HER3 is proven to enhance cell motility and invasion of cells through various mechanisms. HRG is proven to increase motility of breast cancer cell lines through the activation of rac signalling [343] and regulation of factors such as autocrine motility factor [344], G-protein couple receptor 30 [345] and fibroblast growth factor inducible 14 [346]. HRG is demonstrated to regulate focal adhesion formation via paxillin [347, 348], lamellipodia and filopodia formation [349] and also proved to increase expression of matrix metalloproteinases [350]. Activated HER2/HER3 heterodimers also contributed to tumour cell invasion and metastasis *in vivo [351]* further validating the clinical relevance and potency of HRG as an oncoprotein.

The majority of *in vitro* studies into the effects of HRG and HER2/HER3 signalling in the breast to date have been conducted with breast cancer cell lines with little research using normal breast epithelia in the context of surrounding stromal cells.

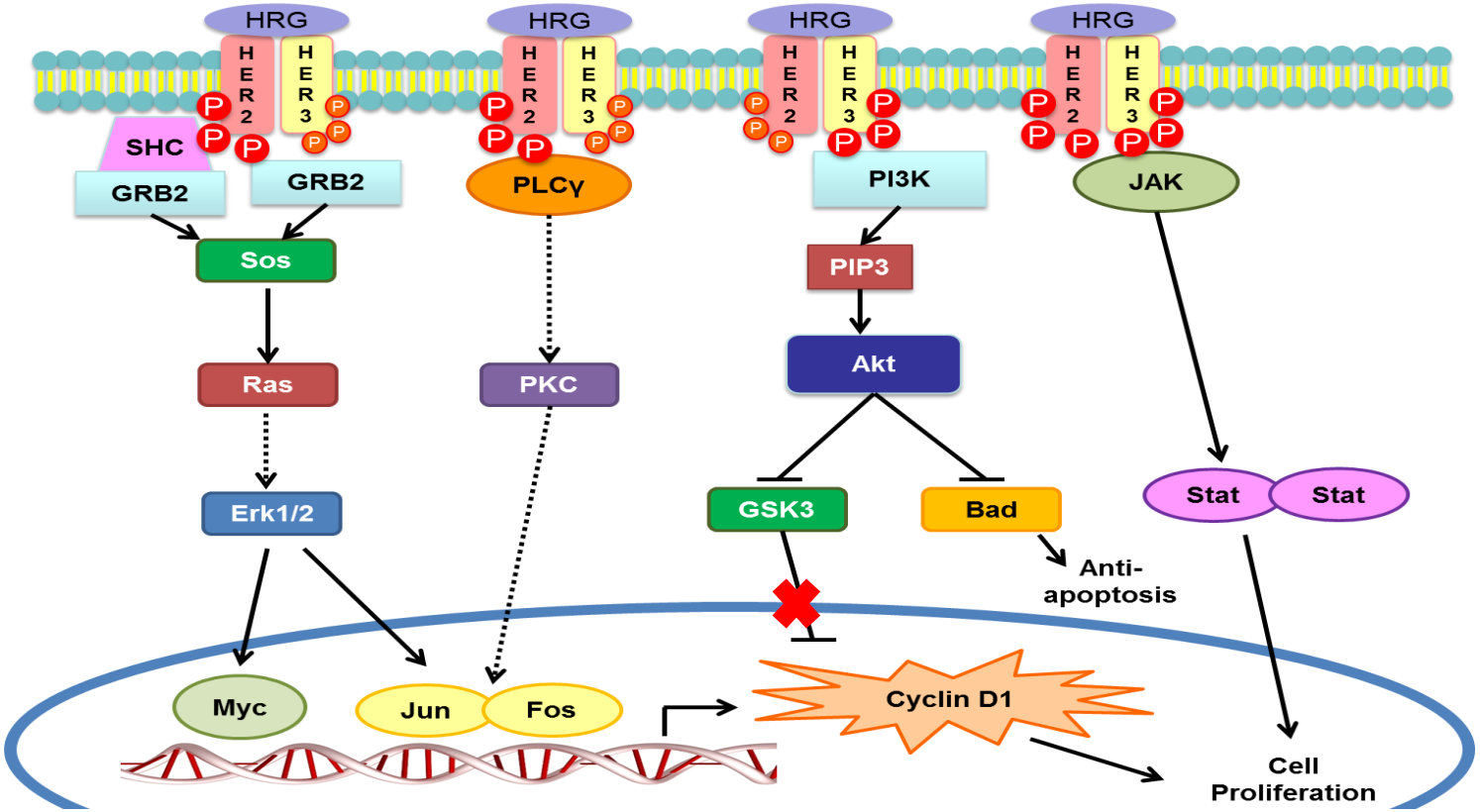

Fig 5.3 Schematic of major signalling pathways stimulated by heregulin and HER2-HER3 heterodimers

Activation of the HER2-HER3 heterodimer by heregulin (HRG) at the plasma membrane initiates downstream signalling of several major pathways resulting in increased cell proliferation and survival. Binding of adaptor proteins such as GRB2 and SHC or kinases such as PLCγ to HER2 activates downstream Ras-Erk1/2 and PKC effectors leading to activation of nuclear transcription factors such as Myc and Jun-Fos. This leads to an increase in Cyclin D1 levels and therefore increases proliferation. Binding of PI3K to HER3 stimulates the Akt pathway inhibiting GSK3 and Bad resulting in antiapoptotic signalling. HER2-HER3 heterodimers also have the capacity to activate JAK-STAT pathways which further enhance cell proliferation through increased transcription.

5.2 Aims

The aim of this series of experiments was to investigate whether HB2 HER2/3OE cells had the capacity to respond to heregulin stimulation in both 3D tri-culture and intracellularly in a manner that reflected studies in the literature. The morphology and phenotype of HB2 HER2/3OE 3D tri-cultures in response to heregulin was assessed and the efficiency of heregulin stimulated intracellular signalling in 2D was examined with a view to elucidating the reasons for the unexpected similar morphology and phenotype of HB2 wildtype and HB2 HER2 and HER3 overexpressing 3D structures observed in Chapter 4. This was addressed by :-

- Comparing the morphology of wildtype and both HER2 and HER3 overexpressing HB2 cells in 3D tri-culture *in vitro* models in response to heregulin stimulation
- Quantifying differences in morphology of HB2 units by assessing area, number and lumen formation from H & E stained gel sections
- Characterising the phenotype of structures by IHC
- Investigating the intracellular signalling pathways within wildtype and both HER2 and HER3 overexpressing HB2 cells in response to heregulin in 2D monolayer using a Proteome Profiler^{TM} human phospho-kinase array

5.3 Materials and Methods

5.3.1 Heregulin stimulation of 3D *in vitro* tri-cultures

3D tri-cultures with HB2 WT and HB2 HER2/3OE cells were prepared as per Chapter 2. For heregulin stimulation, at the time of set up, 3D gels were submerged in media containing 10ng/mL heregulin β1 (Sigma) and control gels in normal heregulin-free media. Thereafter, media was changed twice weekly for the duration of culture with media containing 10ng/mL heregulin β1 for heregulin stimulated gels and normal media for control gels.

5.3.2 Analysis of intracellular signalling pathways induced by heregulin

The intracellular signalling pathways activated by heregulin were analysed using Proteome Profiler™ human phospho-kinase arrays (R & D Systems) according to manufacturer's instructions. Briefly, HB2 WT and HB2 HER2/3OE cells were seeded into 25cm^3 vented cap culture flasks (Corning) at a seeding density of 2 x 10^7 cells per flask. Media was replaced with serum-free media 2 hours prior to stimulation experiments. Heregulin β1 (10ng/mL) was added dropwise onto cells and cells were incubated at 37^{o}C and 5% CO_2 for 15mins. Serum free media was added to separate flasks to serve as negative controls. Working on ice, cells were lysed and protein extracted using lysis buffer provided. Protein concentrations were determined using a DC protein assay (BioRad) as per section 2.11. Protein samples were diluted in assay buffer provided and 300µg of protein sample incubated on each array membrane as per manufacturer's instructions. Membranes were developed using ECL solutions provided and visualised using a ChemiDoc® MP imaging system (BioRad).

Densitometry analysis was performed using BioRad Image Lab 4.1 software by overlaying an image of the array template (provided in kit) onto array membrane image and manually annotating each spot to take a pixel intensity reading. Mean pixel intensity for duplicate pairs of antibody spots was calculated using Microsoft Excel. Background intensity readings taken from PBS negative control spots were subtracted from these means. Mean pixel intensity for

each antibody on the array was then normalised to the internal positive reference control spots to allow separate arrays to be compared.

In order to assess the activation of phospho-kinases specifically in response to heregulin stimulation, mean pixel intensity of phospho-kinases from heregulin stimulated membranes were compared to their respective controls and fold difference calculated using GraphPad Prism 6 software. Where biological replicate experiments were performed, the mean fold difference and SEM were calculated using GraphPad Prism 6 software. In order to focus on phospho-kinases that were considerably differentially activated, a threshold of ≥2-fold difference was set and all phospho-kinases that were <2-fold differentially expressed were not considered.

5.4 Results

5.4.1 Morphology of HER protein overexpressing HB2 cells in 3D *in vitro* tri-culture model in response to heregulin stimulation

Due to the unexpected similarities between the morphology and phenotype of HB2 WT and HB2 HER2/3OE tri-cultures in Chapter 4, HB2 HER2/3OE tri-cultures were stimulated with the heregulin ligand for the HER2/3 heterodimer in order to see if HB2 HER2/3OE cells had the capacity to respond to ligand and disrupt the epithelial architecture in tri-culture and whether these responded in a different manner to HB2 WT cells. The morphology of HB2 WT and HB2 HER2/3OE tri-cultures were assessed in response to stimulation with 10ng/ml heregulin with representative images from three technical replicates presented (Fig 5.4). This demonstrated that in the presence of heregulin, HB2 WT cells formed larger and more elongated units compared to the small rounded units with clear lumen formation without heregulin. HB2 HER2/3OE cells formed much larger, elongated units which featured discohesive cells and distorted lumens in response to heregulin. HB2 HER2/3OE units also presented protrusions from outer edges of units. Quantification of these structures (Fig 5.5) supported these observations. A significant increase in size of HB2 units was demonstrated upon heregulin stimulation with HB2 WT, and HB2 HER2/3OE cells ($p=<0.05$, unpaired t-test). No significant difference was observed in the number of units formed upon heregulin stimulation but there was a significant decrease in lumen formation of HB2 WT units ($p=0.001$, unpaired t-test). No significant difference in lumen formation was demonstrated in HB2 HER2/3OE units ($p=0.197$, unpaired t-test).

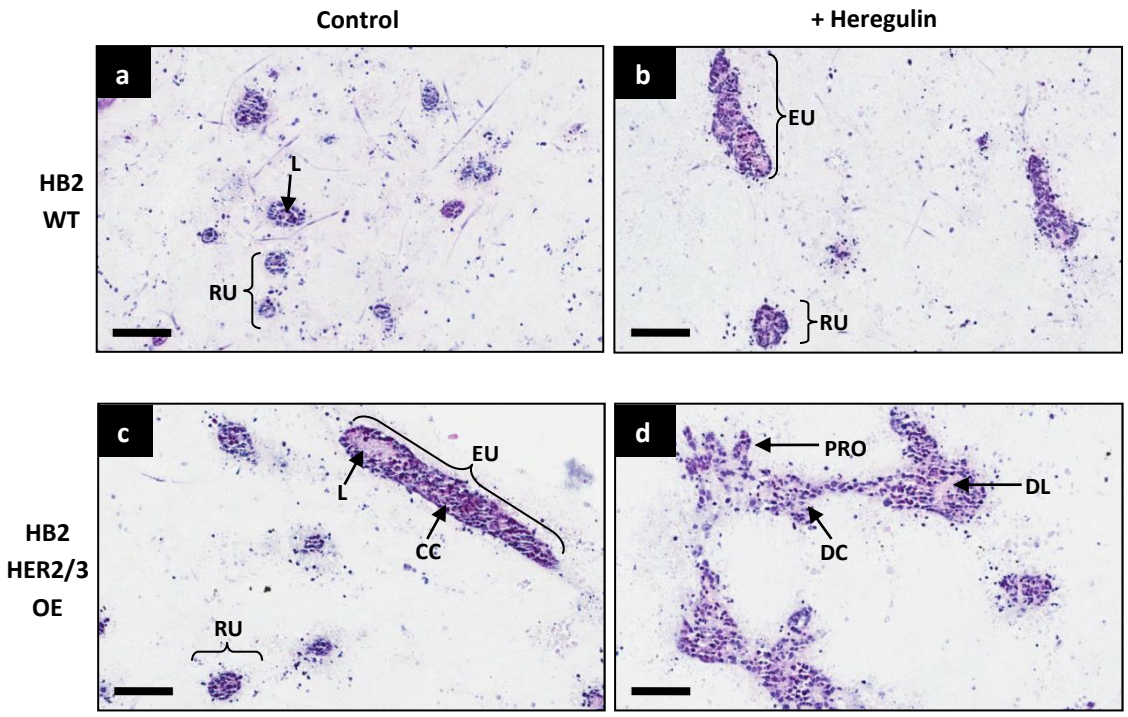

Fig 5.4 H & E staining of 3D *in vitro* tri-culture models containing HER protein overexpressing HB2 cells with or without heregulin

Wildtype (HB2 WT) and both HER2 and HER3 overexpressing (HB2 HER2/3OE) HB2 cells were co-cultured in 3D collagen gels with GFP positive myoepithelial cells (GFP Myo1089) and dsRed positive fibroblast cells (dsRed Fib) for 21 days. These were cultured in the presence or absence of 10ng/ml of heregulin-β1 and 5µm sections of gels H & E stained with representative images from three technical replicates presented. HB2 WT control cells (a) formed cohesive rounded units (RU) with appearance of lumens (L) but formed a mixture of larger more elongated units (EU) and rounded units (RU) in response to heregulin (b). HB2 HER2/3OE cells formed much larger structures with the appearance of protrusions (PRO) from the outer edges of structures, distorted lumens (DL) and consisted of discohesive cells (DC) in response to heregulin (d) when compared to HB2 HER2/3OE control cells (c). Original magnification 20x, scale bars = 100µm.

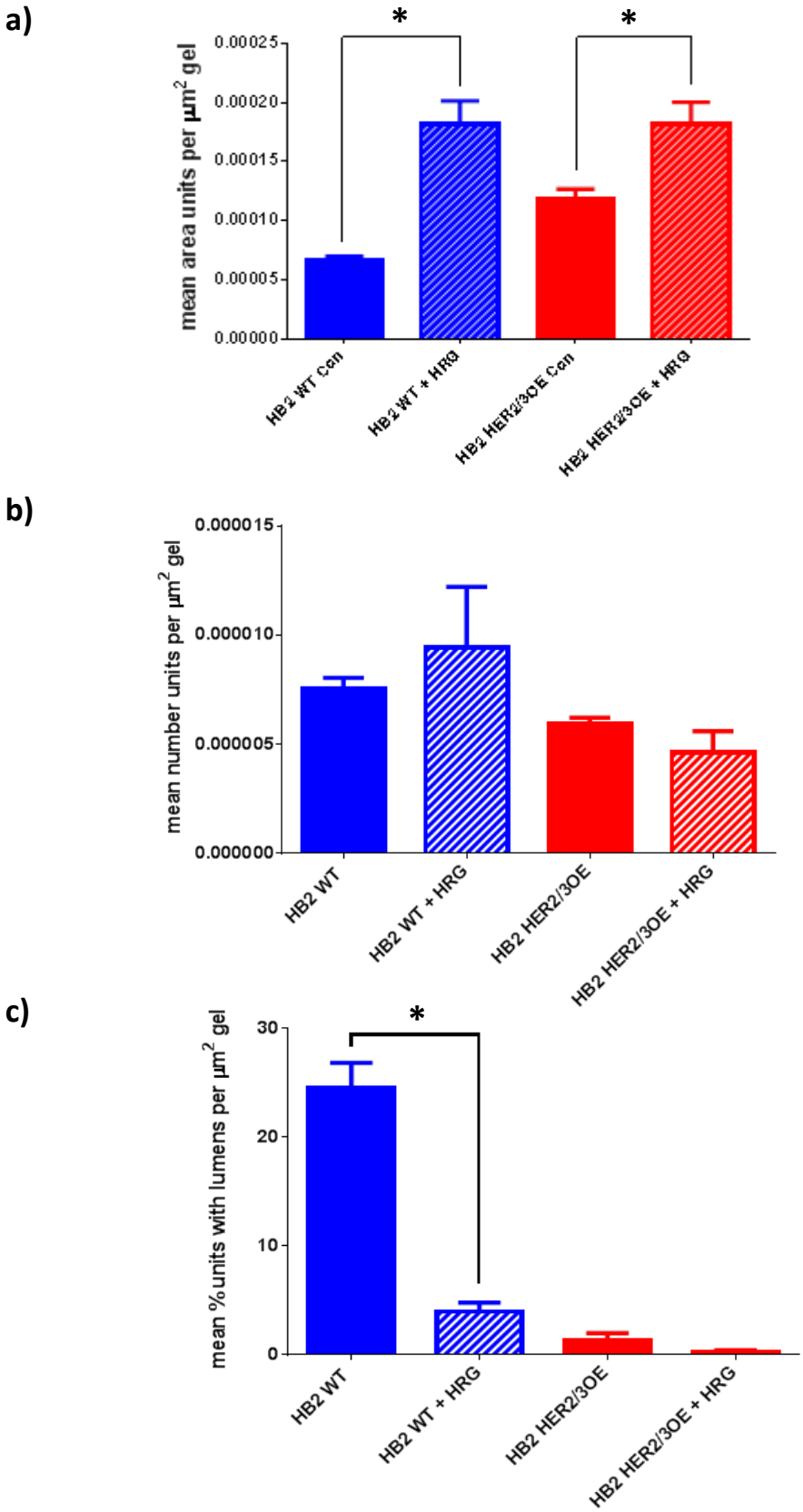

Fig 5.5 Quantification of area, number and lumen formation of HER protein overexpressing HB2 units in 3D tri-culture gels in response to heregulin from H & E stained sections

Size (a), number (b) and lumen formation (c) of wildtype (HB2 WT) and both HER2 and HER3 overexpressing (HB2 HER2/3OE) HB2 cell units in response to 10ng/ml heregulin stimulation

was quantified with Aperio Image scope, analysed with Graph Pad Prism 6 and normalized to total size of each respective collagen gel section. (a) Stimulation with heregulin significantly increased the size of HB2 WT and HB2 HER2/3OE units. (b) No significant difference was observed with the number of HB2 WT and HB2 HER2/3OE units in response to heregulin. (c) Stimulation with heregulin significantly decreased lumen formation in HB2 WT only while no significant difference was observed with HB2 HER2/3OE units. Bars denote mean from three technical replicates and error bars standard error of the mean (SEM). * indicates significant difference to HB2 controls following unpaired t-test ($p=<0.05$).

5.4.2 Phenotype of HB2 wildtype cells in 3D *in vitro* tri-culture model in response to heregulin stimulation

Characterisation of HB2 WT 3D tri-cultures by IHC with or without heregulin stimulation demonstrated that despite lack of HER protein overexpression, the phenotype of HB2 WT units in is altered in response to heregulin. Representative images from three technical replicates are presented (Fig 5.6 & 5.7). While little difference was observed in the membranous pattern of E-Cad expression in response to heregulin, EMA expression was disrupted in response to heregulin as HB2 WT control units showed strong expression concentrated to the apical-lumen interface in the centre of units while ubiquitous cytoplasmic staining was observed in HB2 WT units with heregulin. Strong Ki67 expression was observed across all HB2 WT units regardless of heregulin stimulation confirming the presence of proliferative HB2 cells while apoptosis demonstrated by M30 staining was only detected in the centre of HB2 WT control units and was absent in HB2 WT units + heregulin. Disruption of basement membrane protein production was also observed in response to heregulin as HB2 WT control units displayed strong Coll IV expression neatly distributed around their outer edges while this was lost in HB2 WT units + heregulin. The distribution of GFP Myo1089 cells and LS11-083 dsRed Fibs remained unchanged with tGFP staining detected in rounded cells associated around outer edges of units and dsRed staining detected in long spindle-shaped cells loosely distributed throughout the collagen gels regardless of heregulin stimulation.

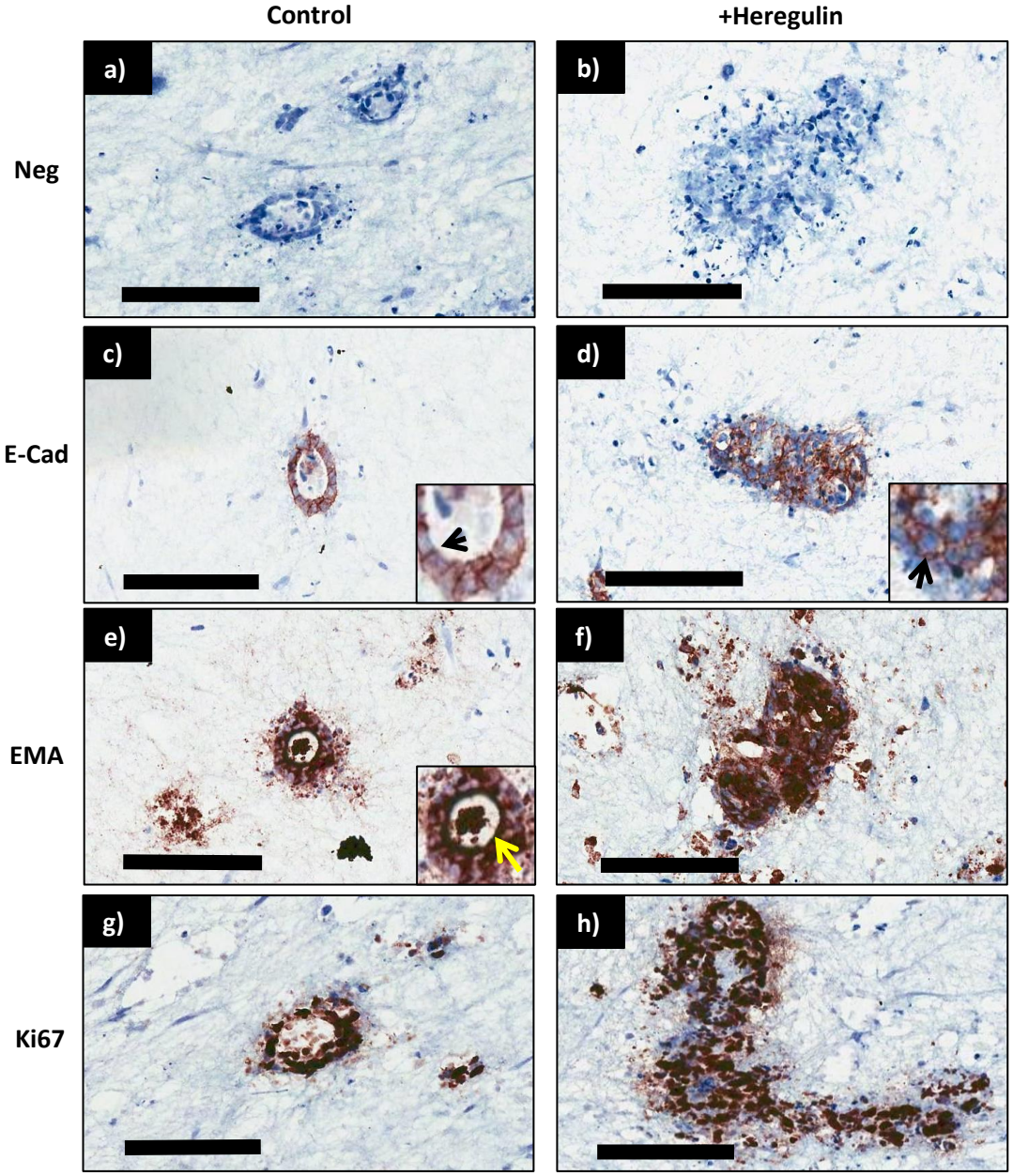

Fig 5.6 Immunohistochemical characterisation of 3D *in vitro* tri-culture models of HB2 WT cells in response to heregulin A

HB2 wildtype (HB2 WT) cell unit phenotype within tri-cultures in response to 10ng/ml heregulin was characterised by IHC to assess cell adhesion, polarisation and proliferation. Representative images from three technical replicates presented. HB2 units were positive for E-cadherin (E-Cad) staining localised between HB2 cell junctions without and with heregulin stimulation (arrows, c & d respectively). Epithelial Membrane Antigen (EMA) staining was concentrated at the apical-lumen interface of cells in the centre of units (yellow arrow, e) but was ubiquitous throughout the cytoplasm of cells in response to heregulin (f). Strong Ki67 staining was observed in all cells of HB2 WT units both without (g) and with heregulin stimulation (h). Primary antibody was omitted to serve as negative (Neg) controls (a & b). Original magnification 20x, scale bars = 100µm.

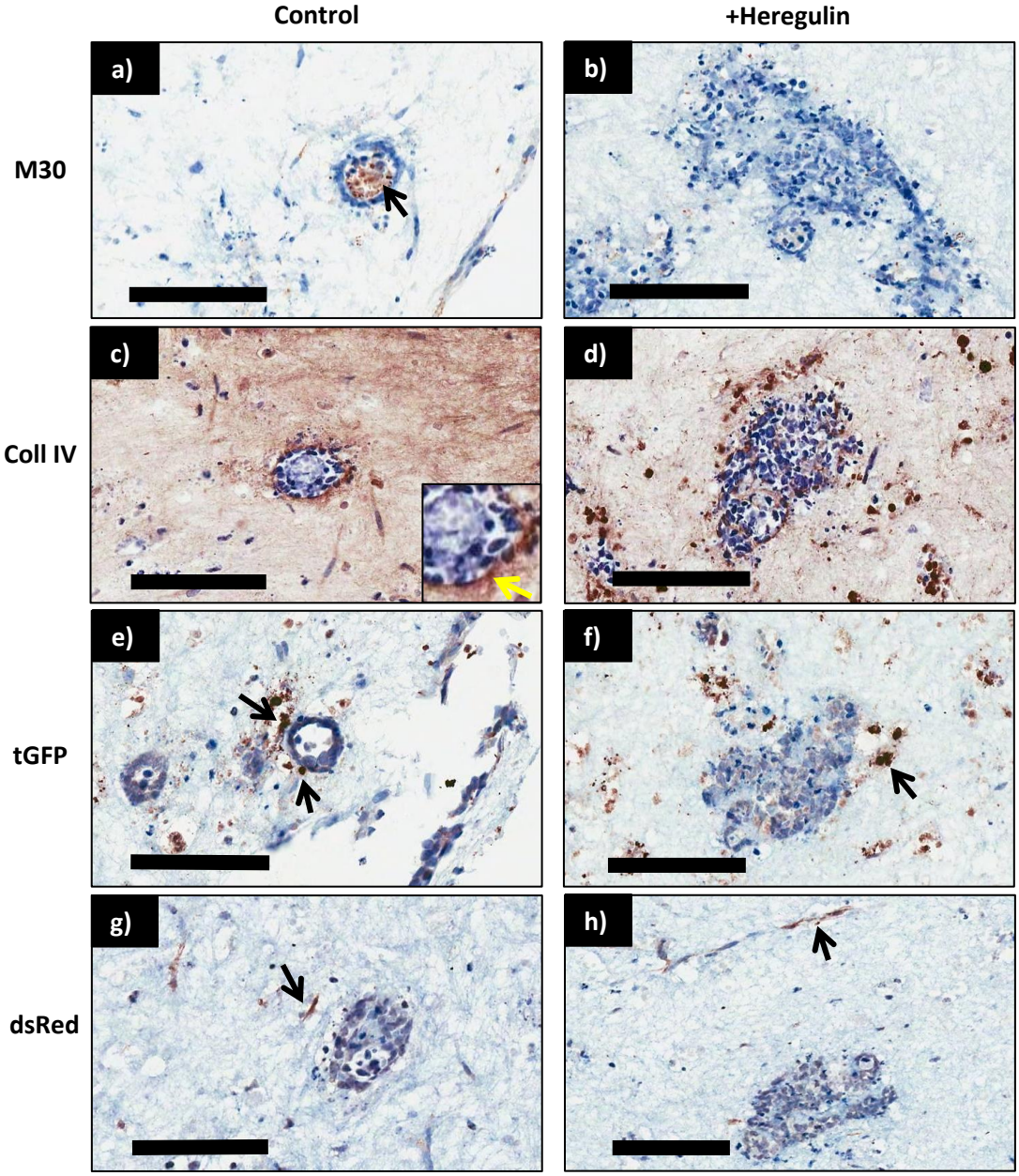

Fig 5.7 Immunohistochemical characterisation of 3D *in vitro* tri-culture models of HB2 WT cells in response to heregulin B

HB2 wildtype (HB2 WT) unit phenotype within tri-cultures in response to 10ng/ml heregulin was characterised by IHC to assess apoptosis and basement membrane production. Representative images from three technical replicates presented. M30 staining was visible in the central lumens of control units (arrow, a) but was absent upon stimulation with heregulin (b). Collagen IV (Coll IV) expression was neatly distributed around outer edges of control units (yellow arrow, c) but was disorganised in response to heregulin stimulation with a lack of concentrated staining around the outer edges of units (d). Both control and heregulin stimulated tri-cultures showed positive staining for tGFP in cells distributed around the outer edges of units (arrows, e & f) and positive staining for dsRed in cells loosely distributed throughout the collagen gel (arrows, g & h). Original magnification 20x, scale bars = 100µm.

5.4.3 Phenotype of HER2 and HER3 overexpressing HB2 cells in 3D *in vitro* tri-culture model in response to heregulin stimulation

Characterisation of HB2 HER2/3OE 3D tri-cultures by IHC with or without heregulin stimulation demonstrated differences in phenotype of HB2 units in response to heregulin suggesting a response from HB2 HER2/3OE cells in 3D tri-culture. Representative images from three technical replicates presented (Fig 5.8 & 5.9). Little difference was observed in the membranous pattern of E-Cad expression, the strong ubiquitous cytoplasmic expression of EMA and strong Ki67 expression across all HB2 HER2/3OE units in response to heregulin stimulation. Apoptotic cells were detected via M30 staining in the centre of HB2 HER2/3OE units regardless of heregulin stimulation. Basement membrane protein production was altered in response to heregulin as HB2 HER2/3OE control units displayed Coll IV expression distributed around their outer edges as well as in their centre while Coll IV was only detected in the centre of HB2 HER2/3OE units + heregulin. The distribution of GFP Myo1089 cells and LS11-083 dsRed Fibs remained unchanged with tGFP staining detected in rounded cells associated around outer edges of units, and dsRed staining detected in long spindle-shaped cells loosely distributed throughout the collagen gels regardless of heregulin stimulation.

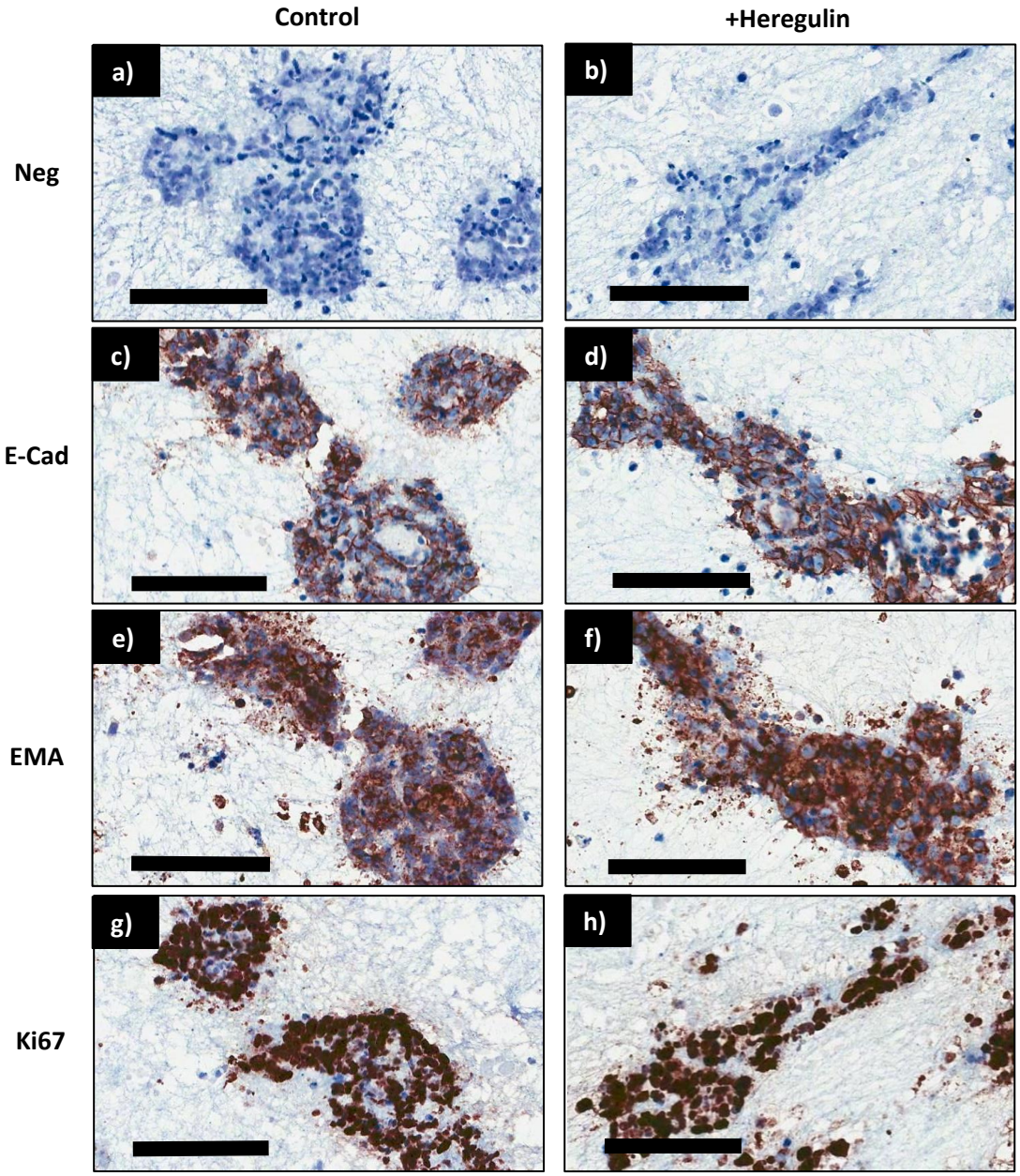

Fig 5.8 Immunohistochemical characterisation of 3D *in vitro* tri-culture models of both HER2 and HER3 overexpressing HB2 cells in response to heregulin

HB2 HER2 and HER3 overexpressing (HB2 HER2/3OE) cell unit phenotype within tri-cultures in response to 10ng/ml heregulin was characterised by IHC to assess cell adhesion, polarisation and proliferation. Representative images from three technical replicates presented. E-cadherin (E-Cad) staining was localised between HB2 cell junctions in control and heregulin stimulated units (c & d respectively). Epithelial Membrane Antigen (EMA) staining was ubiquitous throughout the cytoplasm of HB2 cells in controls (e) and heregulin stimulated HB2 units (f). Strong Ki67 staining was observed in all cells of HB2 control (g) and heregulin stimulated (h) units. Primary antibody was omitted to serve as negative (Neg) controls (a & b). Original magnification 20x, scale bars = 100µm.

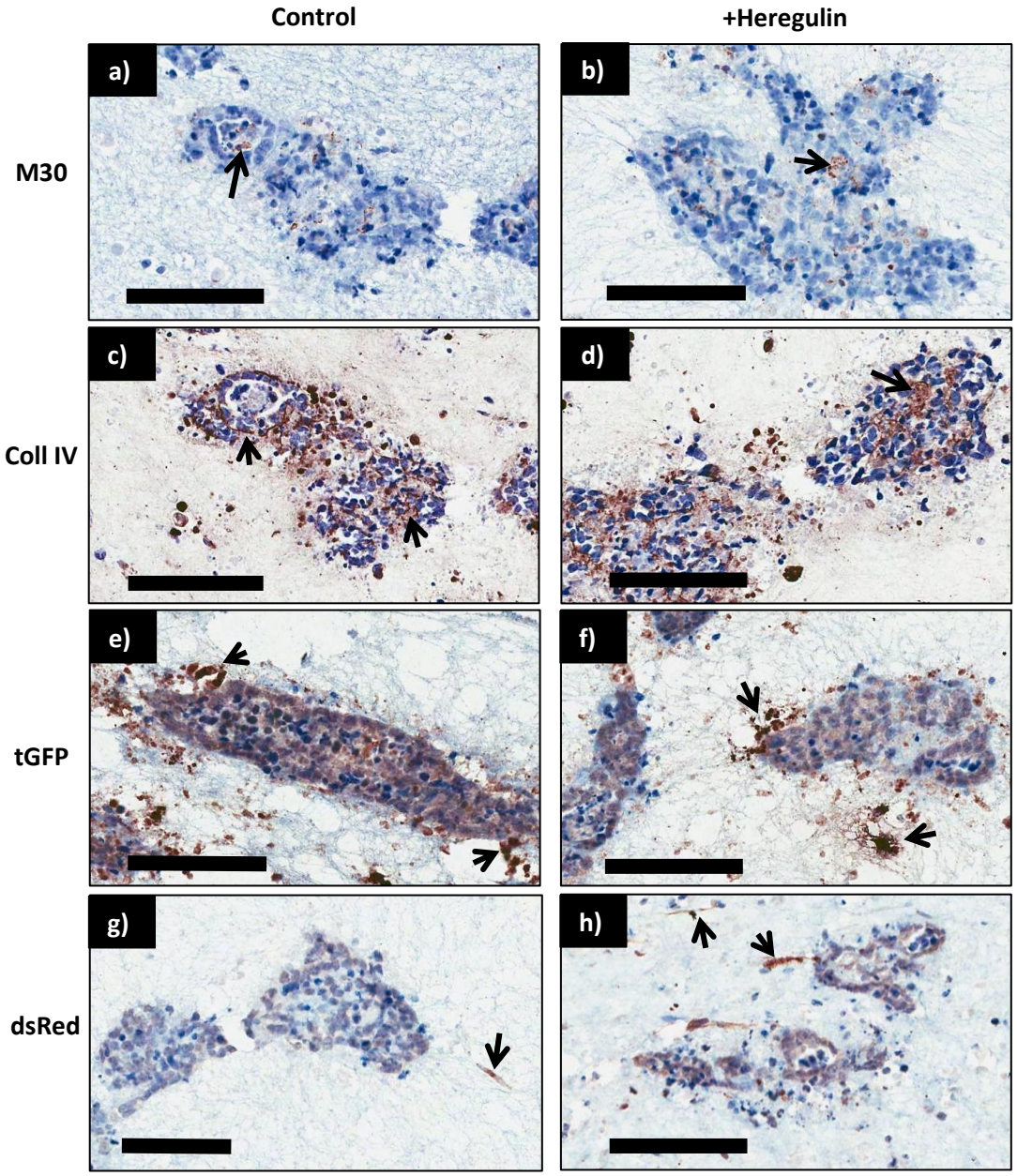

Fig 5.9 Immunohistochemical characterisation of 3D *in vitro* tri-culture models of both HER2 and HER3 overexpressing HB2 cells in response to heregulin

HB2 HER2 and HER3 overexpressing (HB2 HER2/3OE) unit phenotype within tri-cultures in response to 10ng/ml heregulin was characterised by IHC to assess apoptosis and basement membrane production. Representative images from three technical replicates presented. M30 staining was detected in central areas of both HB2 HER2/3OE control (arrow, a) and heregulin stimulated units (arrow, b). Collagen IV (Coll IV) expression was detected both around outer edges and within control units (arrows, c) but was detected in the centre of heregulin stimulated units only (arrow, d). Both control and heregulin stimulated tri-cultures showed positive staining for tGFP in cells distributed around the outer edges of units (arrows, e & f) and positive staining for dsRed in cells loosely distributed throughout the collagen gel (arrows, g & h). Original magnification 20x, scale bars = 100µm.

5.4.4 Analysis of intracellular signalling pathway activation by heregulin in wildtype and HER2 and HER3 overexpressing HB2 cells using a human phospho-kinase Proteome Profiler™ array

In order to further investigate whether HB2 HER2/3OE cells had the capacity to respond to heregulin stimulation in a manner indicated in the literature, the intracellular signalling mechanisms stimulated by heregulin were examined and compared to HB2 WT control cells. This was assessed by comparing HB2 WT and HB2 HER2/3OE control cells to cells stimulated for 15 mins with 10ng/ml heregulin using Proteome Profiler™ human phospho-kinase arrays (R&D Systems) which allowed comparison of activation of 46 different human phospho-kinases. Arrays for HB2 WT control cells and HB2 WT cells + heregulin were compared (Fig 5.10, results from one biological replicate and no technical replicates) and arrays for HB2 HER2/3OE control cells and HB2 HER2/3OE cells + heregulin were compared (Fig 5.11, results from two biological replicates) in order to determine the effect of HER2 and HER3 overexpression in HB2 cells in the presence of heregulin. A subset of phospho-kinases whose phosphorylation were at least two-fold increased or decreased in comparison to control cells were identified for both HB2 WT and HB2 HER2/3OE cells. In the presence of heregulin, expression of phospho-kinases Erk1/2, GSK-3α/β, Akt, PRAS40 and WNK1 were increased and Lck and PDGFRβ decreased in HB2 WT cells (results from one biological replicate). In the presence of heregulin, expression of phospho-kinases Erk1/2, GSK-3α/β, Akt, PRAS40 were also increased and Lck also decreased in HB2 HER2/3OE cells, however, a subset of phospho-kinases were identified which were either increased or decreased in HB2 HER2/3OE which were not identified in HB2 WT cells in response to heregulin. These included an increase in expression of the phospho-kinases Fyn, Hck and FAK and a decrease in expression of eNOS, PLCγ1 and Pyk2. In addition, while WNK1 was increased and PDGFRβ decreased in HB2 WT cells in response to heregulin, these kinases were not differentially expressed in response to heregulin in HB2 HER2/3OE cells.

It was noted that expression of some of the phospho-kinases identified to be at least two-fold increased or decreased following densitometry analysis were not visible on the array membranes following developing. This indicated a need for further validation of phospho-kinase expression in these cells.

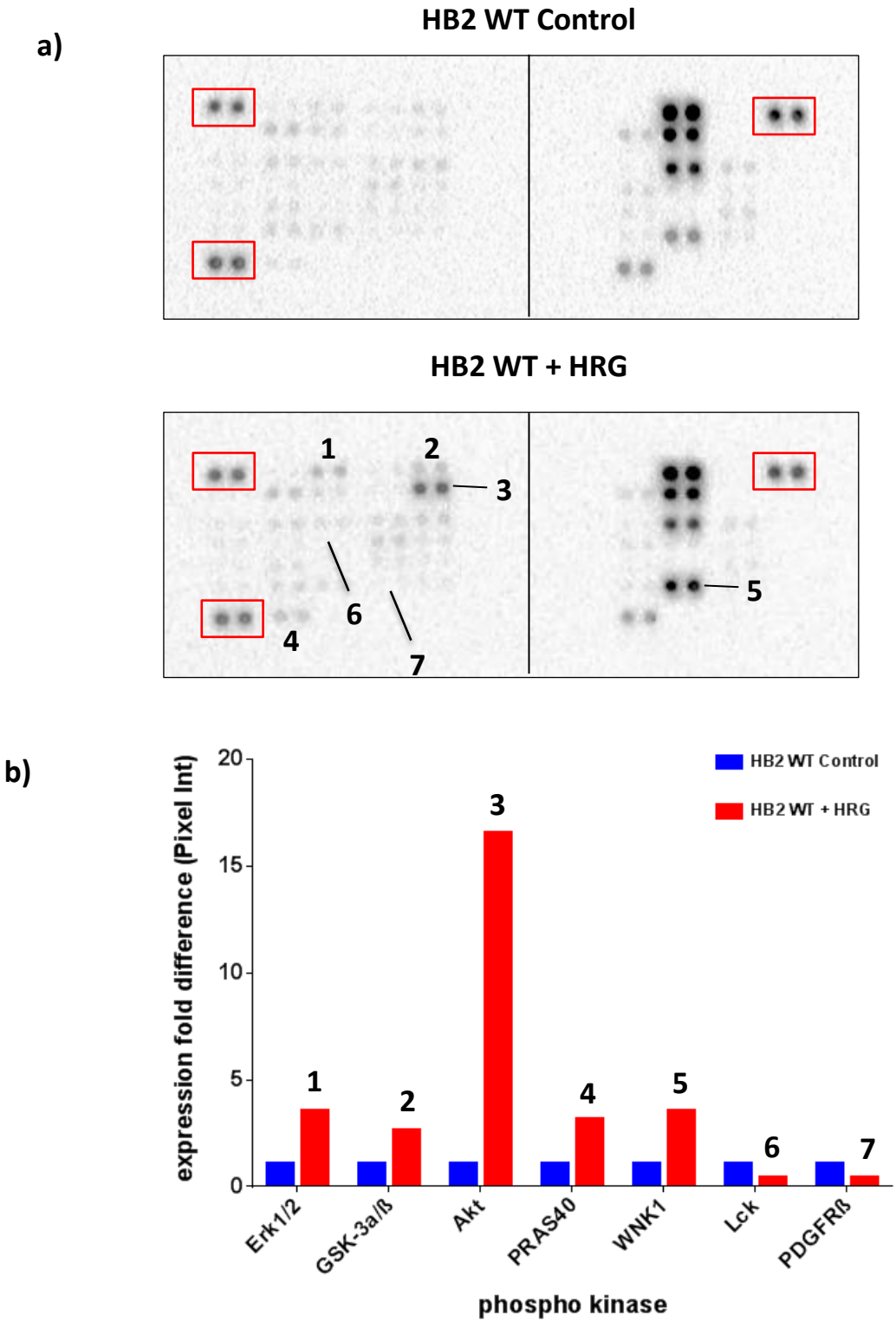

Fig 5.10 Human phospho kinase array analysis of signalling downstream of heregulin in HB2 wildtype cells

a) Human phospho kinase arrays, probed with 46 different phospho-kinase antibodies in duplicate with internal controls, were incubated with lysates from HB2 wildtype cells (HB2 WT) and HB2 WT cells stimulated with 10ng/ml heregulin for 15 minutes (HB2 WT + HRG) and

developed for three minutes. Following heregulin stimulation, specific spots appeared more intense or fainter than HB2 WT controls.

b) Histogram shows quantification of expression of a subset of phospho kinases following densitometry analysis using BioRad Image Lab 4.1 software. Phospho kinase expression was calculated as fold difference to HB2 WT after normalisation to internal positive reference controls (red boxes, a). Phopsho kinases which were differentially expressed by two-fold in comparison to HB2 WT are shown and labelled numbers 1-7 on arrays (a) and histogram (b).

Results from one biological replicate with no technical replicates.

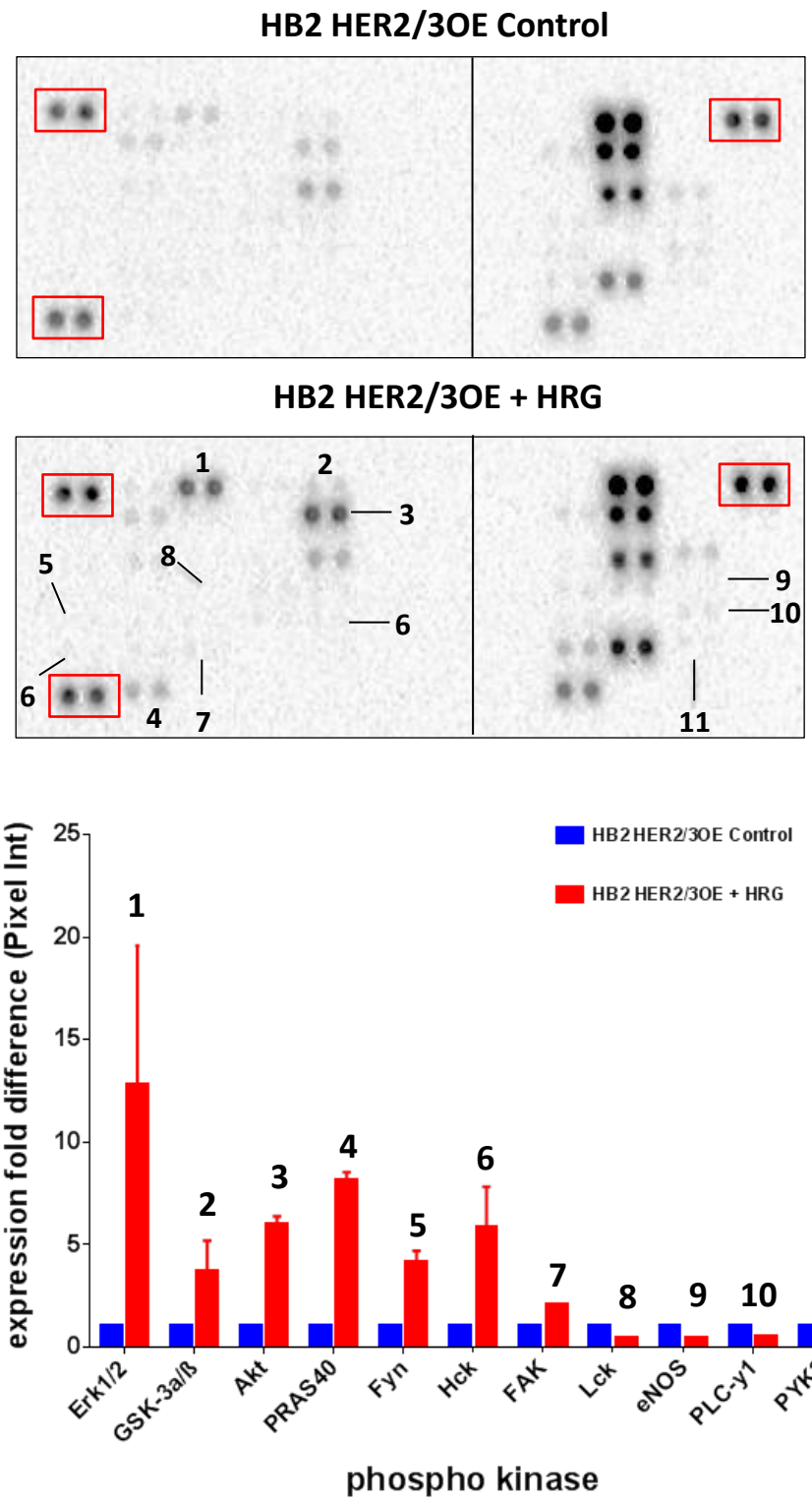

Fig 5.11 Human phospho kinase array analysis of signalling downstream of heregulin in HER2 and HER3 overexpressing HB2 cells

a) Human phospho kinase arrays, probed with 46 different phospho kinase antibodies in duplicate with internal controls, were incubated with lysates from HER2 and HER3 overexpressing HB2 cells (HB2 HER2/3OE control) and HB2 HER2/3OE cells stimulated with

10ng/ml heregulin for 15 minutes (HB2 HER2/3OE + HRG) and developed for three minutes. Representative images of two replicate experiments shown. Following heregulin stimulation, specific spots appeared more intense or fainter than HB2 HER2/3OE controls.

b) Histogram shows quantification of expression of a subset of phospho kinases following densitometry analysis using BioRad Image Lab 4.1 software. Bars denote mean from two biological replicate experiments and error bars standard error of the mean (SEM).Phospho kinase expression was calculated as fold difference to HB2 HER2/3OE controls after normalisation to internal positive reference controls (red boxes, a). Phopsho kinases which were differentially expressed by two-fold in comparison to HB2 HER2/3OE and did so in both replicate experiments are shown and labelled numbers 1-11 on arrays (a) and histogram (b).

Results from two biological replicate experiments.

5.4.5 Validation of the differential expression of both visible and non-visible phospho-kinases identified via Proteome Profiler™ human phospho-kinase arrays in HB2 wildtype and HER2 and HER3 overexpressing HB2 cells by western blot

Phospho-Akt was selected as a representative phospho-kinase clearly visible and phospho-PLCγ1 selected as a representative phospho-kinase not clearly visible on human phospho-kinase array membranes. Protein samples extracted previously for phospho-kinase array analysis were used for western blot analysis of expression of phospho-Akt (Fig 5.12) and phospho-PLCγ1 (Fig 5.13) in HB2 WT and HER2/3OE control and heregulin stimulated cells. Images and results for each antibody presented are from a single experiment run. This confirmed an increase in Akt activation in response to HRG stimulation in both cell lines and that PLCγ1 is only activated in HB2 HER2/3OE control cells and is deactivated in response to HRG in these cells.

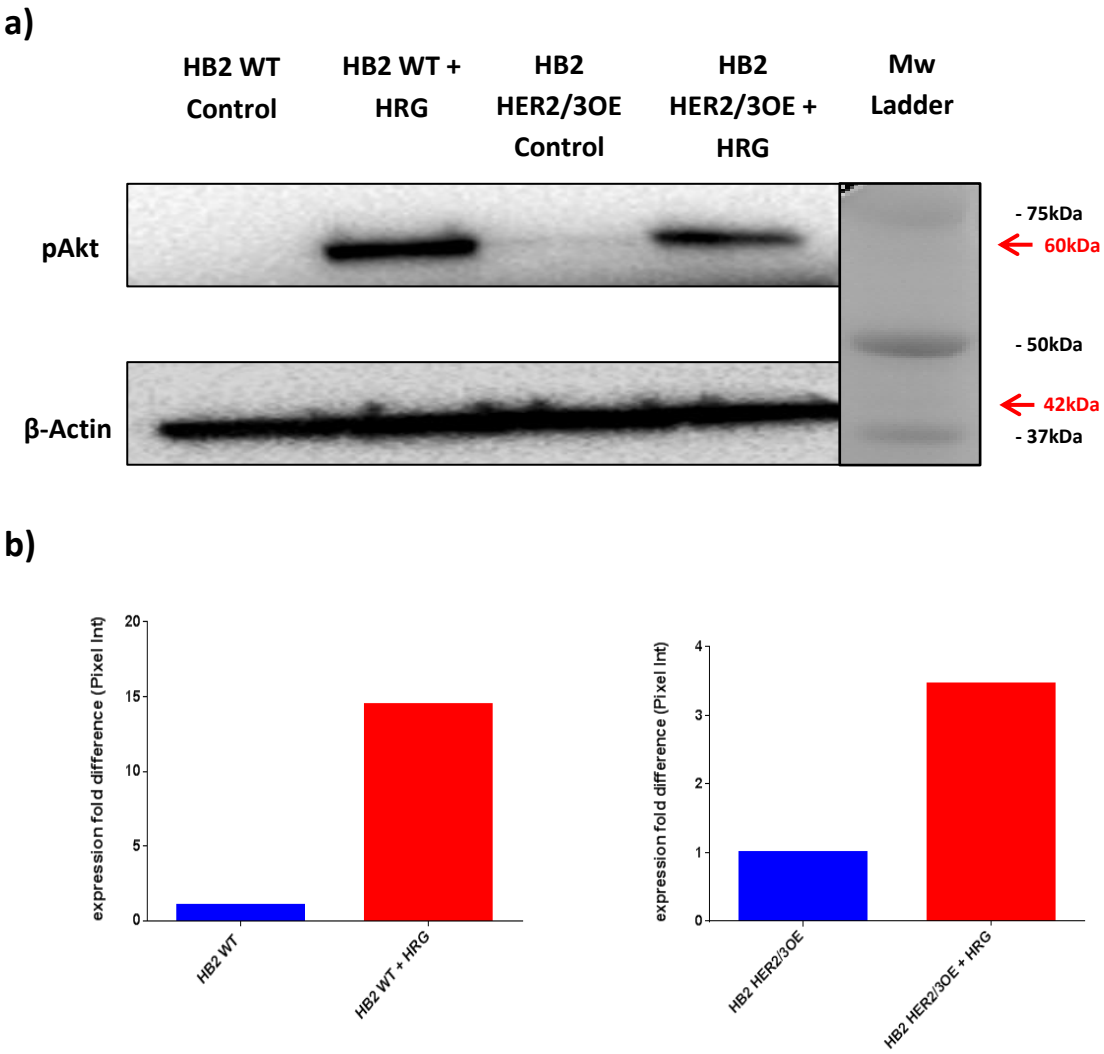

Fig 5.12 Western blots for phospho-Akt in HB2 WT and HB2 HER2/3OE cells stimulated with heregulin.

a) Anti-phospho-Akt IgG was used to detect activated Akt protein in HB2 wildtype cells (HB2 WT) and HB2 cells overexpressing both HER2 and HER3 (HB2 HER2/3OE) in response to stimulation with 10ng/ml heregulin-β1 (HRG). A band of ~60kDa was observed in HB2 WT+HRG and HB2 HER2/3OE+HRG cells. No band was detected in HB2 WT and HB2 HER2/3OE control cells. Anti-β-Actin IgG was used as a loading control for which bands were observed in all samples at ~42kDa.

b) Histogram shows quantification of phospho-Akt expression following densitometry analysis using BioRad Image Lab 4.1 software. Phospho-Akt expression was calculated as fold difference to HB2 control cells after normalization to β-Actin for heregulin stimulated HB2 cells.

Results presented from a single experimental run.

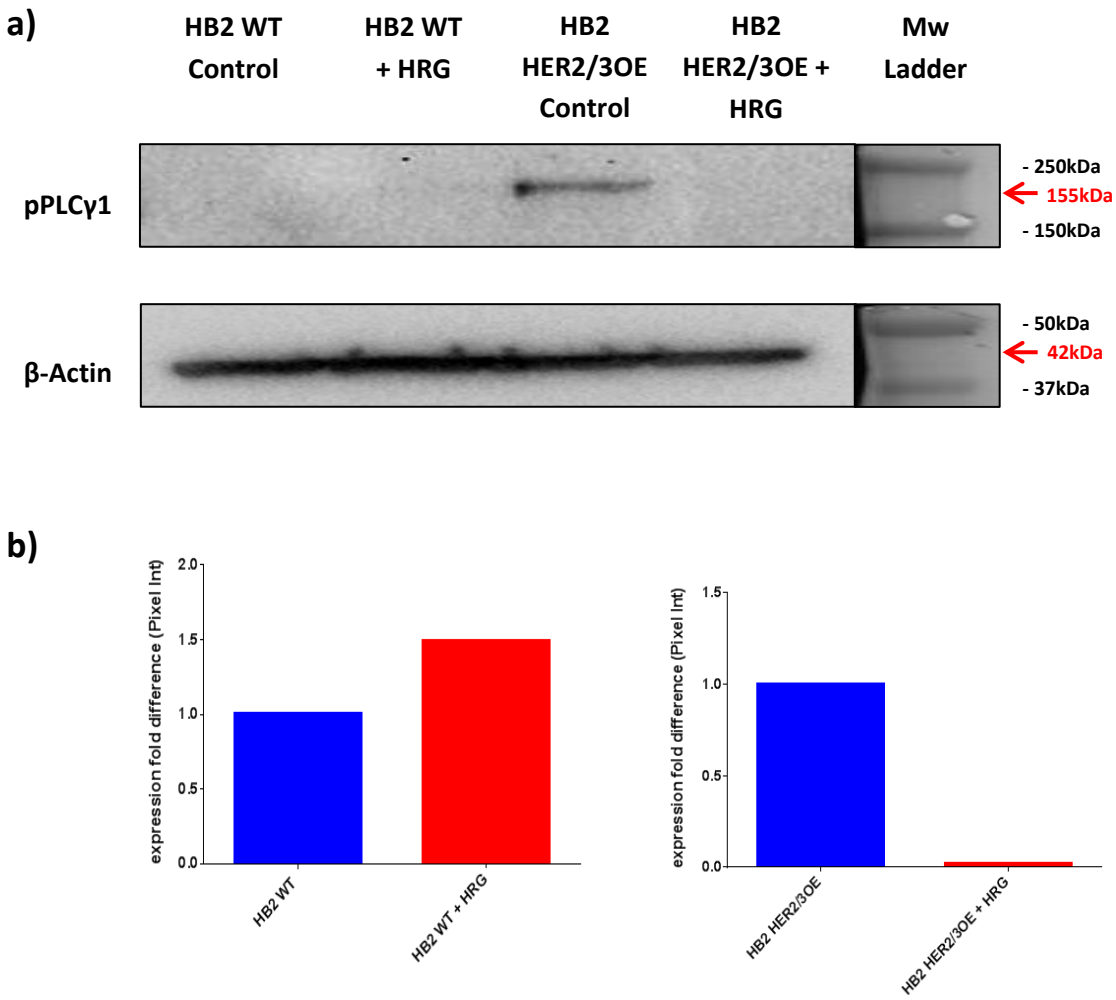

Fig 5.13 Western blots for phospho-PLCγ1 in HB2 WT and HB2 HER2/3OE cells stimulated with heregulin.

a) Anti-phospho-PLCγ1 IgG was used to detect activated PLCγ1 protein in HB2 wildtype cells (HB2 WT) and HB2 cells overexpressing both HER2 and HER3 (HB2 HER2/3OE) in response to stimulation with 10ng/ml heregulin-β1 (HRG). A band of ~155kDa was observed in HB2 HER2/3OE control cells. No band was detected in HB2 WT control, HB2 WT+HRG and HB2 HER2/3OE+HRG cells. Anti-β-Actin IgG was used as a loading control for which bands were observed in all samples at ~42kDa.

b) Histogram shows quantification of phospho-PLCγ1 expression following densitometry analysis using BioRad Image Lab 4.1 software. Phospho-Akt expression was calculated as fold difference to HB2 controls after normalization to β-Actin for heregulin stimulated HB2 cells.

Results presented from a single experimental run.

5.5 Discussion

It has been reported that regardless of HER protein overexpression, it is the stimulation from HER ligands that determines HER receptor heterodimerisation and governs the signalling outcome downstream of HER receptors in epithelial cells [276]. Since HER2-HER3 overexpression in HB2 cells did not affect the structures formed in the tri-culture model in Chapter 4 as expected, we hypothesised that HB2 HER2/3OE cells had the capacity to induce the morphological features described in the literature and were not deficient in their HER2-HER3 signalling capacity but that there were insufficient endogenous levels of the HER2-HER3 heterodimer ligand heregulin in the novel 3D tri-culture system to facilitate a response. We aimed to test this theory by stimulating 3D tri-cultures with heregulin with a view to inducing a morphology and phenotype characteristic of early breast cancer lesions and to validate that the HB2 HER2/3OE cells activate known downstream HER2-HER3 signalling mechanisms intracellularly.

5.5.1 Comparison of wildtype and HER2 and HER3 overexpressing HB2 cell 3D *in vitro* tri-cultures in response to heregulin stimulation

10ng/ml of heregulin-β1 was selected as an appropriate isoform and concentration for HER signalling activation for our experiments as this is considered physiologically relevant and has been widely adopted in the majority of heregulin stimulation studies [352-354]. This has also been validated in studies using HB2 cells [271, 355, 356].

Stimulation of HB2 HER2/3OE tri-cultures with heregulin-β1 induced a morphology and phenotype analogous to HB2 HER2OE tri-cultures observed in Chapter 4. Larger, more branching HB2 units were produced which featured protrusions in comparison to HB2 HER2/3OE control units. This suggested that in 3D tri-culture, HB2 HER2/3OE cells do have the capacity to disrupt normal architecture provided the HER2-HER3 ligand heregulin is present. It was clear that heregulin stimulation of HB2 HER2/3OE cells in the 3D tri-culture context

produced a more tumorigenic phenotype akin to results seen with [276]. However, we also observed that heregulin induced a similar morphology in HB2 WT cells with larger and more elongated units observed and lumen formation significantly decreased. Furthermore, both HB2 WT and HB2 HER2/3OE tri-cultures in response to heregulin exhibited the same phenotype upon examination by IHC. It was expected that an excess of HER2 and HER3 protein expression would dramatically increase the sensitivity of HB2 cells to heregulin ligand stimulation. In these experiments the quantification of the size of HB2 units in response to heregulin-β1 was the same regardless of HER2 and HER3 protein overexpression and these had the same phenotype when analysed by IHC. Analysis of levels of HER2 and HER3 protein expression via western blot demonstrated that HER2 and HER3 proteins were at least 13-fold overexpressed in HB2 HER2/3OE cells in comparison to HB2 WT cells (see Chapter 4). This confirmed that these observations were not due to deficient HER protein overexpression.

This suggested that heregulin stimulation of both HB2 WT and HB2 HER2/3OE cells in 3D tri-culture was sufficient to promote a pro-tumorigenic phenotype regardless of HER2-HER3 overexpression. This correlates with work by Baeckström et al [271] who reported mitogenic effects and increased branching of HB2 WT structures in response to heregulin stimulation in collagen gels without HER2 and HER3 protein overexpression.

Therefore, while we had partly proved our hypothesis in that HB2 HER2/3OE cells have the capacity to induce a pro-tumorigenic morphology as reported in the literature [276] and akin to results with HB2 HER2OE in Chapter 4 in response to heregulin, it was still unclear whether HB2 HER2/3OE cells differed in their HER2-HER3 signalling capacity due to the similar results obtained with HB2 WT cells.

We then sought to investigate which intracellular signalling pathways were activated downstream of heregulin in the HB2 HER2/3OE cells to determine whether observations in our

cultures were due to deficient intracellular signalling processes downstream of the HER2-HER3 heterodimer.

5.5.2 Comparison of intracellular signalling pathway activation by heregulin in HB2 wildtype and HER2 and HER3 overexpressing cells

A time point of 15 minutes for stimulation with heregulin-β1 was selected as an appropriate time point for our experiments as this has been proven to be sufficient for activation of downstream heregulin signalling [325, 357] which has also proven valid for HB2 cells [356].

Heregulin has been reported in multiple studies to induce phosphorylation of Akt [339, 358, 359], GSK3 [360, 361] and Erk1/2 [362-364] in a variety of tissue types. In concordance with these studies, stimulation of HB2 WT and HB2 HER2/3OE cells with heregulin-β1 caused an increase in the levels phospho-Akt, phospho-GSK3α/β and phospho-Erk1/2 when analysed using human phospho-kinase arrays. This provided confidence that the concentration and time point of heregulin stimulation in our experiments was sufficient for downstream heregulin signalling pathway activation. In order to determine if there were any differences between the intracellular signalling pathways of HB2 WT and HB2 HER2/3OE cells in response to heregulin signalling, we first compared HB2 WT control to HB2 WT heregulin stimulated arrays and then HB2 HER2/3OE control to HB2 HER2/3OE heregulin stimulated arrays. We examined which kinases were differentially activated by at least two-fold in response to heregulin signalling for HB2 WT cells and then for HB2 HER2/3OE cells and determined whether there were any differences in the patterns of activation between the two cell types. This was in order to assess whether overexpression of the HER2-HER3 heterodimer caused HB2 cells to respond differently to heregulin stimulation or whether they responded the same therefore explaining the similarity in morphology and phenotype of these cells in the 3D tri-culture system. We identified a subset of kinases differentially activated in both HB2 WT and HER2/3OE cells, some by HB2 WT only, and some in HB2 HER2/3OE cells only. These are summarised in Table 5.2. We

further validated our quantification methods of these arrays by selecting two kinases, one which was easily visible on array membranes and one which was not easily visible and confirmed their expression patterns by western blot.

Kinases phosphorylated in both cell types	Increased or decreased?	Kinases phosphorylated in HB2 WT only	Increased or decreased?	Kinases phosphorylated in HB2 HER2/3OE only	Increased or decreased?
Erk1/2	Increased	**WNK1**	Increased	**Fyn**	Increased
GSK3α/β	Increased	**PDGFRβ**	Decreased	**Hck**	Increased
Akt	Increased			**FAK**	Increased
PRAS40	Increased			**eNOS**	Decreased
Lck	Decreased			**PLCγ1**	Decreased
				Pyk2	Decreased

Table 5.2 Summary of differentially activated kinases between HB2 WT cells and HB2 HER2/3OE cells in response to heregulin stimulation

The increase of phosphorylation of Akt and GSK3α/β suggested that in both cell types, heregulin-β1 stimulated activation of PI3K-Akt signalling. This correlated with the increase in PRAS40 phosphorylation which is a known substrate for activated Akt [365]. Phosphorylation of PRAS40 by Akt relieves inhibition of mTORC1 allowing cell growth through activation of S6K1 [366]. The increase in Erk1/2 phosphorylation suggested that heregulin-β1 also stimulated activation of Ras-Erk signalling in both cell types. The combined effect of this suggests an increase in proliferation, survival and protein translation of these cells in response to heregulin stimulation. Since Lck is a Src family kinase proven to stimulate Ras-Erk pathway [367, 368], the decreased Lck activation in these cells was unexpected. The majority of data available on Lck has been conducted in T cells with few studies addressing Lck function in breast cells and no data available on the effects of heregulin on Lck activation. High levels of Lck expression has been linked to both increased survival of breast cancer patients and increased breast cancer invasiveness [369] making it difficult to speculate the reasons for the decreased activation of

this protein. One theory is that this is attributed to active Syk signalling which is known to inhibit Lck activation in normal breast epithelium [370] but why this would be stimulated by heregulin is not known.

Increased activation of WNK1 protein was specific to HB2 WT cells in response to heregulin. The increased activation of WNK1 can be expected upon increased PI3K-Akt signalling as WNK1 is a substrate for Akt [371]. WNK1 is a serine-threonine kinase which can stimulate Erk5 mediated cell proliferation [372] and is a negative regulator of insulin-stimulated cell proliferation [371]. The reason for lack of increased activation of WNK1 in HB2 HER2/3OE cells is unknown. One theory is that since HER2-HER3 heterodimers are known to co-operate with insulin and insulin-like growth factor signalling [276], HER2-HER3 overexpression enhances insulin-stimulated proliferation thereby overcoming the inhibitory effects of WNK1 in these cells. Little connection could be found between heregulin signalling and PDGFR signalling. However, it has been documented that PDGFR is downregulated by mTOR [373] and since it is likely mTOR is increased in response to heregulin in HB2 WT cells due to the increase in Akt and PRAS40 phosphorylation, this could provide an explanation for PDGFR depletion. However, the reason why this is not the same for HB2 HER2/3OE cells is unknown.

It is clear from these results that despite the lack of HER2 and HER3 protein expression detected by western blot in HB2 WT cells in our study, heregulin had the capacity to induce several of the same major proliferative and anti-apoptotic signalling cascades as HB2 HER2/3OE cells perhaps explaining the similar morphology of these two cell types in response to heregulin in 3D tri-culture. It is likely that HB2 WT cells do indeed express HER2 and HER3 protein which would correlate with findings from the Berditchevski laboratory (personal communication, Dr Fedor Berditchevski). It is feasible that our western blot detection method was not sensitive enough to capture endogenous HER2 and HER3 expression or required prolonged exposure. Since heregulin is specific to HER2/HER3 or HER2/HER4 heterodimers

[317-319], it would be reasonable to suggest that at least HER2 was present in these cells but would need further optimisation of our western blot technique to confirm both this and the expression of HER3 in these cells.

The increase in kinases such as FAK and Fyn in HB2 HER2/3OE cells could be suggestive of increased migratory potential of these cells in response to heregulin. Heregulin has been reported to enhance the formation of filopodia, lamellipodia and increase migration of non-invasive breast cells [267]. Heregulin has the potential to recruit FAK to HER2-HER3 heterodimers [374] and induce its phosphorylation and activation [375]. FAK is well acknowledged as a major regulator of cell migration [376] and is stimulated by phosphorylation by Src kinases such as Fyn [377]. Fyn is reported to be required for cell migration [378] with a capacity to induce actin rearrangement [379]. Both Fyn [380] and FAK [381, 382] are reported to be involved in integrin signalling. Heregulin is also proven to mediate integrin signalling [383] suggesting a possible integrin-HER2-HER3 heterodimer complex formation with activation of FAK and Src downstream effectors in response to heregulin in these cells. The decreased activation of Pyk2 in these cells could be attributed to multiple events in these cells. Increased activation of FAK can downregulate Pyk2 [384]. The recruitment of Fyn to integrin-HER2-HER3 complexes could be competitively inhibiting Fyn association with Pyk2 and the reduction of Lck could cause loss of Pyk2 activation [385].

Though the increased activation of PLCγ in HB2 HER2/3OE control compared with HB2 WT cells was expected as PLCγ1 has been proven to be activated by HER2-HER3 heterodimers [340, 341] the loss of PLCγ1 signalling in HB2 HER2/3OE cells upon heregulin stimulation was unexpected given that heregulin activates the HER2-HER3 heterodimer. However, there is some evidence to suggest that activation of PLCγ1 can be reliant upon kinases such as Fyn and Lck [386, 387]. The recruitment of Fyn to other signalling complexes and the downregulation of Lck in these cells could account for this downregulation of PLCγ1. The reduction in eNOS could

be explained by the reduction in PLCγ1 activity as PLCγ1 can indirectly activate eNOS through increasing intracellular calcium levels [388, 389] and thereby increasing Calmodulin activity [390]. Calmodulin is proven to activate eNOS [391] therefore providing an explanation of loss of eNOS in these cells upon lack of PLCγ1. Another theory is that there is an increase in Caveolin-1 activity in these cells which has been shown to inhibit eNOS [392]. Interestingly, caveolin-1 has also been demonstrated to interact and mobilize Fyn to integrin complexes [380] and could therefore be influencing multiple signalling processes in these cells.

Combined, this suggests that HB2 HER2/3OE cells do have the capacity to respond to heregulin stimulation as expected by up regulating kinases such as Akt and PRAS40 and thus proves our hypothesis that these cells are not deficient in their HER2-HER3 signalling capacity. In addition, the differential activation of kinases such as FAK and Fyn to HB2 WT cells may be indicative of different adhesion and migration properties of these cells.

However, intracellular signalling processes are incredibly complex with a high degree of crosstalk and overlap. Many of the signalling processes highlighted above are clearly context dependent with many of the studies described undertaken in other cell and tissue types to breast. A major limitation of our experimentation here is that the intracellular signalling processes were studied in 2D rather than 3D culture. It is plausible that these effects would not be conserved in 3D and that our observations in 3D were induced by different mechanisms due to different intercellular signalling mechanisms and ligand availability. Therefore, not only are conclusions drawn here based on speculation from crude experimentation, but an inappropriate model system was employed. Further investigation and validation is needed to confirm these theories using appropriate model systems.

Nevertheless, these experiments have confirmed that in 2D monolayer culture, the overexpression of HER2 and HER3 in HB2 cells altered the activation of a subset of phospho-kinases in response to heregulin verifying that HER2 and HER3 overexpression altered

intracellular signalling mechanisms in these cells. This indicated that the lack of a highly mitogenic and migratory morphology and phenotype of HB2 HER2/3OE in comparison to HB2 WT cells was not due to deficient expression, functionality and downstream signalling of the HER2 and HER3 heterodimer from heregulin in these cells but may be due to the external influences of surrounding stromal cells and the microenvironment. This too would require further experimentation in 3D cultures to confirm this theory.

6 Chapter 6: Assessing the suitability of the *in vitro* model to study the role of the stroma on cancer initiation

6.1 Introduction

Over the last few years it has become increasingly apparent that the tumour stroma is not just a passive bystander in the progression of breast tumours. Work by Finak et al [53] proposed that the stromal gene expression signature can be used as a powerful prognostic indicator of clinical outcome of breast cancer patients. However, little is known about how changes in gene expression of stromal cells affect the morphology and phenotype of the normal luminal epithelium and whether these changes are attributed to the initiation of tumorigenesis.

Our tri-culture model included both a fibroblast and a myoepithelial component and validation experiments earlier in this thesis showed that the model was representative of normal breast *in vivo*. To determine whether it had potential to be used as a tool to study the role of gene expression changes in stromal cells on cancer initiation, we selected two protein candidates to knockdown in our fibroblasts and myoepithelial cells and investigated the effect on normal epithelial architecture. These were Dedicator of Cytokinesis 4 (DOCK4) and Estrogen Receptor β1 (ERβ1). These were chosen in concordance with local research interests, the rationales for which are discussed below.

6.1.1 DOCK proteins

Over 60 guanine nucleotide exchange factors (GEFs) have been identified in the human genome. GEFs are a family of proteins which function to activate Rho GTPases [393]. Therefore, through downstream signalling to Rho GTPases, GEFs play a role in regulating cytoskeletal remodelling and thus several key cell functions such as maintaining cell polarity [394], cell migration [395] and even cell proliferation [396].

One family of GEFs identified are the DOCK family proteins. To date, 11 members of the DOCK family have been identified [397]. All DOCK proteins contain a DOCK homology region 1 domain (DHR1) which binds PIP_3 [398] and a bioactive DOCK homology region 2 domain (DHR2) which catalyses the conversion of GDP to GTP [399].

DOCK4 is a member of the DOCK protein family. In addition to containing DHR1 and DHR2 domains, DOCK4 also contains an SH3 domain at its N-terminus and a proline rich motif at its C-terminus contributing to its quaternary structure and aiding inter-molecular protein interactions [400]. Though extensive functional data for the DOCK4 protein is lacking, DOCK4 has been linked to tumorigenesis through its interaction with downstream protein targets such as Rap GTPase regulating cell junction assembly and also metastasis through its role in lymphatic/haematogenous spread [401]. It is also reported that protein complexes containing DOCK4 can increase cell migration and invasion in breast cancer [402]. DOCK4 is a GEF for Rac1 [403]. Rac1 is a Rho GTPase with well documented roles in cancer initiation and progression. Rac1 is commonly overexpressed in breast cancers [404] where it mediates increased migration, invasiveness and anchorage-independent growth of MCF-7 cells via Pak1 activation [405], as well as cyclin D1 induction by heregulin [362]. Currently there is no extensive data available on the abundance and function of DOCK4 in breast tumour cells and fibroblasts. Preliminary work in our group has demonstrated variable DOCK4 expression in fibroblasts in both breast carcinoma samples (Fig 6.1) and in reduction mammoplasty samples (Fig 6.3, section 6.3). The significance of this is currently unknown.

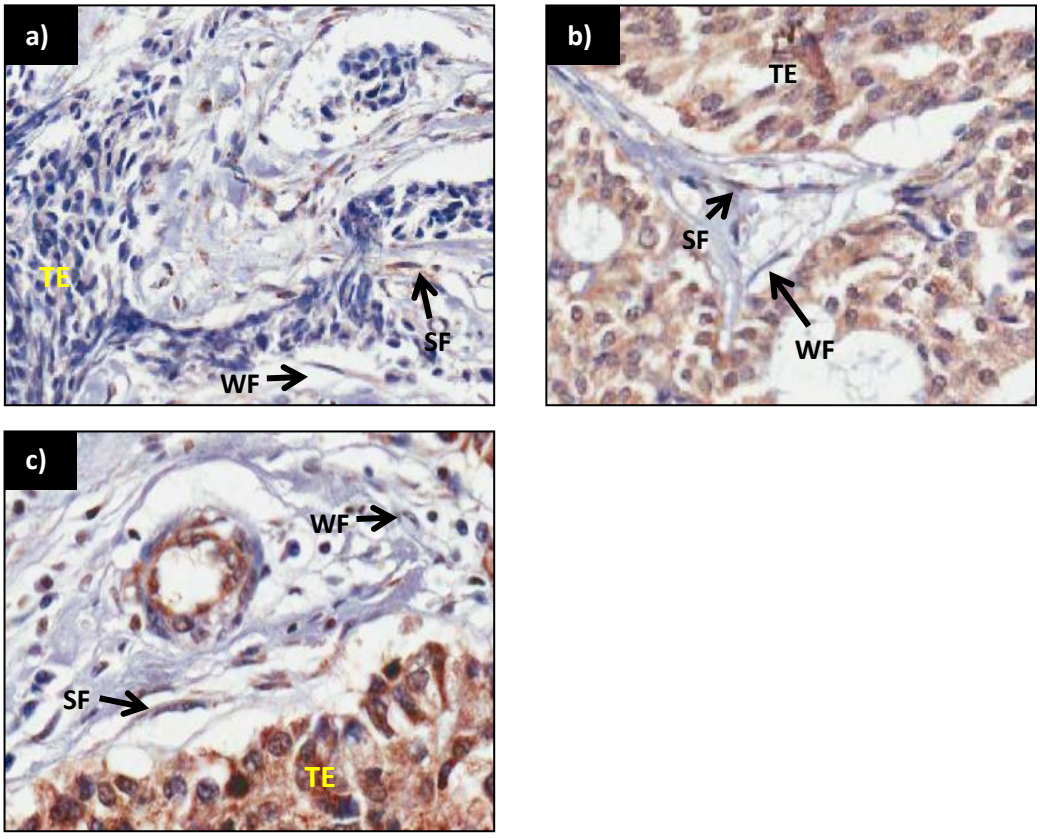

Fig 6.1 Expression of DOCK4 in breast carcinoma samples

Examples of breast carcinoma samples representing weak (a), moderate (b) and strong (c) DOCK4 expression in tumour epithelial cells (TE). In all cases, intensity of DOCK4 expression in fibroblasts varied with each sample regardless of levels in tumour epithelium. Each contained examples of weak DOCK4 expression (WF) and strong expression (SF) in fibroblasts.

Images courtesy of Dr Renu Gahlaut and Dr Georgia Mavria (Leeds Institute of Cancer and Pathology).

6.1.2 ERβ1

In 1986, the first gene encoding a protein receptor responsible for binding 17β estradiol was cloned (now known as ERα) and was long believed to be the only mediator of estrogen signalling [406, 407]. However, a decade later, a second estrogen receptor was identified, first in rat [408], and then in humans [409] and was denoted ERβ. ERβ is expressed in a variety of tissue types and is the major form of ER in the normal adult breast with expression observed in luminal epithelium, myoepithelium and stromal cells [410]. ERβ belongs to the nuclear hormone receptor (NHR) family of proteins which feature common structural compositions. ERβ contains an AF1 domain at its N-terminus which activates transcription irrespective of ligand binding, a DNA binding domain (DBD), an AF2 domain which activates transcription in response to ligand binding and an estrogen ligand binding domain (LBD) [411, 412]. Several isoforms of ERβ have been identified which arise through alternative splicing and differ in their last coding exon [413]. ERβ1 was the first ERβ isoform to be resolved [408] and has since been proven to be the only ligand binding ERβ isoform [414]. Upon activation, ERβ1 can either homodimerise, or form heterodimers with other ERβ isoforms [415] or with ERα [416].

Like other NHRs, the classical ERβ signalling pathway involves the binding of a ligand to ERβ dimers in the cytoplasm causing activation and translocation into the nucleus. Once in the nucleus, ERβ binds DNA via its DNA binding domain to estrogen response elements [417] or serves as a co-regulator for other transcription factors such as AP-1 [418]. Roles for ERβ have also been reported in the mitochondria [419] and in signalling cascades from the plasma membrane [420].

Perhaps due to lack of sufficiently well characterised antibodies, conflicting roles for ERβ have been reported in breast cancer. However, the majority of both clinical and *in vitro* studies to date have reported a tumour suppressive role for ERβ. Several clinical studies have reported a correlation with ERβ expression and increased patient survival [421-423]. In addition, several *in*

vitro studies have reported an anti-proliferative effect of ERβ in breast cancer cells [424-426] as well as decreased cell invasion [427] and increased apoptosis [428].

Given the putative tumour suppressive nature of ERβ in breast cancer as well as the reported tumour suppressive nature of myoepithelial cells [429], it could be proposed that the tumour suppressive role of myoepithelial cells is mediated by ERβ. The loss of both ERβ [430] and myoepithelial cells [431] in the transition from DCIS to invasive cancer may strengthen this proposal.

6.1.3 CAFs and cancer initiation

As a follow up to previous chapters, we were also interested in whether activation of normal fibroblasts can alter the morphology of the normal luminal epithelium further exploring the theory that changes in stromal cell activity can initiate tumorigenesis. Therefore, the effect of pre-exposing our normal fibroblasts to the well characterised HER2 overexpressing tumour cell line SkBr3 on the normal architecture of our model was investigated.

6.2 Aims

In order to determine if the 3D *in vitro* tri-culture model could be used to study the role of gene expression changes in stromal cells on cancer initiation, the effect of DOCK4 protein knockdown in fibroblasts and ERβ1 knockdown in myoepithelial cells on the morphology and phenotype of normal HB2 cells in 3D tri-culture models of normal breast was investigated. In keeping with the theme from previous chapters, the effect of exposing of normal fibroblasts to the conditioned medium of the HER2 overexpressing breast tumour cell line SkBr3 was investigated in an attempt to elucidate whether tumour cells "activate" normal fibroblasts and whether these activated fibroblasts have the capacity to disrupt normal luminal cell architecture. This was addressed by :-

- Induction of stable knockdown of DOCK4 in LS11-045 hTERT immortalised fibroblasts using lentiviral shRNAs and comparison of the morphology and phenotype of HB2 cells in 3D tri-culture *in vitro* models with fibroblasts deficient in DOCK4 and respective controls
- Induction of knockdown of ERβ1 in GFP Myo1089 cells using siRNA and comparison of the morphology and phenotype of HB2 cells in 3D tri-culture *in vitro* models with ERβ1 siRNA GFP Myo1089 cells and respective controls
- Pre-culturing LS11-083 dsRed fibroblasts in SkBr3 conditioned medium and comparison of the morphology and phenotype of HB2 cells in 3D tri-culture *in vitro* models with LS11-083 dsRed fibroblasts pre-conditioned to SkBr3 cells

6.3 Materials and Methods

6.3.1 Downregulation of DOCK4 in LS11-045 hTERT fibroblasts by shRNA transduction

Lentiviral transduction was carried out as per Chapter 2. In order to produce LS11-045 hTERT fibroblasts with stable knockdown of DOCK4 protein, two pGIPZ-tGFP vectors containing shRNA sequences against DOCK4 were used (see Fig 6.2, Thermo Scientific) with the pGIPZ-tGFP empty vector used as a control (see Chapter 3). The shRNA sequences used were as follows:-

- 5'- CTCAGTATTTGCAGATATA - 3' (referred to as DOCK4 shRNA 1)
- 5'- CGCAAGGTCTCTCAGTTAT -3' (referred to as DOCK4 shRNA 2)

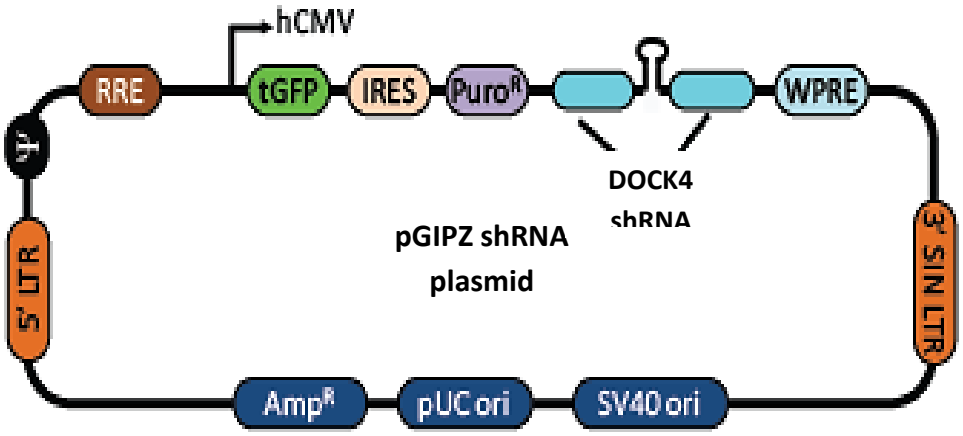

Fig 6.2 Simplified plasmid map of pGIPZ shRNA lentiviral expression plasmid

Diagram represents key elements contained within the expression plasmid used to lentivirally transduce cells with DOCK4 shRNA. Key elements are as follows:- Human Cytomegalovirus promoter (hCMV), TurboGFP gene (tGFP), internal ribosome entry site (IRES), Puromycin resistance gene ($Puro^R$), short hairpin RNA sequence against DOCK4 (DOCK4 shRNA), Woodchuck hepatitis virus post-transcription regulatory element (WPRE), 3'- self inactivating long terminal repeat (3'-SIN LTR), Simian Vacuolating Virus 40 origin of replication (SV40 Ori), pUC origin of replication (pUC), Ampicillin resistance gene (Amp^R), 5'-LTR, psi packaging sequence (ψ) and Rev Response Element (RRE).

Adapted from [http://www.thermoscientificbio.com/shrna/gipz-lentiviral-shrna/].

6.3.2 Lentiviral Transduction for cell tracking

Lentiviral transduction was carried out as per Chapter 2. In order to produce Myo1089 cells that stably expressed dsRed fluorescent protein, the pFURW empty lentiviral expression vector was used (see Chapter 3, Fig 3.2 for a plasmid map of the pFURW vector).

6.3.3 Downregulation of ERβ1 in GFP Myo1089 cells

siRNA transfection

Transfection of siRNAs against ERβ1 in GFP Myo1089 cells was performed according to a method previously optimised by Dr Euan Baxter (Leeds Institute of Cancer and Pathology) shown to give >70% downregulation of ERβ1 in MCF-7 cells (unpublished). ERβ1 siRNA oligonucleotides were supplied lyophilised (Sigma) and were re-suspended in 1x siRNA Buffer (Dharmacon; 20mM KCl, 6mM HEPES-pH 7.5, 0.2mM MgCl2) to obtain standard stock concentrations of 10µM. ERβ1 siRNA sequences used were as follows:-

- 5'- GGGCTTCATCTTTCTGCTG- 3'
- 5'- GGGCATGGAACATCTGCTCAACA -3'

A negative control with a siRNA pool of non-targeting sequences was obtained (Dharmacon #D-001206-13) and is termed scrambled control.

GFP Myo1089 cells were seeded into a 6-well plate and left to adhere for 24 hours ensuring 60% confluency. Cell media was replaced prior to the transfection procedure. Transient transfection was performed using Lipofectamine® RNAiMAX reagent (Invitrogen) according to manufacturer's instructions for a 6-well plate. The final concentration of siRNA in each reaction was 100pmol for both ERβ1 siRNA and scrambled control. In the case of ERβ1, the two different siRNA sequences above were pooled to give a total concentration of 100pmol. Solutions containing siRNA-Lipofectamine® RNAiMAX complexes were added dropwise to GFP Myo1089 cells (250µl per well) and cells left to recover for 72 hours before assessing knockdown efficiency by qPCR.

RNA extraction from cells cultured in 2D

Total RNA was extracted from cells using a Qiagen RNA Easy Plus Mini Kit (Qiagen) according to manufacturer's instructions. Briefly, cells were lysed in situ with lysis buffer containing RNase I. Genomic DNA was removed via gDNA eliminator columns (supplied) before lysate was applied to columns that contain a membrane filter that binds RNA. Total RNA was eluted from the column with 30µl nuclease-free water (supplied). RNA was analysed using a Nanodrop ND-1000 spectrophotometer reading at an optical density of 260nm and 280nm to determine concentration and purity.

RNA Extraction from cells contained in 3D collagen gels

Total RNA was extracted from GFP Myo1089 mono-culture gels as previously described [432]. Briefly, GFP Myo1089 cells were cultured as mono-cultures in 3D collagen gels as per Chapter 2 to give a final cell density of $4x10^5$ cells per mL of gel. After 21 days in culture, the medium was removed from the top and bottom of three replicate gels and gels rinsed twice with ice cold DPBS. Working on ice, collagen gels were removed from inserts using a pre-chilled truncated P1000 pipette tip (Gilson) and transferred into pre-chilled sterile eppendorf tubes. After a soft centrifugation step (1 min, 7500rpm), residual medium supernatant (that had been retained by the collagen gel) as well as collagen overlaying the cell pellet was removed by pipetting. Cell pellet was then lysed immediately and RNA extraction carried out as for cells cultured in 2D (above).

DNase Treatment and cDNA synthesis

RNA (10µg) was treated with DNase using a TURBO DNase kit (Ambion) according to manufacturer's instructions. A total reaction volume of 50µl was used. cDNA was synthesised using a Superscript II kit (Invitrogen). Briefly, 100ng of DNase treated RNA was added to a tube placed on ice, 1µl mixed deoxyribonucleotide triphosphate (dNTPs, 10mM, Promega) and 1µl oligo dT (250ng/µl) (supplied) were added and the volume made up to 12µl with nuclease-free

water (Ambion). Solution was incubated at 65°C for 5 mins and replaced on ice. To this, 1µl RNase (RNase Out), 2µl (0.1M) dithiothreitol and 5µl of 10 x buffer (all supplied) were added. Solution was incubated at 42°C for 2 mins before adding 1µl of Superscript II reverse transcriptase (supplied). Reaction mixture was then incubated for 50 minutes at 42°C and then 15 minutes at 70°C. The cDNA was stored at -20°C until required.

qPCR

The downregulation of ERβ1 was assessed by qPCR. This was performed using Taqman® gene expression assays (Life technologies). All reactions performed in a hood which was UV irradiated prior to use. Total volume of each reaction was 20µl comprising of 2µl of the cDNA template, 1µl of Taqman gene expression assay, 10µl of TaqMan® Gene Expression Master Mix and made up to 20 µl with nuclease free water (all Applied Biosytems). Two types of controls were employed for each gene expression assay, one with cDNA template omitted and one minus RT control per cell type lysed. For each reaction, 20 µl was transferred to a MicroAmp® optical 96-well plate (Applied Biosytems) and plate sealed with optical tape. Reactions were amplified on an ABI 7700 machine (Applied Biosystems) with the following thermocycling parameters: 2 mins 50°C, 10 mins 95°C, and then 40 cycles of 15 secs 95°C and 1 min 60°C. All reactions were performed in triplicate. Relative quantification of ERβ1 mRNA was calculated in relation to the RPLP0 housekeeping gene [433]. The ΔCt was calculated [434] in comparison to RPLP0 and the fold difference to scrambled control calculated to determine efficiency of ERβ1 downregulation.

6.3.4 Pre-conditioning of LS11-083 dsRed Fibs to SkBr3 cells

Conditioned medium from SkBr3 cells was prepared as per Chapter 2. LS11-083 dsRed Fibs were cultured under normal conditions in vented cap cell culture flasks (Corning) until 50% confluency was reached. Cells were rinsed in DPBS and medium replaced with SkBr3 cell conditioned medium either neat or diluted in 1:2 DMEM-GlutaMAX™-I + 10% HI-FCS to give

50% and 100% SkBr3 conditioned medium. Media of control flasks were replaced with fresh DMEM-GlutaMAX^{TM}-I + 10% HI-FCS. LS11-083 dsRed Fibs were then incubated for 24 hours prior to incorporation into 3D tri-culture as per Chapter 2.

6.4 Results

6.4.1 Confirmation of DOCK4 expression in fibroblasts from the LS11-045 normal breast reduction mammoplasty sample

DOCK4 protein expression was examined in the normal breast reduction mammoplasty sample denoted LS11-045 by IHC (Fig 6.3). DOCK4 staining was detected in both the normal breast epithelium and in the majority of surrounding stromal fibroblasts confirming that DOCK4 protein was expressed in original fibroblasts *in vivo* prior to *in vitro* culture. Representative image from three technical replicates presented.

6.4.2 Knockdown of DOCK4 in hTERT fibroblasts

In order to determine the effect of knocking down DOCK4 protein in fibroblasts, LS11-045 hTERT fibroblasts were transduced with lentiviruses harbouring two different shRNA sequences for DOCK4 (DOCK4 shRNA 1 and DOCK4 shRNA 2) or empty vector control (EV) in addition to tGFP. Three fibroblast populations were produced which all retained an elongated spindle-shaped morphology following transduction and with over 95% of cells positive for tGFP (Fig 6.4). Given that with the method of FACS, a population of 95-100% of tGFP positive cells would be considered very high purity [435], and that >95% of our cells were positive for tGFP upon visual inspection without sorting, it was deemed unnecessary to enrich for a tGFP positive cell population any further by FACS sorting.

DOCK4 protein expression was assessed by western blot in untreated LS11-045 hTERT fibroblasts and compared to EV fibroblasts. This not only confirmed that DOCK4 protein expression was retained in fibroblasts following isolation from the original breast reduction mammoplasty specimen and subsequent hTERT transduction, but also that expression was not altered by transduction with the control lentivirus, EV. Representative image from three independent western blots presented. DOCK4 protein expression was then assessed to determine the effectiveness of each shRNA in the knockdown of DOCK4. Fig 6.5 depicts a

decrease in expression of total DOCK4 protein upon treatment with both DOCK4 shRNA plasmids in comparison to EV control fibroblasts. However, a fainter band was observed upon treatment with DOCK4 shRNA 2 than DOCK4 shRNA 1 plasmid. Representative image from three independent western blots presented. Quantification data are presented as expression fold difference to EV controls and confirmed a 2-fold decrease in expression of DOCK4 protein with DOCK4 shRNA 1 and a 7-fold decrease with DOCK4 shRNA 2. This suggested a more efficient knockdown of DOCK4 protein in LS11-045 hTERT fibroblasts transduced with DOCK4 shRNA 2 than DOCK4 shRNA 1. Therefore, hTERT fibroblasts containing DOCK4 shRNA 2 were used for subsequent experimentation and are referred to as DOCK4 shRNA fib and empty vector control fibroblasts referred to as EV fib from here in.

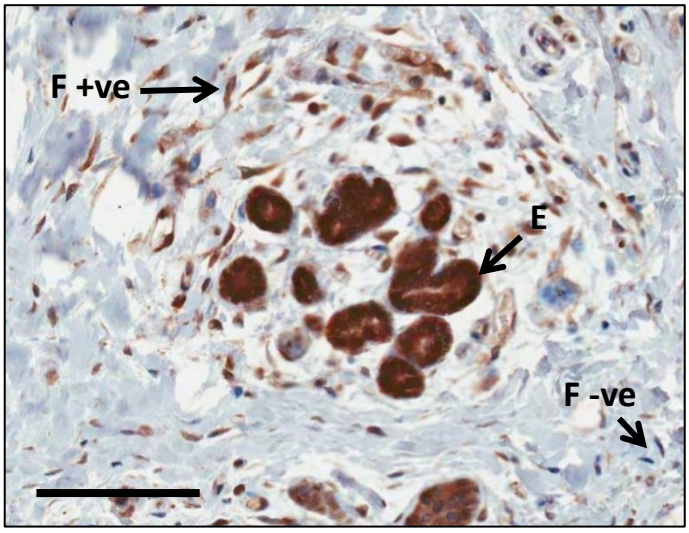

Fig 6.3 Expression of DOCK4 in normal breast tissue

Anti-DOCK4 IgG was used to detect DOCK4 protein expression in LS11-045 normal breast reduction mammoplasty sample by IHC. In addition to the strong DOCK4 staining in the normal breast epithelium (E), DOCK4 was detected in the majority of the surrounding stromal fibroblasts (F +ve). Fibroblasts were also observed which were negative for DOCK4 staining (F – ve) but these were fewer in number than DOCK4 positive fibroblasts. Original magnification 20x, scale bar = 100µm. Representative image from three technical replicates presented.

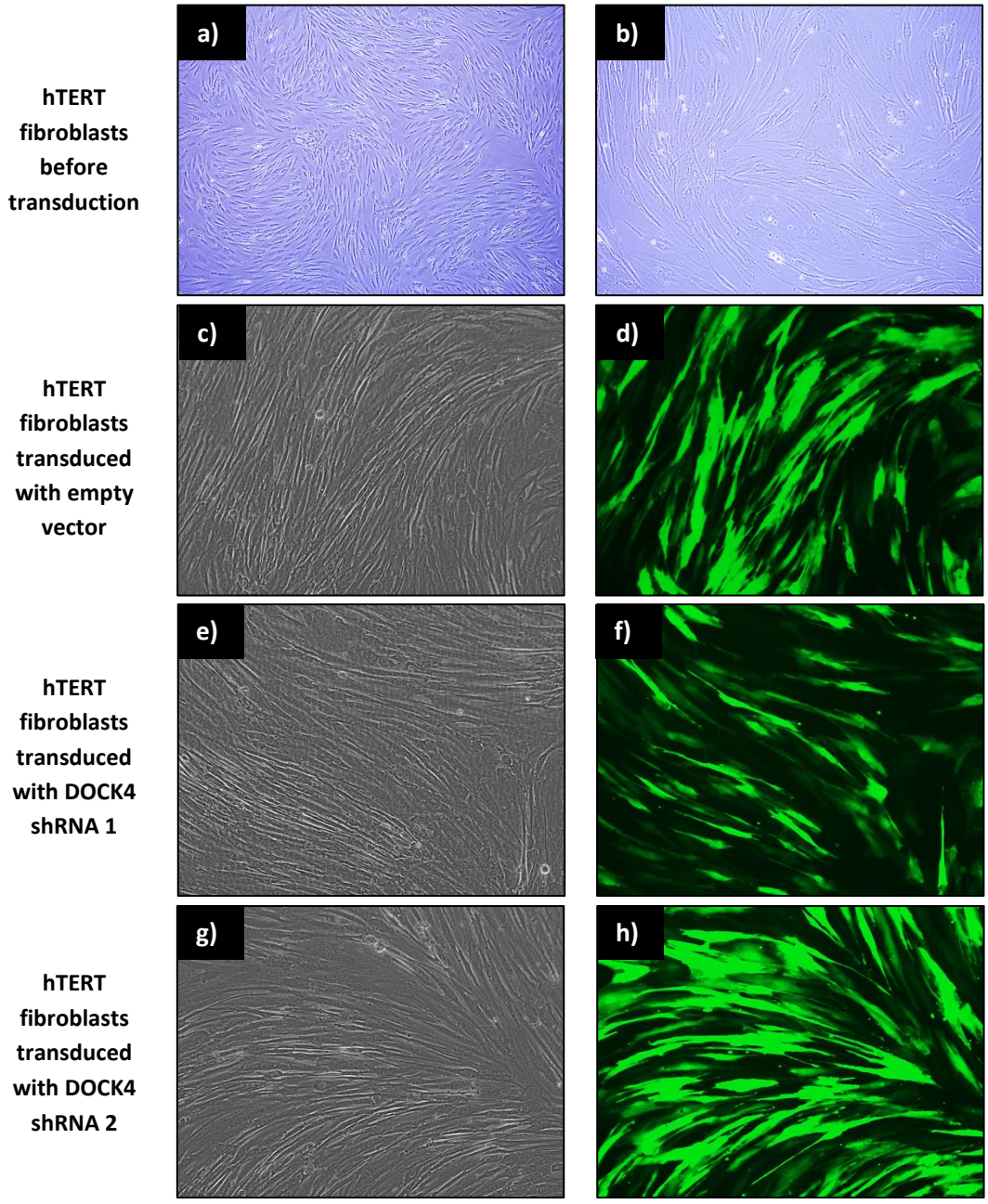

Fig 6.4 Lentiviral transduction of hTERT fibroblasts with DOCK4 shRNA

Phase contrast microscopy of hTERT fibroblasts prior to lentiviral transduction showed a mono layer of dispersed cells (a, original magnification 4x) with elongated spindle-shaped morphology (b, original magnification 10x). hTERT fibroblasts were lentivirally transduced tGFP lentivirus harbouring empty vector (c & d) or tGFP lentiviruses harbouring two different shRNA sequences for the protein DOCK4 labelled here as DOCK4 shRNA 1 (e & f) and DOCK4 shRNA 2 (g & h). Phase contrast microscopy demonstrated that hTERT fibroblasts maintained an elongated spindle-shaped morphology following lentiviral transduction (c, e and g). Fluorescence microscopy for all lentiviral vectors confirmed that over 95% of the cells were positive for the GFP reporter (d, f & h). Original magnification for c-h, 10x. Images acquired with an EVOS fl microscope.

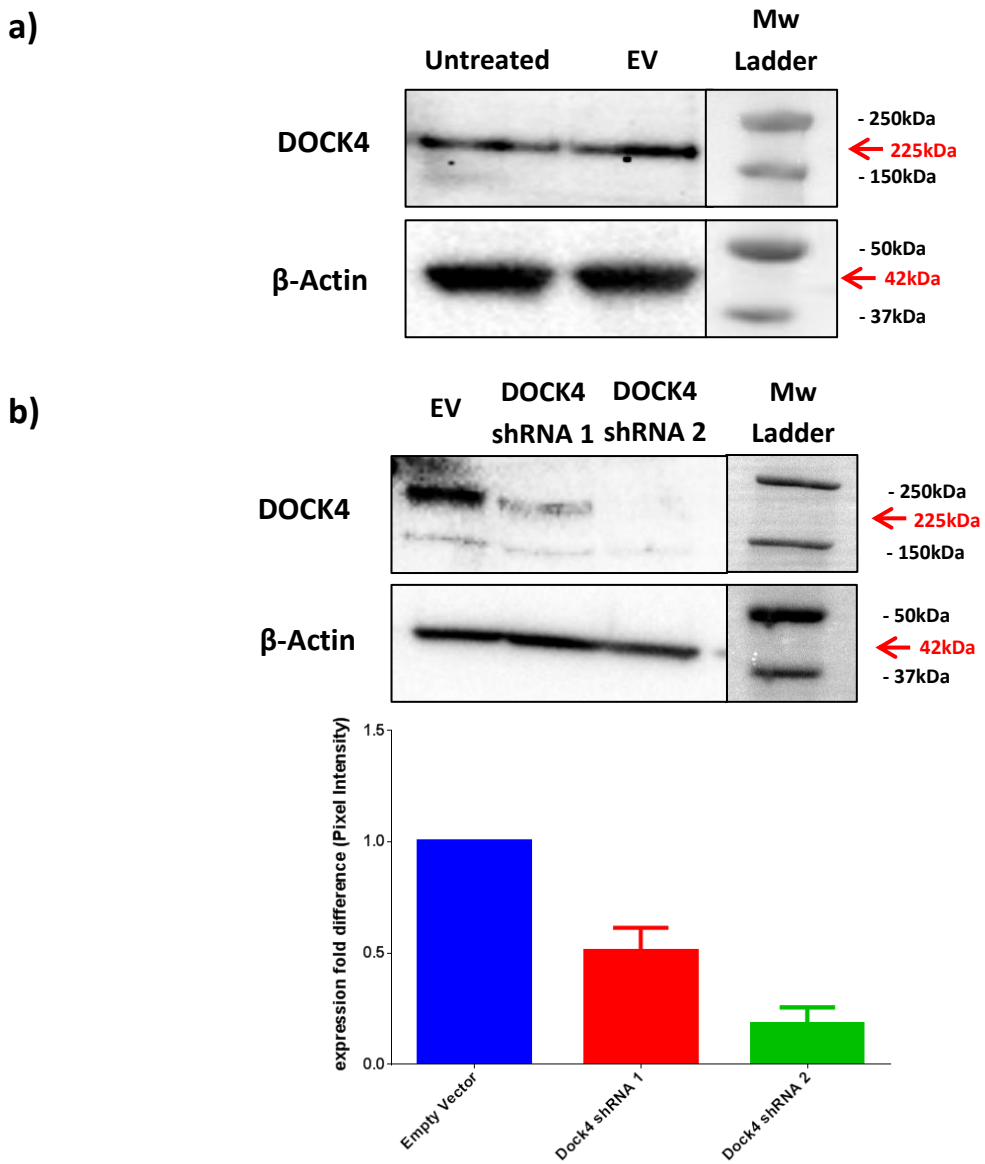

Fig 6.5 Western blot for DOCK4 in fibroblasts transduced with lentiviruses harbouring two DOCK4 shRNAs in comparison to fibroblasts with control lentiviral transduction (EV)

a) Anti-DOCK4 was used to detect total DOCK4 protein in untreated hTERT fibroblasts (untreated) and in empty vector fibroblasts (EV). Bands of ~225kDa were observed in both. Anti-β-Actin IgG was used as a loading control for which bands were observed in both samples at ~42kDa. Representative image from three independent western blots. b) Anti-DOCK4 IgG was used to detect total DOCK4 protein in EV and fibroblasts transduced with lentiviruses harbouring two different DOCK4 shRNAs (DOCK4 shRNA 1 & DOCK4 shRNA 2). Bands of ~255kDa were observed in EV and DOCK4 shRNA 1 cells with EV displaying a more intense band than DOCK4 shRNA 1. No band was detected in DOCK4 shRNA 2. Anti-β-Actin IgG was used as a loading control for which bands were observed in all samples at ~42kDa. Representative image from three independent western blots. Histogram shows quantification of DOCK4 expression following densitometry analysis using the BioRad Image Lab 4.1 software. DOCK4 expression was calculated as fold difference to EV after normalization to β-Actin for each sample. Bars denote mean from three independent western blots and error bars standard error of the mean (SEM).

6.4.3 Production and characterisation of a dsRed positive myoepithelial cell line

Due to the tGFP reporter present in our fibroblasts, to enable the tracking of Myo1089 cells in 3D tri-culture, Myo1089 cells were lentivirally transduced with a lentivirus harbouring the pFURW-dsRed empty vector plasmid. FACS yielded a Myo1089 cell population which was >99% positive for dsRed and retained a stellate-shaped morphology (Fig 6.6). These are referred to as dsRed Myo1089 cells from here in.

6.4.4 Morphology and phenotype of 3D *in vitro* tri-culture models containing fibroblasts with or without DOCK4 protein expression

In order to determine any potential effects of knocking down DOCK4 protein in fibroblasts on epithelial architecture, HB2 WT and dsRed Myo1089 cells were co-cultured with EV fibs or DOCK4 shRNA fibs in the 3D tri-culture system and the morphology of the cultures assessed. Visualisation by H & E demonstrated that in the presence of either EV fibs or DOCK4 shRNA fibs, HB2 WT cells formed small rounded units which consisted of cohesive cells with lumen formation in their centres as per results in previous chapters (Fig 6.7). Representative images from three technical replicates presented. This suggested that knockdown of DOCK4 protein in fibroblasts had no effect on the morphology of HB2 cell architecture.

Similarly, characterisation by IHC showed little difference in the phenotype of HB2 units cultured with EV fibs and DOCK4 shRNA fibs (Fig 6.8 and 6.9, representative images from three technical replicates presented). HB2 unit phenotype was comparable to results from previous chapters whereby E-Cad was observed between HB2 cell junctions and EMA concentrated at the apical-lumen interface with both types of fibroblasts. Ki67 was equally strong and abundant in HB2 cells and M30 staining negligible regardless of fibroblasts used. Basement membrane production was evident with both types of fibroblast with areas of Coll IV staining observed around outer edges of HB2 units. Both EV Fibs and DOCK4 shRNA fibs showed similar distribution within gels with tGFP staining detected both loosely associated with outer edges

of HB2 units and distributed throughout the collagen gel matrix. dsRed Myo1089 cells were also found associated with outer edges of HB2 units in both contexts.

This suggested that knockdown of DOCK4 protein in fibroblasts does not affect the morphology and phenotype of normal mammary epithelial architecture in the 3D *in vitro* tri-culture model of breast.

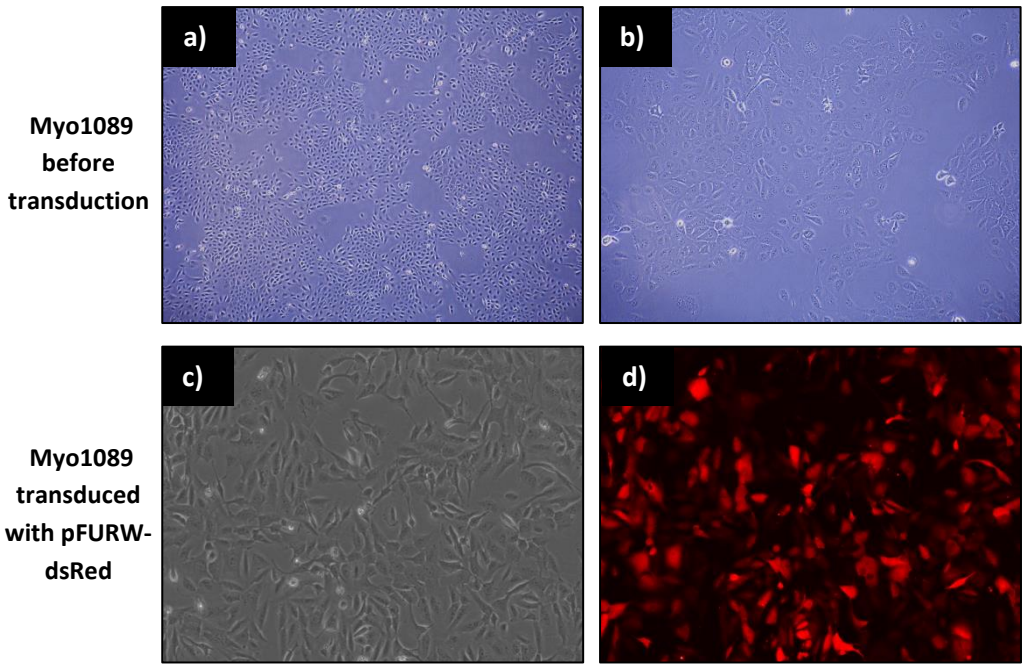

Fig 6.6 Lentiviral transduction of Myo1089 cells with dsRed fluorescent protein

Phase contrast microscopy of Myo1089 cells prior to lentiviral transduction showed a cobblestone monolayer of cohesive cells (a, original magnification 4x) which consisted of an elongated stellate-shaped morphology (b, original magnification 10x). Myo1089 cells were lentivirally transduced with pFURW-dsRed vector. Phase contrast microscopy demonstrated that Myo1089 cells maintained an elongated stellate-shaped morphology following lentiviral transduction (c). Fluorescence microscopy demonstrated over 95% of the cells were positive for the dsRed fluorescent reporter (d). Original magnification for c & d, 10x. Images (a) and (b) acquired using an Olympus CKK41 microscope with an Olympus Camedia C-7070 camera attached. Images (c) and (d) acquired using an EVOS fl microscope.

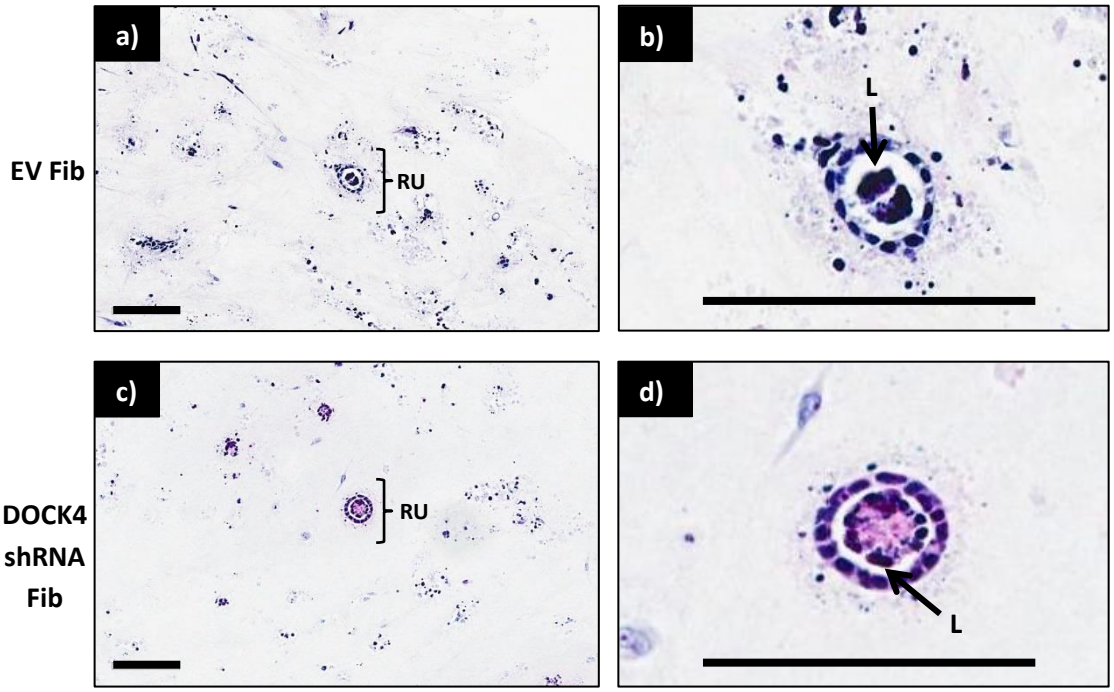

Fig 6.7 Representative H & E staining of 3D *in vitro* tri-culture models containing fibroblasts with or without DOCK4 protein expression

Empty vector control fibroblasts (EV Fibs) and fibroblasts with knockdown of DOCK4 (DOCK4 shRNA Fibs) were co-cultured in 3D collagen gels with dsRed Myo1089 and HB2 wildtype cells for 21 days and 5µm sections of gels were H & E stained. Little difference was observed with knockdown of DOCK4 protein in fibroblasts on the morphology of HB2 units. HB2 cells formed cohesive rounded units (RU) with appearance of lumens (L) both in the presence of EV Fibs (a & b) and DOCK4 shRNA Fibs (c & d). Original magnification 20x, scale bars = 100µm. Representative images from three technical replicates presented.

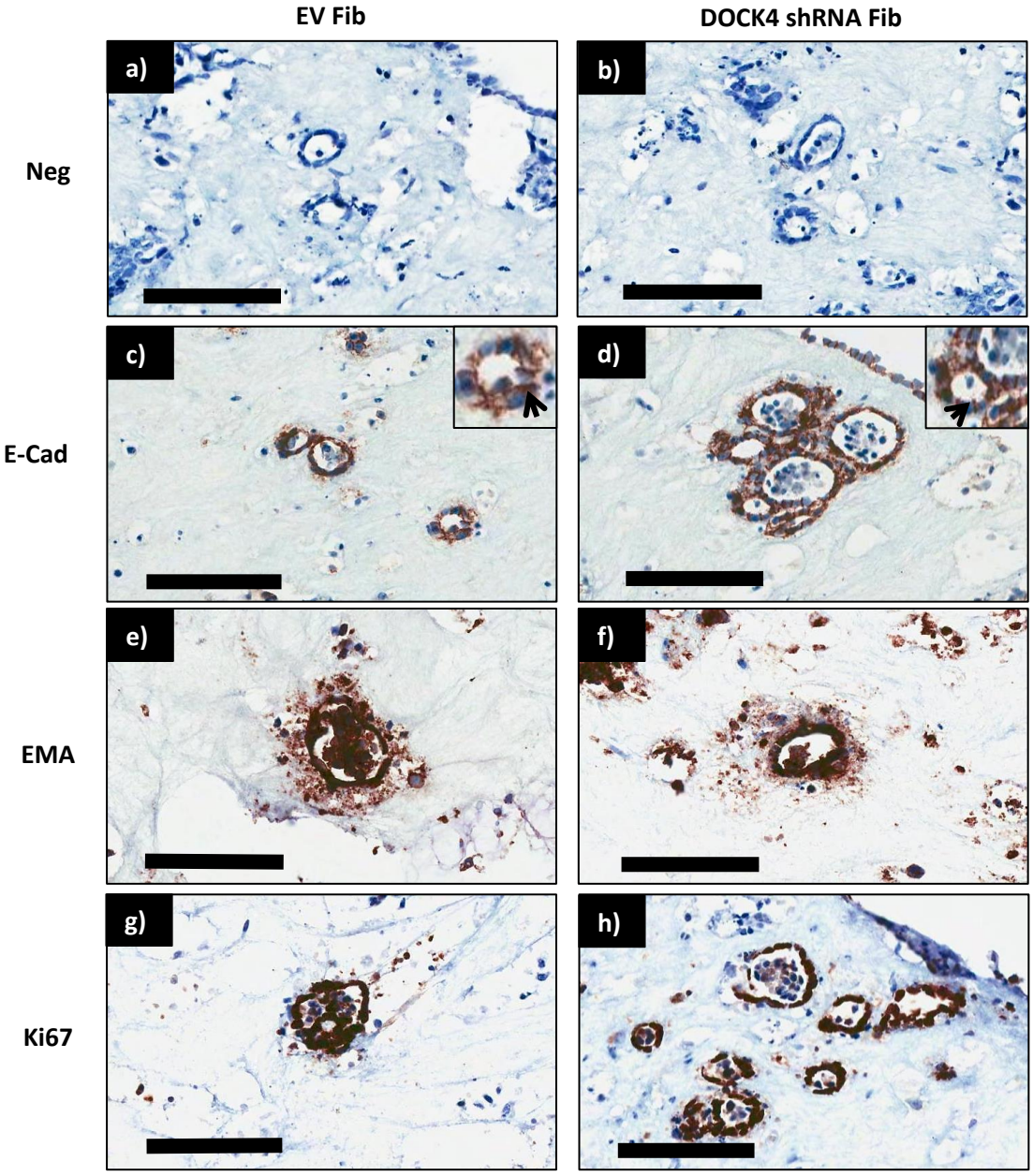

Fig 6.8 IHC characterisation of 3D *in vitro* tri-culture models containing fibroblasts with or without DOCK4 protein expression A

3D *in vitro* tri-culture model containing empty vector control fibroblasts (EV Fibs) and fibroblasts with knockdown of DOCK4 (DOCK4 shRNA Fibs) with HB2 cells and dsRed Myo1089 cells were characterised by IHC. Little difference was observed with the knockdown of DOCK4 protein in fibroblasts on the phenotype of HB2 units. Primary antibody was omitted to serve as a negative control (a & b). E-cadherin (E-Cad) was expressed by HB2 cells at cell-cell junctions (arrow, c) in the presence of EV Fibs (arrow, c) and DOCK4 shRNA Fibs (arrow, d). Strong staining was observed in HB2 cells with both types of fibroblasts (e & f). HB2 cells were positive for Ki67 regardless of fibroblast type (g & h). Original magnification 20x, scale bars = 100µm. Representative images from three technical replicates presented.

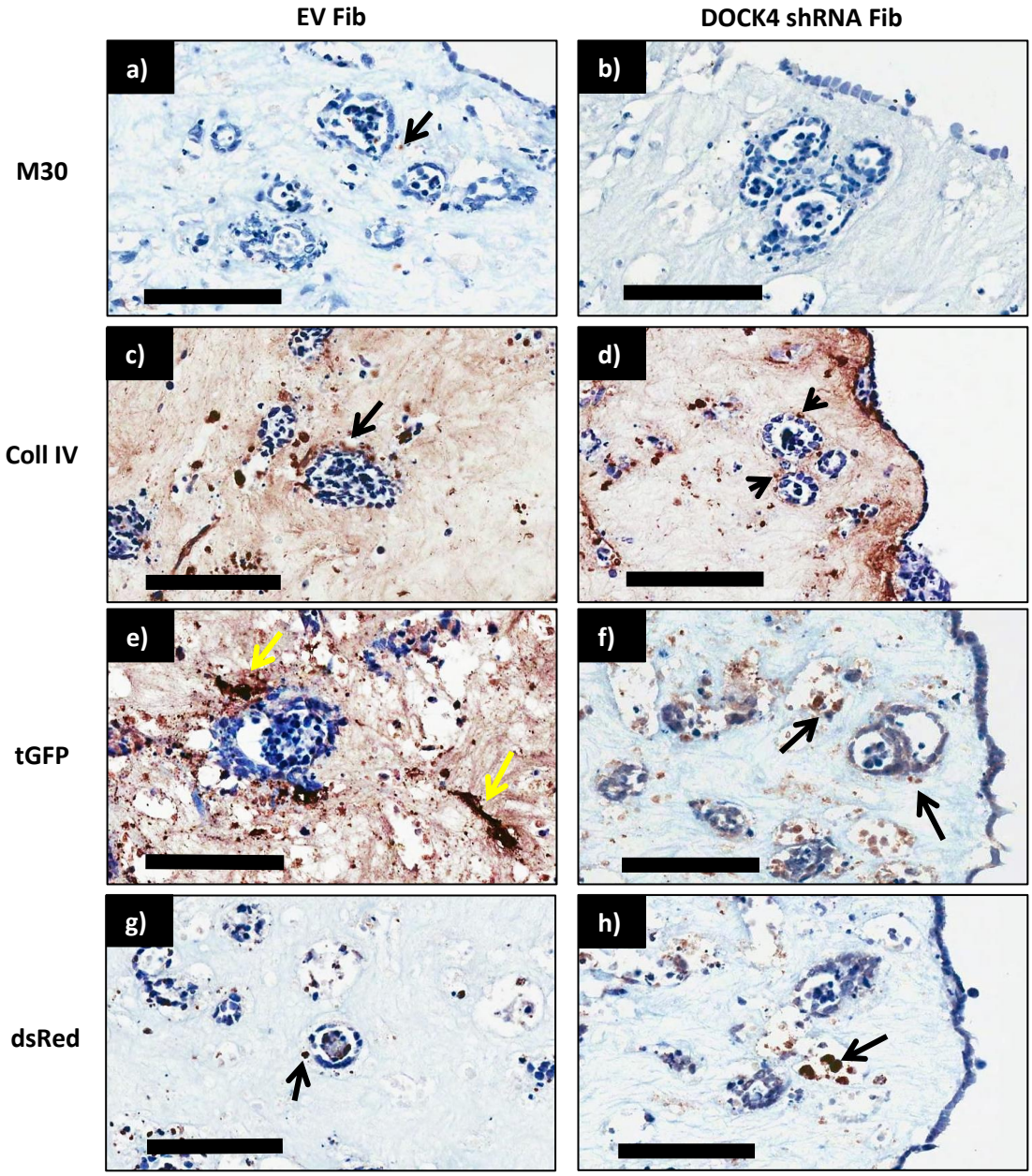

Fig 6.9 IHC characterisation of 3D *in vitro* tri-culture models containing fibroblasts with or without DOCK4 protein expression B

3D *in vitro* tri-culture model containing empty vector control fibroblasts (EV Fibs) and fibroblasts with knockdown of DOCK4 (DOCK4 shRNA Fibs) with HB2 cells and dsRed Myo1089 cells were characterised by IHC. Little difference was observed with the knockdown of DOCK4 protein in fibroblasts on the phenotype of HB2 units. M30 staining was largely negative in cultures containing EV Fibs with a small amount observed in cells on the outer periphery of HB2 units (arrow, a). No M30 was detected with DOCK4 shRNA Fibs (b). Collagen IV (Coll IV) was detected surrounding the outer edges of HB2 units with EV Fibs (arrow, c) while with DOCK4 shRNA Fibs, Coll IV was only detected in small points around the outside of HB2 units (arrows, d). Both EV Fib and DOCK4 shRNA Fib containing tri-cultures showed positive staining for tGFP in cells loosely distributed throughout the collagen gel (arrows, e & f), and dsRed in rounded cells around the outer edges of HB2 units (arrows g & h). Original magnification 20x, scale bars = 100µm. Representative images from three technical replicates presented.

6.4.5 Confirmation of ER expression in GFP Myo1089 cells

In order to assess ER status in GFP Myo1089 cells, immunofluorescence was carried out using antibodies against ERα and ERβ1 (Fig 6.10). This demonstrated that GFP Myo1089 cells are negative for ERα but positive for ERβ1. ERβ1 staining was detected in the cytoplasm of all cells and in speckles in the nuclei of ~25% of cells. This confirmed that GFP Myo1089 cells ERβ1 in 2D. Representative images from three technical replicates presented.

ERβ1 mRNA expression was also assessed in GFP Myo1089 cells using qPCR both in a 2D monolayer and a 3D mono-culture to confirm that expression of ERβ1 was retained in 3D culture. Results from three biological replicates presented. This demonstrated expression of ERβ1 in GFP Myo1089 cells when cultured in both 2D and 3D but showed a 10-fold increase in levels of expression when cultured in a 3D setting. This confirmed that GFP Myo1089 cells expressed ERβ1 in both 2D and 3D and were therefore suitable for subsequent ERβ1 knockdown experiments.

6.4.6 Knockdown of ERβ1 in myoepithelial cells

GFP Myo1089 cells were treated with ERβ1 siRNA in 2D culture in order to knockdown ERβ1 expression (Fig 6.11). Results from three biological replicates presented. Treatment with ERβ1 siRNA caused an 8-fold decrease in the expression of ERβ1 mRNA in comparison to treatment with scrambled control. This confirmed the effectiveness of siRNA treatment in knocking down ERβ1 in these cells.

6.4.7 Morphology and phenotype of 3D *in vitro* tri-culture models containing myoepithelial cells with or without ERβ1 expression

In order to determine the effect of knocking down ERβ1 in myoepithelial cells on epithelial architecture, HB2 WT and LS11-083 dsRed Fibs were co-cultured with GFP Myo1089 cells treated with scrambled control (Control) or GFP Myo1089 cells treated with ERβ1 siRNA (ERβ1 siRNA) and morphology assessed. Visualisation by H & E staining demonstrated that in the

presence of control or ERβ1 siRNA GFP Myo1089 cells, HB2 WT cells formed rounded units which consisted of cohesive cells with lumen formation in their centres (Fig 6.12). Representative images from three technical replicates presented. This suggested the knockdown of ERβ1 with siRNA in GFP Myo1089 cells had no effect on the morphology of HB2 cell architecture.

Similar to DOCK4 knockdown experiments, characterisation by IHC showed little difference in the phenotype of HB2 units cultured with control and ERβ1 siRNA GFP Myo1089 cells (Fig 6.13 & 6.14, representative images from three technical replicates presented). With both types of GFP Myo1089 cells, HB2 units displayed E-Cad staining between cell junctions, EMA at apical-lumen interface and strong Ki67 staining within HB2 cell nuclei. M30 staining was observed in cells around outer edges of HB2 units with both control and ERβ1 siRNA GFP Myo1089 cells and in the centres of units with ERβ1 siRNA GFP Myo1089 cells. Coll IV and tGFP staining was distributed around outer edges of HB2 units confirming basement membrane production and association of GFP Myo1089 cells with HB2 units. dsRed staining was observed in cells loosely distributed throughout the collagen gel.

This suggested that knockdown of ERβ1 in GFP Myo1089 cells does not affect the morphology and phenotype of normal mammary epithelial architecture in the 3D *in vitro* tri-culture model of normal breast.

i)

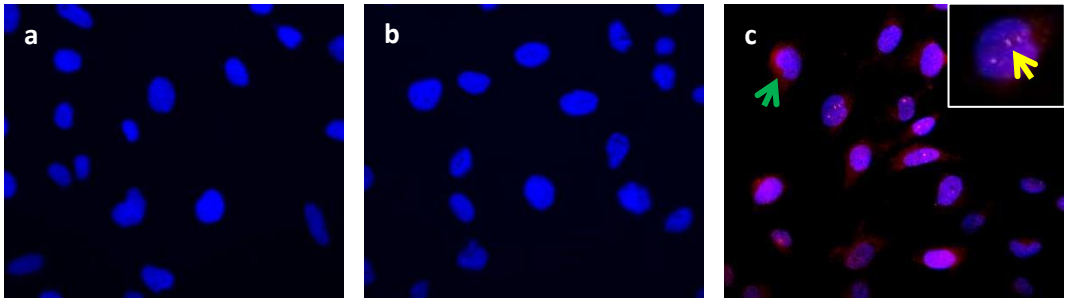

ii)

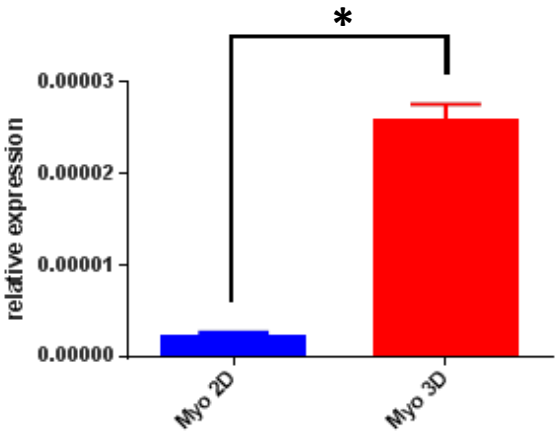

Fig 6.10 Confirmation of ERβ1 expression in GFP Myo1089 cells in 2D by immunofluorescence and comparison to expression in 3D by qPCR

i) The ER status of GFP Myo1089 cells was analysed by immunofluorescence staining and visualised using Texas Red (red) with nuclei visualised using DAPI (blue). Representative images from three biological replicates presented. Primary antibody was omitted to serve as a negative control (a). All cells were negative for ERα (b) but positive for ERβ1 with staining observed both in the cytoplasm of all cells (green arrow, c) and in speckles in the nuclei of ~25% of cells (inset, yellow arrow, c). Original magnification, 63x.

ii) Taqman qPCR was used to detect ERβ1 mRNA expression in GFP Myo1089 cells cultured as a 2D monolayer (Myo 2D) and in 3D as a mono-culture in collagen I (Myo 3D) to confirm expression of ERβ1. Data presented as relative expression and normalised to RPLP0 reference gene. Expression of ERβ1 in GFP Myo1089 cells was significantly higher upon culture in 3D in comparison to 2D with 3D cultures expressing 10x more ERβ1 than 2D cultures. Bars denote mean from three independent experiments and error bars standard error of the mean (SEM). * indicates significant difference following unpaired t-test ($p=<0.01$)

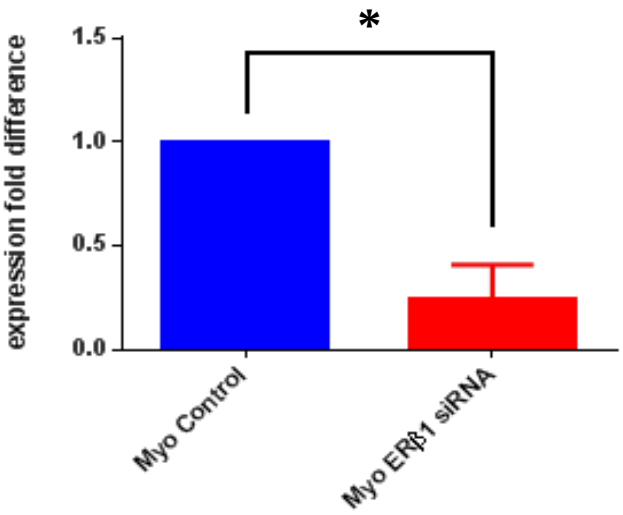

Fig 6.11 Analysis of downregulation of ERβ1 in GFP Myo1089 cells cultured in 2D by qPCR

Taqman qPCR was used to detect ERβ1 mRNA expression in GFP Myo1089 cells cultured in 2D treated with a scrambled control (Myo control) and with ERβ1 siRNA (Myo ERβ1 siRNA) to confirm downregulation of ERβ1. Data presented as expression fold difference to scrambled control and normalised to RPLP0 reference gene. Expression of ERβ1 was significantly lower in GFP Myo1089 cells treated with ERβ1 siRNA and confirmed an 80% downregulation of ERβ1. Bars denote mean from three independent experiments and error bars standard error of the mean (SEM). * indicates significant difference following unpaired t-test ($p=<0.01$)

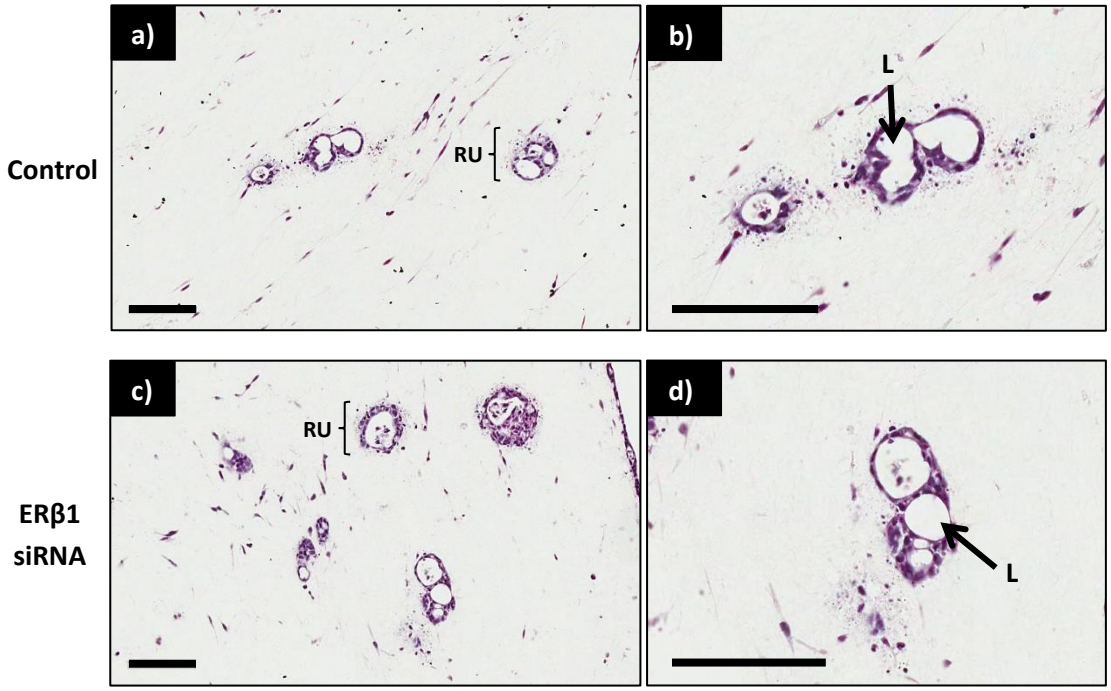

Fig 6.12 Representative H & E staining of 3D *in vitro* tri-culture models containing myoepithelial cells with or without ERβ1 protein expression

Control GFP Myo1089 cells (Control) and GFP Myo1089 cells containing ERβ1 siRNA (ERβ1 siRNA) were co-cultured in 3D collagen gels with dsRed positive fibroblasts (dsRed Fib) and HB2 wildtype cells for 21 days and 5µm sections of gels H & E stained. Representative images from three technical replicates presented. Little difference was observed with the knockdown of ERβ1 protein in GFP Myo1089 cells on the morphology of HB2 units. HB2 cells formed cohesive rounded units (RU) with appearance of lumens (L) both in the presence of control GFP Myo1089 cells (a & b) and ERβ1 siRNA GFP Myo1089 cells (c & d). Original magnification 20x, scale bars = 100µm.

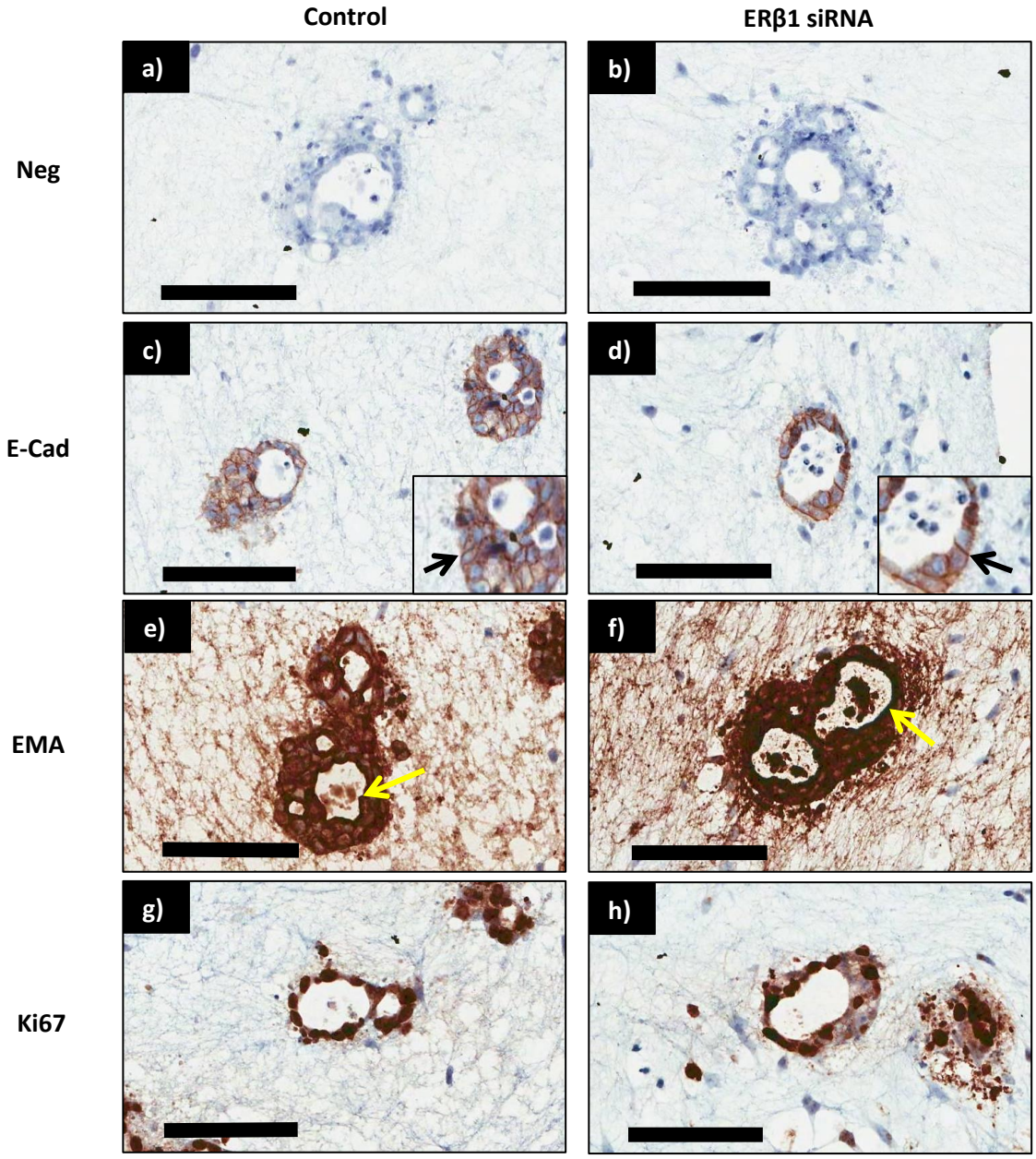

Fig 6.13 IHC characterisation of 3D *in vitro* tri-culture models containing myoepithelial cells with or without ERβ1 protein expression A

3D *in vitro* tri-culture model containing control GFP Myo1089 cells (Control) and GFP Myo1089 cells containing ERβ1 siRNA (ERβ1 siRNA) with HB2 cells and dsRed Fibs were characterised by IHC. Representative images from three technical replicates presented. Little difference was observed with the knockdown of ERβ1 protein in GFP Myo1089 cells on the phenotype of HB2 units. Primary antibody was omitted to serve as a negative control (a & b). E-cadherin (E-Cad) was expressed by HB2 cells at cell-cell junctions (arrow, c) in the presence of control (arrow, c) and ERβ1 siRNA GFP Myo1089 cells (arrow, d). Strong epithelial membrane antigen (EMA) staining was concentrated at the apical-lumen interface in HB2 cells with both types of GFP Myo1089 cells (yellow arrows, e & f). HB2 cells were positive for Ki67 regardless of type of GFP Myo1089 cells (g & h). Original magnification 20x, scale bars = 100µm.

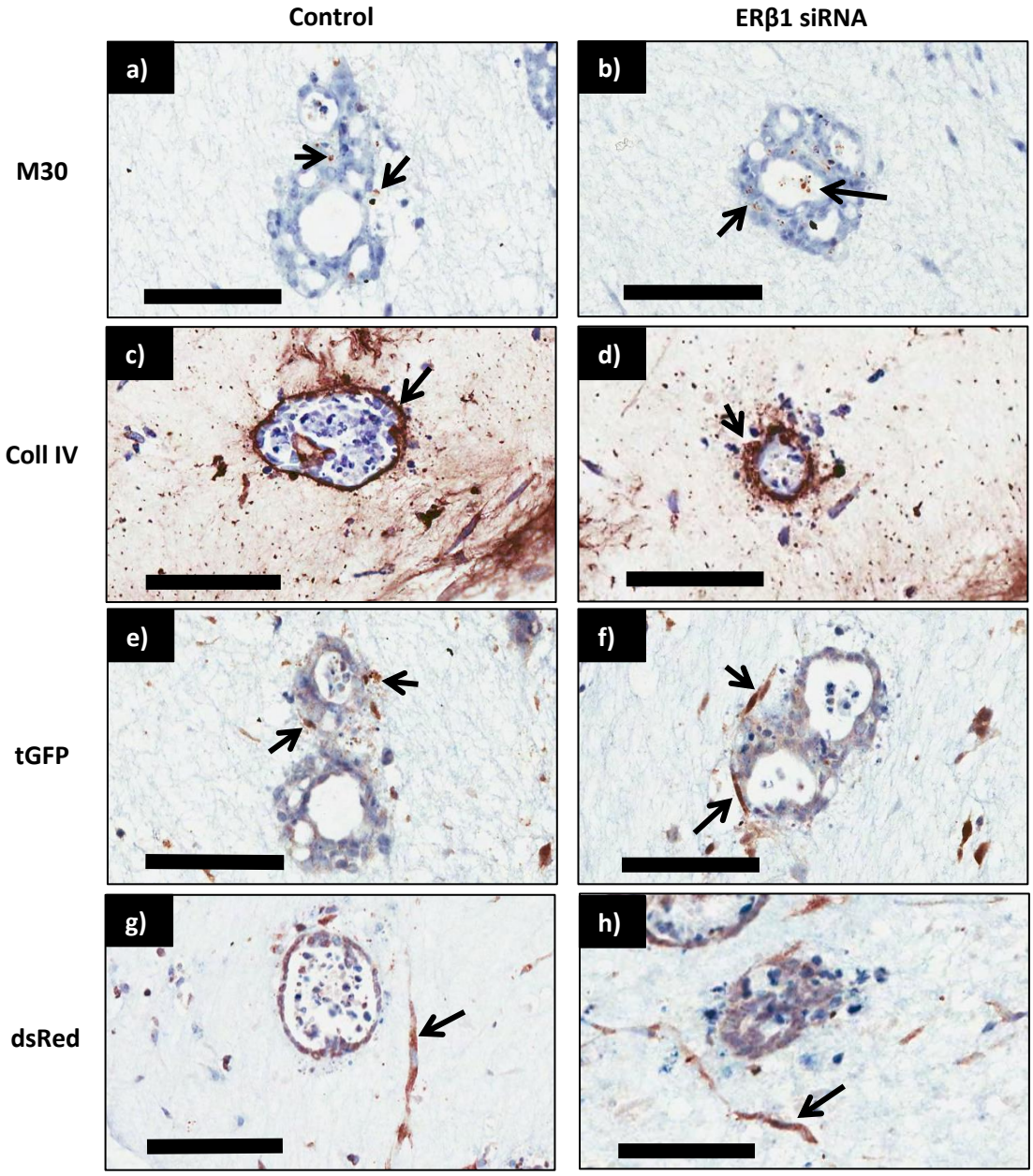

Fig 6.14 IHC characterisation of 3D *in vitro* tri-culture models containing myoepithelial cells with or without ERβ1 protein expression B

3D *in vitro* tri-culture model containing control GFP Myo1089 cells (Control) and GFP Myo1089 cells containing ERβ1 siRNA (ERβ1 siRNA) with HB2 cells and dsRed Fibs were characterised by IHC. Representative images from three technical replicates presented. Little difference was observed with the knockdown of ERβ1 protein in GFP Myo1089 cells on the phenotype of HB2 units. M30 staining was present on the outer periphery of HB2 units with control and ERβ1 siRNA GFP Myo1089 cells (arrows, a & b) as well as in the centre of units containing ERβ1 siRNA GFP Myo1089 cells (arrow, b). Collagen IV (Coll IV) was detected surrounding outer edges of HB2 units with control and ERβ1 siRNA GFP Myo1089 cells (arrows, c & d). Both control and ERβ1 siRNA GFP Myo1089 containing tri-cultures showed positive staining for tGFP in rounded cells around the outer edges of HB2 units (arrows, e & f), and dsRed in cells loosely distributed throughout the collagen gel (arrows g & h). Original magnification 20x, scale bars = 100µm.

6.4.8 Morphology of HER overexpressing HB2 cells in 3D tri-culture with fibroblasts pre-conditioned to SkBr3 cells

In order to investigate whether HER2 positive tumour cells had the capacity to influence normal fibroblast behaviour and produce a HER2 CAF-like fibroblast population and subsequently disrupt epithelial architecture, attempts were made to pre-condition LS11-083 dsRed Fibs to SkBr3 cells with the aim of inducing a HER2 CAF-like phenotype. LS11-083 dsRed Fibs were cultured in a range of dilutions of SkBr3 conditioned medium (from 0% to 100%) prior to tri-culture with HB2 WT or HB2 HER2/3OE cells (Fig 6.15). This did not affect the cell morphology of either HB2 WT units or HB2 HER2/3OE units in 3D tri-cultures. As per previous chapters, HB2 WT units retained a rounded morphology containing lumens and HB2 HER2/3OE units a larger, elongated morphology regardless of condition of LS11-083 dsRed Fibs used. This suggested that LS11-083 dsRed Fibs previously exposed to SkBr3 cells did not have the capacity to disrupt normal cell architecture or enhance to tumorigenicity of HER2/3 overexpressing HB2 cells in the 3D tri-culture model.

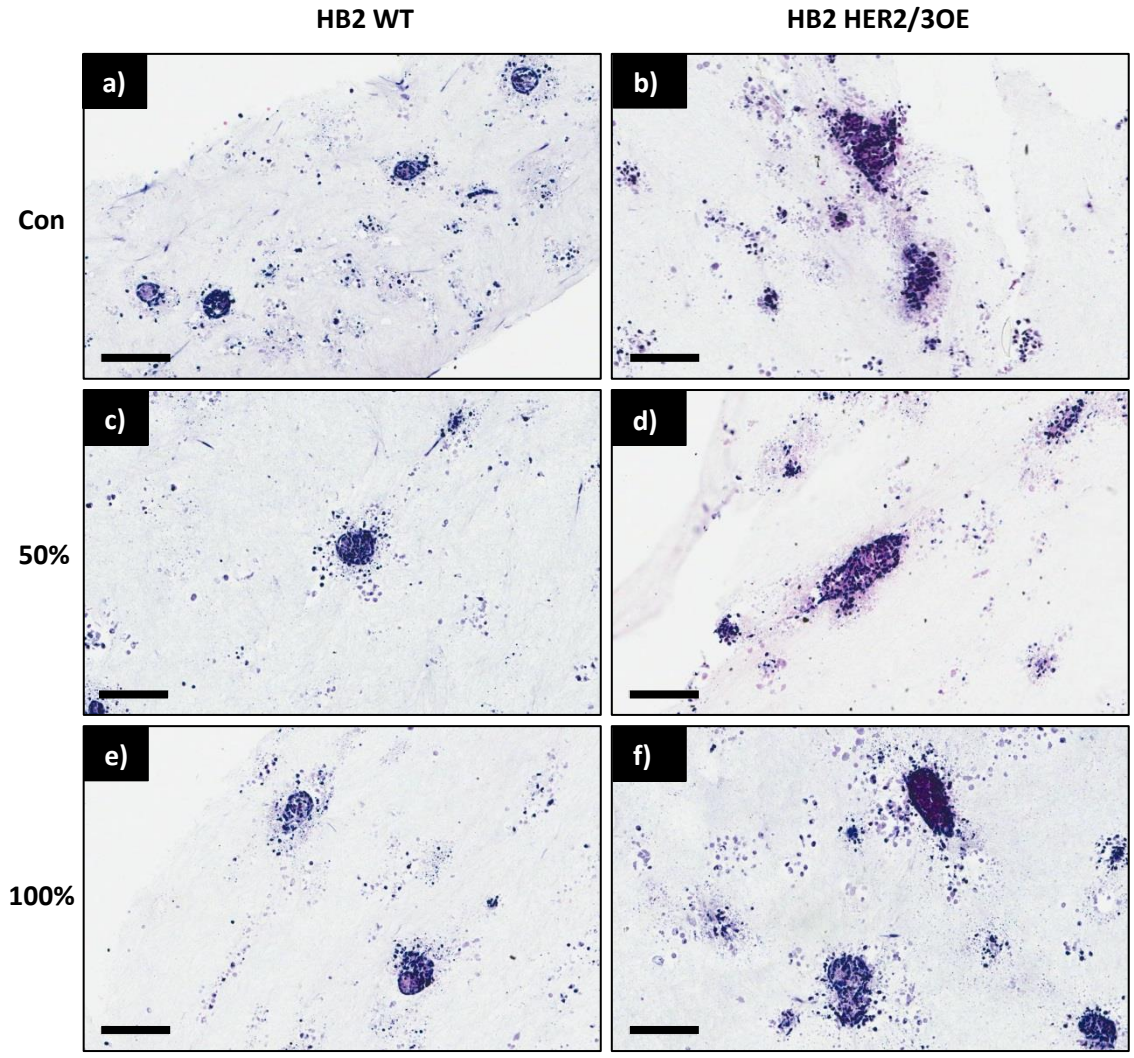

Fig 6.15 Representative H & E staining of 3D *in vitro* tri-culture models containing HER protein overexpressing HB2 cells with fibroblasts with exposed to SkBr3 cell conditioned medium

HB2 wildtype (HB2 WT) and HER2 and HER3 overexpressing HB2 cells (HB2 HER2/3OE) were co-cultured in 3D collagen gels with GFP positive Myo1089 cells (GFP Myo1089) and LS11-083 dsRed positive fibroblasts (LS11-083 dsRed Fibs) which had been exposed to normal media conditions (Con), 50% SkBr3 conditioned medium (50%) or 100% SkBr3 conditioned medium (100%). These were cultured for 21 days and 5µm sections of gels and H & E stained. Little difference was observed with the prior exposure of LS11-083 dsRed Fibs to 50% and 100% SkBr3 conditioned medium on the morphology of HB2 units. HB2 WT cells formed cohesive rounded units in all fibroblast conditions (a, c & e). HB2 HER2/3OE cells formed larger more elongated units to HB2 WT units but these remained unchanged in the presence of fibroblasts exposed to SkBr3 medium (b, d & f). Original magnification 20x, scale bars = 100µm.

6.5 Discussion

Having produced a novel 3D *in vitro* tri-culture model of normal breast that includes both a myoepithelial and fibroblast component, it seemed fitting that this model would be suited to investigating the influence of stromal cells on luminal epithelial architecture. Thus far we had proven the capacity of this model for cancer initiation studies in the luminal epithelium but stromal influence had not been addressed.

6.5.1 The effect of DOCK4 deficient fibroblasts on 3D tri-cultures of normal breast

We first focussed on the fibroblast component of our tri-culture model. Little is known about the function of DOCK4 in the breast. However, DOCK proteins are well known to influence cell migration [395] and since fibroblasts are highly migratory in nature [436-439] we hypothesised that DOCK4 deficient fibroblasts would differ in their ability to interact with the breast epithelium and may induce changes in breast epithelial architecture in our model.

RNA interference (RNAi) is a widely accepted tool to downregulate proteins of interest within a cell. By delivering double stranded RNA sequences identical to the RNA sequence of a target protein, target mRNA is degraded by RISC complexes preventing translation of target mRNA and downregulating the protein [440]. Two RNAi approaches can be taken: siRNAs into the cytoplasm or, for stable downregulation, transduction of the cell with a virus containing a target shRNA which is synthesised by the cell and processed in the cytoplasm providing a continuous source of siRNAs against a target [441].

First we confirmed the expression of DOCK4 in the majority of fibroblasts in the original tissue specimen. Following confirmation that our control empty vector lentivirus had no effect on the levels of DOCK4 expression in our fibroblasts in culture, we applied the concept of shRNA-mediated knockdown of DOCK4 in our LS11-045 hTERT fibroblasts via stable transduction with lentiviral vectors containing two different shRNA sequences. We successfully identified an effective shRNA construct against DOCK4 and produced a LS11-045 hTERT fibroblast cell

population with a significantly reduced level of DOCK4 protein expression as assessed by western blot. In addition, the pGIPZ lentiviral vectors (as described in Chapter 3) contained a tGFP fluorescent reporter allowing us to track these DOCK4 shRNA fibroblasts in culture. In order to distinguish these from Myo1089 cells and HB2 cells in the 3D tri-culture model, Myo1089 cells were transduced with pFURW-dsRed virus.

Incorporation of DOCK4 shRNA fibroblasts into our 3D tri-culture model did not affect the normal architecture of HB2 cells and dsRed Myo1089 cells. Morphology of HB2 units demonstrated retention of a rounded shape with clear lumen formation regardless of DOCK4 knockdown in fibroblasts. This was reflected in their characterisation whereby both these tri-cultures exhibited the same phenotype analogous to the normal HB2 tri-culture phenotype observed in previous chapters when examined by IHC.

DOCK4 functions by activating the Rho GTPase Rac1 and inducing migration through the formation of actin stress fibres and lamellipodia. Knockdown of DOCK4 in NIH3T3 fibroblasts caused a reduction in migration [403]. The lack of altered phenotype of HB2 units in our culture system with DOCK4 shRNA fibroblasts may suggest that cell migration of fibroblasts is not required to mediate their effects on the epithelium. It is feasible that the production of growth factors and paracrine signalling by fibroblasts is not affected by their ability to migrate. It has been reported that fibroblast conditioned media can substitute for the use of fibroblasts in culture [219] supporting the theory that fibroblasts regulate epithelial cell behaviour via paracrine signalling as opposed to cell-cell contact. In addition, little cell contact was observed between fibroblasts and epithelial units within all our tri-cultures which could support this theory.

Another possible explanation for the lack of effect of DOCK4 knockdown in fibroblasts on epithelial cell behaviour is that cell migration was not affected. Despite work by Hiramoto et al [403] showing a reduction of cell migration in NIH3T3 fibroblasts, it is possible that migration

of our fibroblasts was not affected by knockdown of DOCK4. Recent work by Petrie et al [442] has demonstrated that human foetal fibroblasts do not require downstream Rac and Cdc42 to migrate. In this study, fibroblasts migrated via novel lobopodia structures which did not accumulate active Rac and Cdc42. Interestingly, these lobopodia structures were the predominant protrusion structure in fibroblasts cultured in 3D collagen matrix whereas the more commonly reported lamellipodia were predominant in 2D culture. This could offer an explanation for the lack of response to DOCK4 knockdown in our fibroblasts but would need further experimentation to validate this theory. The work by Petrie et al was carried out in human foetal fibroblasts and which had been exposed to a mouse dermal microenvironment so may not be applicable to breast. Nevertheless, a difference in behaviour of fibroblasts in 3D opposed to 2D culture could account for the lack of phenotype observed in our experiments. Though not here, the migratory capacity of these fibroblasts in 2D and 3D culture via real-time imaging and the examination of the growth factors they produce via proteomic techniques could provide answers to these questions.

6.5.2 The effect of ERβ1 deficient myoepithelial cells on 3D tri-cultures of normal breast

We then focussed on the myoepithelial component of our model. As discussed previously, both myoepithelial cells and ERβ have a suspected tumour suppressor role in breast cancer due to their loss in the transition from DCIS to invasive cancer. We therefore postulated that the tumour suppressive nature of myoepithelial cells is reliant on ERβ expression.

To address this, ERβ1 was chosen as a representative of ERβ activity in these cells. ERβ1 is the only ERβ isoform capable of binding ligand [414]. Since we demonstrated that GFP Myo1089 cells are ERα negative, we reasoned that ERβ could not heterodimerise with ERα. Therefore, ERβ signalling would be reliant on heterodimerization with ERβ1 [415]. Consequently, by removing ERβ1 expression, the overall effects of ERβ would be downregulated. Due to the fact

that this cell line was immortalised with vectors containing resistance genes for hygromycin and neomycin [181] and also contain an empty vector containing puromycin resistance gene [personal communication, Dr Mike Allen, Barts Cancer Institute] as well as our tGFP fluorescence reporter gene, we reasoned that stable knockdown of ERβ1 with a virus vector would not have been easily achieved due to inability to select positive clones. We therefore applied the concept of siRNA mediated knockdown of ERβ1 in GFP Myo1089 cells. After confirming the expression of ERβ1 in GFP Myo1089 cells in both 2D and 3D, using a pool of two different siRNA sequence oligonucleotides against ERβ1, we successfully downregulated ERβ1 expression by ~80% as assessed by qPCR.

Similar to results using DOCK4 shRNA fibroblasts, incorporation of ERβ1 siRNA GFP Myo1089 cells into our 3D tri-culture model did not affect the normal architecture of HB2 cells cultured with dsRed fibroblasts. Rounded HB2 units with lumen formation were retained regardless of ERβ1 siRNA. Characterisation of both tri-cultures demonstrated no change in phenotype of HB2 units when examined by IHC. In addition, downregulation of ERβ1 did not appear to change the apoptotic or proliferative nature of GFP Myo1089 cells or their localisation around the outside of HB2 units.

Though it could be construed from these results that ERβ1 is not required for normal GFP Myo1089 activity in our tri-culture model, there were caveats with this experiment. Perhaps the major limitation was the use of siRNAs for this experiment. Knockdown of a target using siRNAs is a transient process with a maximum duration of silencing of 10 days [443]. Given that the 3D tri-culture models were analysed after 21 days in culture, it is possible that ERβ1 signalling gradually resumed following 10 days in culture and resulted in no alterations of epithelial architecture observed at time of analysis. The appearance of rounded HB2 structures following seven days in culture [see chapter 3] suggests that epithelial structures are formed in the early stages of 3D culture and then retained. This indicates that these structures are not

the result of a dynamic rearrangement of cells throughout the length of time in culture. For this reason, it is likely that the knockdown of ERβ1 in GFP Myo1089 cells coincided with the arrangement of epithelial structures in the early stages of culture. This suggests that ERβ1 did not impair the ability of GFP Myo1089 cells in regulating luminal epithelial cell arrangement. However, examination of these structures via real-time imaging would be required to confirm this theory.

Another caveat with this experiment is that we could not confirm a knockdown of ERβ1 protein expression. Though we showed an 80% knockdown of ERβ1 mRNA expression in GFP Myo1089 cells by qPCR, the method of qPCR does not directly correlate with protein expression and only accounts for gene expression [444]. Knockdown of ERβ1 protein expression could not be confirmed due to lack of antibodies suitable for western blotting. In addition, since we demonstrated a 10-fold increase in ERβ1 expression in 3D culture compared to 2D it is possible that the siRNAs which proved adequate for the knockdown of ERβ1 in 2D were not sufficient to knockdown ERβ1 in 3D culture. For both these reasons it is therefore conceivable that there was insufficient knockdown of ERβ1 protein expression in GFP Myo1089 cells when cultured in 3D.

6.5.3 The effect of pre-conditioning normal fibroblasts to SkBr3 cells on 3D tri-cultures of normal breast

The cross-talk between stromal fibroblasts and tumour epithelial cells is a well-documented and widely accepted concept [445, 446]. However, the origin of CAFs is poorly understood. It is currently unknown whether a) established tumour cells signal to normal stromal cells and induce activation of the stroma, or b) stromal cells first undergo changes in phenotype which subsequently trigger pro-tumorigenic responses in the epithelium.

As a follow up to previous chapters, we attempted to investigate whether HER2 positive tumour cells had the capacity to influence normal fibroblast behaviour and produce a HER2

CAF-like fibroblast population. Since CAFs are proven to induce EMT in normal and tumorigenic breast epithelium [303], we predicted that if we were successful in inducing a HER2 CAF-like phenotype in our normal fibroblasts, that these would alter epithelial cell architecture in our normal 3D tri-culture model.

SkBr3 cells are a breast cancer cell line proven to overexpress HER2 protein and are therefore commonly used as a representative of the HER2 sub-group of breast cancers [135]. As mentioned, conditioned media is used as a substitute for direct cell culture *in vitro* [447]. In an attempt to produce a HER2 CAF-like population, we cultured LS11-083 dsRed Fibs in SkBr3 conditioned medium prior to incorporation into our 3D tri-culture models. Different dilutions of SkBr3 conditioned medium were used ranging from 0% (normal medium) to 100%. The morphology of both HB2 WT and HB2 HER2/3OE tri-culture models were unchanged upon culture with LS11-083 dsRed Fibs pre-exposed to all concentrations of SkBr3 conditioned medium.

It is tempting to conclude that SkBr3 cells were incapable of altering the phenotype of normal fibroblasts and that these were therefore unable to disrupt luminal epithelial architecture. However, like the ERβ1 siRNA experiments, there were several limitations with this experiment.

Since signal transduction via growth factors is known to be a rapid process, in this study fibroblasts were pre-cultured in SkBr3 medium for 24 hours prior to incorporation into 3D culture. It is possible that 24 hours in conditioned medium was not sufficient to induce any lasting changes in our normal fibroblasts. This also assumed that all proteins released by SkBr3 cells likely to induce changes in our fibroblasts were growth factors. Several non-growth factor proteins have been identified through cancer cell secretome studies which may affect fibroblast behaviour [448, 449]. These require prolonged culture to elicit their effects. In addition, although morphology of the fibroblasts was assessed and found to be unaltered,

phenotype was not characterised following pre-culture in SkBr3 conditioned medium and prior to 3D culture. For this reason we cannot establish whether a different phenotype was induced by culture in SkBr3 conditioned medium.

Since the conditioned medium produced from SkBr3 cells was not analysed proteomically, we also cannot be certain that there were sufficient proteins and factors present in the medium to induce a change or, if they were present, whether they correlated with known factors secreted by HER2 tumour cells [275, 450, 451].

This experiment also assumed that the tumour cells are solely responsible for inducing an activated phenotype of fibroblasts. Since inflammatory cells are a critical component of tumour progression not accounted for in our study [452], it is likely that this is not the case and that a more complex environment is required for normal fibroblast activation. It is clear that conclusions cannot be made from this investigation. One way to overcome this would be to use fibroblasts originally isolated from HER2 overexpressing patient tumours.

6.5.4 Summary

Despite the lack of success in producing a different phenotype of HB2 cells in the 3D tri-cultures with these experiments, we have established that the model shows great promise in the study of stromal components of the normal breast. We have shown that in addition to luminal epithelial cells, the stromal cells in this model are amenable to genetic engineering and given the right application, could help elucidate the role of stromal cells in cancer initiation.

7 Chapter 7: Final Discussion

7.1 Thesis Summary

Current available 3D *in vitro* models of normal breast tissue lack key components that contribute to normal breast architecture and function such as collagen I ECM and myoepithelial cells. These typically contain either one or at most two different cell types and although show some similarity to normal breast acini, do not accurately reflect normal *in vivo* breast architecture.

The aim of this thesis was to address this by developing a new organotypic 3D *in vitro* model of normal breast tissue that contained three of the major functional cell types of the mammary gland, luminal epithelium, myoepithelium and stromal fibroblasts, in a physiologically relevant collagen I matrix. In Chapter 3, we first attempted to achieve this with the commonly used MCF10A cell line as a representative of luminal epithelium. Despite the success of other researchers in producing acini-like structures with these cells in both Matrigel and collagen matrices [154, 190, 201], we found that in culture with our myoepithelial cell representative (Myo1089) in collagen I that MCF10A cells had a mixed luminal/basal phenotype. This has been reported in 2D culture [180, 220, 221] and we therefore deemed these cells unsuitable for this purpose. However, following a series of optimisation steps, we were successful in producing a 3D *in vitro* model using HB2 cells as the representative luminal epithelium. This model contained HB2 cells with Myo1089 cells and normal breast reduction mammoplasty fibroblasts (isolated and transduced with hTERT in house) and was therefore the first model of its kind to include all three of these components in collagen I. We found that this model accurately reflected acini *in vivo* in both morphology and phenotype when we compared to a breast reduction mammoplasty specimen. Through experiments in subsequent chapters, we demonstrated that these morphological and phenotypical features were reproducible proving that the model is not only representative of normal breast, but is robust. This robustness

coupled with the proven ability to track different cell types by standard histological techniques and quantify any observations and changes in architecture means this model may prove a valuable tool to other researchers.

In order to prove whether our model was suitable for use as a tool to study cancer initiation, in Chapter 4 we selected the protein HER2 as a candidate to test this theory. HER2 is overexpressed in the luminal epithelium of approximately 16% of breast cancers [260] and approximately 50% of cases of DCIS [262]. The stable overexpression of HER2 within HB2 cells of our model resulted in dramatic disruption of the normal architecture with increased branching and protrusions, discohesive HB2 cells and loss of lumen formation. These also showed remarkable resemblance to DCIS *in vivo* validating that our model was indeed suitable for cancer initiation studies and capable of mimicking early lesions of breast in a physiologically relevant context.

In order to reinforce the importance of including myoepithelial cells and fibroblasts in the study of cancer initiation and that the effects of oncogenic events are context dependent, we also set up 3D models of HER overexpressing HB2 cells in mono-culture, in dual-culture with myoepithelial cells or dual culture with fibroblasts. We found that our HER overexpressing mono-culture model correlated with MCF10A and HB2 mono-culture models reported in the literature [274-276], with the HER2-HER3 heterodimer having the most disruptive effect [453]. However, culture of these same cells with myoepithelial cells resulted in the formation of very different structures with myoepithelial cells having a “containment” or tumour suppressive effect. In contrast, dual-culture with fibroblasts had the opposite effect with structures appearing much larger and disordered. These experiments emphasised luminal epithelial organisation is maintained by a delicate balance between the opposing functions of fibroblasts and myoepithelial cells and that the presence of both is vital when interpreting the effects of a genetic insult or oncogenic event on luminal cell transformation.

One unexpected finding from these experiments was that overexpression of both HER2 and HER3 in our tri-culture model did not have the most disruptive effect on normal architecture. As mentioned, reports in the literature suggest that the HER2-HER3 heterodimer is the most potent heterodimer of the HER family [453]. To determine if our observations were due to a deficiency in endogenous heregulin ligand in our cultures or if our HB2 cells did not respond to HER2-HER3 overexpression as expected, in Chapter 5 we conducted stimulation experiments with heregulin and assessed the effects on our tri-culture model and the intracellular signalling pathways activated within these cells. We found that heregulin caused increased disruption of the architecture of our model. In addition, we demonstrated that HER2-HER3 overexpressing HB2 cells had increased activation of Akt and MAPK pathways as well as a subset of phospho-kinases related to cell adhesion/migration which was increased in response to heregulin correlating with published data [339, 362]. Therefore, HER2-HER3 overexpression in our HB2 cells was effective and caused activation of reported downstream signalling pathways. We concluded that the lack of the expected morphology of these cells in our 3D model is likely due to the culture context explaining why these results did not correlate mono-culture models published in the literature. Perhaps in a more physiologically relevant context, HER2-HER3 overexpression alone is not sufficient to completely transform/induce aberrant architecture of luminal epithelium and requires an excess of ligand. This further stressed the importance of an appropriate microenvironment

However, one of the biggest strengths of a tri-culture model such as this is the ability to study the role of stromal cells on cancer initiation. In Chapter 6, we attempted to prove this by selecting DOCK4 and ERβ1 to study in the fibroblasts and myoepithelial cells (respectively) and examining their effect on luminal epithelial architecture/phenotype. The function of DOCK4 is currently unknown in fibroblasts of both the normal breast and breast cancer but has been linked to invasion and migration in breast cancer [402]. Unpublished preliminary work by our collaborators has shown that DOCK4 expression is heterogeneous and may be linked to

increased acquisition of ECM. ERβ1 is reported to be a tumour suppressor [424, 425, 427, 428, 454]. Like myoepithelial cells [431] it is lost in the transition from DCIS to invasive breast cancer [430] but whether these two events are connected and influence tumorigenesis are unclear. Neither the downregulation of DOCK4 in fibroblasts or ERβ1 in myoepithelial cells of our model had any effect on the morphology and phenotype of the luminal epithelium indicating that these proteins do not play a role in breast cancer initiation at least under the conditions of these experiments. In addition, we wanted to assess whether paracrine factors released from established HER2 overexpressing tumour cells had the power to alter normal fibroblast phenotype. To see if these fibroblasts could then go on to influence the normal epithelium and initiate transformation, fibroblasts were "conditioned" to SkBr3 media prior to culture in the normal 3D model. We also found this had no effect on the morphology and phenotype of the luminal epithelium indicating that paracrine factors from SkBr3 cells did not modify fibroblasts and if they did, were not potent enough to change their behaviour in our normal 3D model.

Nevertheless, the work from this thesis addresses topical areas in the breast cancer field. A recent review was undertaken by more than 100 internationally recognised breast cancer scientists, clinicians and healthcare professionals to identify current gaps in knowledge in breast cancer research. Two of the key areas recognised were; the need to better understand the changes that occur in the normal breast that result in tumorigenesis and, the need to develop better 3D culture models that incorporate stromal components, are heterotypic and that accurately reflect physiological *in vivo* conditions [167]. This thesis has addressed both these concepts.

7.2 Comparison of the model to other pre-clinical models of breast

Due to the complexity and heterogeneity of breast tissue and breast cancer there is no single model that can fully recapitulate all aspects of the breast microenvironment. The model

presented in this thesis offers an improvement to 2D *in vitro* culture providing a more biologically relevant *in vivo*-like 3D environment. 2D *in vitro* cultures lack appropriate polarity and extracellular cues that regulate *in vivo* architecture [136]. This novel 3D model also allows the interaction between three different cell types to be studied which cannot be achieved in 2D culture. However, 3D culture in this manner does not allow for easy dissection of complex intracellular signalling pathways and molecular biological processes which can be easily achieved with 2D cultures.

It is clear that the inclusion of myoepithelial cells and the use of collagen I in this model offer an improvement to current 3D *in vitro* models of normal breast as it is more reminiscent of *in vivo* breast. In addition, this model, like others, demonstrated lumen and basement membrane formation and polarisation. It was also proven that the structures formed could be quantified and phenotype analysed easily by IHC. However, unlike other models, due to the use of collagen I, the multicellular structures cannot be analysed easily by immunofluorescence techniques, nor can they be subjected to biochemical analysis using subsequent RNA, DNA, protein extraction easily as mono-culture spheroids/3D *in vitro* models can [455].

Until the advent of 3D *in vitro* culture, animal models, typically mouse xenograft or genetically engineered mice (GEM), were the only method available to study cell interactions and behaviour in an *in vivo* environment. These have been vital in the discovery and development of new drug therapies [456-459]. However, it has been reported that mouse and human physiology differ [460] with the tumours produced in GEM models often not representative of human breast tumours [255]. In addition, mouse models are expensive, labour intensive and time consuming to produce. The 3D model presented here offers an alternative with the ability to study cell interactions and behaviour in a human *in vivo*-like environment. The model has the potential to study tumour progression akin to xenograft models by incorporating tumour epithelial cells as well as cancer initiation via oncogene manipulation similar to GEM models.

What's more, this model is inexpensive, easy to set up and to genetically manipulate and requires no specialist equipment or expertise while maintaining a degree of multicellularity and *in vivo* architecture. However, unlike mouse models, our model does not incorporate a blood supply [461], adipose tissue [462, 463], or an immune system [464, 465] which are all factors known to influence tumour progression and metastasis.

The model presented in this thesis offers an improvement on current 2D and 3D *in vitro* models of normal breast in that it is more representative of human breast tissue and can recapitulate the morphological and phenotypical features achieved with other available *in vitro* models. Also, this model may offer an alternative to the use of expensive and time-consuming mouse models in the study of breast cancer initiation and progression in an *in vivo*-like environment. However, this model cannot be used to address all scientific questions such as the influence of vascularisation, adipose tissue and an immune system on tumour initiation and progression nor can it be used to dissect intricate intracellular events in these processes. Therefore, it is clear that while this model can be used to address a number of scientific questions, a variety of different pre-clinical models still need to be adopted to fully understand breast tumours and their heterogeneity.

7.3 Limitations and solutions

7.3.1 The 3D model

Although our model is an improvement on the current normal *in vitro* models of breast available, it still does not fully recapitulate *in vivo* stromal architecture. Recent studies have proposed that adipocytes (referred to as cancer associated adipocytes) have the capacity to induce breast tumour development and progression through reverting back to a fibroblast-like phenotype and releasing proteases, MMPs and cytokines [239, 466]. In addition, immune cells [237] and vascular endothelial cells [234, 467] have long been acknowledged to induce breast tumour development and progression. Although adipocytes [212] and endothelial cells [468, 469] have been included in normal MCF10A 3D cultures by other researchers, these have generally omitted myoepithelial cells which we have proven play an integral role in maintaining epithelial architecture. Inclusion of one or both of these cell types in our model would further capture the complexity of *in vivo* breast and provide a more accurate platform for cancer initiation studies. However, optimising culture conditions to retain *in vivo*-like characteristics of each cell type in such a model would be challenging. Tracking each of these cell types in culture would be difficult due to limited colours of fluorescent proteins available and difficulties in imaging discussed in Chapter 1.

The expression of fluorescent proteins by the cells in our model gives the opportunity to observe how cells migrate within these gels and how they interact with each other and may be useful for comparative analysis in addition to quantification of structures. This was not addressed in our study but would require sophisticated equipment to allow live cell real time imaging for up to three weeks. Issues with background fluorescence of collagen would also need to be overcome [170]. Use of a well-equipped multiphoton microscope could aid in this process [171].

Although we have produced a 3D model of normal breast tissue in this study, the methods of analysis have not allowed visualisation of the model in 3D. For example, it would be useful to determine if the structures in the model are a branching network of duct-like structures which could be an indicator of how well these structures represent normal ductal/acini epithelium. This could be achieved through digital reconstruction of H & E stained serial sections of our gels, an area which our department has expertise and which is currently being investigated [470]. Previous work in our group has demonstrated the value of 3D reconstructions of DCIS *in vivo* breast tissue [paper in preparation by Booth et al], and is a method which could be applied to the model.

7.3.2 Analysis of cancer initiation

Another area of this work that could be improved is the analysis of epithelial structures following genetic manipulation. Following overexpression of HER proteins in the model, although morphological changes indicative of increased cell migration/invasion were observed, with the exception of E-cadherin, specific markers for these processes were not examined by IHC. Although loss of E-cadherin has been associated with EMT and invasion in breast cancer [471, 472], this was not observed in this study, however, it has recently been proposed that this may not be vital for EMT [473]. This same study highlighted caveolin-1 as an excellent marker for EMT. In addition, markers such as N-cadherin and fibronectin-1 have proven successful in identifying cells undergoing EMT for other researchers using 3D-cultures [276] and may prove better markers for analysing the models.

In addition, throughout this study, EMA was used as a marker of "polarity" due to its localisation at the apical membrane of luminal epithelial cells in normal breast tissue. However, EMA is not a specific marker of polarity and proved difficult to interpret due to its strong staining in HER overexpressing cultures. Desmosomal and tight junction proteins may prove more suitable markers of epithelial cell polarity [16, 474].

One limitation of the model is that biochemical analysis is challenging making quantification of gene/protein expression difficult. Separating cells from the surrounding ECM is problematic [168]. Enzymatic digestion using collagenase is an option but could be damaging to cells and induce changes in phenotype [432]. Although IHC quantification could offer an alternative, this introduces variability in staining intensity both intra- and inter-laboratory as well as between specimens [475]. This could be overcome to some extent by using laser capture microdissection. This would allow changes in gene expression to be detected and quantified [476]. However, this could not be applied to protein expression due to protein degradation through fixing and H & E staining of gel sections.

Although heregulin signalling experiments in Chapter 5 suggested that HER2-HER3 overexpression activates signalling pathways involved in cell migration, these experiments were crude as they were performed in 2D rather than 3D with an insufficient number of biological replicates. As discussed in Chapter 1, the phenotype of cells cultured in 2D may differ from those in 3D. We were also unable to validate the activation of these kinases with subsequent biological replicates and western blotting to determine if migration was affected. Activation of these kinases would need to be examined by IHC in our 3D tri-culture model to determine if they are conserved in a physiologically relevant context. Live real-time cell imaging could prove beneficial in clarifying this.

7.4 Role of stromal cells on cancer initiation

Despite the obvious advantages of having both myoepithelial cells and fibroblasts in our model, we could not definitively conclude that the model can be used to study the role of stroma in cancer initiation. As mentioned above, Caveolin-1 is a robust marker for EMT and has also been shown in our laboratory as well as by other research groups to be lost in the transition from normal to invasive breast cancer [477-479]. However, the effect of

downregulation on normal epithelial architecture and breast cancer initiation is unknown and may prove a better candidate than DOCK4 to focus on in the fibroblasts of our model.

However, interesting findings were observed in Chapter 4 whereby HER overexpressing HB2 cells were dual-cultured with normal fibroblasts. We demonstrated a loss of fibroblasts upon co-culture with HER2 or HER3 overexpressing HB2 cells coupled with a dramatic increase in size and change in morphology of HB2 cell units. This may correlate with findings by Professor Michael Lisanti's group who found that tumour epithelial cells have the capacity to induce aerobic glycolysis and ultimately cell death of fibroblasts, referred to as the "Reverse Warburg" effect [294]. The use of markers such as MCT4 [309] at various time points over three weeks may prove valuable in elucidating if this occurs in our model.

As discussed in Chapter 6, the use of siRNA to downregulate ERβ1 in myoepithelial cells was not an appropriate technique for our model as siRNAs are only effective for a maximum of 10 days and our model is cultured for three weeks. The use of stable shRNA vectors against ERβ1 would be a more appropriate method of downregulation and may help determine if there is a link between the tumour suppressive functions of ERβ1 and myoepithelial cells. Recently, α5β6 integrin has been identified to be upregulated in DCIS which could prove a successful alternative protein candidate to study in our myoepithelial cells [480].

Due to lack of available HER2 positive breast tumour tissue samples, we were unable to culture HER2 CAFs in the model which would have been the ideal alternative to our experiments using fibroblasts conditioned with SkBr3 conditioned media. Experiments examining the effects of CAFs on normal mammary epithelia have so far been conducted in simple mono- or dual cultures. Our model would provide an ideal platform for these experiments and may help determine what are the initiating steps in tumorigenesis, changes in fibroblasts that signal to normal epithelium resulting in cell transformation, or established transformed epithelial cells induce changes in the fibroblasts that feed the epithelium and promote tumorigenesis.

7.5 Future Work

This series of experiments has demonstrated that accurate models of normal breast tissue in 3D can be achieved in the laboratory without the need for complex equipment or expensive reagents. This work could lead to patient benefit through various mechanisms and may not be restricted to breast cancer research.

Current UK government initiatives such as the National Centre for the Replacement, Refinement and Reduction of Animals in Research (NC3Rs) aims to drive innovation of new techniques that will lead to the reduction or replacement of using animals in research [481]. Given that the work in this thesis offers a new model that accurately recapitulates the *in vivo* breast environment, this could go some way to reducing the amount of mouse models needed for research. Many of the genetic, protein and drug compound candidates for cancer research are discovered through experimentation in 2D *in vitro* environment that does not accurately reflect human tissue, excluding important surrounding cell types. Subsequently, these candidates are applied to mouse models with many proving unsuccessful in generating viable drug therapies for patient benefit. Models such as the one developed here could provide an intermediate to test the effectiveness and appropriate targeting of drugs saving unnecessary use of animals and expenditure.

The model also has the potential for incorporating primary patient cells. This could prove valuable for both scientific research and understanding of biological processes, as well as direct patient benefit. The study of normal human breast at different developmental and hormonal stages is currently unexplored. By incorporating primary cells from breast reduction mammoplasties taken from patients of different age and status, we could gain a better understanding of the biological processes that occur in normal breast which may prove key in the understanding of cancer initiation. This coupled with use of primary patient cells extracted from a variety of different tumour types could further understanding of the heterogeneity of

both normal breast tissue and breast tumours. The availability of good quality normal [482] and breast tumour [483] tissues from specialist breast tissue banks can facilitate this process.

8 References

1. Neville, M.C., T.B. McFadden, and I. Forsyth, *Hormonal regulation of mammary differentiation and milk secretion.* J Mammary Gland Biol Neoplasia, 2002. **7**(1): p. 49-66.

2. Petersen, O.W., P.E. Hoyer, and B. van Deurs, *Frequency and distribution of estrogen receptor-positive cells in normal, nonlactating human breast tissue.* Cancer Res, 1987. **47**(21): p. 5748-51.

3. Speirs, V., et al., *Distinct expression patterns of ERα and ERβ in normal human mammary gland.* Journal of Clinical Pathology, 2002. **55**(5): p. 371-374.

4. Clarke, R.B., et al., *Dissociation between steroid receptor expression and cell proliferation in the human breast.* Cancer Res, 1997. **57**(22): p. 4987-91.

5. Gill, S., et al., *Expression of prolactin receptors in normal, benign, and malignant breast tissue: an immunohistological study.* Journal of Clinical Pathology, 2001. **54**(12): p. 956-960.

6. Bartek, J., et al., *Patterns of expression of keratin 19 as detected with monoclonal antibodies in human breast tissues and tumours.* Int J Cancer, 1985. **36**(3): p. 299-306.

7. Taylor-Papadimitriou, J., et al., *Keratin expression in human mammary epithelial cells cultured from normal and malignant tissue: relation to in vivo phenotypes and influence of medium.* Journal of Cell Science, 1989. **94**(3): p. 403-413.

8. Gendler, S.J., et al., *Cloning of partial cDNA encoding differentiation and tumor-associated mucin glycoproteins expressed by human mammary epithelium.* Proc Natl Acad Sci U S A, 1987. **84**(17): p. 6060-4.

9. Emerman, J.T. and A.W. Vogl, *Cell size and shape changes in the myoepithelium of the mammary gland during differentiation.* The Anatomical Record, 1986. **216**(3): p. 405-415.

10. Bocker, W., et al., *An immunohistochemical study of the breast using antibodies to basal and luminal keratins, alpha-smooth muscle actin, vimentin, collagen IV and laminin. Part II: Epitheliosis and ductal carcinoma in situ.* Virchows Arch A Pathol Anat Histopathol, 1992. **421**(4): p. 323-30.

11. Michalczyk, A., et al., *Lactation affects expression of intermediate filaments in human breast epithelium.* Differentiation, 2001. **67**(1–2): p. 41-49.

12. Nagle, R.B., et al., *Characterization of breast carcinomas by two monoclonal antibodies distinguishing myoepithelial from luminal epithelial cells.* J Histochem Cytochem, 1986. **34**(7): p. 869-81.

13. Gusterson, B.A., et al., *Distribution of myoepithelial cells and basement membrane proteins in the normal breast and in benign and malignant breast diseases.* Cancer Res, 1982. **42**(11): p. 4763-70.

14. Pitelka, D.R., et al., *Cell contacts in the mouse mammary gland. I. Normal gland in postnatal development and the secretory cycle.* J Cell Biol, 1973. **56**(3): p. 797-818.

15. Bergstraesser, L.M., Srinivasan, G., Jones, J.C., Stahl, S., Weitzman, S.A., *Expression of hemidesmosomes and component proteins is lost by invasive breast cancer cells.* Am J Pathol, 1995. **146**(6): p. 1823-1839.

16. Bissell, M.J. and D. Bilder, *Polarity determination in breast tissue: desmosomal adhesion, myoepithelial cells, and laminin 1.* Breast Cancer Res, 2003. **5**(2): p. 117-9.

17. Runswick, S.K., et al., *Desmosomal adhesion regulates epithelial morphogenesis and cell positioning.* Nat Cell Biol, 2001. **3**(9): p. 823-30.

18. Jones, J.L., et al., *Modulation of myoepithelial-associated alpha6beta4 integrin in a breast cancer cell line alters invasive potential.* Exp Cell Res, 1997. **235**(2): p. 325-33.

19. Koukoulis, G.K., et al., *Immunohistochemical localization of integrins in the normal, hyperplastic, and neoplastic breast. Correlations with their functions as receptors and cell adhesion molecules.* Am J Pathol, 1991. **139**(4): p. 787-99.

20. Visvader, J.E., *Keeping abreast of the mammary epithelial hierarchy and breast tumorigenesis.* Genes Dev, 2009. **23**(22): p. 2563-77.

21. Villadsen, R., et al., *Evidence for a stem cell hierarchy in the adult human breast.* J Cell Biol, 2007. **177**(1): p. 87-101.

22. Shackleton, M., et al., *Generation of a functional mammary gland from a single stem cell.* Nature, 2006. **439**(7072): p. 84-8.

23. Stingl, J., et al., *Purification and unique properties of mammary epithelial stem cells.* Nature, 2006. **439**(7079): p. 993-7.

24. Visvader, J.E. and G.H. Smith, *Murine mammary epithelial stem cells: discovery, function, and current status.* Cold Spring Harb Perspect Biol, 2011. **3**(2).

25. Asselin-Labat, M.L., et al., *Gata-3 is an essential regulator of mammary-gland morphogenesis and luminal-cell differentiation.* Nat Cell Biol, 2007. **9**(2): p. 201-9.

26. Sleeman, K.E., et al., *CD24 staining of mouse mammary gland cells defines luminal epithelial, myoepithelial/basal and non-epithelial cells.* Breast Cancer Res, 2006. **8**(1): p. 12.

27. Stingl, J., et al., *Characterization of bipotent mammary epithelial progenitor cells in normal adult human breast tissue.* Breast Cancer Res Treat, 2001. **67**(2): p. 93-109.

28. Raouf, A., et al., *Transcriptome analysis of the normal human mammary cell commitment and differentiation process.* Cell Stem Cell, 2008. **3**(1): p. 109-18.

29. Zhao, X., et al., *Derivation of myoepithelial progenitor cells from bipotent mammary stem/progenitor cells.* PLoS ONE, 2012. **7**(4): p. 13.

30. Oakes, S.R., et al., *The Ets transcription factor Elf5 specifies mammary alveolar cell fate.* Genes Dev, 2008. **22**(5): p. 581-6.

31. Li, W., et al., *PML depletion disrupts normal mammary gland development and skews the composition of the mammary luminal cell progenitor pool.* Proc Natl Acad Sci U S A, 2009. **106**(12): p. 4725-30.

32. Press, O.U., *Definition-english-stroma.* 2014.

33. Ronnov-Jessen, L., O.W. Petersen, and M.J. Bissell, *Cellular changes involved in conversion of normal to malignant breast: importance of the stromal reaction.* Physiol Rev, 1996. **76**(1): p. 69-125.

34. Ivarsson, M., et al., *Type I collagen synthesis in cultured human fibroblasts: regulation by cell spreading, platelet-derived growth factor and interactions with collagen fibers.* Matrix Biol, 1998. **16**(7): p. 409-25.

35. Yamazaki, K. and B.P. Eyden, *Characterisation of breast stromal fibroblasts: cell surface distribution of collagen type IV, laminin and fibronectin.* J Submicrosc Cytol Pathol, 1998. **30**(2): p. 217-26.

36. Strutz, F., et al., *Identification and characterization of a fibroblast marker: FSP1.* J Cell Biol, 1995. **130**(2): p. 393-405.

37. Egeblad, M., L.E. Littlepage, and Z. Werb, *The fibroblastic coconspirator in cancer progression.* Cold Spring Harb Symp Quant Biol, 2005. **70**: p. 383-8.

38. Ferlay, J., et al., *Estimates of worldwide burden of cancer in 2008: GLOBOCAN 2008.* International Journal of Cancer, 2010: p. n/a-n/a.

39. Cancer Research UK. *Breast Cancer Statistics*. 2014 7 March 2014]; Available from: http://www.cancerresearchuk.org/cancer-info/cancerstats/types/breast/.

40. Lakhani, S.R., et al., *WHO Classification of Tumours*. Vol. WHO. 2012.

41. Ellis, I.O., et al., *Pathological prognostic factors in breast cancer. II. Histological type. Relationship with survival in a large study with long-term follow-up.* Histopathology, 1992. **20**(6): p. 479-89.

42. Page, D.L., I.O. Ellis, and C.W. Elston, *Histologic grading of breast cancer. Let's do it.* Am J Clin Pathol, 1995. **103**(2): p. 123-4.

43. Perou, C.M., et al., *Molecular portraits of human breast tumours.* Nature, 2000. **406**(6797): p. 747-752.

44. Sørlie, T., et al., *Gene expression patterns of breast carcinomas distinguish tumor subclasses with clinical implications.* Proceedings of the National Academy of Sciences of the United States of America, 2001. **98**(19): p. 10869-10874.

45. Curtis, C., et al., *The genomic and transcriptomic architecture of 2,000 breast tumours reveals novel subgroups.* Nature, 2012. **486**(7403): p. 346-52.

46. Bergamaschi, A., et al., *Extracellular matrix signature identifies breast cancer subgroups with different clinical outcome.* J Pathol, 2008. **214**(3): p. 357-67.

47. DeCosse, J.J., et al., *Embryonic inductive tissues that cause histologic differentiation of murine mammary carcinoma in vitro.* J Natl Cancer Inst, 1975. **54**(4): p. 913-22.

48. Noel, A., et al., *Inhibition of stromal matrix metalloproteases: effects on breast-tumor promotion by fibroblasts.* Int J Cancer, 1998. **76**(2): p. 267-73.

49. Saad, S., et al., *Induction of matrix metalloproteinases MMP-1 and MMP-2 by co-culture of breast cancer cells and bone marrow fibroblasts.* Breast Cancer Res Treat, 2000. **63**(2): p. 105-15.

50. Weaver, V.M., et al., *Reversion of the Malignant Phenotype of Human Breast Cells in Three-Dimensional Culture and In vivo by Integrin Blocking Antibodies.* The Journal of Cell Biology, 1997. **137**(1): p. 231-245.

51. Booth, B.W., et al., *The mammary microenvironment alters the differentiation repertoire of neural stem cells.* Proceedings of the National Academy of Sciences, 2008. **105**(39): p. 14891-14896.

52. Boulanger, C.A., et al., *Interaction with the mammary microenvironment redirects spermatogenic cell fate in vivo.* Proceedings of the National Academy of Sciences, 2007. **104**(10): p. 3871-3876.

53. Finak, G., et al., *Stromal gene expression predicts clinical outcome in breast cancer.* Nat Med, 2008. **14**(5): p. 518-27.

54. Provenzano, P., et al., *Collagen reorganization at the tumor-stromal interface facilitates local invasion.* BMC Medicine, 2006. **4**(1): p. 38.

55. Provenzano, P.P., et al., *Collagen density promotes mammary tumor initiation and progression.* BMC Med, 2008. **6**(11): p. 1741-7015.

56. Egeblad, M. and Z. Werb, *New functions for the matrix metalloproteinases in cancer progression.* Nat Rev Cancer, 2002. **2**(3): p. 161-74.

57. Freije, J.M., et al., *Matrix metalloproteinases and tumor progression.* Adv Exp Med Biol, 2003. **532**: p. 91-107.

58. Moinfar, F., et al., *Concurrent and independent genetic alterations in the stromal and epithelial cells of mammary carcinoma: implications for tumorigenesis.* Cancer Res 2000. **60**(9): p. 2562-6.

59. Kurose, K., et al., *Frequent somatic mutations in PTEN and TP53 are mutually exclusive in the stroma of breast carcinomas.* Nat Genet, 2002. **32**(3): p. 355-7.

60. Sadlonova, A., et al., *Breast fibroblasts modulate epithelial cell proliferation in three-dimensional in vitro co-culture.* Breast Cancer Res, 2005. **7**(1): p. R46 - R59.

61. Skalli, O., et al., *A monoclonal antibody against alpha-smooth muscle actin: a new probe for smooth muscle differentiation.* J Cell Biol, 1986. **103**(6 Pt 2): p. 2787-96.

62. Sappino, A.P., et al., *Smooth-muscle differentiation in stromal cells of malignant and non-malignant breast tissues.* Int J Cancer 1988. **41**(5): p. 707-12.

63. Grisendi, G., et al., *Understanding tumor-stroma interplays for targeted therapies by armed mesenchymal stromal progenitors: the Mesenkillers.* Am J Cancer Res, 2011. **1**(6): p. 787-805.

64. Meng, L., et al., *Tumor necrosis factor alpha and interleukin 11 secreted by malignant breast epithelial cells inhibit adipocyte differentiation by selectively down-regulating CCAAT/enhancer binding protein alpha and peroxisome proliferator-activated receptor gamma: mechanism of desmoplastic reaction.* Cancer Res, 2001. **61**(5): p. 2250-5.

65. Darby, I., O. Skalli, and G. Gabbiani, *Alpha-smooth muscle actin is transiently expressed by myofibroblasts during experimental wound healing.* Lab Invest, 1990. **63**(1): p. 21-9.

66. Garin-Chesa, P., L.J. Old, and W.J. Rettig, *Cell surface glycoprotein of reactive stromal fibroblasts as a potential antibody target in human epithelial cancers.* Proc Natl Acad Sci U S A, 1990. **87**(18): p. 7235-9.

67. Tchou, J., et al., *Human breast cancer associated fibroblasts exhibit subtype specific gene expression profiles.* BMC Med Genomics, 2012. **5**(39): p. 1755-8794.

68. Tyan, S.W., et al., *Breast cancer cells induce cancer-associated fibroblasts to secrete hepatocyte growth factor to enhance breast tumorigenesis.* PLoS ONE, 2011. **6**(1): p. 0015313.

69. Kojima, Y., et al., *Autocrine TGF-beta and stromal cell-derived factor-1 (SDF-1) signaling drives the evolution of tumor-promoting mammary stromal myofibroblasts.* Proc Natl Acad Sci U S A, 2010. **107**(46): p. 20009-14.

70. Hu, M., et al., *Regulation of in situ to invasive breast carcinoma transition.* Cancer Cell, 2008. **13**(5): p. 394-406.

71. Gudjonsson, T., et al., *Normal and tumor-derived myoepithelial cells differ in their ability to interact with luminal breast epithelial cells for polarity and basement membrane deposition.* J Cell Sci, 2002. **115**(1): p. 39-50.

72. Barsky, S.H., *Myoepithelial mRNA expression profiling reveals a common tumor-suppressor phenotype.* Experimental and Molecular Pathology, 2003. **74**(2): p. 113-122.

73. Sternlicht, M.D., et al., *Characterizations of the extracellular matrix and proteinase inhibitor content of human myoepithelial tumors.* Lab Invest, 1996. **74**(4): p. 781-96.

74. Allinen, M., et al., *Molecular characterization of the tumor microenvironment in breast cancer.* Cancer Cell, 2004. **6**(1): p. 17-32.

75. Dupont, W.D. and D.L. Page, *Risk factors for breast cancer in women with proliferative breast disease.* N Engl J Med, 1985. **312**(3): p. 146-51.

76. Simpson, P.T., et al., *Columnar cell lesions of the breast: the missing link in breast cancer progression? A morphological and molecular analysis.* Am J Surg Pathol, 2005. **29**(6): p. 734-46.

77. Aubele, M.M., et al., *Accumulation of chromosomal imbalances from intraductal proliferative lesions to adjacent in situ and invasive ductal breast cancer.* Diagn Mol Pathol, 2000. **9**(1): p. 14-9.

78. O'Connell, P., et al., *Analysis of loss of heterozygosity in 399 premalignant breast lesions at 15 genetic loci.* J Natl Cancer Inst 1998. **90**(9): p. 697-703.

79. Jones, C., et al., *Comparative genomic hybridization analysis of bilateral hyperplasia of usual type of the breast.* The Journal of Pathology, 2003. **199**(2): p. 152-156.

80. Gong, G., et al., *Genetic changes in paired atypical and usual ductal hyperplasia of the breast by comparative genomic hybridization.* Clin Cancer Res, 2001. **7**(8): p. 2410-4.

81. Schnitt, S.J. and A. Vincent-Salomon, *Columnar cell lesions of the breast.* Adv Anat Pathol, 2003. **10**(3): p. 113-24.

82. Fraser, J.L., et al., *Columnar alteration with prominent apical snouts and secretions: a spectrum of changes frequently present in breast biopsies performed for microcalcifications.* Am J Surg Pathol, 1998. **22**(12): p. 1521-7.

83. Dabbs, D.J., et al., *Molecular alterations in columnar cell lesions of the breast.* Mod Pathol, 2006. **19**(3): p. 344-9.

84. Guerra-Wallace, M.M., W.N. Christensen, and R.L. White, Jr., *A retrospective study of columnar alteration with prominent apical snouts and secretions and the association with cancer.* Am J Surg, 2004. **188**(4): p. 395-8.

85. Feeley, L. and C.M. Quinn, *Columnar cell lesions of the breast.* Histopathology, 2008. **52**(1): p. 11-9.

86. Martel, M., et al., *Flat DIN 1 (flat epithelial atypia) on core needle biopsy: 63 cases identified retrospectively among 1,751 core biopsies performed over an 8-year period (1992-1999).* Virchows Arch, 2007. **451**(5): p. 883-91.

87. Lacroix-Triki, M., et al., *Value of cytokeratin 5/6 immunostaining using D5/16 B4 antibody in the spectrum of proliferative intraepithelial lesions of the breast. A comparative study with 34betaE12 antibody.* Virchows Arch, 2003. **442**(6): p. 548-54.

88. Bryan, B.B., S.J. Schnitt, and L.C. Collins, *Ductal carcinoma in situ with basal-like phenotype: a possible precursor to invasive basal-like breast cancer.* Mod Pathol, 2006. **19**(5): p. 617-21.

89. Guray, M. and A.A. Sahin, *Benign breast diseases: classification, diagnosis, and management.* Oncologist, 2006. **11**(5): p. 435-49.

90. Page, D.L., et al., *Atypical lobular hyperplasia as a unilateral predictor of breast cancer risk: a retrospective cohort study.* Lancet, 2003. **361**(9352): p. 125-9.

91. Boecker, W., et al., *Ductal epithelial proliferations of the breast: a biological continuum? Comparative genomic hybridization and high-molecular-weight cytokeratin expression patterns.* J Pathol, 2001. **195**(4): p. 415-21.

92. Xu, S., et al., *Evidence of chromosomal alterations in pure usual ductal hyperplasia as a breast carcinoma precursor.* Oncol Rep, 2008. **19**(6): p. 1469-75.

93. Cleton-Jansen, A.M., *E-cadherin and loss of heterozygosity at chromosome 16 in breast carcinogenesis: different genetic pathways in ductal and lobular breast cancer?* Breast Cancer Res, 2002. **4**(1): p. 5-8.

94. MacGrogan, G., et al., *Impact of immunohistochemical markers, CK5/6 and E-cadherin on diagnostic agreement in non-invasive proliferative breast lesions.* Histopathology, 2008. **52**(6): p. 689-97.

95. Tavassoli, F.A., *Ductal carcinoma in situ: introduction of the concept of ductal intraepithelial neoplasia.* Mod Pathol, 1998. **11**(2): p. 140-54.

96. NHS Cancer Screening Programmes and The Royal College of Pathologists, *Pathology Reporting of Disease*. 2005, NHSBSP.

97. Park, K., et al., *HER2 status in pure ductal carcinoma in situ and in the intraductal and invasive components of invasive ductal carcinoma determined by fluorescence in situ hybridization and immunohistochemistry.* Histopathology, 2006. **48**(6): p. 702-7.

98. Gusterson, B.A., et al., *c-erbB-2 expression in benign and malignant breast disease.* Br J Cancer, 1988. **58**(4): p. 453-7.

99. Sanders, M.E., et al., *The natural history of low-grade ductal carcinoma in situ of the breast in women treated by biopsy only revealed over 30 years of long-term follow-up.* Cancer, 2005. **103**(12): p. 2481-4.

100. Collins, L.C., et al., *Outcome of patients with ductal carcinoma in situ untreated after diagnostic biopsy: results from the Nurses' Health Study.* Cancer 2005. **103**(9): p. 1778-84.

101. Gupta, S.K., et al., *E-cadherin (E-cad) expression in duct carcinoma in situ (DCIS) of the breast.* Virchows Arch, 1997. **430**(1): p. 23-8.

102. Curran, S. and G.I. Murray, *Matrix metalloproteinases: molecular aspects of their roles in tumour invasion and metastasis.* Eur J Cancer, 2000. **36**(13 Spec No): p. 1621-30.

103. Foote, F.W. and F.W. Stewart, *Lobular carcinoma in situ: A rare form of mammary cancer.* Am J Pathol, 1941. **17**(4): p. 491-496.

104. Simpson, P.T., et al., *The diagnosis and management of pre-invasive breast disease: pathology of atypical lobular hyperplasia and lobular carcinoma in situ.* Breast Cancer Res, 2003. **5**(5): p. 258-62.

105. Page, D.L., et al., *Lobular neoplasia of the breast: higher risk for subsequent invasive cancer predicted by more extensive disease.* Hum Pathol, 1991. **22**(12): p. 1232-9.

106. Wellings, S.R., H.M. Jensen, and R.G. Marcum, *An atlas of subgross pathology of the human breast with special reference to possible precancerous lesions.* J Natl Cancer Inst, 1975. **55**(2): p. 231-73.

107. Carley, A.M., et al., *Frequency and clinical significance of simultaneous association of lobular neoplasia and columnar cell alterations in breast tissue specimens.* Am J Clin Pathol, 2008. **130**(2): p. 254-8.

108. Abdel-Fatah, T.M., et al., *High frequency of coexistence of columnar cell lesions, lobular neoplasia, and low grade ductal carcinoma in situ with invasive tubular carcinoma and invasive lobular carcinoma.* Am J Surg Pathol, 2007. **31**(3): p. 417-26.

109. Abdel-Fatah, T.M., et al., *Morphologic and molecular evolutionary pathways of low nuclear grade invasive breast cancers and their putative precursor lesions: further evidence to support the concept of low nuclear grade breast neoplasia family.* Am J Surg Pathol, 2008. **32**(4): p. 513-23.

110. Fitzgibbons, P.L., D.E. Henson, and R.V. Hutter, *Benign breast changes and the risk for subsequent breast cancer: an update of the 1985 consensus statement. Cancer Committee of the College of American Pathologists.* Arch Pathol Lab Med, 1998. **122**(12): p. 1053-5.

111. Boulos, F.I., et al., *Histologic associations and long-term cancer risk in columnar cell lesions of the breast: a retrospective cohort and a nested case-control study.* Cancer, 2008. **113**(9): p. 2415-21.

112. Rosenblum, M.K., R. Purrazzella, and P.P. Rosen, *Is microglandular adenosis a precancerous disease? A study of carcinoma arising therein.* Am J Surg Pathol, 1986. **10**(4): p. 237-45.

113. Acs, G., et al., *Microglandular adenosis with transition into adenoid cystic carcinoma of the breast.* Am J Surg Pathol, 2003. **27**(8): p. 1052-60.

114. Khalifeh, I.M., et al., *Clinical, histopathologic, and immunohistochemical features of microglandular adenosis and transition into in situ and invasive carcinoma.* Am J Surg Pathol, 2008. **32**(4): p. 544-52.

115. Geyer, F.C., et al., *Microglandular adenosis or microglandular adenoma? A molecular genetic analysis of a case associated with atypia and invasive carcinoma.* Histopathology, 2009. **55**(6): p. 732-43.

116. Shin, S.J., et al., *Molecular evidence for progression of microglandular adenosis (MGA) to invasive carcinoma.* Am J Surg Pathol, 2009. **33**(4): p. 496-504.

117. Allred, D.C., et al., *Ductal carcinoma in situ and the emergence of diversity during breast cancer evolution.* Clin Cancer Res, 2008. **14**(2): p. 370-8.

118. Miller, F.R., *Xenograft models of premalignant breast disease.* J Mammary Gland Biol Neoplasia, 2000. **5**(4): p. 379-91.

119. Nowell, P.C., *The clonal evolution of tumor cell populations.* Science, 1976. **194**(4260): p. 23-8.

120. Lakhani, S.R., et al., *Genetic alterations in 'normal' luminal and myoepithelial cells of the breast.* J Pathol, 1999. **189**(4): p. 496-503.

121. Larson, P.S., et al., *Loss of heterozygosity or allele imbalance in histologically normal breast epithelium is distinct from loss of heterozygosity or allele imbalance in co-existing carcinomas.* Am J Pathol, 2002. **161**(1): p. 283-90.

122. Stingl, J., et al., *Phenotypic and functional characterization in vitro of a multipotent epithelial cell present in the normal adult human breast.* Differentiation, 1998. **63**(4): p. 201-13.

123. Dontu, G., et al., *In vitro propagation and transcriptional profiling of human mammary stem/progenitor cells.* Genes Dev 2003. **17**(10): p. 1253-70.

124. Reya, T., et al., *Stem cells, cancer, and cancer stem cells.* Nature, 2001. **414**(6859): p. 105-11.

125. Tu, S.M., S.H. Lin, and C.J. Logothetis, *Stem-cell origin of metastasis and heterogeneity in solid tumours.* Lancet Oncol, 2002. **3**(8): p. 508-13.

126. Prat, A. and C.M. Perou, *Mammary development meets cancer genomics.* Nat Med, 2009. **15**(8): p. 842-4.

127. Lim, E., et al., *Aberrant luminal progenitors as the candidate target population for basal tumor development in BRCA1 mutation carriers.* Nat Med, 2009. **15**(8): p. 907-13.

128. Molyneux, G., et al., *BRCA1 basal-like breast cancers originate from luminal epithelial progenitors and not from basal stem cells.* Cell Stem Cell, 2010. **7**(3): p. 403-17.

129. Nash, C. and V. Speirs, *Pre-Clinical Modelling of Breast Cancer: Which Model to Choose?*, in *Breast Cancer Metastasis and Drug Resistance. Progress and Prospects*, A. Ahmad, Editor. 2013, Springer.

130. Forozan, F., et al., *Molecular cytogenetic analysis of 11 new breast cancer cell lines.* Br J Cancer, 1999. **81**(8): p. 1328-1334.

131. Miller, F.R., et al., *MCF10DCIS.com Xenograft Model of Human Comedo Ductal Carcinoma In Situ.* Journal of the National Cancer Institute, 2000. **92**(14): p. 1185a-1186.

132. Charafe-Jauffret, E., C. Ginestier, and D. Birnbaum, *Breast cancer stem cells: tools and models to rely on.* BMC Cancer, 2009. **9**(1): p. 202.

133. Holliday, D. and V. Speirs, *Choosing the right cell line for breast cancer research.* Breast Cancer Research, 2011. **13**(4): p. 215.

134. Burdall, S.E., et al., *Breast cancer cell lines: friend or foe?* Breast Cancer Research, 2003. **5**(2): p. 89.

135. Neve, R.M., et al., *A collection of breast cancer cell lines for the study of functionally distinct cancer subtypes.* Cancer Cell, 2006. **10**(6): p. 515-527.

136. Weigelt, B. and M. Bissell, *Unraveling the microenvironmental influences on the normal mammary gland and breast cancer.* Seminars in Cancer Biology, 2008. **18**(5): p. 311-321.

137. Bissell, M.J. and D. Radisky, *Putting tumours in context.* Nat Rev Cancer, 2001. **1**(1): p. 46-54.

138. Cukierman, E., R. Pankov, and K.M. Yamada, *Cell interactions with three-dimensional matrices.* Curr Opin Cell Biol, 2002. **14**(5): p. 633-9.

139. Zwezdaryk, K.J., et al., *Rotating cell culture systems for human cell culture: human trophoblast cells as a model.* J Vis Exp, 2012. **18**(59).

140. Foty, R., *A simple hanging drop cell culture protocol for generation of 3D spheroids.* J Vis Exp 2011. **(51).**(pii): p. 2720. doi: 10.3791/2720.

141. Naber, H.P., et al., *Spheroid assay to measure TGF-beta-induced invasion.* J Vis Exp, 2011. **16**(57).

142. Nagelkerke, A., et al., *Hypoxia stimulates migration of breast cancer cells via the PERK/ATF4/LAMP3-arm of the unfolded protein response.* Breast Cancer Res, 2013. **15**(1).

143. Ivascu, A. and M. Kubbies, *Rapid generation of single-tumor spheroids for high-throughput cell function and toxicity analysis.* J Biomol Screen, 2006. **11**(8): p. 922-32.

144. Zhang, X., et al., *Development of an in vitro multicellular tumor spheroid model using microencapsulation and its application in anticancer drug screening and testing.* Biotechnol Prog, 2005. **21**(4): p. 1289-96.

145. Smart, C.E., et al., *In vitro analysis of breast cancer cell line tumourspheres and primary human breast epithelia mammospheres demonstrates inter- and intrasphere heterogeneity.* PLoS ONE, 2013. **8**(6).

146. Farnie, G., et al., *Novel cell culture technique for primary ductal carcinoma in situ: role of Notch and epidermal growth factor receptor signaling pathways.* J Natl Cancer Inst, 2007. **99**(8): p. 616-27.

147. Shaw, F.L., et al., *A detailed mammosphere assay protocol for the quantification of breast stem cell activity.* J Mammary Gland Biol Neoplasia, 2012. **17**(2): p. 111-7.

148. Leeper, A.D., et al., *Long-term culture of human breast cancer specimens and their analysis using optical projection tomography.* J Vis Exp, 2011. **29**(53).

149. Holliday, D.L., et al., *Novel multicellular organotypic models of normal and malignant breast: tools for dissecting the role of the microenvironment in breast cancer progression.* Breast Cancer Research, 2009. **11**(1): p. R3.

150. Debnath, J. and J.S. Brugge, *Modelling glandular epithelial cancers in three-dimensional cultures.* Nat Rev Cancer, 2005. **5**(9): p. 675-88.

151. Kenny, P.A., et al., *The morphologies of breast cancer cell lines in three-dimensional assays correlate with their profiles of gene expression.* Mol Oncol, 2007. **1**(1): p. 84-96.

152. Streuli, C.H., N. Bailey, and M.J. Bissell, *Control of mammary epithelial differentiation: basement membrane induces tissue-specific gene expression in the absence of cell-cell interaction and morphological polarity.* The Journal of Cell Biology, 1991. **115**(5): p. 1383-1395.

153. Wang, F., et al., *Phenotypic Reversion or Death of Cancer Cells by Altering Signaling Pathways in Three-Dimensional Contexts.* Journal of the National Cancer Institute, 2002. **94**(19): p. 1494-1503.

154. Petersen, O.W., et al., *Interaction with basement membrane serves to rapidly distinguish growth and differentiation pattern of normal and malignant human breast epithelial cells.* Proc Natl Acad Sci U S A, 1992. **89**(19): p. 9064-8.

155. Lee, G.Y., et al., *Three-dimensional culture models of normal and malignant breast epithelial cells.* Nat Methods, 2007. **4**(4): p. 359-65.

156. Novitskaya, V., et al., *Tetraspanin CD151 Regulates Growth of Mammary Epithelial Cells in Three-Dimensional Extracellular Matrix: Implication for Mammary Ductal Carcinoma In situ.* Cancer Research, 2010. **70**(11): p. 4698-4708.

157. Ilina, O. and P. Friedl, *Mechanisms of collective cell migration at a glance.* J Cell Sci, 2009. **122**(Pt 18): p. 3203-8.

158. Wolf, K., et al., *Physical limits of cell migration: Control by ECM space and nuclear deformation and tuning by proteolysis and traction force.* The Journal of Cell Biology, 2013. **201**(7): p. 1069-1084.

159. Liu, H., et al., *Polarity and proliferation are controlled by distinct signaling pathways downstream of PI3-kinase in breast epithelial tumor cells.* The Journal of Cell Biology, 2004. **164**(4): p. 603-612.

160. Leone, A., et al., *Transfection of human nm23-H1 into the human MDA-MB-435 breast carcinoma cell line: effects on tumor metastatic potential, colonization and enzymatic activity.* Oncogene, 1993. **8**(9): p. 2325-33.

161. Howlett, A.R., et al., *A novel function for the nm23-H1 gene: overexpression in human breast carcinoma cells leads to the formation of basement membrane and growth arrest.* J Natl Cancer Inst, 1994. **86**(24): p. 1838-44.

162. Spancake, K.M., et al., *E7-transduced human breast epithelial cells show partial differentiation in three-dimensional culture.* Cancer Res, 1999. **59**(24): p. 6042-5.

163. Chen, H.-M., et al., *AZU-1: A Candidate Breast Tumor Suppressor and Biomarker for Tumor Progression.* Molecular Biology of the Cell, 2000. **11**(4): p. 1357-1367.

164. Muschler, J., et al., *A Role for Dystroglycan in Epithelial Polarization.* Cancer Research, 2002. **62**(23): p. 7102-7109.

165. Muthuswamy, S.K., et al., *ErbB2, but not ErbB1, reinitiates proliferation and induces luminal repopulation in epithelial acini.* Nat Cell Biol, 2001. **3**(9): p. 785-92.

166. Bersini, S., et al., *A microfluidic 3D in vitro model for specificity of breast cancer metastasis to bone.* Biomaterials, 2014. **35**(8): p. 2454-61.

167. Eccles, S.A., et al., *Critical research gaps and translational priorities for the successful prevention and treatment of breast cancer.* Breast Cancer Res, 2013. **15**(5).

168. O'Brien, L.E., et al., *Morphological and biochemical analysis of Rac1 in three-dimensional epithelial cell cultures.* Methods Enzymol, 2006. **406**: p. 676-91.

169. Dickinson, M.E., *Multimodal imaging of mouse development: tools for the postgenomic era.* Dev Dyn, 2006. **235**(9): p. 2386-400.

170. Kubow, K.E. and A.R. Horwitz, *Reducing background fluorescence reveals adhesions in 3D matrices.* Nat Cell Biol, 2011. **13**(1): p. 3-5.

171. Zipfel, W.R., R.M. Williams, and W.W. Webb, *Nonlinear magic: multiphoton microscopy in the biosciences.* Nat Biotechnol, 2003. **21**(11): p. 1369-77.

172. Huang, D., et al., *Optical coherence tomography.* Science, 1991. **254**(5035): p. 1178-81.

173. Sharpe, J., et al., *Optical projection tomography as a tool for 3D microscopy and gene expression studies.* Science, 2002. **296**(5567): p. 541-5.

174. Sameni, M., et al., *MAME models for 4D live-cell imaging of tumor: microenvironment interactions that impact malignant progression.* J Vis Exp, 2012. **17**(60).

175. Leeper, A.D., et al., *Long-term culture of human breast cancer specimens and their analysis using optical projection tomography.* J Vis Exp, 2011(53).

176. Leeper, A.D., et al., *Determining tamoxifen sensitivity using primary breast cancer tissue in collagen-based three-dimensional culture.* Biomaterials, 2012. **33**(3): p. 907-915.

177. Hood, C.J. and D.M. Parham, *A Simple Method of Tumour Culture.* Pathology - Research and Practice, 1998. **194**(3): p. 177-181.

178. Holliday, D.L., et al., *The practicalities of using tissue slices as preclinical organotypic breast cancer models.* J Clin Pathol, 2013. **66**(3): p. 253-5.

179. Berdichevsky, F., et al., *Branching morphogenesis of human mammary epithelial cells in collagen gels.* J Cell Sci, 1994. **107**(Pt 12): p. 3557-68.

180. Soule, H.D., et al., *Isolation and characterization of a spontaneously immortalized human breast epithelial cell line, MCF-10.* Cancer Res, 1990. **50**(18): p. 6075-86.

181. O'Hare, M.J., et al., *Conditional immortalization of freshly isolated human mammary fibroblasts and endothelial cells.* Proc Natl Acad Sci U S A, 2001. **98**(2): p. 646-51.

182. Trempe, G.L., *Human breast cancer in culture.* Recent Results Cancer Res, 1976. **57**: p. 33-41.

183. Gomm, J.J., et al., *Isolation of pure populations of epithelial and myoepithelial cells from the normal human mammary gland using immunomagnetic separation with Dynabeads.* Anal Biochem, 1995. **226**(1): p. 91-9.

184. EPFL. *Lentivectors Toolbox*. 2012 26/02/2014]; Available from: http://tronolab.epfl.ch/lentivectors.

185. Addgene. *Plasmid 1774: pBABE-neo-hTERT*. 2014 7 March 2014]; Available from: https://www.addgene.org/1774/.

186. Bissell, M.J., et al., *The organizing principle: microenvironmental influences in the normal and malignant breast.* Differentiation, 2002. **70**(9-10): p. 537-546.

187. Hebner, C., V.M. Weaver, and J. Debnath, *Modeling Morphogenesis and Oncogenesis in Three-Dimensional Breast Epithelial Cultures.* Annual Review of Pathology: Mechanisms of Disease, 2008. **3**(1): p. 313-339.

188. Lopez, J.I., J.K. Mouw, and V.M. Weaver, *Biomechanical regulation of cell orientation and fate.* Oncogene, 2008. **27**(55): p. 6981-6993.

189. Kleinman, H.K., et al., *Isolation and characterization of type IV procollagen, laminin, and heparan sulfate proteoglycan from the EHS sarcoma.* Biochemistry, 1982. **21**(24): p. 6188-6193.

190. Debnath, J., S.K. Muthuswamy, and J.S. Brugge, *Morphogenesis and oncogenesis of MCF-10A mammary epithelial acini grown in three-dimensional basement membrane cultures.* Methods, 2003. **30**(3): p. 256-268.

191. Wisdom, B.J., et al., *Type IV Collagen of Engelbreth-Holm-Swarm Tumor Matrix: Identification of Constituent Chains.* Connective Tissue Research, 1992. **27**(4): p. 225-234.

192. Vaillant, F., G. Lindeman, and J. Visvader, *Jekyll or Hyde: does Matrigel provide a more or less physiological environment in mammary repopulating assays?* Breast Cancer Research, 2011. **13**(3): p. 108.

193. Parmar, H. and G.R. Cunha, *Epithelial-stromal interactions in the mouse and human mammary gland in vivo.* Endocr Relat Cancer, 2004. **11**(3): p. 437-458.

194. Provenzano, P.P., et al., *Matrix density-induced mechanoregulation of breast cell phenotype, signaling and gene expression through a FAK-ERK linkage.* Oncogene, 2009. **28**(49): p. 4326-43.

195. Dhimolea, E., et al., *The role of collagen reorganization on mammary epithelial morphogenesis in a 3D culture model.* Biomaterials, 2010. **31**(13): p. 3622-3630.

196. Maskarinec, G., et al., *Mammographic density as a predictor of breast cancer survival: the Multiethnic Cohort.* Breast Cancer Res, 2013. **15**(1).

197. Alowami, S., et al., *Mammographic density is related to stroma and stromal proteoglycan expression.* Breast Cancer Res, 2003. **5**(5): p. R129 - R135.

198. Krause, S., et al., *A novel 3D in vitro culture model to study stromal-epithelial interactions in the mammary gland.* Tissue Eng Part C Methods, 2008. **14**(3): p. 261-71.

199. Berdichevsky, F., et al., *Branching morphogenesis of human mammary epithelial cells in collagen gels.* Journal of Cell Science, 1994. **107**(12): p. 3557-3568.

200. Tait, L., H.D. Soule, and J. Russo, *Ultrastructural and immunocytochemical characterization of an immortalized human breast epithelial cell line, MCF-10.* Cancer Res, 1990. **50**(18): p. 6087-94.

201. Krause, S., et al., *A Novel 3D In vitro Culture Model to Study Stromal–Epithelial Interactions in the Mammary Gland.* Tissue Engineering Part C: Methods, 2008. **14**(3): p. 261-271.

202. Bartek, J., et al., *Efficient immortalization of luminal epithelial cells from human mammary gland by introduction of simian virus 40 large tumor antigen with a recombinant retrovirus.* Proc Natl Acad Sci U S A 1991. **88**(9): p. 3520-4.

203. Shekhar, M.P.V., J. Werdell, and L. Tait, *Interaction with Endothelial Cells Is a Prerequisite for Branching Ductal-Alveolar Morphogenesis and Hyperplasia of Preneoplastic Human Breast Epithelial Cells: Regulation by Estrogen.* Cancer Research, 2000. **60**(2): p. 439-449.

204. Wang, X., et al., *Preadipocytes stimulate ductal morphogenesis and functional differentiation of human mammary epithelial cells on 3D silk scaffolds.* Tissue Eng Part A, 2009. **15**(10): p. 3087-98.

205. Olsen, C., et al., *Human mammary fibroblasts stimulate invasion of breast cancer cells in a three-dimensional culture and increase stroma development in mouse xenografts.* BMC Cancer, 2010. **10**(1): p. 444.

206. Egeblad, M. and Z. Werb, *New functions for the matrix metalloproteinases in cancer progression.* Nat Rev Cancer, 2002. **2**(3): p. 161-174.

207. Gilles, C., et al., *Implication of collagen type 1-induced membrane-type 1 matrix metalloproteinase expression and matrix metalloproteinase-2 activation in the metastatic progression of breast carcinoma.* Laboratory Investigation, 1997. **76**(5): p. 651-660.

208. Jones, J.L., et al., *Primary breast myopithelial cells exert an invasion-suppressor effect on breast cancer cells via paracrine down-regulation of MMP expresssion in fibroblasts and tumour cells.* Journal of Pathology, 2003. **201**(4): p. 562-572.

209. Addgene. *Plasmid 14882: FUW*. 2014 12/03/14]; Available from: http://www.addgene.org/14882/.

210. Thermo Fisher Scientific Inc. *GIPZ Lentiviral shRNA*. 2014 12/03/2014]; Available from: http://www.thermoscientificbio.com/shrna/gipz-lentiviral-shrna/.

211. O'Hare, M.J., et al., *Characterization in vitro of luminal and myoepithelial cells isolated from the human mammary gland by cell sorting.* Differentiation, 1991. **46**(3): p. 209-21.

212. Wang, X., et al., *A complex 3D human tissue culture system based on mammary stromal cells and silk scaffolds for modeling breast morphogenesis and function.* Biomaterials, 2010. **31**(14): p. 3920-3929.

213. Damiani, S., et al., *Myoepithelial cells and basal lamina in poorly differentiated in situ duct carcinoma of the breast - An immunocytochemical study.* Virchows Archiv, 1999. **434**(3): p. 227-234.

214. Runswick, S.K., et al., *Desmosomal adhesion regulates epithelial morphogenesis and cell positioning.* Nat Cell Biol, 2001. **3**(9): p. 823-830.

215. Cockrell, A.S. and T. Kafri, *Gene delivery by lentivirus vectors.* Mol Biotechnol, 2007. **36**(3): p. 184-204.

216. Rizzo, M.A., M.W. Davidson, and D.W. Piston, *Fluorescent protein tracking and detection: applications using fluorescent proteins in living cells.* Cold Spring Harb Protoc, 2009. **12**(10).

217. Page, M.J., et al., *Proteomic definition of normal human luminal and myoepithelial breast cells purified from reduction mammoplasties.* Proc Natl Acad Sci U S A, 1999. **96**(22): p. 12589-94.

218. Grinnell, F., *Fibroblast biology in three-dimensional collagen matrices.* Trends in Cell Biology, 2003. **13**(5): p. 264-269.

219. Green, C.A., *Further defining the role of ERβ in the mammary gland.* PhD Thesis, University of Leeds, 2009.

220. DiRenzo, J., et al., *Growth factor requirements and basal phenotype of an immortalized mammary epithelial cell line.* Cancer Res, 2002. **62**(1): p. 89-98.

221. Yusuf, R. and K. Frenkel, *Morphologic transformation of human breast epithelial cells MCF-10A: dependence on an oxidative microenvironment and estrogen/epidermal growth factor receptors.* Cancer Cell International, 2010. **10**(1): p. 30.

222. Saleh, M.K.H.A., *Characterization of CSMD1 in Cancer.* PhD Thesis, University of Leeds, 2010.

223. Stingl, J., et al., *Epithelial progenitors in the normal human mammary gland.* Journal of Mammary Gland Biology and Neoplasia, 2005. **10**(1): p. 49-59.

224. Narayanan, A.S., R.C. Page, and J. Swanson, *Collagen synthesis by human fibroblasts. Regulation by transforming growth factor-beta in the presence of other inflammatory mediators.* Biochem J, 1989. **260**(2): p. 463-9.

225. Tomasek, J.J., et al., *Myofibroblasts and mechano-regulation of connective tissue remodelling.* Nat Rev Mol Cell Biol, 2002. **3**(5): p. 349-63.

226. Sadlonova, A., et al., *Human breast fibroblasts inhibit growth of the MCF10AT xenograft model of proliferative breast disease.* Am J Pathol, 2007. **170**(3): p. 1064-76.

227. Chhetri, R.K., et al., *Longitudinal study of mammary epithelial and fibroblast co-cultures using optical coherence tomography reveals morphological hallmarks of pre-malignancy.* PLoS ONE, 2012. **7**(11): p. 12.

228. Sung, K.E., et al., *Understanding the impact of 2D and 3D fibroblast cultures on in vitro breast cancer models.* PLoS ONE, 2013. **8**(10).

229. Jeanes, A.I., A. Maya-Mendoza, and C.H. Streuli, *Cellular Microenvironment Influences the Ability of Mammary Epithelia to Undergo Cell Cycle.* PLoS ONE, 2011. **6**(3): p. e18144.

230. Lee, K.M., K.H. Choi, and M.M. Ouellette, *Use of exogenous hTERT to immortalize primary human cells.* Cytotechnology, 2004. **45**(1-2): p. 33-8.

231. Chapman, E.J., et al., *Expression of hTERT immortalises normal human urothelial cells without inactivation of the p16//Rb pathway.* Oncogene, 2006. **25**(36): p. 5037-5045.

232. Coppe, J.P., et al., *Secretion of vascular endothelial growth factor by primary human fibroblasts at senescence.* J Biol Chem, 2006. **281**(40): p. 29568-74.

233. Davis, J., *Basic Cell Culture*. Practical Approach Series. Vol. 254. 2002: Oxford University Press.

234. Toi, M., et al., *Tumor angiogenesis in breast cancer: its importance as a prognostic indicator and the association with vascular endothelial growth factor expression.* Breast Cancer Res Treat, 1995. **36**(2): p. 193-204.

235. Schneider, B.P. and K.D. Miller, *Angiogenesis of breast cancer.* J Clin Oncol, 2005. **23**(8): p. 1782-90.

236. Boudreau, N. and C. Myers, *Breast cancer-induced angiogenesis: multiple mechanisms and the role of the microenvironment.* Breast Cancer Res, 2003. **5**(3): p. 140-6.

237. DeNardo, D.G. and L.M. Coussens, *Inflammation and breast cancer. Balancing immune response: crosstalk between adaptive and innate immune cells during breast cancer progression.* Breast Cancer Res, 2007. **9**(4): p. 212.

238. Leek, R.D. and A.L. Harris, *Tumor-associated macrophages in breast cancer.* J Mammary Gland Biol Neoplasia, 2002. **7**(2): p. 177-89.

239. Dirat, B., et al., *Cancer-associated adipocytes exhibit an activated phenotype and contribute to breast cancer invasion.* Cancer Res, 2011. **71**(7): p. 2455-65.

240. Ingthorsson, S., et al., *Endothelial cells stimulate growth of normal and cancerous breast epithelial cells in 3D culture.* BMC Res Notes, 2010. **3**(184): p. 1756-0500.

241. van der Geer, P., T. Hunter, and R.A. Lindberg, *Receptor protein-tyrosine kinases and their signal transduction pathways.* Annu Rev Cell Biol, 1994. **10**: p. 251-337.

242. Tzahar, E., et al., *A hierarchical network of interreceptor interactions determines signal transduction by Neu differentiation factor/neuregulin and epidermal growth factor.* Mol Cell Biol, 1996. **16**(10): p. 5276-87.

243. Klapper, L.N., et al., *The ErbB-2/HER2 oncoprotein of human carcinomas may function solely as a shared coreceptor for multiple stroma-derived growth factors.* Proc Natl Acad Sci U S A, 1999. **96**(9): p. 4995-5000.

244. Shi, F., et al., *ErbB3/HER3 intracellular domain is competent to bind ATP and catalyze autophosphorylation.* Proc Natl Acad Sci U S A, 2010. **107**(17): p. 7692-7.

245. Garrett, T.P., et al., *The crystal structure of a truncated ErbB2 ectodomain reveals an active conformation, poised to interact with other ErbB receptors.* Mol Cell, 2003. **11**(2): p. 495-505.

246. Karunagaran, D., et al., *ErbB-2 is a common auxiliary subunit of NDF and EGF receptors: implications for breast cancer.* Embo J, 1996. **15**(2): p. 254-64.

247. Worthylake, R., L.K. Opresko, and H.S. Wiley, *ErbB-2 amplification inhibits down-regulation and induces constitutive activation of both ErbB-2 and epidermal growth factor receptors.* J Biol Chem, 1999. **274**(13): p. 8865-74.

248. Prigent, S.A. and W.J. Gullick, *Identification of c-erbB-3 binding sites for phosphatidylinositol 3'-kinase and SHC using an EGF receptor/c-erbB-3 chimera.* Embo J, 1994. **13**(12): p. 2831-41.

249. Hellyer, N.J., K. Cheng, and J.G. Koland, *ErbB3 (HER3) interaction with the p85 regulatory subunit of phosphoinositide 3-kinase.* Biochem J, 1998. **333 (Pt 3)**: p. 757-63.

250. Kurokawa, H., et al., *Inhibition of HER2/neu (erbB-2) and mitogen-activated protein kinases enhances tamoxifen action against HER2-overexpressing, tamoxifen-resistant breast cancer cells.* Cancer Res, 2000. **60**(20): p. 5887-94.

251. Shou, J., et al., *Mechanisms of Tamoxifen Resistance: Increased Estrogen Receptor-HER2/neu Cross-Talk in ER/HER2–Positive Breast Cancer.* Journal of the National Cancer Institute, 2004. **96**(12): p. 926-935.

252. Proietti, C.J., et al., *Activation of Stat3 by Heregulin/ErbB-2 through the Co-Option of Progesterone Receptor Signaling Drives Breast Cancer Growth.* Molecular and Cellular Biology, 2009. **29**(5): p. 1249-1265.

253. Yang, S., et al., *Mapping ErbB receptors on breast cancer cell membranes during signal transduction.* Journal of Cell Science, 2007. **120**(16): p. 2763-2773.

254. Stern, D.F., *ErbBs in mammary development.* Experimental Cell Research, 2003. **284**(1): p. 89-98.

255. Cardiff, R.D., et al., *The mammary pathology of genetically engineered mice: the consensus report and recommendations from the Annapolis meeting.* Oncogene, 2000. **19**(8): p. 968-988.

256. Jackson-Fisher, A.J., et al., *ErbB2 is required for ductal morphogenesis of the mammary gland.* Proceedings of the National Academy of Sciences of the United States of America, 2004. **101**(49): p. 17138-17143.

257. Jones, F.E. and D.F. Stern, *Expression of dominant-negative ErbB2 in the mammary gland of transgenic mice reveals a role in lobuloalveolar development and lactation.* Oncogene, 1999. **18**(23): p. 3481-90.

258. Sebastian, J., et al., *Activation and function of the epidermal growth factor receptor and erbB-2 during mammary gland morphogenesis.* Cell Growth Differ, 1998. **9**(9): p. 777-85.

259. Choritz, H., G. Busche, and H. Kreipe, *Quality assessment of HER2 testing by monitoring of positivity rates.* Virchows Arch, 2011. **459**(3): p. 283-9.

260. Kallioniemi, O.P., et al., *ERBB2 amplification in breast cancer analyzed by fluorescence in situ hybridization.* Proc Natl Acad Sci U S A, 1992. **89**(12): p. 5321-5.

261. Slamon, D.J., et al., *Human breast cancer: correlation of relapse and survival with amplification of the HER-2/neu oncogene.* Science, 1987. **235**(4785): p. 177-82.

262. Guy, C.T., R.D. Cardiff, and W.J. Muller, *Activated neu Induces Rapid Tumor Progression.* Journal of Biological Chemistry, 1996. **271**(13): p. 7673-7678.

263. Muller, W.J., et al., *Single-step induction of mammary adenocarcinoma in transgenic mice bearing the activated c-neu oncogene.* Cell, 1988. **54**(1): p. 105-115.

264. Korkaya, H., et al., *HER2 regulates the mammary stem/progenitor cell population driving tumorigenesis and invasion.* Oncogene, 2008. **27**(47): p. 6120-30.

265. Kumar, R., et al., *Overexpression of HER2 modulates bcl-2, bcl-XL, and tamoxifen-induced apoptosis in human MCF-7 breast cancer cells.* Clinical Cancer Research, 1996. **2**(7): p. 1215-1219.

266. Knowlden, J.M., et al., *Elevated Levels of Epidermal Growth Factor Receptor/c-erbB2 Heterodimers Mediate an Autocrine Growth Regulatory Pathway in Tamoxifen-Resistant MCF-7 Cells.* Endocrinology, 2003. **144**(3): p. 1032-1044.

267. Adam, L., et al., *Heregulin Regulates Cytoskeletal Reorganization and Cell Migration through the p21-activated Kinase-1 via Phosphatidylinositol-3 Kinase.* Journal of Biological Chemistry, 1998. **273**(43): p. 28238-28246.

268. Spencer, K.S.R., et al., *ErbB2 Is Necessary for Induction of Carcinoma Cell Invasion by Erbb Family Receptor Tyrosine Kinases.* The Journal of Cell Biology, 2000. **148**(2): p. 385-397.

269. Adelsman, M.A., J.B. McCarthy, and Y. Shimizu, *Stimulation of β1-Integrin Function by Epidermal Growth Factor and Heregulin-β Has Distinct Requirements for erbB2 but a Similar Dependence on Phosphoinositide 3-OH Kinase.* Molecular Biology of the Cell, 1999. **10**(9): p. 2861-2878.

270. Xu, F.J., et al., *Heregulin and agonistic anti-p185(c-erbB2) antibodies inhibit proliferation but increase invasiveness of breast cancer cells that overexpress p185(c-erbB2): Increased invasiveness may contribute to poor prognosis.* Clinical Cancer Research, 1997. **3**(9): p. 1629-1634.

271. Baeckstrom, D., D. Alford, and J. Taylor-Papadimitriou, *Morphogenetic and proliferative responses to heregulin of mammary epithelial cells in vitro are dependent on HER2 and HER3 and differ from the responses to HER2 homodimerisation or hepatocyte growth factor.* Int J Oncol, 2000. **16**(6): p. 1081-90.

272. D'Souza, B., et al., *Collagen-induced morphogenesis and expression of the alpha 2-integrin subunit is inhibited in c-erbB2-transfected human mammary epithelial cells.* Oncogene, 1993. **8**(7): p. 1797-806.

273. Ozbay, T. and R. Nahta, *Delphinidin Inhibits HER2 and Erk1/2 Signaling and Suppresses Growth of HER2-Overexpressing and Triple Negative Breast Cancer Cell Lines.* Breast Cancer (Auckl), 2011. **5**: p. 143-54.

274. Pradeep, C.R., et al., *Modeling invasive breast cancer: growth factors propel progression of HER2-positive premalignant lesions.* Oncogene, 2012. **31**(31): p. 3569-83.

275. Aceto, N., et al., *Co-expression of HER2 and HER3 receptor tyrosine kinases enhances invasion of breast cells via stimulation of interleukin-8 autocrine secretion.* Breast Cancer Research, 2012. **14**(5): p. R131.

276. Wolf-Yadlin, A., et al., *Effects of HER2 overexpression on cell signaling networks governing proliferation and migration.* Mol Syst Biol, 2006. **2**(54): p. 3.

277. Dittmar, T., et al., *Induction of cancer cell migration by epidermal growth factor is initiated by specific phosphorylation of tyrosine 1248 of c-erbB-2 receptor via epidermal growth factor receptor.* The FASEB Journal, 2002.

278. Lombaerts, M., et al., *E-cadherin transcriptional downregulation by promoter methylation but not mutation is related to epithelial-to-mesenchymal transition in breast cancer cell lines.* Br J Cancer, 2006. **94**(5): p. 661-71.

279. Hazan, R.B. and L. Norton, *The epidermal growth factor receptor modulates the interaction of E-cadherin with the actin cytoskeleton.* J Biol Chem, 1998. **273**(15): p. 9078-84.

280. Najy, A.J., K.C. Day, and M.L. Day, *The ectodomain shedding of E-cadherin by ADAM15 supports ErbB receptor activation.* J Biol Chem, 2008. **283**(26): p. 18393-401.

281. Kufe, D.W., *MUC1-C oncoprotein as a target in breast cancer: activation of signaling pathways and therapeutic approaches.* Oncogene, 2013. **32**(9): p. 1073-81.

282. Milross, C.G., et al., *The Effect of Tumor Size on Necrosis and Polarographically Measured pO2.* Acta Oncologica, 1997. **36**(2): p. 183-189.

283. *Consensus conference on the classification of ductal carcinoma in Situ.* Cancer, 1997. **80**(9): p. 1798-1802.

284. Barnes, D.M., et al., *Overexpression of the c-erbB-2 oncoprotein: Why does this occur more frequently in ductal carcinoma in situ than in invasive mammary carcinoma and is this of prognostic significance?* European Journal of Cancer, 1992. **28**(2–3): p. 644-648.

285. Gudjonsson, T., et al., *Normal and tumor-derived myoepithelial cells differ in their ability to interact with luminal breast epithelial cells for polarity and basement membrane deposition.* J Cell Sci, 2002. **115**(Pt 1): p. 39-50.

286. Shao, Z.-M., et al., *The Human Myoepithelial Cell Exerts Antiproliferative Effects on Breast Carcinoma Cells Characterized by p21WAF1/CIP1Induction, G2/M Arrest, and Apoptosis.* Experimental Cell Research, 1998. **241**(2): p. 394-403.

287. Fu, H.L., et al., *Ultrastructural localization of laminin and type IV collagen in normal human breast.* Ultrastruct Pathol, 2002. **26**(2): p. 77-80.

288. Sternlicht, M.D., et al., *The human myoepithelial cell is a natural tumor suppressor.* Clin Cancer Res, 1997. **3**(11): p. 1949-58.

289. Kalluri, R. and M. Zeisberg, *Fibroblasts in cancer.* Nat Rev Cancer, 2006. **6**(5): p. 392-401.

290. Mueller, M.M. and N.E. Fusenig, *Friends or foes - bipolar effects of the tumour stroma in cancer.* Nat Rev Cancer, 2004. **4**(11): p. 839-49.

291. Studebaker, A.W., et al., *Fibroblasts isolated from common sites of breast cancer metastasis enhance cancer cell growth rates and invasiveness in an interleukin-6-dependent manner.* Cancer Res, 2008. **68**(21): p. 9087-95.

292. Sadlonova, A., et al., *Breast fibroblasts modulate epithelial cell proliferation in three-dimensional in vitro co-culture.* Breast Cancer Res, 2005. **7**(1): p. 8.

293. Bhowmick, N.A., et al., *TGF-beta signaling in fibroblasts modulates the oncogenic potential of adjacent epithelia.* Science, 2004. **303**(5659): p. 848-51.

294. Seslar, S.P., T. Nakamura, and S.W. Byers, *Regulation of fibroblast hepatocyte growth factor/scatter factor expression by human breast carcinoma cell lines and peptide growth factors.* Cancer Res, 1993. **53**(6): p. 1233-8.

295. Sung, K.E., et al., *Understanding the Impact of 2D and 3D Fibroblast Cultures on In vitro Breast Cancer Models.* PLoS ONE, 2013. **8**(10): p. 0076373.

296. Sadlonova, A., et al., *Identification of molecular distinctions between normal breast-associated fibroblasts and breast cancer-associated fibroblasts.* Cancer Microenviron, 2009. **2**(1): p. 9-21.

297. Grille, S.J., et al., *The protein kinase Akt induces epithelial mesenchymal transition and promotes enhanced motility and invasiveness of squamous cell carcinoma lines.* Cancer Res 2003. **63**(9): p. 2172-8.

298. Barsky, S.H., et al., *Loss of basement membrane components by invasive tumors but not by their benign counterparts.* Lab Invest, 1983. **49**(2): p. 140-7.

299. Nakano, S., et al., *Differential tissular expression and localization of type IV collagen alpha1(IV), alpha2(IV), alpha5(IV), and alpha6(IV) chains and their mRNA in normal breast and in benign and malignant breast tumors.* Lab Invest, 1999. **79**(3): p. 281-92.

300. Davies, B., et al., *Activity of type IV collagenases in benign and malignant breast disease.* Br J Cancer, 1993. **67**(5): p. 1126-31.

301. Noel, A., et al., *Modulation of collagen and fibronectin synthesis in fibroblasts by normal and malignant cells.* Journal of Cellular Biochemistry, 1992. **48**(2): p. 150-161.

302. Pechoux, C., et al., *Human mammary luminal epithelial cells contain progenitors to myoepithelial cells.* Dev Biol, 1999. **206**(1): p. 88-99.

303. Soon, P.S.H., et al., *Breast cancer-associated fibroblasts induce epithelial-to-mesenchymal transition in breast cancer cells.* Endocrine-Related Cancer, 2013. **20**(1): p. 1-12.

304. Benson, J.R., et al., *Synthesis and secretion of transforming growth factor beta isoforms by primary cultures of human breast tumour fibroblasts in vitro and their modulation by tamoxifen.* Br J Cancer, 1996. **74**(3): p. 352-8.

305. Park, I.-S., et al., *Expression of Transforming Growth Factor-β and Type IV Collagen in Early Streptozotocin-Induced Diabetes.* Diabetes, 1997. **46**(3): p. 473-480.

306. Azuma, M., et al., *Different signalling pathways involved in transforming growth factor-beta 1-induced morphological change and type IV collagen synthesis in simian virus-40-immortalized normal human salivary gland duct and myoepithelial cell clones.* Arch Oral Biol, 1996. **41**(5): p. 413-24.

307. Tang, B., et al., *TGF-β switches from tumor suppressor to prometastatic factor in a model of breast cancer progression.* The Journal of Clinical Investigation, 2003. **112**(7): p. 1116-1124.

308. Pavlides, S., et al., *The reverse Warburg effect: aerobic glycolysis in cancer associated fibroblasts and the tumor stroma.* Cell Cycle, 2009. **8**(23): p. 3984-4001.

309. Whitaker-Menezes, D., et al., *Evidence for a stromal-epithelial "lactate shuttle" in human tumors: MCT4 is a marker of oxidative stress in cancer-associated fibroblasts.* Cell cycle (Georgetown, Tex.), 2011. **10**(11): p. 1772-1783.

310. Wallasch, C., et al., *Heregulin-dependent regulation of HER2/neu oncogenic signaling by heterodimerization with HER3.* Embo J, 1995. **14**(17): p. 4267-75.

311. Alimandi, M., et al., *Cooperative signaling of ErbB3 and ErbB2 in neoplastic transformation and human mammary carcinomas.* Oncogene 1995. **10**(9): p. 1813-21.

312. Falls, D.L., *Neuregulins: functions, forms, and signaling strategies.* Exp Cell Res, 2003. **284**(1): p. 14-30.

313. Steinthorsdottir, V., et al., *Multiple novel transcription initiation sites for NRG1.* Gene, 2004. **342**(1): p. 97-105.

314. Holmes, W.E., et al., *Identification of heregulin, a specific activator of p185erbB2.* Science 1992. **256**(5060): p. 1205-10.

315. Shirakabe, K., et al., *Roles of Meltrin beta /ADAM19 in the processing of neuregulin.* J Biol Chem, 2001. **276**(12): p. 9352-8.

316. Montero, J.C., et al., *Differential shedding of transmembrane neuregulin isoforms by the tumor necrosis factor-alpha-converting enzyme.* Mol Cell Neurosci, 2000. **16**(5): p. 631-48.

317. Sliwkowski, M.X., et al., *Coexpression of erbB2 and erbB3 proteins reconstitutes a high affinity receptor for heregulin.* J Biol Chem 1994. **269**(20): p. 14661-5.

318. Tzahar, E., et al., *ErbB-3 and ErbB-4 function as the respective low and high affinity receptors of all Neu differentiation factor/heregulin isoforms.* J Biol Chem, 1994. **269**(40): p. 25226-33.

319. Fitzpatrick, V.D., et al., *Formation of a high affinity heregulin binding site using the soluble extracellular domains of ErbB2 with ErbB3 or ErbB4.* FEBS Lett, 1998. **431**(1): p. 102-6.

320. Li, L., et al., *The breast proto-oncogene, HRGalpha regulates epithelial proliferation and lobuloalveolar development in the mouse mammary gland.* Oncogene, 2002. **21**(32): p. 4900-7.

321. Jones, F.E., et al., *Heregulin induces in vivo proliferation and differentiation of mammary epithelium into secretory lobuloalveoli.* Cell Growth Differ, 1996. **7**(8): p. 1031-8.

322. Jones, J.T., R.W. Akita, and M.X. Sliwkowski, *Binding specificities and affinities of egf domains for ErbB receptors.* FEBS Lett, 1999. **447**(2-3): p. 227-31.

323. Krane, I.M. and P. Leder, *NDF/heregulin induces persistence of terminal end buds and adenocarcinomas in the mammary glands of transgenic mice.* Oncogene, 1996. **12**(8): p. 1781-8.

324. Weinstein, E.J. and P. Leder, *The extracellular region of heregulin is sufficient to promote mammary gland proliferation and tumorigenesis but not apoptosis.* Cancer Res, 2000. **60**(14): p. 3856-61.

325. Atlas, E., et al., *Heregulin is sufficient for the promotion of tumorigenicity and metastasis of breast cancer cells in vivo.* Mol Cancer Res, 2003. **1**(3): p. 165-75.

326. Aguilar, Z., et al., *Biologic effects of heregulin/neu differentiation factor on normal and malignant human breast and ovarian epithelial cells.* Oncogene, 1999. **18**(44): p. 6050-62.

327. Peles, E., et al., *Cell-type specific interaction of Neu differentiation factor (NDF/heregulin) with Neu/HER-2 suggests complex ligand-receptor relationships.* Embo J, 1993. **12**(3): p. 961-71.

328. Lupu, R., et al., *Interaction between erbB-receptors and heregulin in breast cancer tumor progression and drug resistance.* Semin Cancer Biol, 1995. **6**(3): p. 135-45.

329. Menendez, J.A., I. Mehmi, and R. Lupu, *Trastuzumab in combination with heregulin-activated Her-2 (erbB-2) triggers a receptor-enhanced chemosensitivity effect in the absence of Her-2 overexpression.* J Clin Oncol, 2006. **24**(23): p. 3735-46.

330. de Alava, E., et al., *Neuregulin expression modulates clinical response to trastuzumab in patients with metastatic breast cancer.* J Clin Oncol, 2007. **25**(19): p. 2656-63.

331. Normanno, N., et al., *Expression of messenger RNA for amphiregulin, heregulin, and cripto-1, three new members of the epidermal growth factor family, in human breast carcinomas.* Breast Cancer Res Treat, 1995. **35**(3): p. 293-7.

332. Esteva, F.J., et al., *Expression of erbB/HER receptors, heregulin and P38 in primary breast cancer using quantitative immunohistochemistry.* Pathol Oncol Res, 2001. **7**(3): p. 171-7.

333. Marshall, C., et al., *Neuregulins 1-4 are expressed in the cytoplasm or nuclei of ductal carcinoma (in situ) of the human breast.* Breast Cancer Res Treat, 2006. **96**(2): p. 163-8.

334. Haas, S., et al., *Expression of heregulin, phosphorylated HER-2, HER-3 and HER-4 in HER-2 negative breast cancers.* Oncol Rep, 2009. **21**(2): p. 299-304.

335. Huang, H.E., et al., *A recurrent chromosome breakpoint in breast cancer at the NRG1/neuregulin 1/heregulin gene.* Cancer Res, 2004. **64**(19): p. 6840-4.

336. Hanahan, D. and Robert A. Weinberg, *Hallmarks of Cancer: The Next Generation.* Cell, 2011. **144**(5): p. 646-674.

337. Ricci, A., et al., *Analysis of protein-protein interactions involved in the activation of the Shc/Grb-2 pathway by the ErbB-2 kinase.* Oncogene, 1995. **11**(8): p. 1519-29.

338. Marshall, C.J., *MAP kinase kinase kinase, MAP kinase kinase and MAP kinase.* Curr Opin Genet Dev, 1994. **4**(1): p. 82-9.

339. Manning, B.D. and L.C. Cantley, *AKT/PKB signaling: navigating downstream.* Cell, 2007. **129**(7): p. 1261-74.

340. Fazioli, F., et al., *The erbB-2 mitogenic signaling pathway: tyrosine phosphorylation of phospholipase C-gamma and GTPase-activating protein does not correlate with erbB-2 mitogenic potency.* Mol Cell Biol, 1991. **11**(4): p. 2040-8.

341. Peles, E., et al., *Oncogenic forms of the neu/HER2 tyrosine kinase are permanently coupled to phospholipase C gamma.* Embo J, 1991. **10**(8): p. 2077-86.

342. Liu, J. and J.A. Kern, *Neuregulin-1 activates the JAK-STAT pathway and regulates lung epithelial cell proliferation.* Am J Respir Cell Mol Biol, 2002. **27**(3): p. 306-13.

343. Yang, C., et al., *Essential role for Rac in heregulin beta1 mitogenic signaling: a mechanism that involves epidermal growth factor receptor and is independent of ErbB4.* Mol Cell Biol, 2006. **26**(3): p. 831-42.

344. Talukder, A.H., et al., *Heregulin regulation of autocrine motility factor expression in human tumor cells.* Cancer Res, 2000. **60**(2): p. 474-80.

345. Ruan, S.Q., et al., *Heregulin-beta1-induced GPR30 upregulation promotes the migration and invasion potential of SkBr3 breast cancer cells via ErbB2/ErbB3-MAPK/ERK pathway.* Biochem Biophys Res Commun, 2012. **420**(2): p. 385-90.

346. Asrani, K., et al., *The HER2- and heregulin beta1 (HRG)-inducible TNFR superfamily member Fn14 promotes HRG-driven breast cancer cell migration, invasion, and MMP9 expression.* Mol Cancer Res, 2013. **11**(4): p. 393-404.

347. Vadlamudi, R., et al., *Transcriptional up-regulation of paxillin expression by heregulin in human breast cancer cells.* Cancer Res, 1999. **59**(12): p. 2843-6.

348. Vadlamudi, R., et al., *Serine phosphorylation of paxillin by heregulin-beta1: role of p38 mitogen activated protein kinase.* Oncogene, 1999. **18**(51): p. 7253-64.

349. Adam, L., et al., *Heregulin regulates cytoskeletal reorganization and cell migration through the p21-activated kinase-1 via phosphatidylinositol-3 kinase.* J Biol Chem, 1998. **273**(43): p. 28238-46.

350. Kim, S., et al., *A functional comparison between the HER2(high)/HER3 and the HER2(low)/HER3 dimers on heregulin-beta1-induced MMP-1 and MMP-9 expression in breast cancer cells.* Exp Mol Med, 2012. **44**(8): p. 473-82.

351. Xue, C., et al., *ErbB3-dependent motility and intravasation in breast cancer metastasis.* Cancer Res, 2006. **66**(3): p. 1418-26.

352. Ram, T.G., et al., *Mitogenic activity of neu differentiation factor/heregulin mimics that of epidermal growth factor and insulin-like growth factor-I in human mammary epithelial cells.* J Cell Physiol, 1995. **163**(3): p. 589-96.

353. Hutcheson, I.R., et al., *Heregulin beta1 drives gefitinib-resistant growth and invasion in tamoxifen-resistant MCF-7 breast cancer cells.* Breast Cancer Res, 2007. **9**(4).

354. Yao, J., et al., *Multiple signaling pathways involved in activation of matrix metalloproteinase-9 (MMP-9) by heregulin-beta1 in human breast cancer cells.* Oncogene, 2001. **20**(56): p. 8066-74.

355. Lindberg, L.E., S. Hedjazifar, and D. Baeckstrom, *c-erbB2-induced disruption of matrix adhesion and morphogenesis reveals a novel role for protein kinase B as a negative regulator of alpha(2)beta(1) integrin function.* Mol Biol Cell, 2002. **13**(8): p. 2894-908.

356. Sun, Y., et al., *Induction or suppression of expression of cytochrome C oxidase subunit II by heregulin beta 1 in human mammary epithelial cells is dependent on the levels of ErbB2 expression.* J Cell Physiol, 2002. **192**(2): p. 225-33.

357. Labriola, L., et al., *Heregulin induces transcriptional activation of the progesterone receptor by a mechanism that requires functional ErbB-2 and mitogen-activated protein kinase activation in breast cancer cells.* Mol Cell Biol, 2003. **23**(3): p. 1095-111.

358. Hellyer, N.J., M.S. Kim, and J.G. Koland, *Heregulin-dependent activation of phosphoinositide 3-kinase and Akt via the ErbB2/ErbB3 co-receptor.* J Biol Chem, 2001. **276**(45): p. 42153-61.

359. Liu, W., J. Li, and R.A. Roth, *Heregulin regulation of Akt/protein kinase B in breast cancer cells.* Biochem Biophys Res Commun, 1999. **261**(3): p. 897-903.

360. Khaleque, M.A., et al., *Induction of heat shock proteins by heregulin beta1 leads to protection from apoptosis and anchorage-independent growth.* Oncogene, 2005. **24**(43): p. 6564-73.

361. Jabbour, A., et al., *A recombinant human neuregulin-1 peptide improves preservation of the rodent heart after prolonged hypothermic storage.* Transplantation 2011. **91**(9): p. 961-7. doi: 10.1097/TP.0b013e3182115b4b.

362. Yang, C., et al., *Heregulin beta1 promotes breast cancer cell proliferation through Rac/ERK-dependent induction of cyclin D1 and p21Cip1.* Biochem J, 2008. **410**(1): p. 167-75.

363. Lessor, T., et al., *Regulation of heregulin beta1-induced differentiation in a human breast carcinoma cell line by the extracellular-regulated kinase (ERK) pathway.* J Cell Biochem, 1998. **70**(4): p. 587-95.

364. Tan, M., R. Grijalva, and D. Yu, *Heregulin beta1-activated phosphatidylinositol 3-kinase enhances aggregation of MCF-7 breast cancer cells independent of extracellular signal-regulated kinase.* Cancer Res, 1999. **59**(7): p. 1620-5.

365. Kovacina, K.S., et al., *Identification of a proline-rich Akt substrate as a 14-3-3 binding partner.* J Biol Chem, 2003. **278**(12): p. 10189-94.

366. Sancak, Y., et al., *PRAS40 is an insulin-regulated inhibitor of the mTORC1 protein kinase.* Mol Cell, 2007. **25**(6): p. 903-15.

367. Franklin, R.A., P.A. Atherfold, and J.A. McCubrey, *Calcium-induced ERK activation in human T lymphocytes occurs via p56(Lck) and CaM-kinase.* Mol Immunol, 2000. **37**(11): p. 675-83.

368. Giglione, C., S. Gonfloni, and A. Parmeggiani, *Differential actions of p60c-Src and Lck kinases on the Ras regulators p120-GAP and GDP/GTP exchange factor CDC25Mm.* Eur J Biochem, 2001. **268**(11): p. 3275-83.

369. Elsberger, B., et al., *Is expression or activation of Src kinase associated with cancer-specific survival in ER-, PR- and HER2-negative breast cancer patients?* Am J Pathol, 2009. **175**(4): p. 1389-97.

370. Chakraborty, G., et al., *Hypoxia regulates cross-talk between Syk and Lck leading to breast cancer progression and angiogenesis.* J Biol Chem, 2006. **281**(16): p. 11322-31.

371. Jiang, Z.Y., et al., *Identification of WNK1 as a substrate of Akt/protein kinase B and a negative regulator of insulin-stimulated mitogenesis in 3T3-L1 cells.* J Biol Chem, 2005. **280**(22): p. 21622-8.

372. Xu, B.E., et al., *WNK1: analysis of protein kinase structure, downstream targets, and potential roles in hypertension.* Cell Res, 2005. **15**(1): p. 6-10.

373. Zhang, H., et al., *PDGFRs are critical for PI3K/Akt activation and negatively regulated by mTOR.* J Clin Invest, 2007. **117**(3): p. 730-8.

374. Vartanian, T., et al., *Neuregulin induces the rapid association of focal adhesion kinase with the erbB2-erbB3 receptor complex in schwann cells.* Biochem Biophys Res Commun 2000. **271**(2): p. 414-7.

375. Vadlamudi, R.K., et al., *Heregulin and HER2 signaling selectively activates c-Src phosphorylation at tyrosine 215.* FEBS Lett 2003. **543**(1-3): p. 76-80.

376. Mitra, S.K., D.A. Hanson, and D.D. Schlaepfer, *Focal adhesion kinase: in command and control of cell motility.* Nat Rev Mol Cell Biol, 2005. **6**(1): p. 56-68.

377. Cary, L.A., J.F. Chang, and J.L. Guan, *Stimulation of cell migration by overexpression of focal adhesion kinase and its association with Src and Fyn.* J Cell Sci, 1996. **109**(Pt 7): p. 1787-94.

378. Yadav, V. and M.F. Denning, *Fyn is induced by Ras/PI3K/Akt signaling and is required for enhanced invasion/migration.* Mol Carcinog, 2011. **50**(5): p. 346-52.

379. Xu, D., et al., *Involvement of Fyn tyrosine kinase in actin stress fiber formation in fibroblasts.* FEBS Lett, 2007. **581**(27): p. 5227-33.

380. Wary, K.K., et al., *A requirement for caveolin-1 and associated kinase Fyn in integrin signaling and anchorage-dependent cell growth.* Cell, 1998. **94**(5): p. 625-34.

381. Guan, J.L., *Role of focal adhesion kinase in integrin signaling.* Int J Biochem Cell Biol, 1997. **29**(8-9): p. 1085-96.

382. Serrels, B. and M.C. Frame, *FAK and talin: who is taking whom to the integrin engagement party?* J Cell Biol, 2012. **196**(2): p. 185-7.

383. Kawano, S., et al., *Interaction of integrin alpha(6)beta(4) with ErbB3 and implication in heregulin-induced ErbB3/ErbB2-mediated DNA synthesis.* Genes Cells, 2010. **15**(9): p. 995-1001.

384. Du, Q.S., et al., *Inhibition of PYK2-induced actin cytoskeleton reorganization, PYK2 autophosphorylation and focal adhesion targeting by FAK.* J Cell Sci, 2001. **114**(Pt 16): p. 2977-87.

385. Ganju, R.K., et al., *RAFTK, a novel member of the focal adhesion kinase family, is phosphorylated and associates with signaling molecules upon activation of mature T lymphocytes.* J Exp Med, 1997. **185**(6): p. 1055-63.

386. Archuleta, M.M., et al., *7,12-Dimethylbenz[a]anthracene activates protein-tyrosine kinases Fyn and Lck in the HPB-ALL human T-cell line and increases tyrosine phosphorylation of phospholipase C-gamma 1, formation of inositol 1,4,5-trisphosphate, and mobilization of intracellular calcium.* Proc Natl Acad Sci U S A, 1993. **90**(13): p. 6105-9.

387. Kuruvilla, A., C. Pielop, and W.T. Shearer, *Platelet-activating factor induces the tyrosine phosphorylation and activation of phospholipase C-gamma 1, Fyn and Lyn kinases, and phosphatidylinositol 3-kinase in a human B cell line.* J Immunol, 1994. **153**(12): p. 5433-42.

388. Patterson, R.L., et al., *Phospholipase C-gamma: diverse roles in receptor-mediated calcium signaling.* Trends Biochem Sci, 2005. **30**(12): p. 688-97.

389. Hisatsune, C., et al., *Amplification of Ca2+ signaling by diacylglycerol-mediated inositol 1,4,5-trisphosphate production.* J Biol Chem, 2005. **280**(12): p. 11723-30.

390. Yap, K.L., et al., *Diversity of conformational states and changes within the EF-hand protein superfamily.* Proteins, 1999. **37**(3): p. 499-507.

391. Presta, A., et al., *Substrate binding and calmodulin binding to endothelial nitric oxide synthase coregulate its enzymatic activity.* Nitric Oxide, 1997. **1**(1): p. 74-87.

392. Chen, Z., et al., *Nitric oxide-dependent Src activation and resultant caveolin-1 phosphorylation promote eNOS/caveolin-1 binding and eNOS inhibition.* Mol Biol Cell, 2012. **23**(7): p. 1388-98.

393. Etienne-Manneville, S. and A. Hall, *Rho GTPases in cell biology.* Nature, 2002. **420**(6916): p. 629-35.

394. Pruyne, D. and A. Bretscher, *Polarization of cell growth in yeast.* J Cell Sci, 2000. **113**(Pt 4): p. 571-85.

395. Small, J.V., et al., *The lamellipodium: where motility begins.* Trends Cell Biol, 2002. **12**(3): p. 112-20.

396. Olson, M.F., A. Ashworth, and A. Hall, *An essential role for Rho, Rac, and Cdc42 GTPases in cell cycle progression through G1.* Science, 1995. **269**(5228): p. 1270-2.

397. Cote, J.F. and K. Vuori, *GEF what? Dock180 and related proteins help Rac to polarize cells in new ways.* Trends Cell Biol, 2007. **17**(8): p. 383-93.

398. Cote, J.F., et al., *A novel and evolutionarily conserved PtdIns(3,4,5)P3-binding domain is necessary for DOCK180 signalling.* Nat Cell Biol, 2005. **7**(8): p. 797-807.

399. Yang, J., et al., *Activation of Rho GTPases by DOCK exchange factors is mediated by a nucleotide sensor.* Science, 2009. **325**(5946): p. 1398-402.

400. Mayer, B.J., *SH3 domains: complexity in moderation.* J Cell Sci, 2001. **114**(Pt 7): p. 1253-63.

401. Yajnik, V., et al., *DOCK4, a GTPase activator, is disrupted during tumorigenesis.* Cell, 2003. **112**(5): p. 673-84.

402. Hiramoto-Yamaki, N., et al., *Ephexin4 and EphA2 mediate cell migration through a RhoG-dependent mechanism.* J Cell Biol, 2010. **190**(3): p. 461-77.

403. Hiramoto, K., M. Negishi, and H. Katoh, *Dock4 is regulated by RhoG and promotes Rac-dependent cell migration.* Exp Cell Res, 2006. **312**(20): p. 4205-16.

404. Schnelzer, A., et al., *Rac1 in human breast cancer: overexpression, mutation analysis, and characterization of a new isoform, Rac1b.* Oncogene, 2000. **19**(26): p. 3013-20.

405. Vadlamudi, R.K., et al., *Regulatable expression of p21-activated kinase-1 promotes anchorage-independent growth and abnormal organization of mitotic spindles in human epithelial breast cancer cells.* J Biol Chem, 2000. **275**(46): p. 36238-44.

406. Green, S., et al., *Human oestrogen receptor cDNA: sequence, expression and homology to v-erb-A.* Nature, 1986. **320**(6058): p. 134-9.

407. Greene, G.L., et al., *Sequence and expression of human estrogen receptor complementary DNA.* Science, 1986. **231**(4742): p. 1150-4.

408. Kuiper, G.G., et al., *Cloning of a novel receptor expressed in rat prostate and ovary.* Proc Natl Acad Sci U S A, 1996. **93**(12): p. 5925-30.

409. Mosselman, S., J. Polman, and R. Dijkema, *ER beta: identification and characterization of a novel human estrogen receptor.* FEBS Lett, 1996. **392**(1): p. 49-53.

410. Speirs, V., et al., *Distinct expression patterns of ER alpha and ER beta in normal human mammary gland.* J Clin Pathol, 2002. **55**(5): p. 371-4.

411. Beato, M., P. Herrlich, and G. Schutz, *Steroid hormone receptors: many actors in search of a plot.* Cell, 1995. **83**(6): p. 851-7.

412. Beato, M., *Gene regulation by steroid hormones.* Cell, 1989. **56**(3): p. 335-44.

413. Moore, J.T., et al., *Cloning and characterization of human estrogen receptor beta isoforms.* Biochem Biophys Res Commun, 1998. **247**(1): p. 75-8.

414. Peng, B., et al., *Putative functional characteristics of human estrogen receptor-beta isoforms.* J Mol Endocrinol, 2003. **30**(1): p. 13-29.

415. Leung, Y.K., et al., *Estrogen receptor (ER)-beta isoforms: a key to understanding ER-beta signaling.* Proc Natl Acad Sci U S A, 2006. **103**(35): p. 13162-7.

416. Cowley, S.M., et al., *Estrogen receptors alpha and beta form heterodimers on DNA.* J Biol Chem, 1997. **272**(32): p. 19858-62.

417. Huang, J., et al., *Binding of estrogen receptor beta to estrogen response element in situ is independent of estradiol and impaired by its amino terminus.* Mol Endocrinol, 2005. **19**(11): p. 2696-712.

418. Maruyama, S., et al., *Suppression by estrogen receptor beta of AP-1 mediated transactivation through estrogen receptor alpha.* J Steroid Biochem Mol Biol, 2001. **78**(2): p. 177-84.

419. Chen, J.Q., et al., *ERbeta shifts from mitochondria to nucleus during estrogen-induced neoplastic transformation of human breast epithelial cells and is involved in estrogen-induced synthesis of mitochondrial respiratory chain proteins.* Biochim Biophys Acta, 2007. **12**(46): p. 29.

420. Levin, E.R. and R.J. Pietras, *Estrogen receptors outside the nucleus in breast cancer.* Breast Cancer Res Treat, 2008. **108**(3): p. 351-61.

421. Honma, N., et al., *Clinical importance of estrogen receptor-beta evaluation in breast cancer patients treated with adjuvant tamoxifen therapy.* J Clin Oncol, 2008. **26**(22): p. 3727-34.

422. Nakopoulou, L., et al., *The favourable prognostic value of oestrogen receptor beta immunohistochemical expression in breast cancer.* J Clin Pathol, 2004. **57**(5): p. 523-8.

423. Iwase, H., et al., *Clinical significance of the expression of estrogen receptors alpha and beta for endocrine therapy of breast cancer.* Cancer Chemother Pharmacol, 2003. **52**(1): p. 19.

424. Strom, A., et al., *Estrogen receptor beta inhibits 17beta-estradiol-stimulated proliferation of the breast cancer cell line T47D.* Proc Natl Acad Sci U S A, 2004. **101**(6): p. 1566-71.

425. Paruthiyil, S., et al., *Estrogen receptor beta inhibits human breast cancer cell proliferation and tumor formation by causing a G2 cell cycle arrest.* Cancer Res, 2004. **64**(1): p. 423-8.

426. Lazennec, G., et al., *ER beta inhibits proliferation and invasion of breast cancer cells.* Endocrinology, 2001. **142**(9): p. 4120-30.

427. Platet, N., et al., *Unliganded and liganded estrogen receptors protect against cancer invasion via different mechanisms.* Mol Endocrinol, 2000. **14**(7): p. 999-1009.

428. Hodges-Gallagher, L., et al., *Estrogen receptor beta increases the efficacy of antiestrogens by effects on apoptosis and cell cycling in breast cancer cells.* Breast Cancer Res Treat, 2008. **109**(2): p. 241-50.

429. Sternlicht, M.D., et al., *The human myoepithelial cell is a natural tumor suppressor.* Clinical Cancer Research, 1997. **3**(11): p. 1949-1958.

430. Iwao, K., et al., *Quantitative analysis of estrogen receptor-beta mRNA and its variants in human breast cancers.* Int J Cancer, 2000. **88**(5): p. 733-6.

431. Man, Y.G. and Q.X. Sang, *The significance of focal myoepithelial cell layer disruptions in human breast tumor invasion: a paradigm shift from the "protease-centered" hypothesis.* Exp Cell Res, 2004. **301**(2): p. 103-18.

432. Heidebrecht, F., et al., *Improved protocols for protein and RNA isolation from three-dimensional collagen sandwich cultures of primary hepatocytes.* Anal Biochem, 2009. **393**(1): p. 141-4.

433. de Cremoux, P., et al., *Inter-laboratory quality control for hormone-dependent gene expression in human breast tumors using real-time reverse transcription-polymerase chain reaction.* Endocr Relat Cancer, 2004. **11**(3): p. 489-95.

434. Ponchel, F., et al., *Real-time PCR based on SYBR-Green I fluorescence: an alternative to the TaqMan assay for a relative quantification of gene rearrangements, gene amplifications and micro gene deletions.* BMC Biotechnol, 2003. **3**: p. 18.

435. Basu, S., et al., *Purification of specific cell population by fluorescence activated cell sorting (FACS).* J Vis Exp, 2010. **10**(41).

436. Kole, T.P., et al., *Intracellular mechanics of migrating fibroblasts.* Mol Biol Cell, 2005. **16**(1): p. 328-38.

437. Abercrombie, M., J.E. Heaysman, and S.M. Pegrum, *The locomotion of fibroblasts in culture. 3. Movements of particles on the dorsal surface of the leading lamella.* Exp Cell Res, 1970. **62**(2): p. 389-98.

438. Abercrombie, M., J.E. Heaysman, and S.M. Pegrum, *The locomotion of fibroblasts in culture. II. "RRuffling".* Exp Cell Res, 1970. **60**(3): p. 437-44.

439. Abercrombie, M., J.E. Heaysman, and S.M. Pegrum, *The locomotion of fibroblasts in culture. I. Movements of the leading edge.* Exp Cell Res, 1970. **59**(3): p. 393-8.

440. Fire, A., et al., *Potent and specific genetic interference by double-stranded RNA in Caenorhabditis elegans.* Nature, 1998. **391**(6669): p. 806-11.

441. Kutter, C. and P. Svoboda, *miRNA, siRNA, piRNA: Knowns of the unknown.* RNA Biol, 2008. **5**(4): p. 181-8.

442. Petrie, R.J., et al., *Nonpolarized signaling reveals two distinct modes of 3D cell migration.* J Cell Biol, 2012. **197**(3): p. 439-55.

443. Inc, T.F.S. *RNA interference (RNAi) is an evolutionarily conserved mechanism for silencing gene expression*. 2014 27/02/2014]; Available from: http://www.lifetechnologies.com/uk/en/home/references/ambion-tech-support/rnai-sirna/tech-notes/duration-of-sirna-induced-silencing.html.

444. Heid, C.A., et al., *Real time quantitative PCR.* Genome Res, 1996. **6**(10): p. 986-94.

445. Cirri, P. and P. Chiarugi, *Cancer associated fibroblasts: the dark side of the coin.* Am J Cancer Res, 2011. **1**(4): p. 482-97.

446. Pietras, K. and A. Ostman, *Hallmarks of cancer: interactions with the tumor stroma.* Exp Cell Res 2010. **316**(8): p. 1324-31. doi: 10.1016/j.yexcr.2010.02.045. Epub 2010 Mar 6.

447. Dowling, P. and M. Clynes, *Conditioned media from cell lines: a complementary model to clinical specimens for the discovery of disease-specific biomarkers.* Proteomics, 2011. **11**(4): p. 794-804.

448. Xue, H., B. Lu, and M. Lai, *The cancer secretome: a reservoir of biomarkers.* J Transl Med, 2008. **6**(52): p. 1479-5876.

449. Pavlou, M.P. and E.P. Diamandis, *The cancer cell secretome: a good source for discovering biomarkers?* J Proteomics, 2010. **73**(10): p. 1896-906.

450. Davalos, A.R., et al., *Senescent cells as a source of inflammatory factors for tumor progression.* Cancer Metastasis Rev, 2010. **29**(2): p. 273-83.

451. Hartman, Z.C., et al., *HER2 overexpression elicits a proinflammatory IL-6 autocrine signaling loop that is critical for tumorigenesis.* Cancer Res, 2011. **71**(13): p. 4380-91.

452. Coussens, L.M. and Z. Werb, *Inflammation and cancer.* Nature, 2002. **420**(6917): p. 860-7.

453. Muthuswamy, S.K., et al., *ErbB2, but not ErbB1, reinitiates proliferation and induces luminal repopulation in epithelial acini.* Nat Cell Biol, 2001. **3**(9): p. 785-792.

454. Lazennec, G., et al., *ERβ Inhibits Proliferation and Invasion of Breast Cancer Cells.* Endocrinology, 2001. **142**(9): p. 4120-4130.

455. McMahon, K.M., et al., *Characterization of changes in the proteome in different regions of 3D multicell tumor spheroids.* J Proteome Res, 2012. **11**(5): p. 2863-75.

456. Ahmed, F., et al., *GFP expression in the mammary gland for imaging of mammary tumor cells in transgenic mice.* Cancer Res, 2002. **62**(24): p. 7166-9.

457. Baselga, J., et al., *Recombinant humanized anti-HER2 antibody (Herceptin) enhances the antitumor activity of paclitaxel and doxorubicin against HER2/neu overexpressing human breast cancer xenografts.* Cancer Res, 1998. **58**(13): p. 2825-31.

458. Israyelyan, A.H., et al., *Effective treatment of human breast tumor in a mouse xenograft model with herpes simplex virus type 1 specifying the NV1020 genomic deletion and the gBsyn3 syncytial mutation enabling high viral replication and spread in breast cancer cells.* Hum Gene Ther, 2007. **18**(5): p. 457-73.

459. Lyons, S.K., et al., *The generation of a conditional reporter that enables bioluminescence imaging of Cre/loxP-dependent tumorigenesis in mice.* Cancer Res, 2003. **63**(21): p. 7042-6.

460. Rangarajan, A., et al., *Species- and cell type-specific requirements for cellular transformation.* Cancer Cell, 2004. **6**(2): p. 171-183.

461. Longatto Filho, A., J.M. Lopes, and F.C. Schmitt, *Angiogenesis and breast cancer.* J Oncol, 2010. **2010**.

462. Celis, J.E., et al., *Identification of Extracellular and Intracellular Signaling Components of the Mammary Adipose Tissue and Its Interstitial Fluid in High Risk Breast Cancer Patients.* Molecular & Cellular Proteomics, 2005. **4**(4): p. 492-522.

463. Iyengar, P., et al., *Adipocyte-derived collagen VI affects early mammary tumor progression in vivo, demonstrating a critical interaction in the tumor/stroma microenvironment.* The Journal of Clinical Investigation, 2005. **115**(5): p. 1163-1176.

464. Chen, J., et al., *CCL18 from Tumor-Associated Macrophages Promotes Breast Cancer Metastasis via PITPNM3.* Cancer Cell, 2011. **19**(4): p. 541-555.

465. Nakayama, T., L. Yao, and G. Tosato, *Mast cell–derived angiopoietin-1 plays a critical role in the growth of plasma cell tumors.* The Journal of Clinical Investigation, 2004. **114**(9): p. 1317-1325.

466. Tan, J., et al., *Adipocyte is a non-trivial, dynamic partner of breast cancer cells.* Int J Dev Biol, 2011. **55**(7-9): p. 851-9.

467. Price, D.J., et al., *Role of vascular endothelial growth factor in the stimulation of cellular invasion and signaling of breast cancer cells.* Cell Growth Differ, 2001. **12**(3): p. 129-35.

468. Ingthorsson, S., et al., *Endothelial cells stimulate growth of normal and cancerous breast epithelial cells in 3D culture.* BMC Research Notes, 2010. **3**(1): p. 184.

469. Buchanan, C.F., et al., *Cross-talk between endothelial and breast cancer cells regulates reciprocal expression of angiogenic factors in vitro.* J Cell Biochem, 2012. **113**(4): p. 1142-51.

470. Roberts, N., et al., *Toward Routine Use of 3D Histopathology as a Research Tool.* The American Journal of Pathology, 2012. **180**(5): p. 1835-1842.

471. Singhai, R., et al., *E-Cadherin as a diagnostic biomarker in breast cancer.* N Am J Med Sci, 2011. **3**(5): p. 227-33.

472. Kowalski, P.J., M.A. Rubin, and C.G. Kleer, *E-cadherin expression in primary carcinomas of the breast and its distant metastases.* Breast Cancer Res, 2003. **5**(6): p. 26.

473. Hollestelle, A., et al., *Loss of E-cadherin is not a necessity for epithelial to mesenchymal transition in human breast cancer.* Breast Cancer Res Treat, 2013. **138**(1): p. 47-57.

474. Fanning, A.S., et al., *The tight junction protein ZO-1 establishes a link between the transmembrane protein occludin and the actin cytoskeleton.* J Biol Chem, 1998. **273**(45): p. 29745-53.

475. Grunkin, M., J. Raundahl, and N.T. Foged, *Practical considerations of image analysis and quantification of signal transduction IHC staining.* Methods Mol Biol, 2011. **717**: p. 143-54.

476. Verghese, E.T., et al., *Role of miR-26b in carcinoma-associated fibroblasts and effect on migration and invasion of breast cancer epithelial cells.* The Lancet, 2014. **383**: p. S103.

477. Simpkins, S.A., et al., *Clinical and functional significance of loss of caveolin-1 expression in breast cancer-associated fibroblasts.* J Pathol, 2012. **227**(4): p. 490-8.

478. Martinez-Outschoorn, U.E., et al., *Tumor cells induce the cancer associated fibroblast phenotype via caveolin-1 degradation: implications for breast cancer and DCIS therapy with autophagy inhibitors.* Cell Cycle, 2010. **9**(12): p. 2423-33.

479. Sotgia, F., et al., *Caveolin-1-/- null mammary stromal fibroblasts share characteristics with human breast cancer-associated fibroblasts.* Am J Pathol, 2009. **174**(3): p. 746-61.

480. Allen, M.D., et al., *Altered Microenvironment Promotes Progression of Preinvasive Breast Cancer: Myoepithelial Expression of alphavbeta6 Integrin in DCIS Identifies High-risk Patients and Predicts Recurrence.* Clin Cancer Res, 2014. **20**(2): p. 344-57.

481. NC3Rs. *The National Centre for the Replacement Refinement & Reduction of Animals in Research*. 2014 12/03/2014]; Available from: http://www.nc3rs.org.uk/.

482. The Komen Tissue Bank. *Susan G. Komen for the Cure Tissue Bank*. 2012 08 May 2012]; Available from: http://komentissuebank.iu.edu/.

483. Breast Cancer Campaign Tissue Bank. *About-Tissue-Bank*. 2012 08 May 2012]; Available from: http://breastcancertissuebank.org/about-tissue-bank.php.

9 Appendix

NHS
National Research Ethics Service
Leeds (East) Research Ethics Committee
Room 5.2, Clinical Sciences Building
St James's University Hospital
Beckett Street
Leeds
LS9 7TF

Telephone: 0113 3926768
Facsimile: 0113 3926768

20 January 2010

Dr Valerie Speirs
Leeds Institute of Molecular Medicine
Wellcome Trust Brenner Building
Leeds
LS9 7TF

Dear Dr Speirs

Title of the Research Tissue Bank: **Leeds Breast Research Tissue Bank**
REC reference: **09/H1306/108**
Designated Individual: **Dr Patricia Harnden**

Thank you for your letter of 14 January 2010, responding to the Committee's request for further information on the above research tissue bank and submitting revised documentation.

The further information has been considered on behalf of the Committee by the Chair.

Confirmation of ethical opinion

On behalf of the Committee, I am pleased to confirm a favourable ethical opinion of the above research tissue bank on the basis described in the application form and supporting documentation as revised.

The Committee has also confirmed that the favourable ethical opinion applies to all research projects conducted in the UK using tissue or data supplied by the tissue bank, provided that the release of tissue or data complies with the attached conditions. It will not be necessary for these researchers to make project-based applications for ethical approval. They will be deemed to have ethical approval from this committee. You should provide the researcher with a copy of this letter as confirmation of this. The Committee should be notified of all projects receiving tissue and data from this tissue bank by means of an annual report.

Duration of ethical opinion

The favourable opinion is given for a period of five years from the date of this letter and provided that you comply with the conditions set out in the attached document. You are advised to study the conditions carefully. The opinion may be renewed for a further period of up to five years on receipt of a fresh application. It is suggested that the fresh application is made 3-6 months before the 5 years expires, to ensure continuous approval for the research tissue bank.

This Research Ethics Committee is an advisory committee to Yorkshire and The Humber Strategic Health Authority
The National Research Ethics Service (NRES) represents the NRES Directorate within the National Patient Safety Agency and Research Ethics Committees in England

Approved documents

The documents reviewed and approved at the meeting were:

Document	Version	Date
Covering Letter		05 November 2009
REC application		06 November 2009
Protocol for Management of the Tissue Bank	1	16 October 2009
Annex H - SOPs		01 April 2009
Approval Letter - Study 06/Q1206/180		17 November 2006
Approval Letter - Study 06/Q1205/156		24 July 2006
Approval Letter - Study 04/Q1206/112		22 October 2004
HTA License		
SOPs (Tissue Bank) - Leeds NHST		02 November 2009
Participant Information Sheet	2	13 January 2010
Participant Consent Form	2	13 January 2011
Response to Request for Further Information		14 January 2010

Licence from the Human Tissue Authority

Thank you for providing a copy of the above licence.

Research governance

A copy of this letter is being sent to the R&D office responsible for Leeds Teaching Hospitals NHS Trust. You are advised to check their requirements for approval of the research tissue bank.

Under the Research Governance Framework (RGF), there is no requirement for NHS research permission for the establishment of research tissue banks in the NHS. Applications to NHS R&D offices through IRAS are not required as all NHS organisations are expected to have included management review in the process of establishing the research tissue bank.

Research permission is also not required by collaborators at tissue collection centres (TCCs) who provide tissue or data under the terms of a supply agreement between the organisation and the research tissue bank. TCCs are not research sites for the purposes of the RGF.

Research tissue bank managers are advised to provide R&D offices at all TCCs with a copy of the REC application for information, together with a copy of the favourable opinion letter when available. All TCCs should be listed in Part C of the REC application.

NHS researchers undertaking specific research projects using tissue or data supplied by a research tissue bank must apply for permission to R&D offices at all organisations where the research is conducted, whether or not the research tissue bank has ethical approval.

Site-specific assessment (SSA) is not a requirement for ethical review of research tissue banks. There is no need to inform Local Research Ethics Committees.

Statement of compliance

The Committee is constituted in accordance with the Governance Arrangements for Research Ethics Committees (July 2001) and complies fully with the Standard Operating Procedures for Research Ethics Committees in the UK.

After ethical review

Now that you have completed the application process please visit the National Research Ethics Service website > After Review

Here you will find links to the following:

a) Providing feedback. You are invited to give your view of the service that you have received from the National Research Ethics Service and the application procedure. If you wish to make your views known please use the feedback form available on the website.
b) Annual Reports. Please refer to the attached conditions of approval.
c) Amendments. Please refer to the attached conditions of approval.

We would also like to inform you that we consult regularly with stakeholders to improve our service. If you would like to join our Reference Group please email reference.group@nres.npsa.nhs.uk

09/H1306/108	**Please quote this number on all correspondence**

Yours sincerely

Dr Carol Chu
Chair

E-mail: laura.milnes@leedsth.nhs.uk

Enclosures: *Standard approval conditions*

Copy to: *Patricia Herriden*

Leeds Teaching Hospitals Trust